Guidelines for the use of advanced numerical analysis

SUPPORTED BY

European Commission, Directorate-General XII for Science, Research and Development
Co-operation in Science and Technology (COST) Action C7
Soil–Structure Interaction in Urban Civil Engineering
Working Group A, Advanced Numerical Analysis

EDITORS

David Potts, Kennet Axelsson, Lars Grande, Helmut Schweiger and Michael Long

LEGAL NOTICE

Thomas Telford

Published by Thomas Telford Publishing, Thomas Telford Ltd, 1 Heron Quay, London E14 4JD.
URL: http://www.thomastelford.com

Distributors for Thomas Telford books are

USA: ASCE Press, 1801 Alexander Bell Drive, Reston, VA 20191-4400, USA
Japan: Maruzen Co. Ltd, Book Department, 3–10 Nihonbashi 2-chome, Chuo-ku, Tokyo 103
Australia: DA Books and Journals, 648 Whitehorse Road, Mitcham 3132, Victoria

First published 2002

A catalogue record for this book is available from the British Library

ISBN: 07277 3125 4

Designed and typeset by Keyword Publishing Services
Printed and bound in Great Britain by MPG Books, Bodmin, Cornwall

Contents

Foreword

Urban development is currently being undertaken in many cities around the world and the level of activity is likely to increase in the future. Because of limited surface space, much of this development involves exploitation underground. New construction will have to be carried out among existing buildings and services and the close proximity of the various different forms of construction will provoke considerable interaction between them. This will have to be considered in the design of new constructions to ensure they are both safe and economic. Consequently, calculations will have to be performed which quantify the interaction effects.

Advanced numerical analysis, which has undergone major development during the past ten years, is the ideal tool for performing these calculations. However, such analysis procedures are relatively new and several issues have to be resolved before their use can be generally accepted. One of these issues is the provision of guidelines for the use of numerical analysis. This report attempts to provide such a set of guidelines.

This document has been prepared as part of the Co-operation in Science and Technology (COST) Action C7 for Soil–Structure Interaction in Urban Civil Engineering. COST C7 consists of 67 members representing 17 countries and was formed and funded by the European Commission, with the aim of stimulating European integration and strengthening European competitiveness.

The authors of this report were:

Professor D. Potts	Imperial College, London, United Kingdom
Professor K. Axelsson	Jönköping College, Sweden
Professor L. Grande	NTNU Trondheim, Norway
Professor H. Schweiger	Graz University of Technology, Graz, Austria
Dr M. Long	University College, Dublin, Ireland
Professor C. Sagaseta	University Cantabria, Santander, Spain
Dr M. Dolezalova	Belvederem, Prague, Czech Republic
Dr G. Anagnostou	OMETE AE Consulting Engineers, Athens, Greece
Dr P. de la Fuente	Ciudad University, Madrid, Spain
Dr J. Laue	ETH Zürich, Switzerland
Dr I. Herle	Czech Academy of Sciences, Prague, Czech Republic
Professor D. Battelino	Trieste University, Trieste, Italy

Input and advice from Mr O. Kjekstad from the Norwegian Geotechnical Institute, Norway, chairman of the COST C7 Action, is gratefully acknowledged.

Other handbooks prepared by COST C7 include:

Hidden aspects of urban planning—surface and underground development
Interaction between structural and geotechnical engineers
Avoiding damage caused by soil–structure interaction, lessons learned by case histories

COST

Founded in 1971, COST is an intergovernmental framework for European co-operation in the field of scientific and technical research. COST Actions cover basic and pre-competitive research as well as activities of public interest.

The goal of COST is to ensure that Europe holds a strong position by increasing European co-operation and interaction. Ease of access for institutions from non-member countries also makes COST a successful tool for handling topics of a truly global nature.

To emphasize that the initiative came from the scientists and technical experts themselves and from those with a direct interest in furthering international collaboration, the founding fathers of COST opted for a flexible and pragmatic approach. COST activities have in the past paved the way for community activities, and its flexibility allows COST Actions to be used as a testing and exploratory field for emerging topics.

The member countries participate on an '*à la carte* principle', and activities are launched using a bottom-up approach. COST has a geographical scope beyond the European Union, and most of the Central and Eastern European countries are members. COST also welcomes the participation of interested institutions from non-COST-member states without any geographical restriction.

COST has developed into one of the largest frameworks for research co-operation in Europe and is a valuable mechanism for co-ordinating national research activities in Europe. Today it has almost 200 Actions and involves nearly 30 000 scientists from 32 European member countries and more than 50 participating institutions from 11 non-member countries.

COST Action C7 on Soil–Structure Interaction in Urban Civil Engineering was launched in 1996 and comprises 67 experts from 17 COST countries. Its main objective, as formulated in the Memorandum of Understanding of the Action, is to prepare recommendations for a more efficient, integrated approach to planning, designing and management of construction on and in the ground.

The present volume is tangible proof of the success of COST Action C7. Other handbooks that have been prepared are listed in the Foreword. Thanks to strong momentum in Action, the ambitious plan for deliverables, and the quality of the team of European experts, this Action, initially scheduled to terminate in 2000, was prolonged until May 2002 by the Committee of Senior Officials of COST.

Oddvar Kjekstad
Chairman of COST Action C7

Executive summary

Guidelines for the use of advanced numerical analysis aims to provide guidelines for practising engineers involved in urban development. Although primarily aimed at geotechnical engineers, the book should also be useful to structural engineers.

Urban development involves new construction adjacent to existing buildings and services (i.e. tunnels, gas and water pipelines). Owing to the lack of surface space a considerable part of this new construction is underground (i.e. tunnels and basements). Design involves assessing and accounting for the interaction between new and existing construction. This in turn involves quantifying the degree of soil–structure interaction. In this respect conventional geotechnical analysis is of limited use and advanced analysis based on numerical methods must be employed. However, the use of such methods for analysing soil–structure interaction problems is relatively new and consequently limited experience is available.

To perform useful numerical analysis an engineer requires specialist knowledge in a range of subjects. Firstly, a sound understanding of soil mechanics, structural engineering and the theory behind numerical methods is required. Secondly, an in-depth understanding and appreciation of the limitations of the various constitutive models that are currently available is needed. Lastly, users must be fully conversant with the manner in which the software they are using works. Unfortunately, it is not easy for an engineer to gain all these skills, as it is very rare for all of them to be part of a single undergraduate or postgraduate degree course. It is perhaps, therefore, not surprising that many engineers, who carry out such analyses and/or use the results from such analyses, are not aware of the potential restrictions and pitfalls involved.

This report provides guidelines and advice to help rectify this situation. To do this, it has to discuss many of the approximations that form part of any numerical analysis. In particular, the report

- discusses the major approximations involved in non-linear numerical analysis; this should enable the reader to judge the accuracy of any software being used;
- describes some of the more popular constitutive models currently available and explores their strengths and weaknesses;
- discusses the determination of material parameters for defining soil behaviour;
- describes and compares the various options for modelling structural components and their interface with the soil;
- discusses the various boundary conditions that are appropriate in geotechnical analysis and the assumptions implied when they are used;
- discusses the modelling of specific types of soil–structure interaction that are common in urban development, providing guidelines for best practice;
- describes some of the more common restrictions and pitfalls associated with numerical analysis; and
- discusses the role of benchmarking and provides guidelines by examining the results from several benchmarking exercises.

The report is written for engineers with experience in soil mechanics and numerical analysis. Consequently, there is no in-depth description of the different forms of numerical methods nor the theory behind basic soil mechanics. Rather, emphasis is given to the main assumptions involved and how these may affect the accuracy of any analysis involving soil–structure interaction. Once these are appreciated, the guidelines for best practice become a logical conclusion.

Introduction

Urban planning and civil engineering are disciplines that are facing a great challenge as development of cities becomes more and more complex. This challenge has technical, economical and environmental dimensions.

One of the consequences of urban development will be the greater use of underground space in the form of new tunnels and basements, the construction of which will interact with existing building foundations and services. For such construction to be both safe and economical a clear understanding of its interaction with the existing infrastructure is necessary. In this respect many of the potential problems will involve soil–structure interaction. Some examples of situations that may be encountered are shown in Figures 1.1 to 1.3.

Figure 1.1 shows a common situation in which a basement to a new building is to be constructed adjacent to a road beneath which there is a service pipeline or tunnel. During construction, support to the sides of the excavation will be required. Although there are many design issues associated with such a construction, a major concern is the effect of the excavation on the service pipeline/tunnel. This is particularly so if the pipeline carries gas or water under pressure. In this respect it should be noted that many high-pressure urban water mains are constructed from cast iron which behaves in a brittle manner and can therefore be sensitive to ground movements. Design decisions will have to be made as to the type of support wall (sheet pile, secant pile, diaphragm wall, etc.), its method of construction and the degree of propping provided. To enable a safe and economic solution to be derived, analysis must be performed to estimate the likely movements of, and loads induced in, the pipeline. Conventional calculation methods can only provide crude estimates of these quantities.

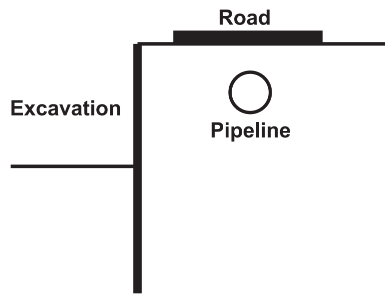

Figure 1.1 Basement construction

Figure 1.2 shows a more complex situation where a basement and the foundations to a new building are to be constructed. Adjacent to the basement are existing buildings, on either piled or raft foundations, and below the basement are two railway tunnels. Construction of the basement will involve an excavation which in turn will require support. These activities will disturb the ground, promoting movements which in turn will affect the ability of the foundations of the adjacent buildings to resist their applied loads and the loads in, and movement of, the tunnel linings. Such effects must be sufficiently small, otherwise unacceptable movements or even failure may be induced. For example, excessive movements of the tunnels could result in trains rubbing against the tunnel sides, whereas differential movements of the foundations of the adjacent buildings could result in cracking to the building's superstructure. In an extreme situation the support provided by the soil could be reduced and either the tunnel linings overstressed and/or the bearing capacity of the foundations reduced.

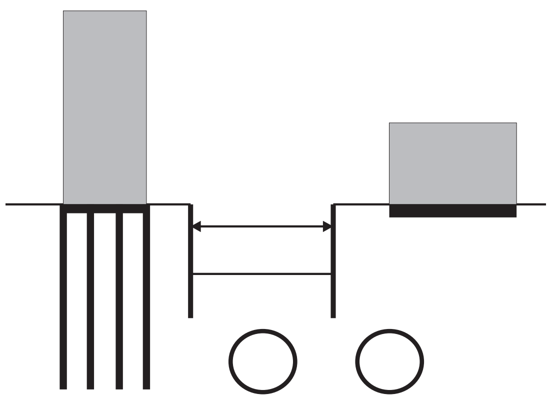

Figure 1.2 Basement construction in an urban environment

Figure 1.3 shows another common scenario where a new metro tunnel is to be constructed beneath an existing building. The tunnel construction must not adversely affect the ability of the existing foundations to resist the building loads or cause excessive movements which would threaten the functionality of the building. The alternative scenario in which the tunnel exists and the building is constructed above it is also common in large cities with an established underground system. In such a situation construction of

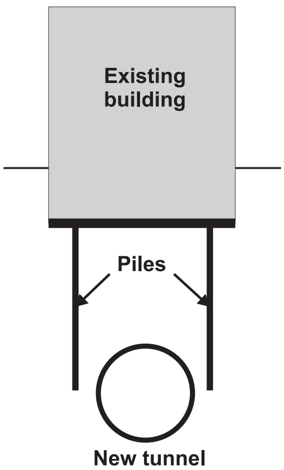

Figure 1.3 Tunnel construction

the new foundations will impose changes in the loads within, and movements of, the tunnel lining.

The design of new developments must account for the interaction between new and existing construction. This requires calculations to be performed to quantify the likely effects (i.e. induced loads and displacements). In this respect it should be noted that the presence of existing structures and services will influence the behaviour of any new construction. Unfortunately such calculations are not straightforward and are probably the most difficult to be performed by structural and geotechnical engineers. In the past much use has been made of empirical information and, because of insufficient information, this has often restricted new developments. However, over the past ten years numerical analyses, which require the use of a powerful computer, have been developed to analyse soil–structure interaction problems.

These methods are extremely powerful and have the potential for dealing with most of the likely scenarios that may arise in urban development. However, there are several issues that have still to be reconciled before the use of these methods can become generally accepted. Firstly, as the problems involve both the ground and various structural elements, an understanding of both structural and ground behaviour is necessary. This implies collaboration between geotechnical and structural engineers, much closer than in the past. Secondly, engineers have to be fully conversant with the new methods of analysis. This involves a knowledge of the numerical method being used and the constitutive models used to represent the various soil strata and structural members, and a thorough understanding of the way the software being used works.

Guidelines for the use of advanced numerical analyses are therefore required and this report is a first attempt to provide such a document. It is based on European practice and is restricted to soil–structure interaction problems. It does not directly address problems in which the ground consists of rock, or where dynamic loading is significant.

The report consists of twelve chapters. *Chapter 2* provides a brief overview of geotechnical analysis and provides a framework that can be used to judge the relative merits of advanced numerical analysis over conventional methods of analysis. An overview of the more common constitutive models used to represent soil behaviour is provided in *Chapter 3*. Both the relevant merits and drawbacks of the models are discussed. *Chapter 4* looks at the various methods available for determining the material parameters necessary for defining soil behaviour. Non-linear numerical analysis is discussed in *Chapter 5*. The sources of non-linearity (i.e. material, geometric and coupled) are described and some of the numerical techniques that are used to deal with it are compared. The special facilities that are needed for modelling structural elements are briefly reviewed in *Chapter 6*, and the boundary conditions appropriate to soil–structure interaction analysis in *Chapter 7*. Guidelines for the input and output of data for numerical analysis are given in *Chapter 8*. Modelling of specific types of interaction problems is discussed in *Chapter 9* and some of the restrictions and pitfalls associated with numerical analysis are presented in *Chapter 10*. *Chapter 11* reviews the important subject of benchmarking and describes the outcome from several examples where such exercises have been undertaken.

2

Geotechnical analysis

2.1 Introduction

Nearly all civil engineering structures involve the ground in some way. Cut slopes, earth and rockfill embankments (see **Figure 2.1**), are made from geological materials. The soil (or rock) provides both the destabilizing and stabilizing forces which maintain equilibrium of the structure. Raft and piled foundations transfer loads from buildings, bridges and offshore structures to be resisted by the ground. Retaining walls enable vertical excavations to be made. In most situations the soil provides both the activating and resisting forces, with the wall and its structural support providing a transfer mechanism. Geotechnical engineering, therefore, plays a major role in the design of civil engineering structures.

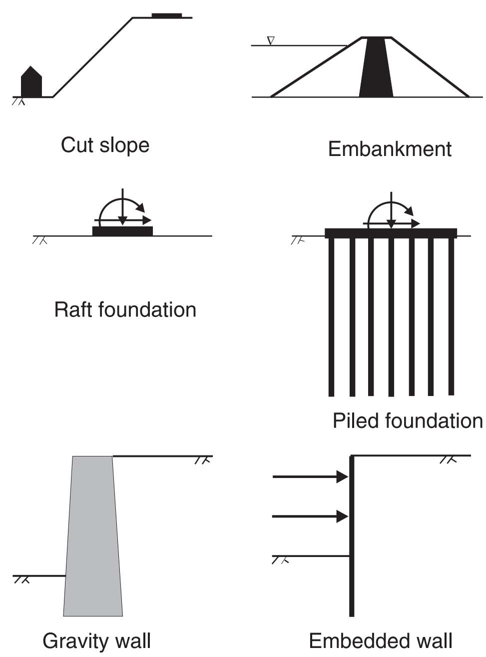

Figure 2.1 Examples of geotechnical structures

The design engineer must assess the forces imposed in the soil and structural members, and the potential movements of both the structure and the surrounding soil. Usually these have to be determined under both working and ultimate load conditions.

Traditionally, geotechnical design has been carried out using simplified analyses or empirical approaches. Most design codes or advice manuals are based on such approaches. The introduction of inexpensive, but sophisticated, computer hardware and software has resulted in considerable advances in the analysis and design of geotechnical structures. Much progress has been made in attempting to model the behaviour of geotechnical structures in service and to investigate the mechanisms of soil–structure interaction.

At present, there are many different methods of calculation available for analysing geotechnical structures. This can be very confusing to an inexperienced geotechnical engineer. This chapter introduces *geotechnical analysis*. The basic theoretical considerations are discussed and the various methods of analysis categorized. The main objectives are to describe the analysis procedures that are in current use and to provide a framework in which the different methods of analysis may be compared. Having established the place of numerical analysis in this overall framework, it is then possible to identify its potential advantages.

2.2 Design objectives

When designing any geotechnical structure, the engineer must ensure that it is stable. Stability can take several forms.

Firstly, the structure and support system must be stable as a whole. There must be no danger of rotational, vertical or translational failure (see **Figure 2.2**).

Secondly, overall stability must be established. For example, if a retaining structure supports sloping ground, the possibility of the construction promoting an overall slope failure should be investigated (see **Figure 2.3**).

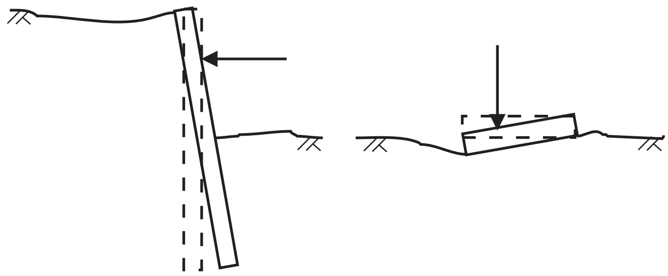

Figure 2.2 Local stability

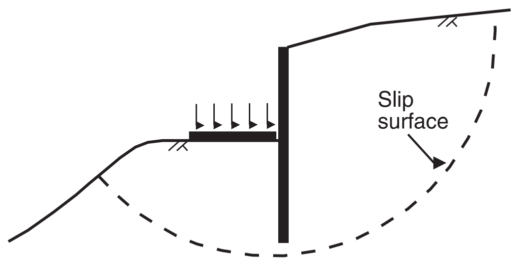

Figure 2.3 Overall stability

The loads on any structural elements involved in the construction must also be calculated, so that these elements may be designed to carry them safely.

Movements must be estimated, both of the structure and of the ground. This is particularly important if there are adjacent buildings and/or sensitive services. For example, if an excavation is to be made in an urban area close to existing services and buildings (see **Figure 2.4**), one of the key design constraints is the effect that the excavation has on the adjacent structures and services. It may be necessary to predict any structural forces induced in these existing structures and/or services.

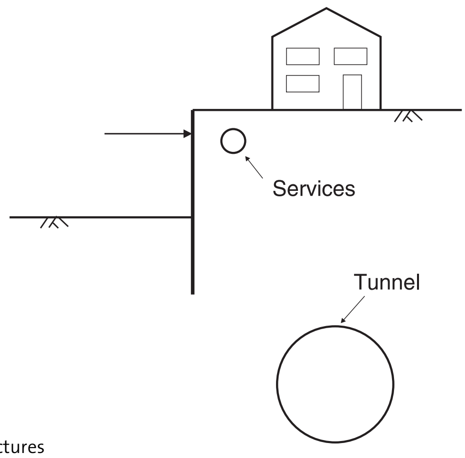

Figure 2.4 Interaction of structures

As part of the design process, it is necessary for an engineer to perform calculations to provide estimates of the above quantities. *Analysis* provides the mathematical framework for such calculations. A good analysis, which simulates real behaviour, allows the engineer to understand problems better. While an important part of the design process, analysis only provides the engineer with a tool to quantify effects once material properties and loading conditions have been set. The design process involves considerably more than *analysis*.

2.3 Design requirements

Before the design process can begin, a considerable amount of information must be assembled. The basic geometry and loading conditions must be established. These are usually defined by the nature of the engineering project.

A geotechnical site investigation is then required to establish the ground conditions. Both the soil stratigraphy and soil properties should be determined. In this respect it will be necessary to determine the strength of the soil and, if ground movements are important, to evaluate its stiffness too. The position of the groundwater table, and whether or not there is underdrainage or artesian conditions, must also be established. The possibility of any changes to these water conditions should be investigated. For example, in many major cities around the world the groundwater level is rising.

The site investigation should also establish the location of any services (gas, water, electricity, telecommunications, sewers and/or tunnels) that are in the vicinity of the proposed construction. The type (strip, raft and/or piled) and depth of the foundations of any adjacent buildings should also be determined. The allowable movements of these services and foundations should then be established.

Any restrictions on the performance of the new geotechnical structure must be identified. Such restrictions can take many different forms. For example, due to the close proximity of adjacent services and structures there may be restrictions imposed on ground movements.

Once the above information has been collected, the design constraints on the geotechnical structure can be established. These should cover the construction period and the design life of the structure. This process also implicitly identifies which types of structure are and are not appropriate. For example, when designing an excavation, if there is a restriction on the movement of the retained ground, propped or anchored embedded retaining walls are likely to be more appropriate than gravity or reinforced earth walls. The design constraints also determine the type of design analysis that needs to be undertaken.

2.4 Theoretical considerations

2.4.1 Requirements for a general solution

In general, a theoretical solution must satisfy *equilibrium*, *compatibility*, the material *constitutive behaviour* and *boundary conditions* (both *force* and *displacement*). Each of these conditions is considered separately below.

2.4.2 Equilibrium

To quantify how forces are transmitted through a continuum, engineers use the concept of stress (force/unit area). The magnitude and direction of a stress and the manner in which it varies spatially indicates how the forces are transferred. However, these stresses cannot vary randomly but must obey certain rules.

For example, consider a concrete beam, supported by two reactions on its lower surface and loaded by a load L on its upper surface, as presented in **Figure 2.5**. Clearly, for overall equilibrium the reactions must be $2L/3$ and $L/3$. What is not so clear, however, is how the load is transferred through the beam. As noted above, engineers use the concept of stress to investigate the load transfer. Stresses are essentially fictitious quantities. For example, the manner in which the major principal stress varies through the beam is given in Figure 2.5. The length of the trajectories represents the magnitude of the stress and their orientation its direction.

Stress is a tensor consisting of six components (see **Figure 2.6**) and there are rules which control the manner in which the stress components vary throughout a continuum. Neglecting inertia effects and all body forces, except self-weight, stresses in a soil mass must satisfy the following three equations (Timoshenko and Goodier, 1951):

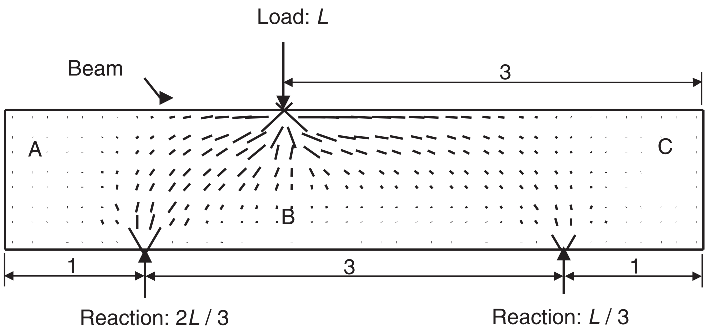

Figure 2.5 Stress trajectories

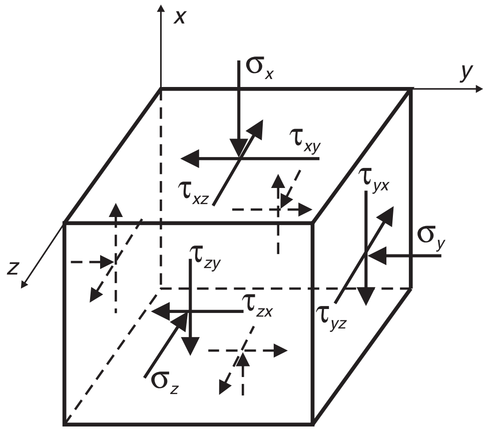

Figure 2.6 Stresses on a typical element

$$
\begin{aligned}
&\frac{\partial \boldsymbol{\sigma}_x}{\partial x}+\frac{\partial \tau_{yx}}{\partial y}+\frac{\partial \tau_{zx}}{\partial z}+\gamma=0\\
&\frac{\partial \tau_{xy}}{\partial x}+\frac{\partial \boldsymbol{\sigma}_y}{\partial y}+\frac{\partial \tau_{zy}}{\partial z}=0\\
&\frac{\partial \tau_{xz}}{\partial x}+\frac{\partial \tau_{yz}}{\partial y}+\frac{\partial \boldsymbol{\sigma}_z}{\partial z}=0
\end{aligned}
\tag{2.1}
$$

The following should be noted:

- self-weight γ acts in the x direction;
- compressive stresses are assumed positive;
- the equilibrium equations (2.1) are in terms of total stresses;
- stresses must satisfy the boundary conditions (i.e. at the boundaries the stresses must be in equilibrium with the applied surface traction forces).

2.4.3 Compatibility

2.4.3.1 Physical compatibility

Compatible deformation involves no overlapping of material and no generation of holes. The physical meaning of compatibility can be explained by considering a plate composed of smaller plate elements, as shown in **Figure 2.7(a)**. After straining, the plate elements may be so distorted that they form the array shown in **Figure 2.7(b)**. This condition might represent failure by rupture. Alternatively, deformation might be such that the various plate elements fit together (i.e. no holes created and no overlapping) as shown in **Figure 2.7(c)**. This condition represents a compatible deformation.

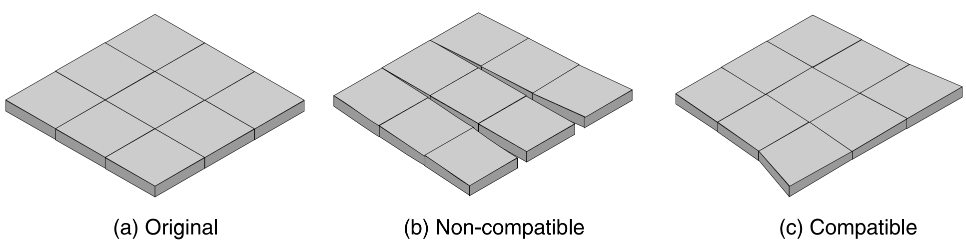

Figure 2.7 Modes of deformation

2.4.3.2 Mathematical compatibility

The above physical interpretation of compatibility can be expressed mathematically by considering the definition of strains. If deformations are defined by continuous functions u, v and w in the x, y and z directions respectively, the strains (assuming small strain theory and a compression positive sign convention) are defined as (Timoshenko and Goodier, 1951):

$$
\begin{array}{lll}
\varepsilon_x = -\dfrac{\partial u}{\partial x}; & \varepsilon_y = -\dfrac{\partial v}{\partial y}; & \varepsilon_z = -\dfrac{\partial w}{\partial z} \\
\gamma_{xy} = -\dfrac{\partial v}{\partial x} - \dfrac{\partial u}{\partial y}; & \gamma_{yz} = -\dfrac{\partial w}{\partial y} - \dfrac{\partial v}{\partial z}; & \gamma_{xz} = -\dfrac{\partial w}{\partial x} - \dfrac{\partial u}{\partial z}
\end{array}
\tag{2.2}
$$

As the six strains are a function of only three displacements, they are not independent. It can be shown mathematically that, for a compatible displacement field to exist, all the above components of strain and their derivatives must exist and be continuous to at least the second order. The displacement field must satisfy any specified displacements or restraints imposed on the boundary.

2.4.4 Equilibrium and compatibility conditions

Combining the equilibrium (Equations (2.1)) and compatibility conditions (Equations (2.2)), gives:

Unknowns:	6 stresses + 6 strains + 3 displacements	= 15
Equations:	3 equilibrium + 6 compatibility	= 9

To obtain a solution therefore requires six more equations. These come from the constitutive relationships.

2.4.5 Constitutive behaviour

This is a description of material behaviour. In simple terms it is the stress–strain behaviour of the soil. It usually takes the form of a relationship between stresses and strains and therefore provides a link between equilibrium and compatibility. For calculation purposes the constitutive behaviour has to be expressed mathematically:

$$
\begin{Bmatrix} \Delta\sigma_x \\ \Delta\sigma_y \\ \Delta\sigma_z \\ \Delta\tau_{xy} \\ \Delta\tau_{xz} \\ \Delta\tau_{zy} \end{Bmatrix} = \begin{bmatrix} D_{11} & D_{12} & D_{13} & D_{14} & D_{15} & D_{16} \\ D_{21} & D_{22} & D_{23} & D_{24} & D_{25} & D_{26} \\ D_{31} & D_{32} & D_{33} & D_{34} & D_{35} & D_{36} \\ D_{41} & D_{42} & D_{43} & D_{44} & D_{45} & D_{46} \\ D_{51} & D_{52} & D_{53} & D_{54} & D_{55} & D_{56} \\ D_{61} & D_{62} & D_{63} & D_{64} & D_{65} & D_{66} \end{bmatrix} \begin{Bmatrix} \Delta\varepsilon_x \\ \Delta\varepsilon_y \\ \Delta\varepsilon_z \\ \Delta\gamma_{xy} \\ \Delta\gamma_{xz} \\ \Delta\gamma_{zy} \end{Bmatrix}
\tag{2.3}
$$

or

$$\Delta\sigma = [\mathbf{D}]\ \Delta\varepsilon$$

For example, for a linear elastic material the [**D**] matrix takes the following form:

$$
\frac{E}{(1+\mu)} \begin{bmatrix} (1-\mu) & \mu & \mu & 0 & 0 & 0 \\ \mu & (1-\mu) & \mu & 0 & 0 & 0 \\ \mu & \mu & (1-\mu) & 0 & 0 & 0 \\ 0 & 0 & 0 & (1/2-\mu) & 0 & 0 \\ 0 & 0 & 0 & 0 & (1/2-\mu) & 0 \\ 0 & 0 & 0 & 0 & 0 & (1/2-\mu) \end{bmatrix}
\tag{2.4}
$$

where E and μ are the Young's modulus and Poisson's ratio respectively.

Because soil usually behaves in a non-linear manner, it is more realistic for the constitutive equations to relate increments of stress and strain, as indicated in Equation (2.3), and for the [**D**] matrix to depend on the current and past stress history.

The constitutive behaviour can be expressed in terms of either total or effective stresses. If specified in terms of effective stresses, the principle of effective stress ($\sigma = \sigma' + \sigma_f$) may be invoked to obtain total stresses required for use with the equilibrium equations:

$$\Delta\sigma' = [\mathbf{D}']\Delta\varepsilon; \qquad \Delta\sigma_f = [\mathbf{D}_f]\Delta\varepsilon; \qquad \text{therefore } \Delta\sigma = ([\mathbf{D}'] + [\mathbf{D}_f])\Delta\varepsilon \tag{2.5}$$

where $[\mathbf{D}_f]$ is a constitutive relationship relating the change in pore fluid pressure $\Delta\sigma_f$ to the change in strain. For undrained behaviour, the change in pore fluid pressure is related to the volumetric strain (which is small) via the bulk compressibility of the pore fluid (which is large).

2.5 Geometric idealization

In order to apply the above concepts to a real geotechnical problem, certain assumptions and idealizations must be made. In particular, it is necessary to specify soil behaviour in the form of a mathematical constitutive relationship. It may also be necessary to simplify and/or idealize the geometry and/or boundary conditions of the problem.

2.5.1 Plane strain

Owing to the special geometric characteristics of many of the physical problems treated in soil mechanics, additional simplifications of considerable magnitude can be applied. Problems, such as the analysis of retaining walls, continuous footings and the stability of slopes, generally have one dimension very large in comparison with the other two (see **Figure 2.8**). Hence, if the force and/or applied displacement boundary conditions are perpendicular to, and independent of, this dimension, all cross-sections will be the same. If the *z* dimension of the problem is large, and it can be assumed that the state existing in the *x*–*y* plane holds for all planes parallel to it, the displacement of any *x*–*y* cross-section relative to any parallel *x*–*y* cross-section is zero. This means that $w = 0$, and the displacements *u* and *v* are independent of the *z* coordinate. The conditions consistent with these approximations are said to define the very important case of *plane strain*:

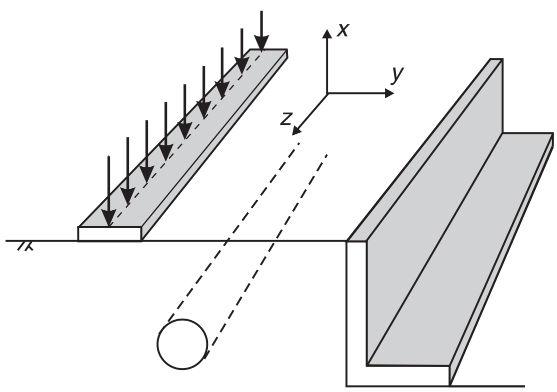

Figure 2.8 Examples of plane strain

$$\varepsilon_z = -\frac{\partial w}{\partial z} = 0; \qquad \gamma_{yz} = -\frac{\partial w}{\partial y} - \frac{\partial v}{\partial z} = 0; \qquad \gamma_{xz} = -\frac{\partial w}{\partial x} - \frac{\partial u}{\partial z} = 0 \tag{2.6}$$

The constitutive relationship then reduces to

$$\begin{Bmatrix} \Delta\sigma_x \\ \Delta\sigma_y \\ \Delta\sigma_z \\ \Delta\tau_{xy} \\ \Delta\tau_{xz} \\ \Delta\tau_{zy} \end{Bmatrix} = \begin{bmatrix} D_{11} & D_{12} & D_{14} \\ D_{21} & D_{22} & D_{24} \\ D_{31} & D_{32} & D_{34} \\ D_{41} & D_{42} & D_{44} \\ D_{51} & D_{52} & D_{54} \\ D_{61} & D_{62} & D_{64} \end{bmatrix} \begin{Bmatrix} \Delta\varepsilon_x \\ \Delta\varepsilon_y \\ \Delta\gamma_{xy} \end{Bmatrix} \tag{2.7}$$

However, for elastic and the majority of material idealizations currently used to represent soil behaviour $D_{52} = D_{51} = D_{54} = D_{61} = D_{62} = D_{64} = 0$, and consequently $\Delta\tau_{xz} = \Delta\tau_{zy} = 0$. This results in four non-zero stress changes, $\Delta\sigma_x$, $\Delta\sigma_y$, $\Delta\sigma_z$ and $\Delta\tau_{xy}$.

It is common to consider only the stresses σ_x, σ_y and τ_{xy} when performing analysis for plane strain problems. This is acceptable if D_{11}, D_{12}, D_{14}, D_{21}, D_{22}, D_{24}, D_{41}, D_{42} and D_{44} are not dependent on σ_z. This condition is satisfied if the soil is assumed to be elastic. It is also true if the Tresca or Mohr–Coulomb failure condition is adopted and it is assumed that the intermediate stress $\sigma_2 = \sigma_z$. *Such an assumption is usually adopted for the simple analysis of geotechnical problems*. It should be noted, however, that these are special cases.

2.5.2 Axi-symmetry

Some problems possess rotational symmetry. For example, a uniform or centrally loaded circular footing, acting on a homogeneous or horizontally layered foundation, has rotational symmetry about a vertical axis through the centre of the foundation. Cylindrical triaxial samples, single piles and caissons are other examples where such symmetry may exist (see **Figure 2.9**).

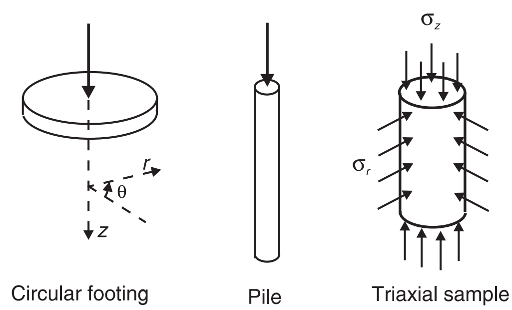

Figure 2.9 Examples of axi-symmetry

In this type of problem it is usual to carry out analyses using cylindrical coordinates *r* (radial direction), *z* (vertical direction) and θ (circumferential direction). Because of the symmetry, there is no displacement in the θ direction and the displacements in the *r* and *z* directions are independent of θ and therefore the strains reduce to (Timoshenko and Goodier, 1951)

$$\varepsilon_r = -\frac{\partial u}{\partial r}; \qquad \varepsilon_z = -\frac{\partial v}{\partial z}; \qquad \varepsilon_\theta = -\frac{u}{r}; \qquad \gamma_{rz} = -\frac{\partial v}{\partial r} - \frac{\partial u}{\partial z}; \qquad \gamma_{r\theta} = \gamma_{z\theta} = 0 \tag{2.8}$$

where *u* and *v* are the displacements in the *r* and *z* directions respectively.

This is similar to the plane strain situation discussed above and, consequently, the same arguments concerning the [**D**] matrix apply here too. As for plane strain, there are four non-zero stress changes, $\Delta\sigma_r$, $\Delta\sigma_z$, $\Delta\sigma_\theta$ and $\Delta\tau_{rz}$.

2.6 Methods of analysis

As noted above, fundamental considerations assert that for an exact theoretical solution the requirements of *equilibrium, compatibility, material behaviour* and *boundary conditions*, both force and displacement, must all be satisfied. It is therefore useful to review the broad categories of analysis currently in use against these theoretical requirements.

Current methods of analysis can be conveniently grouped into the following categories: closed form, simple and numerical analysis. Each of these categories is considered separately. The ability of each method to satisfy the fundamental theoretical requirements and provide design information is summarized in **Tables 2.1 and 2.2** respectively.

Table 2.1 Basic solution requirements satisfied by the various methods of analysis

Method of analysis	Solution requirements				
	Equilibrium	Compatibility	Constitutive behaviour	Boundary conditions[a]	
				Force	Displacement
Closed form	S	S	Linear elastic	S	S
Limit equilibrium	S	NS	Rigid with a failure criterion	S	NS
Stress field	S	NS	Rigid with a failure criterion	S	NS
Limit analysis:					
Lower bound	S	NS	Ideal plasticity with associated flow rule	S	NS
Upper bound	NS	S		NS	S
Beam–spring approaches	S	S	Soil modelled by springs or elastic interaction factors	S	S
Full numerical analysis	S	S	Any	S	S

[a] S - Satisfied; NS - Not satisfied

2.7 Closed form solutions

For a particular geotechnical structure, if it is possible to establish a realistic constitutive model for material behaviour, identify the boundary conditions, and combine these with the equations of equilibrium and compatibility, an exact theoretical solution can be obtained. The solution is exact in the theoretical sense but is still approximate for the real problem, as assumptions about geometry, the applied boundary conditions and the constitutive behaviour have been made in idealizing the real physical problem into an equivalent mathematical form. In principle, it is possible to obtain a solution that predicts the behaviour of a problem from first loading (construction/excavation) through to the long term and to provide information on movements and stability from a single analysis.

A closed form solution is, therefore, the ultimate method of analysis. In this approach all solution requirements are satisfied and the theories of mathematics are used to obtain complete analytical expressions defining the full behaviour of the problem. However, as soil is a highly complex multi-phase material which behaves non-linearly when loaded, complete

Table 2.2 Design requirements satisfied by the various methods of analysis

Method of analysis	Design requirements		
	Stability	Movements	Adjacent structures
Closed form (linear elastic)	No	Yes	Yes
Limit equilibrium	Yes	No	No
Stress field	Yes	No	No
Limit analysis:			
Lower bound	Yes	No	No
Upper bound	Yes	Crude estimate	No
Beam-spring approaches	Yes	Yes	No
Full numerical analysis	Yes	Yes	Yes

analytical solutions to realistic geotechnical problems are not usually possible. Solutions can be obtained only for two very simple classes of problem.

Firstly, there are solutions in which the soil is assumed to behave in an isotropic linear elastic manner. While these can be useful for providing a first estimate of movements and structural forces, they are of little use for investigating stability. Comparison with observed behaviour indicates that such solutions do not provide realistic predictions.

Secondly, there are some solutions for problems that contain enough geometric symmetries for the problem to reduce to being essentially one-dimensional. Expansion of spherical and infinitely long cylindrical cavities in an infinite elasto-plastic continuum are examples.

2.8 Simple methods

To enable more realistic solutions to be obtained, approximations must be introduced. This can be done in one of two ways. Firstly, the constraints on satisfying the basic solution requirements may be relaxed, but mathematics is still used to obtain an approximate analytical solution. This is the approach used by the pioneers of geotechnical engineering. Such approaches are considered as ‘simple methods’ in what follows. The second way, by which more realistic solutions can be obtained, is to introduce numerical approximations. All requirements of a theoretical solution are considered, but may be satisfied only in an approximate manner. This latter approach is considered in more detail in the next section.

Limit equilibrium, *stress field* and *limit analysis* fall into the category of ‘simple methods’. All methods essentially assume the soil is at failure, but differ in the manner in which they arrive at a solution.

2.8.1 Limit equilibrium

In this method of analysis an 'arbitrary' failure surface is adopted (assumed) and *equilibrium* conditions are considered for the failing soil mass, assuming that the failure criterion holds everywhere along the failure surface. The failure surface may be planar, curved or some combination of these. Only the global equilibrium of the 'blocks' of soil between the failure surfaces and the boundaries of the problem are considered. The internal stress distribution within the blocks of soil is not considered. Coulomb's wedge analysis and the method of slices are examples of limit equilibrium calculations.

2.8.2 Stress field solution

In this approach the soil is assumed to be at the point of failure everywhere and a solution is obtained by combining the failure criterion with the equilibrium equations. For plane strain conditions and the Mohr–Coulomb failure criterion this gives the following:

Equilibrium equations:

$$\begin{aligned}\frac{\partial \sigma_x}{\partial x} + \frac{\partial \tau_{xy}}{\partial y} &= 0 \\ \frac{\partial \tau_{xy}}{\partial x} + \frac{\partial \sigma_y}{\partial y} &= \gamma\end{aligned} \tag{2.9}$$

Mohr–Coulomb failure criterion (from **Figure 2.10**):

$$\sigma_1' - \sigma_3' = 2c' \cos\varphi' + (\sigma_1' + \sigma_3') \sin\varphi' \tag{2.10}$$

Noting that

$$\begin{aligned}s &= c' \cot\varphi' + \tfrac{1}{2}(\sigma_1' + \sigma_3') \\ &= c' \cot\varphi' + \tfrac{1}{2}(\sigma_x' + \sigma_y')\end{aligned}$$

$$t = \tfrac{1}{2}(\sigma_1' - \sigma_3') = [\tfrac{1}{4}(\sigma_x' - \sigma_y')^2 + \tau_{xy}^2]^{0.5}$$

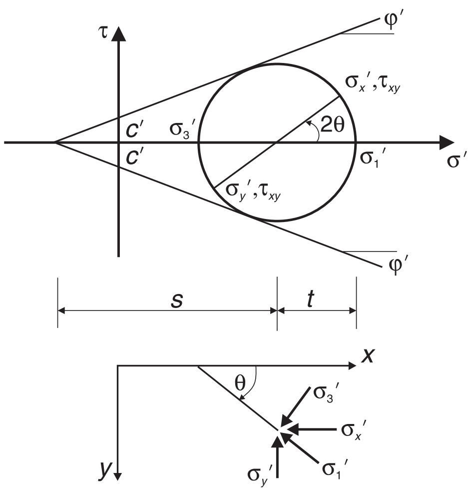

Figure 2.10 Mohr's circle of stress

and substituting in Equation (2.10) give the following alternative equations for the Mohr–Coulomb criterion

$$t = s \sin \varphi' \tag{2.11}$$

$$[\tfrac{1}{4}(\sigma'_x - \sigma'_y)^2 + \tau_{xy}^2]^{0.5} = [c' \cot \varphi' + \tfrac{1}{2}(\sigma'_x + \sigma'_y)] \sin \varphi' \tag{2.12}$$

The equilibrium equations (2.9) and the failure criterion (2.12) provide three equations in terms of three unknowns. It is therefore theoretically possible to obtain a solution. Combining the above equations gives

$$\left.\begin{aligned}(1 + \sin \varphi' \cos 2\theta)\frac{\partial s}{\partial x} + \sin \varphi' \sin 2\theta \frac{\partial s}{\partial y} + 2s \sin \varphi' \left(\cos\ 2\theta \frac{\partial \theta}{\partial y} - \sin 2\theta \frac{\partial \theta}{\partial x} \right) &= 0 \\ \sin \varphi' \sin 2\theta \frac{\partial s}{\partial x} + (1 - \sin \varphi' \cos 2\theta)\frac{\partial s}{\partial y} + 2s \sin \varphi' \left(\sin 2\theta \frac{\partial \theta}{\partial y} + \cos 2\theta \frac{\partial \theta}{\partial x} \right) &= \gamma \end{aligned}\right\} \tag{2.13}$$

These two partial differential equations can be shown to be of the hyperbolic type. A solution is obtained by considering the characteristic directions and obtaining equations for the stress variation along these characteristics (Atkinson and Potts, 1975). The differential equations of the stress characteristics are

$$\begin{aligned}\frac{dy}{dx} &= \tan[\theta - (\pi/4 - \varphi'/2)] \\ \frac{dy}{dx} &= \tan[\theta + (\pi/4 - \varphi'/2)]\end{aligned} \tag{2.14}$$

Along these characteristics the following equations hold:

$$\left.\begin{aligned}ds - 2s \tan \varphi' d\theta &= \gamma(dy - \tan \varphi' dx) \\ ds + 2s \tan \varphi' d\theta &= \gamma(dy + \tan \varphi' dx)\end{aligned}\right\} \tag{2.15}$$

Equations (2.14) and (2.15) provide four differential equations with four unknowns x, y, s and θ which, in principle, can be solved mathematically. However, to date, it has been possible to obtain analytical solutions only for very simple problems and/or if the soil is assumed to be weightless, $\gamma = 0$. Generally, they are solved numerically by adopting a finite difference approximation.

Solutions based on the above equations usually provide only a partial stress field which does not cover the whole soil mass but is restricted to the zone of interest. In general, they are therefore not lower bound solutions (see *Section 2.8.3*).

The above equations provide what appears to be, and sometimes is, static determinacy, in the sense that there are the same number of equations as unknown stress components. In most practical problems, however, the boundary conditions involve both forces and displacements and the static determinacy is misleading. Compatibility is not considered in this approach.

Rankine active and passive stress fields and the earth pressure tables obtained by Sokolovski (1960, 1965) and used in some codes of practice are examples of stress field solutions. Stress fields also form the basis of analytical solutions to the bearing capacity problem.

2.8.3 Limit analysis

The theorems of limit analysis (Chen, 1975) are based on the following assumptions:

- Soil behaviour exhibits perfect or ideal plasticity, work hardening/softening does not occur. This implies that there is a single yield surface separating elastic and elasto-plastic behaviour.
- The yield surface is convex in shape and the plastic strains can be derived from the yield surface through the normality condition.
- Changes in geometry of the soil mass that occur at failure are insignificant. This allows the equations of virtual work to be applied.

With these assumptions it can be shown that a unique failure condition will exist. The bound theorems enable estimates of the collapse loads, which occur at failure, to be obtained. Solutions based on the 'safe' theorem are safe estimates of these loads, while those obtained using the 'unsafe' theorem are unsafe estimates. Use of both theorems enable bounds to the true collapse loads to be obtained.

2.8.3.1 Unsafe theorem

An unsafe solution to the true collapse loads (for the ideal plastic material) can be found by selecting any kinematically possible failure mechanism and performing an appropriate work rate calculation. The loads so determined are either on the unsafe side or equal to the true collapse loads.

This theorem is often referred to as the 'upper bound' theorem. As equilibrium is not considered, there is an infinite number of solutions that can be found. The accuracy of the solution depends on how close the assumed failure mechanism is to the real one.

2.8.3.2 Safe theorem

If a statically admissible stress field covering the whole soil mass can be found, which nowhere violates the yield condition, then the loads in equilibrium with the stress field are on the safe side or equal to the true collapse loads.

This theorem is often referred to as the 'lower bound' theorem. A statically admissible stress field consists of an equilibrium distribution of stress which balances the applied loads and body forces. As compatibility is not considered, there is an infinite number of solutions. The accuracy of the solution depends on how close the assumed stress field is to the real one.

If safe and unsafe solutions can be found which give the same estimates of collapse loads, then this is the correct solution for the ideal plastic material. It should be noted that in such a case all the fundamental solution requirements are satisfied. This can rarely be achieved in practice. However, two such cases in which it has been achieved are (i) the solution of the undrained bearing capacity of a strip footing, on a soil with a constant undrained shear strength S_u (Chen, 1975), and (ii) the solution for the undrained lateral load capacity of an infinitely long rigid pile embedded in an infinite continuum of soil, with a constant undrained shear strength (Randolph and Houlsby, 1984).

2.8.4 Comments

The ability of these simple methods to satisfy the basic solution requirements is shown in Table 2.1. Inspection of this table clearly shows that none of the methods satisfy all the basic requirements and therefore they do not necessarily produce an exact theoretical solution. All methods are therefore approximate and it is, perhaps, not surprising that there are many different solutions to the same problem.

As these approaches assume the soil to be everywhere at failure, they are not strictly appropriate for investigating behaviour under working load conditions. When applied to geotechnical problems, they do not distinguish between different methods of construction (e.g. excavation versus backfilling), nor account for *in situ* stress conditions. Information is provided on local stability, but no information on soil or structural movements is given and separate calculations are required to investigate overall stability (see Table 2.2).

Notwithstanding the above limitations, simple methods form the mainstay of most design approaches. Where they have been calibrated against field observation their use may be appropriate. However, it is for cases with more complex soil–structure interaction, where calibration is more difficult, that these simple methods are perhaps less reliable. Because of their simplicity and ease of use, it is likely that they will always play an important role in the design of geotechnical structures. In particular, they are appropriate at the early stages of the design process to obtain first estimates of both stability and structural forces.

2.9 Numerical analysis

2.9.1 Beam–spring approach

This approach is used to investigate soil–structure interaction. For example, it can be used to study the behaviour of axially and laterally loaded piles, raft foundations, embedded retaining walls and tunnel linings. The major approximation is the assumed soil behaviour, and two approaches are commonly used. The soil behaviour is either approximated by a set of unconnected vertical and horizontal springs (Borin, 1989), or by a set of linear elastic interaction factors (Papin *et al*., 1985). Only a single structure can be accommodated in the analysis. Consequently, only a single pile or retaining wall can be analysed. Further approximations must be introduced if more than one pile, retaining wall or foundation interact. Any structural support, such as props or anchors (retaining wall problems), are represented by simple springs (see **Figure 2.11**).

To enable limiting pressures to be obtained, for example on each side of a retaining wall, 'cut-offs' are usually applied to the spring forces and interaction factors representing soil behaviour.

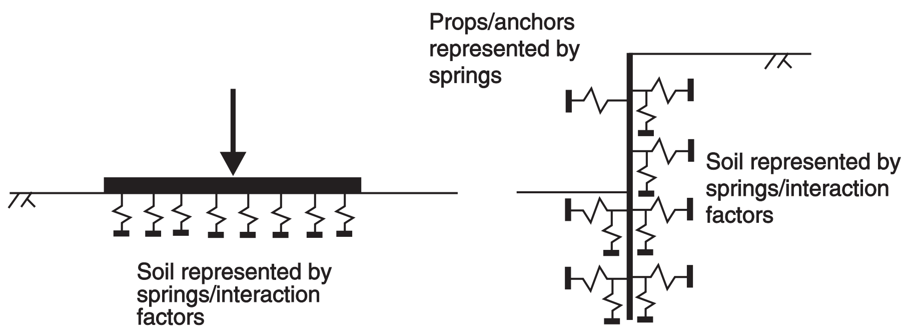

Figure 2.11 Examples of beam–spring problems

These cut-off pressures are usually obtained from one of the simple analysis procedures discussed above (i.e. limit equilibrium, stress fields or limit analysis). It is important to appreciate that these limiting pressures are not a direct result of the beam–spring calculation, but are obtained from separate approximate solutions and then imposed on the beam–spring calculation process.

With the boundary value problem reduced to one of studying the behaviour of a single isolated structure (e.g. a pile, a footing or a retaining wall) and gross assumptions made about soil behaviour, a complete theoretical solution to the problem is sought. Because of the complexities involved, this is usually achieved using a computer. The structural member (e.g. pile, footing or retaining wall) is represented using either finite differences or finite elements and a solution that satisfies all the fundamental solution requirements is obtained by iteration.

Sometimes computer programs that perform such calculations are identified as finite difference or finite element programs. However, it must be noted that it is only the structural member that is represented in this manner and these programs should not be confused with those that involve full discretization of both the soil and structural members by finite differences or finite elements (see *Section 2.9.2*).

As solutions obtained in this way include limits to the earth pressures that can develop adjacent to the structure, they can provide information on local stability. This is often indicated by a failure of the program to converge. However, numerical instability may occur for other reasons and therefore a false impression of instability may be given. Solutions from these calculations include forces and movements of the structure. They do not provide information about global stability or movements in the adjacent soil. Nor do they consider adjacent structures.

2.9.2 Full numerical analysis

This category of analysis includes methods that attempt to satisfy all theoretical requirements, include realistic soil constitutive models and incorporate boundary conditions that simulate field conditions. Because of the complexities involved and the non-linearities in soil behaviour, all methods are numerical in nature. Approaches based on finite difference and finite element methods are those most widely used in geotechnical engineering. The boundary element method and the cell method (Tonti, 2001; Pani *et al.*, 2001) are used to a lesser extent. These methods essentially involve a computer simulation of the history of the boundary value problem from green field conditions, through construction and in the long term.

Their ability to accurately reflect field conditions essentially depends on (i) the ability of the constitutive model to represent real soil behaviour and (ii) correctness of the boundary conditions imposed. The user has only to define the appropriate geometry, construction procedure, soil parameters and boundary conditions. Structural members may be added and withdrawn during the numerical simulation to model field conditions. Retaining structures composed of several retaining walls, interconnected by structural components, can be considered and, because the soil mass is modelled in the analysis, the complex interaction between raking struts or ground anchors and the soil can be accounted for. The effect of time on the development of pore water pressures can also be simulated by including coupled consolidation. No postulated failure mechanism or mode of behaviour of the problem is required, as these are predicted by the analysis. The analysis allows the complete history of the boundary value problem to be predicted and a single analysis can provide information on all design requirements.

Potentially, the methods can solve fully three-dimensional problems and suffer none of the limitations discussed previously for the other methods. At present, the speed of computer hardware restricts analysis of most practical problems to two-dimensional plane strain or axi-symmetric sections. However, with the rapid development in computer hardware and its reduction in cost, the possibilities of full three-dimensional simulations are imminent.

Full numerical analyses are complex and should be performed by qualified and experienced staff. The operator must understand soil mechanics and, in particular, the constitutive models that the software uses, and be familiar with the software package to be employed for the analysis. Non-linear numerical analysis is not straightforward and at present there are several algorithms available for solving the non-linear system of governing equations. Some of these are more accurate than others and some are dependent on increment size. There are approximations within these algorithms and errors associated with discretization. However, these can be controlled by the experienced user so that accurate predictions can be obtained.

Full numerical analysis can be used to predict the behaviour of complex field situations. It can also be used to investigate the fundamentals of soil–structure interaction and to calibrate some of the simple methods discussed above.

Numerical analysis and its use in analysing geotechnical structures is the subject of the remaining chapters of this handbook.

3

Constitutive models

3.1 Basic soil behaviour

3.1.1 Introduction

Soil is a complex material and its behaviour, as observed from tests in the laboratory or *in situ*, depends on a number of issues, the most important of which are the soil composition (grain size, clay content, etc.), the loading history (degree of consolidation, stress paths, etc.) and drainage conditions. Soil is a multi-phase material. The mineral particles constitute the solid phase in the form of a soil skeleton. The pores in this skeleton might contain the phases of liquid (pore water) and/or gas (pore air). Each of these phases behaves in a different way. Without doubt, the most difficult to model is the soil skeleton which determines the deformation behaviour of the whole composite (e.g. the Terzaghi principle of effective stress). As soil behaviour is a complex subject, it is not possible, given the limited space, to cover every aspect of it in this handbook. Consequently, attention will be given to the most important features so as to provide the necessary background for understanding the framework of the different soil models and their applications.

3.1.2 Compression of the soil skeleton

The compressibility of soils is traditionally investigated by oedometer tests. By plotting the void ratio, e, of the sample against the vertical effective stress, σ_v' (on a linear scale), at least two characteristic features can be observed. The compression is (highly) *non-linear* (**Figure 3.1(a)**), and, when unloaded from some stress state, *irreversible deformation* is observed. When reloading, the response is much stiffer than during the virgin compression. However, when the virgin compression line (VCL) is again reached at the *preconsolidation pressure*, the compressive stiffness rapidly reduces to that of the virgin soil.

When the vertical compression is plotted against the logarithm of the vertical effective stress, a more or less straight VCL is obtained, at least for clays (**Figure 3.1(b)**). In an overconsolidated state the response is essentially *elastic* and might, for many purposes, be regarded as linear elastic. Further, the unloading and reloading lines might be assumed to coincide. However, a

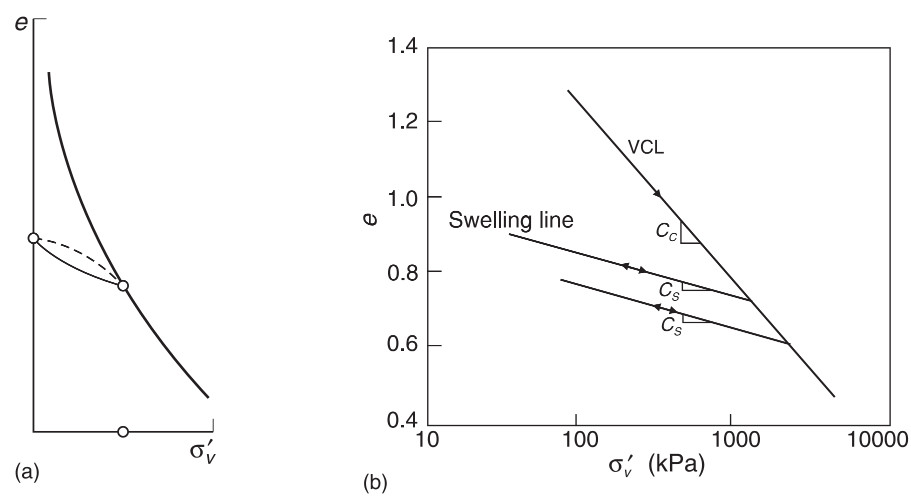

Figure 3.1 (a) Compression of soil. (b) Usual interpretation of soil compression

more detailed description of the unloading–reloading branches should account for the hysteretic behaviour observed.

The true volumetric response of soils can be investigated using triaxial tests by increasing the mean effective pressure while keeping the deviatoric stress as zero. In this case, the volumetric strain, or the void ratio, is plotted against the mean effective pressure. Compression lines similar to those in Figure 3.1 are obtained.

When the compression lines of clays and sands are compared, the compressive stiffness of the latter is much higher than that of the former. For sands and coarser soils, the non-linear VCL is more like a potential function than a logarithmic curve. It can thus be concluded that volumetric compression of soils is highly non-linear as well as elastic–plastic. The preconsolidation pressure then plays the role of a yield stress. When this preconsolidation pressure is reached in reloading, and the VCL is followed again, the preconsolidation pressure increases as a result of plastic (volumetric) strain hardening of the soil.

3.1.3 Shearing of the soil skeleton

The shear response of soils is traditionally investigated using simple shear, direct shear or standard triaxial tests, the last of which gives the most thorough information. Even more information can be obtained from true triaxial or hollow cylinder tests; however, such complex tests are usually only used by academia. In order to capture the behaviour of the soil skeleton drained shear tests should be performed, very slowly for clays because of their low permeability, while sands drain quite fast if saturated. In addition, information about the behaviour of the clay skeleton can be drawn from stress paths obtained from undrained triaxial tests (see below).

3.1.3.1 Contractant soils

Figure 3.2(a) shows two idealized shear curves, plotted in a $q - \varepsilon_q$ plane, for a normally or lightly over-consolidated soil, and corresponding to drained triaxial tests. Here $q = \sigma_1 - \sigma_3$ is the deviatoric stress (or second deviatoric stress invariant) and $\varepsilon_q = 2/3(\varepsilon_1 - \varepsilon_3)$ is the deviatoric strain (or second deviatoric strain invariant). One of the curves represents a soil sheared under a mean effective pressure p'_1 while the other curve is obtained for the very same soil sheared under a higher mean effective pressure $p'_2 > p'_1$ (**Figure 3.2(b)**). Hence, the deviatoric response of the soil skeleton depends on the effective mean pressure applied. The higher this pressure is, the stiffer the response and the higher the failure stress.

The shear curves in Figure 3.2(a) are highly non-linear from the very start of shearing, i.e. the shear stiffness reduces as the soil is sheared. For higher shear strains, this reduction weakens and, in the limit, the shear curve asymptotically approaches a limiting value of the

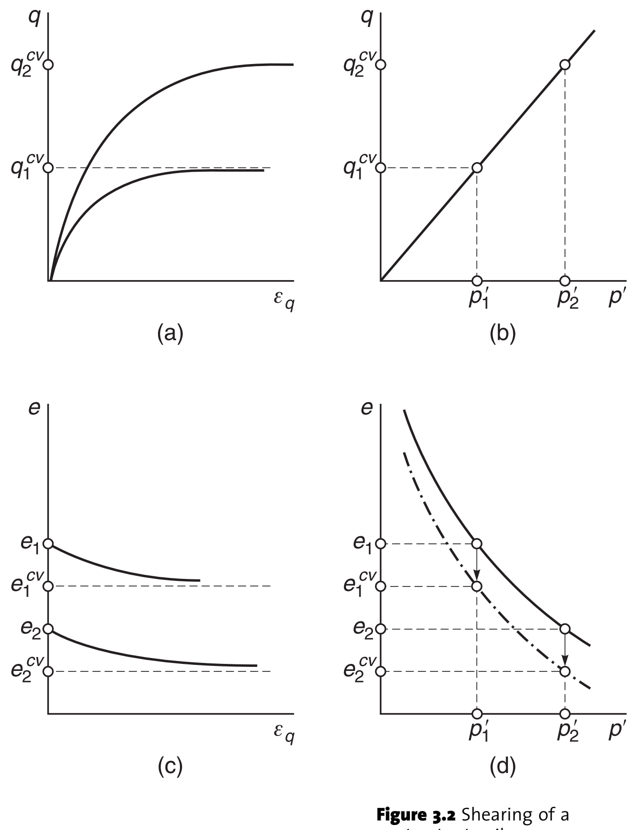

Figure 3.2 Shearing of a contractant soil

deviatoric stress, q_1^{cv} and q_2^{cv} respectively, corresponding to points on the failure line in the q–p' plot (Figure 3.2(b)). Furthermore, unloading, from some deviatoric stress level, would reveal irreversible strains and hence an elastic–plastic deviatoric response. In addition, if reloading takes place after such an unloading, the response is fairly elastic up to the stress level from which the unloading started. From this two conclusions can be drawn. Firstly, this stress plays the role of a deviatoric yield stress and, secondly, deviatoric strain hardening has taken place.

Another important feature, observed from drained shear tests on normally consolidated or lightly overconsolidated soils, is that shearing is accompanied by a volume decrease of the test sample, i.e. contractancy occurs (**Figure 3.2(c)**). For higher shear strains, this volume change reduces and the sample takes a constant volume at the same time as the deviatoric stress reaches its limiting value (see Figures 3.2(a) and 3.2(b). Hence, during the shearing that corresponds to the shear curve ($p' = p_1'$), the void ratio of the sample decreases from e_1 at the start of shearing to the limiting value e_1^{cv}, the so-called critical void ratio (Figure 3.2(c) and (d)). Tests show that these critical void ratios, e.g. e_1^{cv} and e_2^{cv}, together constitute the critical state line (CSL), which plots below the VCL, (**Figure 3.2(d)**). In an $e - \ln p'$ plot these two lines are observed to be parallel (**Figure 3.3**).

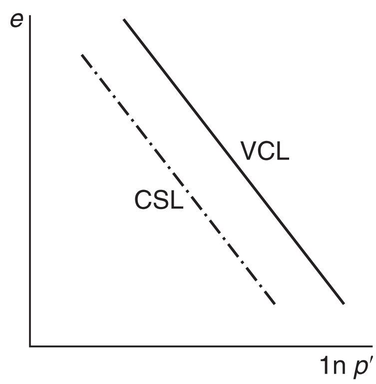

Figure 3.3 VCL and CSL lines

3.1.3.2 Dilatant soils

It is not only the mean effective pressure, acting on the test sample, that influences the drained shear response but also, to a large extent, the degree of preconsolidation. In **Figure 3.4** shearing of a heavily overconsolidated soil is schematically displayed. The soil has, during its history of loading, experienced a considerably higher mean effective pressure p_2' than the current one p_1' (Figure 3.4(d)). When sheared, a sample of such an overconsolidated soil initially displays a stiff response (Figure 3.4(a)). The behaviour in this phase is often considered as elastic, but not necessarily linear elastic. The high initial shear stiffness then gradually decreases and after a moderate shear strain the deviator stress generally reaches a peak value q_1^{max}, after which it decreases to a critical state value q_1^{cv}.

Shearing of a highly overconsolidated soil is in the initial phase generally accompanied by some contractancy, whereafter the volume of the sample starts to increase, i.e. it dilates (Figure 3.4(c)). In the limit, when the critical state stress q_1^{cv}, (Figure 3.4(a)), is approached, the rate of volume change reduces and the sample takes a constant volume, (Figure 3.4(c)), represented by the critical void ratio e_1^{cv}. This void ratio is the same as that reached in the limit when a

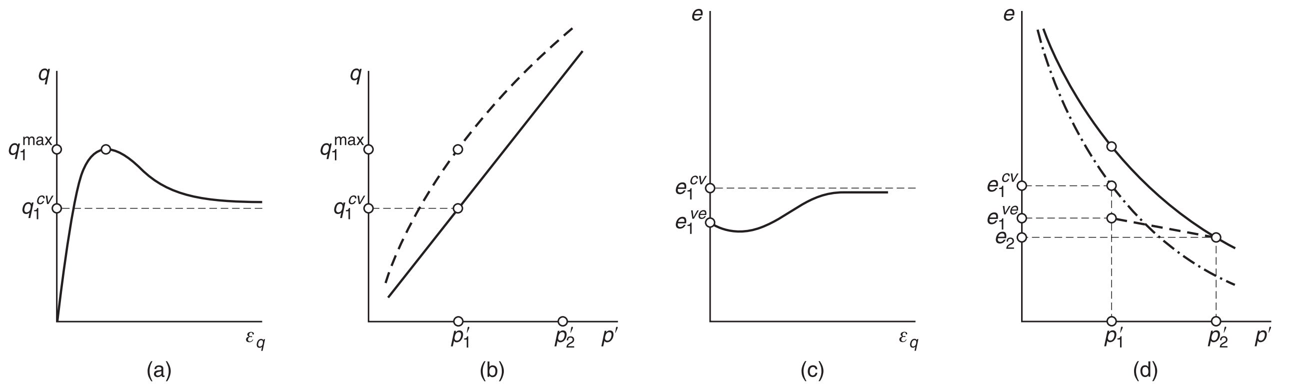

Figure 3.4 Shearing of dilatant soil

normally consolidated sample of the very same soil is sheared with the very same confining pressure p_1' (Figure 3.2(c)). Further, the critical state stress q_1^{cv} in Figure 3.4(a) equals the limiting deviator stress q_1^{cv} for the same soil and confining pressure in Figure 3.2(a); the dashed shear curve in Figure 3.4(a) is the same as that in Figure 3.2(a). Clearly, when approaching this limit state, the soil has forgotten its stress history.

If failure for the overconsolidated soil is based on critical state deviator stresses for different mean effective pressures, a failure line identical to that based on limit stresses for the same normally consolidated soil is obtained, the solid curve in Figure 3.4(b). However, if failure is based on peak values of the deviator stress, the dashed failure line in Figure 3.4(b) might be obtained.

3.1.3.3 Real soil behaviour: clays and sands

The above conceptual behaviour of the soil skeleton under compression and shearing is often taken as a basis for the qualitative design of constitutive soil models. Of course, real soil behaviour might differ from this general pattern to some degree. For example, sands, gravels, etc. have often been deposited under such conditions that they mainly display a dilatant behaviour. Tests on sands show that the so-called phase transformation point, where the initial contraction turns to dilation, depends on the degree of preconsolidation and thus on the density. Further, the critical state is not easily reached in either conventional testing equipment or in many practical problems, but only in tests performed in special high-pressure equipment.

Other attributes of real soil behaviour may also have to be considered in soil modelling, e.g. anisotropy and time dependence. Both clays and sands often display anisotropy, i.e. strength and stiffness depend not only on the magnitude but also on the orientation of applied stresses. With respect to stiffness, the soil might be cross-anisotropic (transversely isotropic) in both the elastic and plastic ranges. Due to their stress history, clays often display K_o-anisotropy which, however, tends to be wiped out by large shear strains. In some situations, it may be necessary to account for time dependence and creep in clays; e.g. when computing long-term settlements, the secondary (or creep) consolidation of clay should be accounted for.

3.1.4 Undrained behaviour of soils

Clays are generally saturated and their low permeability seldom leads to fully drained conditions. In the laboratory, drained clay tests are very time consuming and, therefore, considerable knowledge on clay behaviour has been gained from undrained tests. In addition, not only the fully drained behaviour of a soil but also its fully undrained behaviour can be modelled at the constitutive level, whereas partially drained conditions must be handled as a two-phase problem involving development of both effective stress and pore pressure.

In an undrained shear test, the effective stress path (ESP) in $p' - q$ stress space can reveal information on the soil properties. For contractant soils, the ESP bends to the left because of the pore pressure increase that is needed in the undrained case to eliminate the volume decrease of the soil skeleton (**Figure 3.5**). For large shear strains, the ESP approaches the CSL and undrained failure. For the same confining pressure the undrained failure stress is lower than the drained shear stress at failure.

For dilatant soils, on the other hand, the effective stress path generally bends to the right because of the pore pressure decrease needed to eliminate the volume increase of the soil skeleton (Figure 3.5). During the early stages of shearing, the effective stress path often starts to bend to the left, as a result of the contractancy during the first phase of shearing, after which it bends to the right. In the limit, the ESP approaches the CSL. In this case, the undrained failure stress is higher than the drained failure stress.

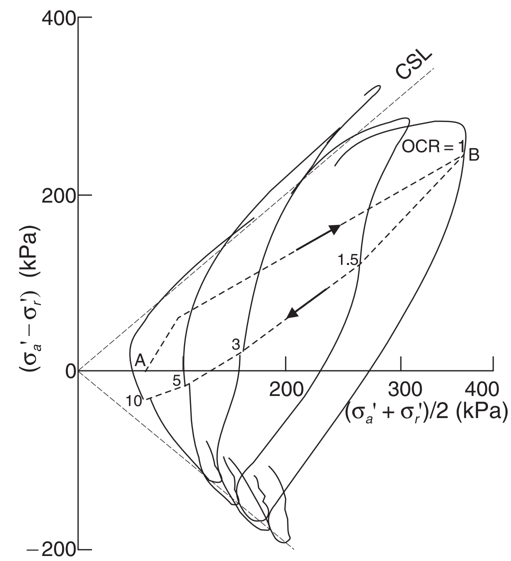

Figure 3.5 Undrained shearing of soils

3.2 Soil models

3.2.1 Introduction

Over the last four decades, constitutive soil models have undergone considerable improvement, in parallel with the development of numerical methods and with a mutual influence between them. The user of any of the commercially available finite element packages can choose between several soil constitutive models, which a few years ago were available only for researchers and specialists. The correct selection of a soil model is important, in order to avoid either a too simple model that does not consider the relevant features of the problem, or a too complex one, which could mask the main aspects of the solution and require the determination of obscure material properties.

A soil model must be sufficiently general and formulated independently of the problem considered as stress/strain paths cannot be estimated in advance. Stress level, porosity and other state variables can change dramatically as well during the calculation (consider for instance the zone beneath the edge of a spread foundation). A constitutive relation is represented by an equation describing the relationship between the stresses, strains and state variables (see *Section 2.4.5*). In geomechanics, incremental constitutive relations are generally used, which are formulated only for increments of the considered variables, since the non-conservative (dissipative, path-dependent) behaviour of soils and rocks does not usually enable the formulation of finite relationships. Only in exceptional cases can finite relations be defined, e.g. the semi-logarithmic compression law for clays.

Mechanical properties of soils and rocks are parameters of the constitutive models. Consequently, often used parameters like E (Young's modulus) or Φ (angle of shearing resistance) make sense only in relation to the corresponding constitutive models. These parameters should not change during the calculation and should not be problem-dependent because they must characterize the materials and thus be constants in the mathematical equations.

State variables (stress, porosity, orientation of grain contacts, degree of saturation, temperature, deformation rate, etc.), on the contrary, describe the actual state of the material and can change during the calculation over a wide (physically allowed) range. It should be possible to measure state variables directly (at least theoretically) at any moment in time. It is worth mentioning that the deformation, or strain, tensor is not a state variable for geomaterials since it cannot be measured. It is only possible to determine strain increments related to the known initial state. In the initial state, consider for example, a laboratory specimen before testing, the deformation tensor has no meaning and can be chosen arbitrarily.

3.2.2 First generation of constitutive models

3.2.2.1 Deformation and limit state analysis

The first generation of soil models covers the long period between the work of Coulomb in 1773 and the rise and development of computers and finite element methods in 1960–70. From a practical point of view, the objectives of conventional geotechnical analyses were (i) the ground deformation (mainly the vertical settlements) under the design loads, and (ii) the value of the load leading to failure. The available calculation methods were based on analytical solutions, requiring a considerable simplification of geometrical and mechanical boundary conditions. This led to the separation of the two analyses: a model of (linear) elasticity was applied for the service conditions and a rigid–plastic one for the limit equilibrium analyses.

3.2.2.2 Elasticity models

3.2.2.2.1 Linear elasticity

In the *linear isotropic elasticity model* by Hooke the material is characterized by just two parameters, Young's modulus E' and the Poisson ratio μ', or preferably, for a soil skeleton, the bulk modulus K' and the shear modulus G. Because of its simplicity it has been widely applied in conventional soil mechanics where boundary value problems had to be solved analytically. It was also used as a soil model in the early years of the finite element method. However, linear isotropic elastic models do not reproduce any of the important features of real soil behaviour. By selecting appropriate values of the two elasticity parameters it is sometimes possible to capture one feature but to fail in predicting the others. For instance, in a numerical simulation of tunnel construction one can obtain the correct maximum settlement of the surface but the wrong settlement distribution with depth (Dolezalová *et al*., 1998).

For an isotropic material the stress state can be described by three (independent) stress invariants, e.g. the three principal stresses, or, more conveniently for soils, the mean effective pressure p' (or first stress invariant), the second deviatoric stress invariant J and the Lode's angle θ:

$$p = \frac{\sigma_1' + \sigma_2' + \sigma_3'}{3} \tag{3.1}$$

$$J = \frac{1}{\sqrt{6}} \sqrt{(\sigma_1' - \sigma_2')^2 + (\sigma_1' - \sigma_3')^2 + (\sigma_2' - \sigma_3')^2} \tag{3.2}$$

$$\theta = \tan^{-1}\left[\frac{1}{\sqrt{3}}\left(2\frac{(\sigma_2' - \sigma_3')}{(\sigma_1' - \sigma_3')} - 1\right)\right] \tag{3.3}$$

Linear elasticity can suffice in deformation problems provided the range of stresses and strains is very small (e.g. for some problems in soil dynamics), or in determination of the approximate distribution of vertical stresses under foundations (Hoeg *et al.*, 1968; Nuebel *et al.*, 1999). It can also be useful for an initial rough estimate of solutions and for calibration of numerical methods and codes where analytical solutions are available.

Extension to a *linear anisotropic elasticity model* does not really improve the situation. For soils the transversely anisotropic elastic model has gained some interest, as it can capture the different stiffness properties of isotropic (horizontal) planes of deposition and of the planes in the (vertical) direction of deposition, as would be the case for layered soils. This model requires five independent parameters and the stress state is characterized by six independent stress variables.

3.2.2.2.2 Non-linear elasticity

A model involving *non-linear elasticity* is a substantial improvement over the linear one. With this model, for example, the non-linear relation between the shear (or deviator) stress and the shear (or deviator) strain can be captured. A widely used model of this type is the hyperbolic one (Kondner, 1963), in which the shear modulus decreases from an initial value G_0 to a zero value at failure (**Figure 3.6(a)**). Such a shear response corresponds well to the shear curve obtained for normally consolidated clays and loose sands. This model was implemented into a finite element code for the first time by Duncan and Chang (1970). The hyperbolic model requires two parameters (**Figure 3.6(b)**), which can be determined from experimental results. Recently, non-linear elastic constitutive models have been developed to describe stiffness

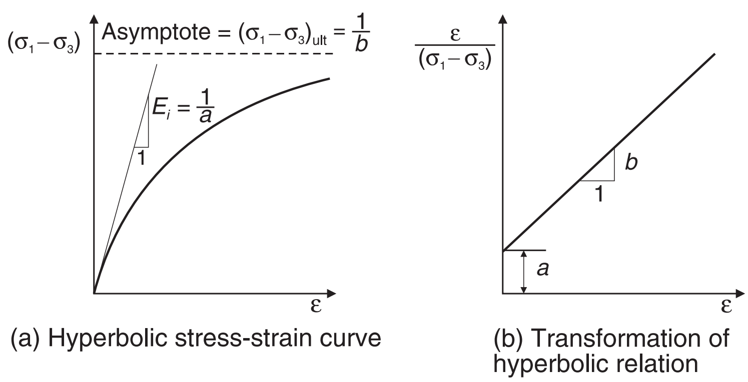

Figure 3.6 Hyperbolic model

changes in the range of small strains (Jardine *et al.*, 1986). Using such models, the deformation behaviour of deep excavations and tunnels can be more accurately predicted.

The hyperbolic model for shear behaviour must, of course, be supplemented by a model for compression behaviour. These two models are often formulated independently; i.e., the shear and compression responses are decoupled from each other. It is then not unusual to combine a non-linear elastic model for shear behaviour with a linear elastic model for compression behaviour, which is governed by a constant bulk modulus.

A further improvement is obtained by using the *K–G* model where the tangent bulk modulus is assumed to be a linear function of mean effective pressure (Naylor *et al.*, 1981):

$$K_t = K_o + \alpha_K p' \quad (3.4)$$

and where the tangent shear modulus is expressed as

$$G_t = G_o + \alpha_G p' + \beta_G J \quad (3.5)$$

implying compression and shear curves according to **Figure 3.7**. In this model, not only are these response curves realistically modelled, but the dependence of the shear modulus on the mean effective pressure is also accounted for. As seen from the above equations, the *K–G* model requires five independent parameters.

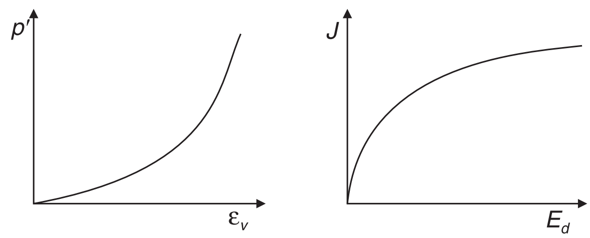

Figure 3.7 K–G model

A typical example of elastic non-linear compression is the Terzaghi equation for the semi-logarithmic compressibility (VCL) which yields the tangent elastic compression modulus $M = d\sigma'_v/d\varepsilon_v$ proportional to the vertical effective stress σ'_v. A more general non-linear elasticity model for vertical compression was proposed by Ohde (1939), $M = M_o(\sigma'_v/\sigma'_{vo})^\alpha$ (sometimes wrongly attributed to Janbu (1963)).

Non-linear–elastic models can simulate well monotonic curves of experimentally measured stress–strain relations for specific loading paths (triaxial, oedometric). However, their extrapolation beyond the calibration curves is practically impossible. These models are mostly focused on a single feature of the soil behaviour (stress–strain curve) and do not take into account other important aspects (stress paths dependence, volume change during shear, etc.). They also share many of the disadvantages of linear elastic models (e.g. no hysteretic behaviour during cyclic loading) and, in contrast to linear elastic models, they lack a sound theoretical background.

3.2.2.2.3 Perfect plasticity and failure

In comparison with elastic models, the framework of the theory of plasticity represents a distinct qualitative step forward. It limits the allowed stress range and enables dilatancy, and to a certain degree hysteretic behaviour, to be captured.

In a *perfect plasticity model*, where plastic yield coincides with the failure condition, a yield condition is defined which does not change as a result of plastic straining (no hardening or softening). Within the corresponding fixed yield surface in stress space the behaviour is elastic, whereas on this yield surface it is perfectly plastic. In conventional soil mechanics many solutions are based on limit analysis/limit equilibrium and perfect plasticity concepts, e.g. slope stability, earth pressure distribution and bearing capacity problems.

The oldest failure criterion, for materials in general, is the *Mohr–Coulomb criterion*, based on the failure line defined by Coulomb (1776) and the stress circle representation by Mohr (1882). Failure, or perfectly plastic yielding, is governed by the cohesion c' and the angle of shearing resistance ϕ'. Most failure computations in conventional soil mechanics are based on the Mohr–Coulomb criterion, examples being bearing capacity and earth pressure.

In 3D principal stress space the Mohr–Coulomb failure/yield criterion is represented by a hexagonal cone, **Figure 3.8(a)**. When extending this criterion to become a complete constitutive model, formulated within the framework of the theory of perfect plasticity, the Mohr–Coulomb yield cone has to be accompanied by a flow rule (or plastic potential) governing the increments of plastic strains. It should be noted here that an associated flow rule, where the yield function is taken as the plastic potential function, leads to excessive dilatancy for soils. Within the yield cone, an isotropic linear elasticity model is normally assumed. Such an elastic–perfectly plastic constitutive model thus requires four parameters, two strength parameters defining the yield cone and two elastic parameters.

For numerical implementation a drawback of the Mohr–Coulomb model is the corners on the hexagonal yield cone. To avoid this problem Drucker and Prager (1952) proposed a circular yield cone, **Figure 3.8(b)**, which can be regarded as an extension of the Mises criterion (as the Mohr–Coulomb criterion can be regarded as an extension of the Tresca criterion).

In spite of the common opinion that the angle of shearing resistance ϕ' and the cohesion c' are standard parameters of soils and rocks, one must realize that these two parameters are linked to the Mohr–Coulomb failure criterion. This criterion is only one of many failure (yield) conditions. Besides the Drucker–Prager condition, which is very popular for programming but very unsuitable for the description of real soil behaviour, there exist failure conditions derived

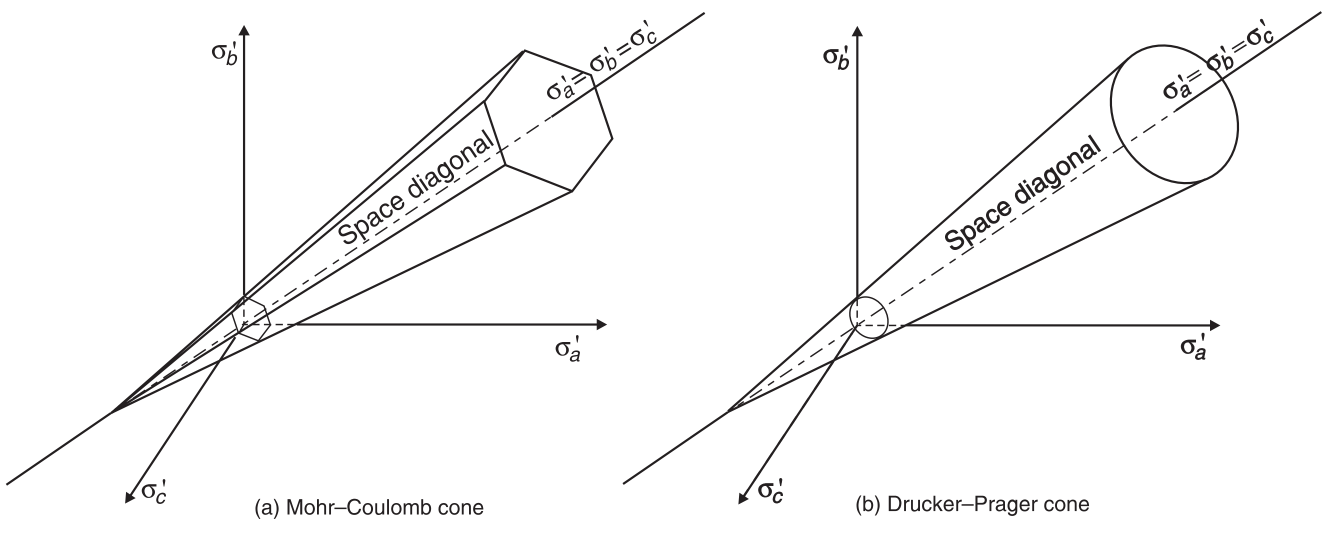

Figure 3.8 Perfectly plastic yield surfaces

from experimental results in true triaxial apparatuses, e.g. Lade and Duncan (1973), or Matsuoka and Nakai (1977).

In combination with linear elasticity, perfect plasticity still represents the most widely used constitutive framework for geomaterials. However, such a fact does not imply anything about its suitability. One can find many drawbacks of the framework: for example, it does not take into account the history of deformation. Consequently, it is not possible to distinguish between 'primary loading', 'unloading' or 'reloading' inside the failure surface. As a result, the calculated heave of the bottom of an excavation or tunnel can be unrealistically high. The elastic behaviour can be contractant only, whereas the volume increase due to dilatancy during plastic shearing is unlimited. Compressive stresses inside the open yield cone remain elastic and thus cause an infinite compression of the material, and so on.

Notwithstanding the limitations of the elastic–perfectly plastic model, there still remain many appropriate geotechnical applications for it, especially if the model is enhanced with non-linear elasticity. In particular, problems with monotonic stress/strain paths leading to the limit stress states, like embankment calculations, can be sufficiently well captured by the model.

3.2.3 Second generation of constitutive models

3.2.3.1 An early cone-cap model

In order to avoid some of the above-mentioned drawbacks of the perfectly plastic model, especially the unbounded elastic compressive strain, Drucker *et al*. (1957) closed the fixed Drucker–Prager yield cone with a movable yield cap, **Figure 3.9(a)**, and thus introduced volumetric plastic strain hardening into the model. The strain hardening, and thus the movement of the yield cap, is governed by the volumetric plastic strain. Hence, in addition to the four model parameters in the elastic–perfectly plastic model, a volumetric hardening parameter is required. For stresses on the yield cap associated plasticity was assumed, i.e. the yield cap was also taken as the plastic potential. With this cone-cap model it was thus possible to capture irreversible volumetric and deviatoric plastic strains and it became possible to distinguish between primary loading and reloading (for stresses on the cap).

3.2.3.2 Critical state models

At about the same time as the development of the cone-cap model, Roscoe *et al*. (1958) introduced the concept of critical state into soil mechanics and Calladine (1963) advocated hardening plasticity to be a proper framework for soil modelling. The Cam clay model, based on the critical state concept, was presented by Roscoe and Schofield (1963) and Schofield and Wroth (1968), and the modified Cam clay model by Roscoe and Burland (1968). In the latter, an elliptical yield locus is assumed in the p'–J plane **Figure 3.9(b)**, together with an associated flow rule and isotropic hardening/softening. The actual size of the yield surface is determined by a scalar internal variable which represents the 'memory' of the material and evolves as a function of the accumulated plastic volumetric strain. Except for modifications to its size, the yield surface keeps its shape and orientation in principal stress space.

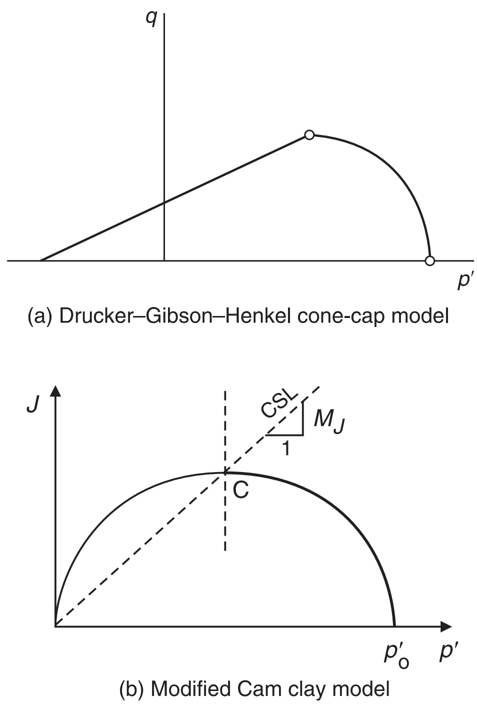

Figure 3.9 Soil yield criteria

The Cam clay models are able to simulate both consolidation and shearing of soils. The models require five parameters of which three (v_1, κ, λ) are consolidation parameters, one (M_J or ϕ'_{cs}) is a drained strength parameter and one (G or μ) is an elastic parameter. Here, λ denotes the inclination of the straight virgin consolidation line, κ the inclination of the likewise straight swelling lines in the v–ln p' plane (**Figure 3.10**) and v_1 the specific volume for ln $p' = 1$ (note specific volume $v = 1 + e$). Further, M_J is the inclination of the critical state line in the p'–J plane (Figure 3.9(b)), corresponding to the angle of shearing resistance ϕ'_{cs} at the critical state.

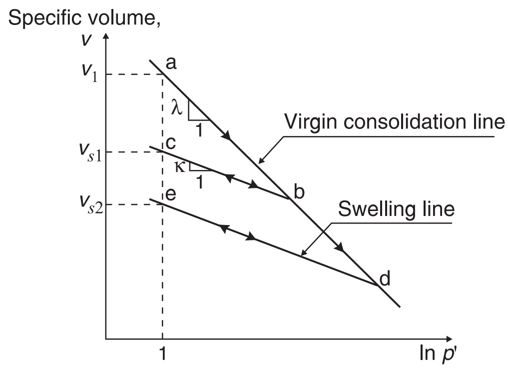

Figure 3.10 Cam clay under isotropic compression

It should be noted that the undrained shear strength S_u does not appear as a model parameter. However, it is possible to express S_u in terms of the above model parameters and the initial stress conditions of the soil (see Potts and Zdravkovic, 1999). Further, the Cam clay models are formulated in triaxial stress space. Extension of the models to general stress space, a necessity for finite element analyses, has been done in many different ways, but unfortunately not always very well documented.

The Cam clay models have achieved a high popularity due to both their logical theoretical structure and their good predictive capabilities. **Figure 3.11(a)** shows drained triaxial tests and **Figure 3.11(b)** undrained triaxial tests as predicted by modified Cam clay (after Potts and Zdravkovic, 1999).

3.2.3.3 Cone-cap models

A number of modifications to the original Cam clay models have been proposed throughout the years, many of them still based on the critical state concept. A drawback of the Cam clay models is that the supercritical yield surface (dry side) significantly overestimates peak failure stresses. In an early computational application of the modified Cam clay model, Zienkiewicz and Naylor (1973) exchanged the Cam clay surface in the supercritical region with the failure surface of Hvorslev (1937) (**Figure 3.12(a)**). However, to avoid excessive dilatancy, as well as an inconsistency at the critical state point, they used a non-associated flow rule with dilatancy increasing from zero at the critical state to some fixed value at $p' = 0$. In similar models the supercritical Cam clay surface has been used as a plastic potential in combination with the Hvorslev surface.

Instead of the Hvorslev surface, Di Maggio and Sandler (1971) and Sandler *et al.* (1976) used a fixed curved surface in the supercritical region, closed with a cap surface which was allowed to move as a function of the volumetric plastic strain (**Figure 3.12(b)**). Hence, this model can predict

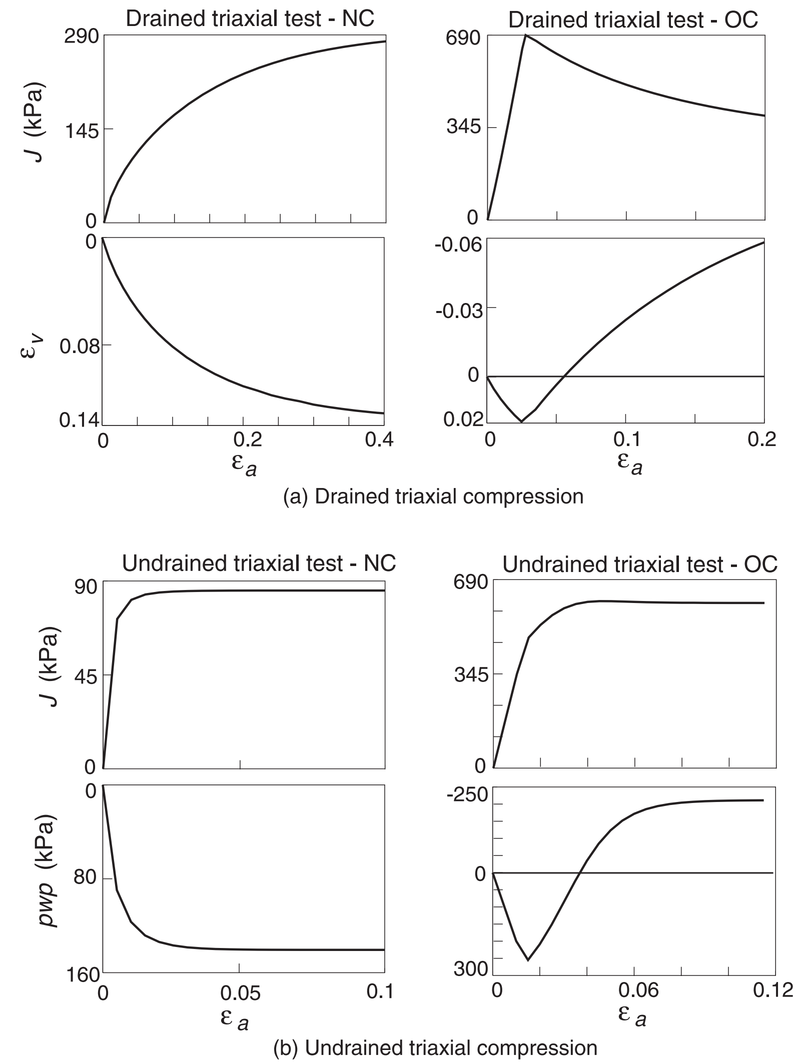

Figure 3.11 Triaxial compression tests with modified Cam clay model

hardening for normally consolidated and slightly overconsolidated soils, but no softening for heavily overconsolidated soils. This model and similar ones have been applied in a number of numerical analyses.

3.2.3.4 K_o consolidated soils

In situ-consolidated clays normally display so-called K_o (i.e. $\sigma'_h = K_o\ \sigma'_v$) anisotropy. However, the formulation of the basic Cam clay models was based on results from triaxial tests on isotropically consolidated samples. To capture this anisotropy, the Cam clay yield ellipse can be 'rotated' and centred on the K_o line in the p'–J plane instead of on the p'-axis (**Figure 3.13(a)**). A model of this type is the MELANIE model proposed by Mouratides and Magnan (1983), based on extensive experimental tests on Canadian soft clays at the University of Laval (Tavenas, 1981). This model uses a non-associated flow rule, with strain increment vectors D_i as shown in Figure 3.13(a). Other similar models have been proposed by Ohta and Wroth (1976) and Sekiguchi and Ohta (1977) (**Figure 3.13(b)**). For describing the MELANIE model an anisotropy parameter as well as a dilatancy parameter are needed, in addition to those governing the Cam clay models. Magnan *et al*. (1982) reported a numerical comparison between analyses of an embankment on soft clay using the MELANIE and Cam clay models. Predictions were compared with field measurements. This comparison proved to be inconclusive and did not indicate any superior performance of the anisotropic model.

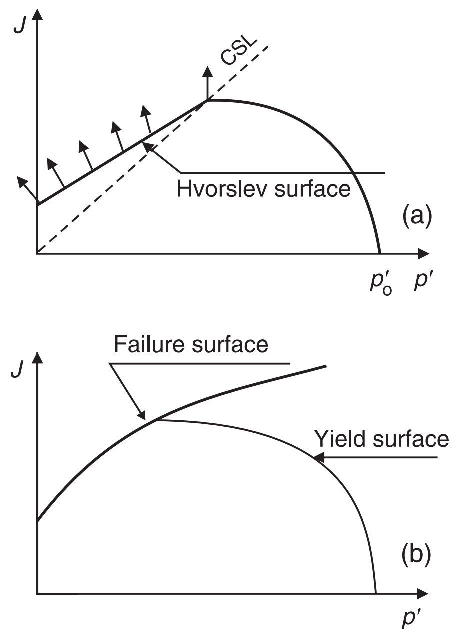

Figure 3.12 Modifications of the Cam clay supercritical surface: (a) Hvorslev surface; (b) cone-cap model

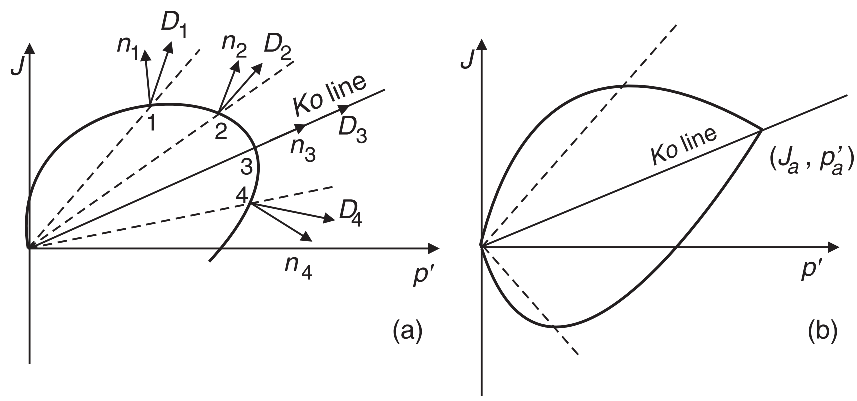

Figure 3.13 Yield surfaces for K_o consolidated soils: (a) MELANIE model; (b) Sekiguchi–Ohta model

3.2.3.5 Associated versus non-associated plasticity

One can distinguish between plasticity models with an associated flow rule and those with a non-associated flow rule, where the yield surface is different from the plastic potential surface. The models of the first group have a simpler mathematical structure, with a lower number of material parameters, and they benefit from some theoretical properties (e.g. they obey the postulates of uniqueness and stability). Unfortunately, their applications for soils and rocks are limited to soft clays and loose sands, i.e. to contractant geomaterials. If used for overconsolidated clays or dense sands, the calculated dilatancy is often too high, as for example in the Mohr–Coulomb model where the angle of shearing resistance must correspond to the dilatancy angle. Moreover, even in the case of soft soils there are serious limitations for applications of associated plasticity. For instance, it is not possible to obtain the softening branch of a stress–strain curve during undrained shearing, which is important in the modelling of static liquefaction (Nova, 1989).

3.2.4 Third generation of constitutive models

3.2.4.1 Extended hardening concepts

The second generation of soil models referred to above, formulated within the framework of isotropic hardening/softening elasto-plasticity and generally based on the concept of a critical state, can accurately reproduce a number of facets of real soil behaviour such as yield phenomena, irreversible behaviour and shear-induced contractancy/dilatancy. Nevertheless, monotonic deformation processes with relatively large displacements remain as the optimum application range for this class of plasticity models. It is not possible to make realistic predictions of cyclic behaviour, sharp changes of stress/strain paths or even rotation of principal stress axes. Particular formulations suffer from additional problems, like a too stiff response in undrained simulations, or an overestimation of values of the earth pressure at rest (Pande and Pietruszczak, 1986).

3.2.4.1.1 Combined hardening

The size of the yield surface of the models belonging to the second generation is determined by an isotropic hardening/softening rule with a scalar hardening parameter based only on the size of the plastic volumetric strain. In a first step to extending such models, the plastic shear strains are allowed to influence the change of size of the yield surface. Hence, in the rule of combined hardening, the scalar hardening parameter, governing the isotropic hardening/softening, is taken as a function of both plastic volumetric and shear strains (Nova and Wood, 1979).

3.2.4.1.2 Double hardening

Triaxial tests on sands of different densities indicate the existence of shear yield surfaces (Stroud, 1971; Tatsuoka and Ishihara, 1974). A shear yield surface is a cone-like surface which hardens or softens as a function only of the plastic shear strain (represented for example by the deviatoric invariant of the plastic strain tensor, **Figure 3.14(a)**). On the basis of this observation, soil models have been developed with two active yield surfaces: a conical shear yield surface,

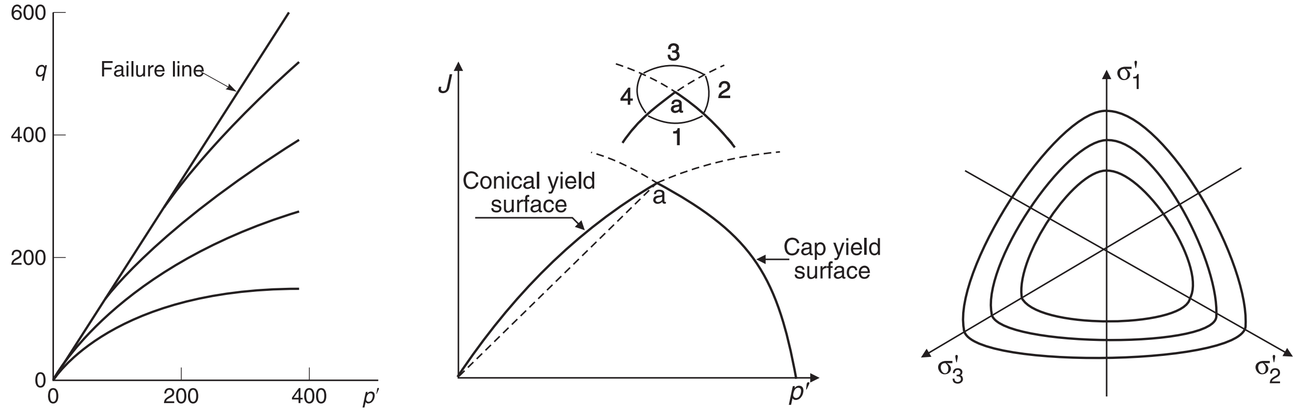

(a) Shear yield surface (b) Two active yield surfaces (c) Yield surface in deviatoric plane

Figure 3.14 Shear yield surface and double hardening

moving as a function only of the plastic shear strain, and a cap yield surface moving as a function only of the plastic volumetric strain (**Figure 3.14(b)**).

Double hardening was first proposed by Prevost and Hoeg (1975) and somewhat later by Lade (1977) as a modification of an earlier proposed model for sand (Lade and Duncan, 1975). A similar model with two active yield surfaces and double hardening has been proposed by Vermeer (1982). Both the Lade model and the Vermeer model account for the third stress invariant having a yield locus in the deviatoric plane of the form shown in **Figure 3.14(c)**, and both models are appropriate for simulating granular soils. In the Lade model a conical failure surface defines the limit of yielding (Figure 3.14(b)). This model is governed by 14 parameters, three of which control the non-linear elastic response and the others the plastic strains as well as shear and volume hardening. These model parameters can be determined from standard laboratory tests, although the model is applicable to general stress states.

3.2.4.1.3 Kinematic hardening

The soil models referred to above can simulate soils under radial loading and unloading, in compression as well as in shear. However, in order to capture non-recoverable behaviour and memory effects of soils under non-radial loading, e.g. cyclic loading, these models have to be extended by using the kinematic hardening concept; i.e., plastic hardening is associated with a pure translation of the yield surface. In this way the Bauschínger effect on load reversal, first observed for metals, can be simulated.

Kinematic hardening imposes some mathematical complexities on the formulation of soil models. The kinematics of yield surfaces must be formulated using evolution equations of tensorial internal state variables, and the permissible mutual positions of yield surfaces are constrained by several conditions. Kinematic hardening is often combined with isotropic hardening thus allowing also for changes of the size of the yield surface. In such a model a tensorial variable controls the position of the yield surface and a scalar variable the size.

3.2.4.2 Bounding surface plasticity

A conventional yield surface separates elastic behaviour (for stress states within the yield surface) from elasto-plastic behaviour (for stress states on the yield surface). Hence, for stress paths within the yield surface only recoverable strains occur. However, real soils often exhibit non-recoverable behaviour on unloading and reloading. The soil models of the second generation thus display limitations when applied, for example, to cyclic loading problems of medium to high amplitude (typically for strains greater than 10^{-4} to 10^{-3}). Such a model will produce, at best, a non-linear closed hysteresis loop that is repeated again and again, because the unloading branches are always elastic.

In **Figure 3.15** the classical liquefaction tests by Castro (1969) on loose sand are shown. The first cycle is well reproduced by any model of the second generation type, because the undrained

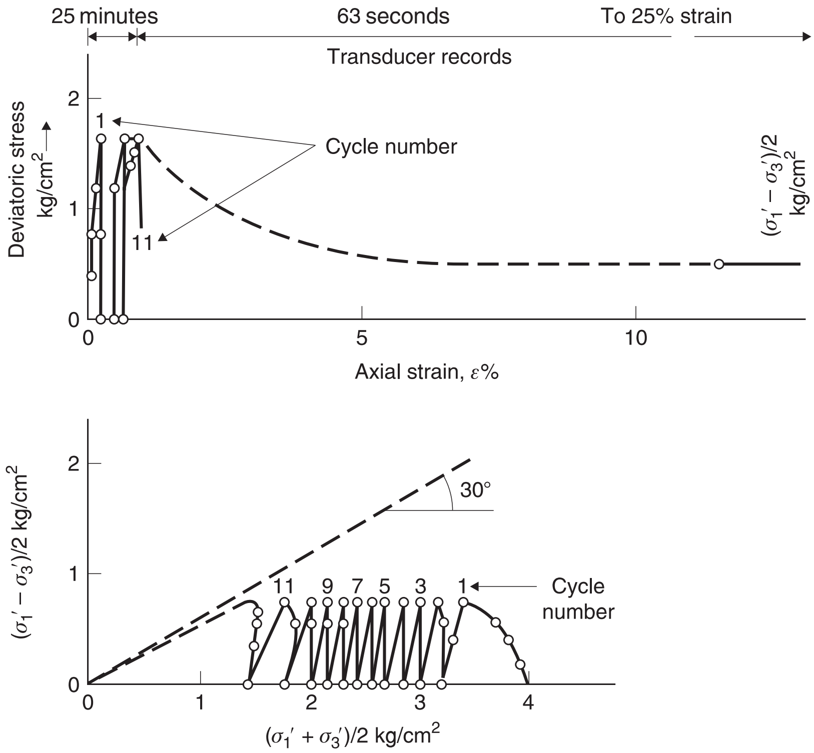

Figure 3.15 Liquefaction of a loose sand under undrained cyclic loading

loading stress path follows closely the yield surface of a modified Cam clay type. However, after the first cycle, the rest of the soil response will be elastic, and the stress path will not go to the left of point 1. None of these models can therefore reproduce the pore pressure build-up, accumulating for increasing number of cycles and leading eventually to liquefaction.

Several attempts have been made in the last 20 years to overcome this limitation. The general basic idea is to consider the yield surface associated with the preconsolidation pressure as a bounding surface, subjected to isotropic hardening, inside which there are irrecoverable strains (of smaller magnitude than those developed at the outer bounding surface).

3.2.4.3 Multi-surface models

The multi-surface model, first proposed by Mroz (1967) for metals and later extended to soils (Mroz and Norris, 1982), considers a finite number of intermediate nested yield surfaces that are progressively activated as the stress path touches each of them (**Figure 3.16**). The innermost surface encloses the true elastic domain. All the surfaces are dragged by the stress point (kinematic hardening) along its path. Special algorithms must be applied in order that the surfaces are tangent at their contacts and do not intersect each other. When the stress path reaches the outer surface, this can expand or shrink as in the classical critical state type models.

With such a multi-surface concept, the gradual transition from an initially fully elastic state to a fully plastic state in the limit can be modelled. However, a large number of parameters is needed to define all the yield surfaces and their movements. In order to reduce the number of model parameters but still be able to capture essential features of cyclic loading plasticity, two-surface models have been developed, termed bounding surface models.

3.2.4.4 Bounding surface models

In the bounding surface model (Dafalias, 1975; Krieg, 1975; Dafalias and Popov, 1975), an inner initial yield surface is surrounded by a bounding surface representing full plastic flow (**Figure 3.17**). The bounding surface resembles many features of a conventional yield surface, but plastic straining is allowed within this surface while the inner yield surface defines the limit of the elastic region. During loading into the plastic range, the initial inner yield surface expands by some law of isotropic or combined isotropic and kinematic hardening.

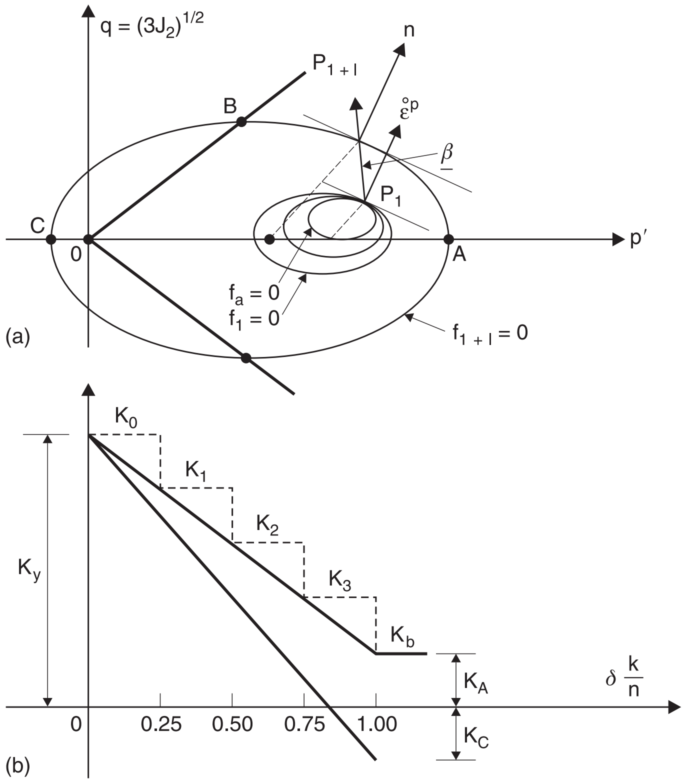

Figure 3.16 Multi-surface model

A mapping rule is used for the plastic strains in terms of the ratio of the distances from the origin to the current stress point and the conjugate or 'image' point on the outer bounding surface (Figure 3.17). Thus plastic strains vary from zero at the origin to full plastic flow at the bounding surface. With respect to the multi-surface models, this reduces considerably the number of parameters involved and simplifies the algorithms. In turn, the flexibility of the model to reproduce the actual soil behaviour is lost to some extent.

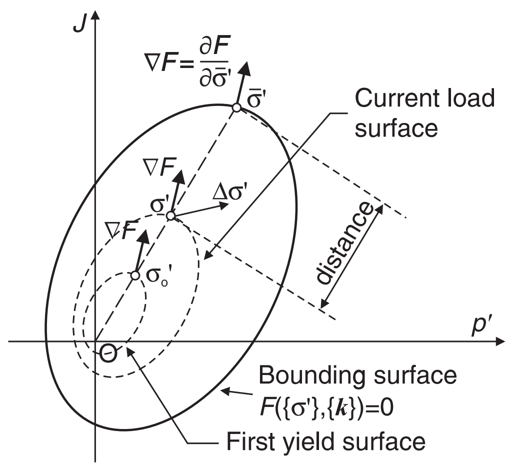

Figure 3.17 Bounding surface model

As an example of a well-established bounding surface model, the *MIT-E3 model* (Whittle, 1987, 1991, 1993; Hashash, 1992) is noteworthy. This model is loosely based on modified Cam clay but extended to, among other things, small-strain non-linear hysteretic elasticity, an anisotropic yield surface and bounding surface plasticity (**Figure 3.18(a)**). In the elastic range, the model uses a non-linear bulk modulus but a constant Poisson's ratio. The advanced form of the bulk modulus *K* expresses hysteric elasticity so that the non-linear nature of over-consolidated soils in an unload–reload cycle can be simulated (**Figure 3.18(b)**). The bounding surface is an anisotropic form of the modified Cam clay yield ellipsoid and is formulated in general stress space to be able to reproduce anisotropic soil behaviour. A hardening law controls not only the size of the bounding surface but also its orientation, i.e. the inclination of its principal axis. This enables simulation of a fading anisotropy observed for anisotropic soils under large straining. The bounding surface is combined with a critical state cone (**Figure 3.19**), and a non-associated flow rule enables the model to reach a critical state at this cone. Stress states inside the bounding surface represent over-consolidation; however, plastic states are allowed also inside this surface. A first yield surface defines the elastic limit. During loading, this surface expands as a loading surface (see Figure 3.17).

The MIT-E3 model is thus able to simulate most of the typical features displayed by soils under general loading. This, however, makes the model quite complex, with the associated difficulties

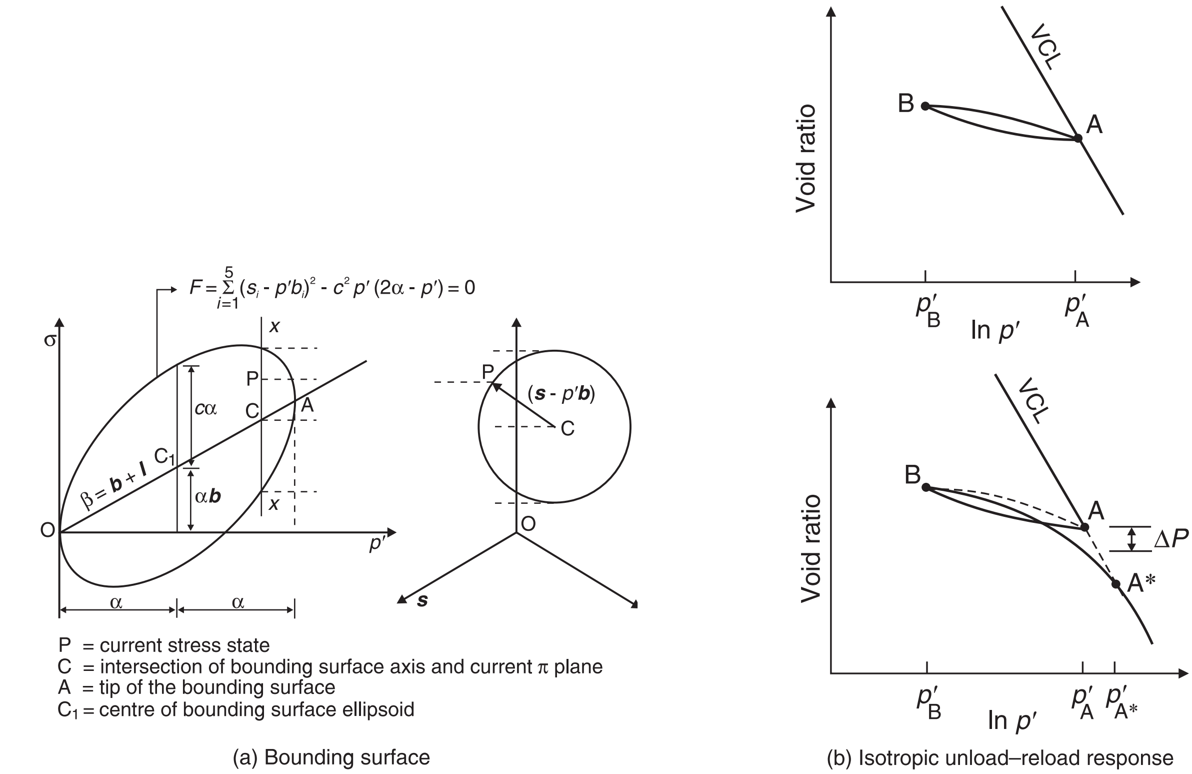

Figure 3.18 MIT-E3 model

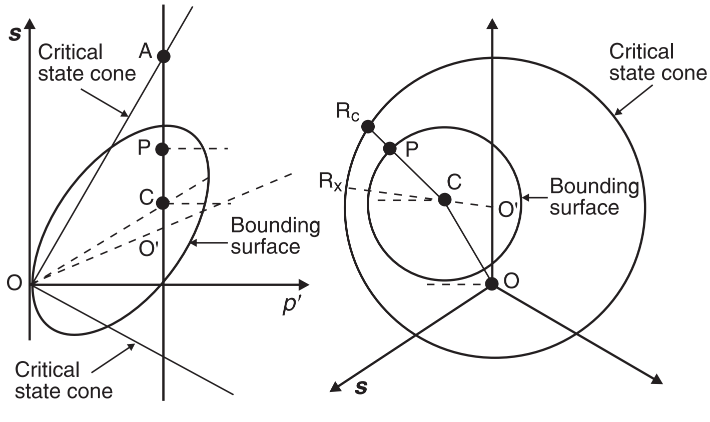

O' = intersection of axis of critical state cone and current π plane
R_c = the projection of vector CP onto the critical state cone
R_x = the projection of vector O'C onto the critical state cone

Figure 3.19 MIT-E3 bounding surface and the critical state cone

of evaluating all of its 15 model parameters. A thorough discussion of the MIT-3 model can be found in Ganendra (1993) and Ganendra and Potts (1995).

3.2.4.5 Bubble models

The bubble model can be considered as a further development of the bounding surface model. Although the latter is quite efficient in capturing soil behaviour, it still has some deficiencies with regard to cyclic loading and hysteretic soil behaviour within the bounding surface; during unloading the soil is assumed to behave elastically, whereas real soils display a narrow elastic range before reversed plastic yielding is reached. To this end Al-Tabbaa (1987) and Al-Tabbaa and Wood (1989) introduced a small kinematic yield surface, called the bubble, inside the bounding surface (**Figure 3.20**). Elastic behaviour is defined only inside this bubble, the movement of which is governed by a kinematic hardening law as it is dragged by the stress point. For the sizes of the kinematic yield surface and the bounding surface, a scaling law is applied.

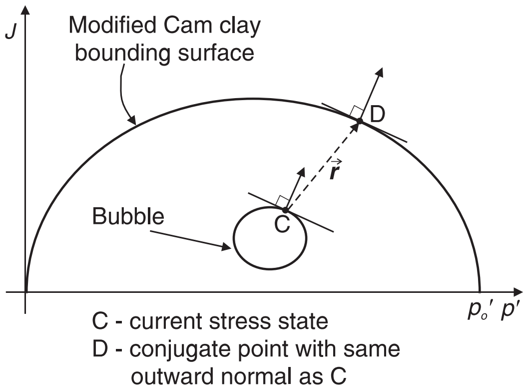

Figure 3.20 Bubble model

The bubble model of Al-Tabbaa and Wood was developed for triaxial stress space and requires just seven input parameters. It has been extended to general stress space by Stallebrass and Taylor (1997) who also introduced a second bubble (the history surface), nested outside the first one. The inner bubble defines stress states representing true linear elastic behaviour, whereas stress states in the zone between the inner and outer bubble and the outer bubble and the bounding surface produce elasto-plastic behaviour. Similar models are presented by Puzrin and Burland (1998), Kavvadas and Amorosi (2000) and Rouainia and Muir Wood (2000).

3.2.4.6 The use of advanced models

By using advanced constitutive models, such as bounding surface models and bubble models, it is theoretically possible to describe numerous phenomena observed in sophisticated experiments on geometarials, e.g. cyclic loading behaviour, anisotropy. However, it is questionable whether several different phenomena can be captured simultaneously by one and the same model. It is often the case that improvement of one effect spoils another one. In any case, these models become quite complex and, therefore, have limited practical application.

Since the internal structure of soils and rocks is modelled by geometrical transformations of yield surfaces, the actual sizes of yield surfaces and their positions and orientations in stress space represent the state variables of the material under consideration. Although the state variables should be (at least theoretically) measurable and interpretable, this is rarely the case. Consequently, application of such models for practical problems is extremely difficult because of troubles in determining the initial state. The identification of material parameters can be problematic as well, if the number of parameters is very high and special experiments are required.

3.2.5 Alternative frameworks for soil models

There is a number of constitutive models for soils and rocks which remain on the boundary of the plasticity framework or even outside of it. They are often based on rational continuum mechanics (Truesdell and Noll, 1965) and the laws of thermodynamics. As an example, one can consider endochronic models (Valanis, 1971, 1982; Bazant, 1978). They include a monotonically increasing internal variable, called intrinsic time, which traces the deformation history and controls the calculation of strains.

Hypoplastic models represent a novel approach. They do not split strains into their elastic and plastic parts, which makes it possible to obtain an elegant and relatively simple mathematical formulation (Wu and Bauer, 1994; Chambon *et al*., 1994; Kolymbas *et al*., 1995; Gudehus, 1996; Nieminis and Herle, 1997).

Another example of a non-traditional approach to constitutive modelling is the multilaminate model (Pande and Sharma, 1983; Pietruszczak and Pande, 1987). It assumes a finite number of slip surfaces inside the material. Considering a simple elasto–perfectly plastic model on these surfaces, the resulting deformation is obtained from displacements of the quasi-blocks.

A novel approach to constitutive modelling is the disturbed state concept of Desai (1999). This essentially uses two models, one for the intact material and one for the fully reconstituted material. The degradation of the soil from one state to the other is controlled by algorithms that are dependent on the degree of disturbance. In principle, the two models can be based on any of the frameworks discussed above, but usually they are based on strain hardening/softening plasticity.

Determination of material parameters

4.1 Direct determination of physical parameters

4.1.1 Types of soil parameters

Material parameters (physical parameters) of a soil constitute some or all of the *model parameters* in the constitutive models used for capturing the behaviour of the same soil. These material parameters express the properties of the soil and have a constant value for a particular soil. Examples of such material parameters are the Poisson ratio μ, the angle of shearing resistance at the critical state, φ'_{cs} (or M), and the inclinations of the virgin consolidation line (VCL), λ, and the swelling lines, κ. These parameters should not change during the calculation and they should not be problem dependent because they must characterize the soils and, thus, they are constants in any mathematical equations.

Material parameters are of two main types, parameters characterizing the stiffness of the soil and parameters characterizing its strength. The above-mentioned parameters λ and κ belong to the former group which also includes parameters obtained from one-dimensional compression tests, e.g. the gradients C_c and C_s. To the group of material parameters characterizing soil strength belong the angle of shearing resistance ϕ' and the apparent cohesion c'.

State variables (stress, porosity, orientation of grain contacts, degree of saturation, temperature, deformation rate, etc.) describe the actual state of a material and can change during the calculation over a wide (physically allowable) range. It should be possible to measure state variables directly (at least theoretically) at any moment in time.

It is worth mentioning that the deformation (strain) tensor is not a state variable for geomaterials since it cannot be measured. It is only possible to determine strain increments related to the known initial state. In the initial state (consider, for example, a laboratory specimen before testing), the deformation tensor has no meaning and can be chosen arbitrarily.

In some more advanced soil constitutive models not only material parameters but also state-dependent parameters are used as model parameters.

A third category of model parameters is *hidden* (or *internal*) *parameters*. These are normally state dependent but cannot be directly measured. An example of a hidden parameter is the tensor defining the translation of the yield surface when a kinematic hardening rule is applied. A way to determine such hidden model parameters for a certain soil is to use parameter optimization, as outlined in *Section 4.2*.

In addition to the above-mentioned soil parameters, *empirical parameters* should also be mentioned. These are parameters in empirical expressions, e.g. expressions relating stiffness or strength to standard penetration test (SPT) values, and are based on observations of behaviour in the field.

4.1.2 Determination of consolidation and stiffness properties

Material parameters characterizing the consolidation of soils are usually determined in the laboratory on undisturbed samples using an *oedometer*. By such a test, the gradient C_c of the VCL and the gradient C_s of swelling lines in an e-$\log_{10}\sigma'_v$ plot can be determined. Additional information can be obtained from an isotropic compression test in a *triaxial apparatus*. In this way, the gradient λ of the VCL and the gradient κ of the swelling lines in a v-ln p' plot are determined.

Stiffness characteristics of natural soils, varying from very small to large strains, can be determined in the laboratory, provided:

- the samples are relatively undisturbed;
- some type of local (specimen-mounted) transducer is used to measure strains.

Recently use has been made of bender elements, embedded into the end platens (or elsewhere) of various laboratory devices, in order to measure shear wave velocity and hence the stiffness (G_{max}) at very small strains (i.e. elastic plateau). The resonant column device has been used for some time for the same purpose. For more advanced studies into stiffness anisotropy, recent research has made use of the true triaxial device and the hollow cylinder apparatus where all three principal stresses can be varied in both magnitude and angle of inclination.

Geophysical techniques, mostly using seismic waves directed from the surface or cross-hole and detected by special cone penetrometer devices such as the seismic cone, are also used to measure initial small-strain stiffness in the field. The literature on this subject is extensive. Reference should be made to:

- the Xth European Conference on Soil Mechanics and Foundation Engineering held in Florence in 1991;
- the XIVth International Conference on Soil Mechanics and Foundation Engineering held in Hamburg in 1997;
- and also to the series of conferences on 'Pre-Failure Deformation Behaviour of Geomaterials' held in Hokkaido in 1994, in London in 1997 and in Torino in 1999.

In situ test devices such as the pressuremeter and dilatometer are frequently used to obtain stiffness parameters. Again, a full discussion on these instruments is beyond the scope of this document and the reader is referred initially to the textbook by Clarke (1995) and to Marchetti (1997).

In some countries *in situ* testing techniques such as the standard penetration test (SPT) are also used to obtain stiffness parameters (e.g. Riggs, 1982). Frequently, local correlations are used and these must be treated with caution if used in wider application.

4.1.3 Determination of strength properties

Shear behaviour of soils can be investigated in a range of apparatus, from direct and simple shear to conventional triaxial cells, or even true triaxial cells and hollow cylinders. The direct shear cell gives information on the relationship between the shear stress and shear strain, as well as the strength, as a function of the vertical pressure applied to the sample. In this way, the strength parameters, the angle of shearing resistance φ' and the apparent cohesion c' can be determined. However, the most common test is the conventional triaxial test. As many soil models are formulated in triaxial stress space, the triaxial test gives the best information on those material parameters that are to be used in these models. For example, in the original Cam clay model the angle of shearing resistance φ'_{cs} has to be determined from triaxial tests.

In order to obtain more detailed information for some advanced constitutive models, true triaxial tests, hollow cylinder tests and other such sophisticated tests are needed. For example, the dependence on the third stress invariant cannot be determined by conventional triaxial tests.

For many years use has been made of the field vane test to measure the undrained shear strength of soft to firm clays. Although this test suffers from interpretation difficulties due to vane insertion disturbance effects, rate of rotation and anisotropy, sufficient experience of its use exists to render it a useful device. It is particularly useful when designing embankments on soft clays. The ASTM Special Technical Publication, STP 1014, published in 1988, contains several very useful papers on the use and interpretation of the test results from this device.

Perhaps the device that has been most frequently and successfully used in site investigation to determine strength is the cone penetrometer (CPT) or piezocone (CPTU). Both the undrained shear strength of clays and the effective angle of shearing resistance of sands (also the relative density) can be reliably determined with this device. The available literature on the use of and interpretation of piezocone test results is vast. The reader is referred to the textbook by Lunne *et al*. (1997) for further information.

Additional information concerning the determination of both stiffness and strength parameters from laboratory and *in situ* field tests can be found in Potts and Zdravkovic (2001a).

4.2 Parameter determination by optimization

4.2.1 General

Complex soil models may contain model parameters which do not necessarily have a physical meaning or which are not possible to determine directly by laboratory or field tests. The predictions from using such constitutive models, for a certain soil type, must be evaluated against as many tests on that soil as possible, for different stress paths, under drained as well as undrained conditions. The model parameters should then be chosen in such a way that the model 'on average' predicts results as good as possible for different loading conditions and stress paths.

A way to find such parameter values for a certain soil model is to simulate several laboratory or field tests and measure the difference between experimental and theoretical values of stresses, strains and pore pressures. The model parameter set which minimizes these differences is then searched for and determined by optimization.

To be able to simulate a variety of tests, the constitutive equations, obtained in strain-driven form, should be reformulated in a mixed form, enabling simulation of, for example, triaxial tests.

4.2.2 Tangent relationships under mixed control

4.2.2.1 Mixed control: decomposition of stresses and strains

Constitutive equations for soils, based on the flow theory of plasticity, are considered. These are incremental (rate) relations between total stress rates $\dot{\boldsymbol{\sigma}}$ and strain rates $\dot{\varepsilon}$. In general, this tangential relationship is given in strain-driven format, i.e.

$$\dot{\boldsymbol{\sigma}} = \mathbf{D}^{\mathrm{ep}} \cdot \dot{\varepsilon} \tag{4.1}$$

where $\mathbf{D}^{\mathrm{ep}}$ is the elastic–plastic stiffness matrix. However, in many laboratory and field tests, not only strain components but also stress components might act as control variables. Hence, in order to be able to simulate different types of test, the constitutive relation has to be reformulated in a mixed form. To this end, the increments of total stresses $\dot{\boldsymbol{\sigma}}$ and strains $\dot{\varepsilon}$ associated with the co-ordinate system of the test, have to be decomposed and rearranged in energy conjugate portions into subvectors

$$\dot{\boldsymbol{\sigma}} = \begin{bmatrix} \dot{\boldsymbol{\sigma}}_1 \\ \dot{\boldsymbol{\sigma}}_2 \end{bmatrix}, \qquad \dot{\varepsilon} = \begin{bmatrix} \dot{\varepsilon}_1 \\ \dot{\varepsilon}_2 \end{bmatrix} \tag{4.2}$$

in such a way that the stress rate components $\dot{\boldsymbol{\sigma}}_1$ and the strain rate components $\dot{\varepsilon}_2$ represent control variables, while the strain rate components, $\dot{\varepsilon}_1$ and stress rate components $\dot{\boldsymbol{\sigma}}_2$ represent response variables. Other vectors and matrices are decomposed in the same way. The quantities can be transformed back to the physical co-ordinate system at any time.

Correspondingly, the increments of the effective stresses

$$\dot{\boldsymbol{\sigma}}' = \dot{\boldsymbol{\sigma}} - \delta \cdot \dot{u} \tag{4.3a}$$

where δ is a diagonal matrix with elements 1 and $\dot{u}$ are the pore pressure increments, are decomposed into the subvectors

$$\dot{\boldsymbol{\sigma}}' = \begin{bmatrix} \dot{\boldsymbol{\sigma}}_1' \\ \dot{\boldsymbol{\sigma}}_2' \end{bmatrix} \tag{4.3b}$$

where $\dot{\boldsymbol{\sigma}}_1'$ are control variables and $\dot{\boldsymbol{\sigma}}_2'$ response variables.

4.2.2.2 Mixed tangent relationship under drained conditions

With the effective stress increments $\dot{\boldsymbol{\sigma}}_1'$, and the strain increments, $\dot{\varepsilon}_2$ acting as control variables, and their energy conjugates $\dot{\varepsilon}_1$ and $\dot{\boldsymbol{\sigma}}_2'$ acting as response variables, the mixed tangent relationship for the soil skeleton (i.e. for the drained case) can be written

$$\begin{bmatrix} \dot{\varepsilon}_1 \\ \dot{\boldsymbol{\sigma}}_2' \end{bmatrix} = \begin{bmatrix} D_{11} & D_{12} \\ D_{21} & D_{22} \end{bmatrix} \begin{bmatrix} \dot{\boldsymbol{\sigma}}_1' \\ \dot{\varepsilon}_2 \end{bmatrix} \tag{4.4a}$$

where the tangent matrix under plastic loading has the form

$$\begin{bmatrix} D_{11} & D_{12} \\ D_{21} & D_{22} \end{bmatrix} = \begin{bmatrix} D_{11}^{\mathrm{e}} & D_{12}^{\mathrm{e}} \\ D_{21}^{\mathrm{e}} & D_{22}^{\mathrm{e}} \end{bmatrix} + \frac{1}{K} \begin{bmatrix} \hat{m}_1 \hat{n}_1^{\mathrm{T}} & \hat{m}_1 \hat{n}_2^{\mathrm{T}} \\ -\hat{m}_2 \hat{n}_1^{T} & -\hat{m}_2 \hat{n}_2^{T} \end{bmatrix} \tag{4.4b}$$

Here, the first matrix on the right-hand side is a partitioned version of the elastic tangential matrix $\mathbf{D}^{e}$ for the soil skeleton, K is a generalized plastic modulus, $\hat{n}_1$ and $\hat{n}_2$ are transformations of the gradient $\mathbf{n}$ of the yield function, and $\hat{m}_1$ and $\hat{m}_2$, are transformations of the flow vector $\mathbf{m}$. For a detailed derivation of the mixed tangential relationship (4.4), see Runesson *et al*. (1992) or Mattsson *et al*. (1997).

4.2.2.3 Mixed tangent relationship under undrained conditions

In standard field and laboratory testing, undrained conditions often prevail. It is thus necessary to formulate constitutive equations also for this case. The mixed tangent relationship under undrained conditions can be written

$$\begin{bmatrix} \dot{\varepsilon}_1 \\ \dot{\sigma}_2 \end{bmatrix} = \begin{bmatrix} D_{u11} & D_{u12} \\ D_{u21} & D_{u22} \end{bmatrix} \begin{bmatrix} \dot{\sigma}_1 \\ \dot{\varepsilon}_2 \end{bmatrix} \tag{4.5a}$$

where the tangent matrix under plastic loading has the form

$$\begin{bmatrix} D_{u11} & D_{u12} \\ D_{u21} & D_{u22} \end{bmatrix} = \begin{bmatrix} D^{e}_{u11} & D^{e}_{u12} \\ D^{e}_{u21} & D^{e}_{u22} \end{bmatrix} + \frac{1}{K_u} \begin{bmatrix} \hat{m}_{u1}\hat{n}^{T}_{u1} & \hat{m}_{u1}\hat{n}^{T}_{u2} \\ -\hat{m}_{u2}\hat{n}^{T}_{u1} & -\hat{m}_{u2}\hat{n}^{T}_{u2} \end{bmatrix} \tag{4.5b}$$

Here, the first matrix on the right-hand side is a partitioned version of the undrained elastic tangential matrix $\mathbf{D}^{e}_{u}$, K_u is the undrained generalized plastic modulus, $\hat{n}_{u1}$ and $\hat{n}_{u2}$ are transformations of the undrained gradient $\mathbf{n}_u$ of the yield function, and $\hat{m}_{u1}$ and $\hat{m}_{u2}$ are transformations of the undrained plastic flow vector $\mathbf{m}_u$ (Runesson *et al.*, 1992).

Further, the pore pressure increment under undrained conditions takes the form

$$\dot{u} = c_1 \left(\bar{\delta}_1 + \frac{1}{K_u} \hat{m}_{1v} \hat{n}_{u1} \right)^{T} \dot{\sigma}_1 + c_1 \left(\bar{\delta}_2 + \frac{1}{K_u} \hat{m}_{1v} \hat{n}_{u2} \right)^{T} \dot{\varepsilon}_2 \tag{4.6}$$

where c_1 is the elastic complementary energy, $\bar{\delta}_1$ and $\bar{\delta}_2$ are transformations of the Kronecker delta, and $\hat{m}_{1v}$ is the volumetric portion of $\hat{m}_1$.

4.2.2.4 Uniqueness of solutions

It can be shown that non-zero values of the drained and undrained generalized plastic moduli, $K > 0$, and $K_u > 0$, provide the criteria for a unique response (by giving an unambiguous loading criterion) and should therefore be computed as part of the scheme. The choice of control variables has a major influence on the uniqueness of the stress–strain behaviour (Runesson *et al.*, 1992; Klisinski *et al.*, 1992). For example, for drained behaviour under pure stress control, the material must be strictly hardening.

The constitutive equations in the mixed form described here do not apply to multi-surface plasticity models where more than one yield surface can be loaded at the same time. An extension of the mixed control concept to multi-surface plasticity has been presented by Klisinski (1998).

4.2.3 Integration algorithm

The constitutive equations under mixed control in Equations (4.4) and (4.5) must be numerically integrated. In Mattsson *et al.* (1999), explicit as well as implicit integration algorithms have been applied. Implicit integration of the elastic–plastic tangent relations under mixed control for drained and undrained response is addressed in Alawaji *et al.* (1992). In the example of parameter optimization given below, however, only the explicit integration algorithm of the forward Euler (FE) type has been applied.

A numerical problem that might appear in plastic loading, when using explicit integration, is caused by drift from the yield surface which primarily arises from the use of the rate consistency condition when establishing the tangential constitutive matrix. Such drift might give rise to a cumulative discrepancy that, in the worst case, can totally destroy a solution.

Therefore, a drift correction method, for the explicit integration of the mixed tangential relations in soil plasticity for drained and undrained response, has been formulated (Mattsson *et al*., 1997).

4.2.4 Optimization of model parameters

The key idea here, to properly select model parameters for more or less complex soil models in plasticity, is to consider the parameters obtained when stimulating different tests with different load paths etc., and then use an optimization strategy to select the 'best' set of these parameters (Mattsson *et al*., 2000).

The mathematical procedure of optimization basically consists of two parts; the formulation of an objective function measuring the difference between theoretical and experimental results, and the selection of an optimization strategy to enable the search for the minimum of this function.

4.2.4.1 Formulation of an objective function

In the optimization problem to be formulated, the parameters of the constitutive model considered play the role of optimization variables. In general, more reliable model parameters can be obtained if many (qualitatively different) experimental tests form a basis for the optimization.

For each test, the difference between the experimental result and the theoretical prediction is measured by a norm value, referred to as an individual norm. The individual norms of the tests form an objective function $F(x)$. The optimization problem involves the minimization of this objective function

$$F(\boldsymbol{x}) \rightarrow \min \tag{4.7a}$$

where $\boldsymbol{x}$ is a vector containing the optimization variables. Bound constraints are introduced on the optimization variables

$$\boldsymbol{x}_\ell \leq \boldsymbol{x} \leq x_{\mathrm{u}} \tag{4.7b}$$

where $\boldsymbol{x}_\ell$ and $\boldsymbol{x}_{\mathrm{u}}$ are, respectively, the lower and upper bounds of $\boldsymbol{x}$.

As a first step in the formulation of an objective function, an expression for the individual norm has to be established. The individual norm is based on Euclidean measures between discrete points, composed by the experimental and the theoretical result, in a seven-dimensional space spanned by normalized versions of the principal total stresses σ_1, σ_2 and σ_3, the principal strains ε_1, ε_2 and ε_3, and the pore pressure u, i.e.

$$d = \left[\frac{1}{\sigma_{\mathrm{o}}^2}\sum_{i=1}^{3}\left(\sigma_i^{\mathrm{exptl}} - \sigma_i^{\mathrm{theor}}\right)^2 + \frac{1}{\varepsilon_{\mathrm{o}}^2}\sum_{i=1}^{3}\left(\varepsilon_o^{\mathrm{exptl}} - \varepsilon_i^{\mathrm{theor}}\right)^2 + \frac{1}{u_{\mathrm{o}}^2}\left(u^{\mathrm{exptl}} - u^{\mathrm{theor}}\right)^2\right]^{\frac{1}{2}} \tag{4.8}$$

where the scaling factors σ_{o}, ε_{o} and u_{o} are necessary for the comparison of stresses and strains. The scaling factors are chosen as the maximum absolute values of all the total stresses, strains and pore pressures respectively in the discrete points involved in the computation of the individual norm.

The minimum distance $d_{\min}$ between experimental points and the prediction curve, for each experimental point included in the test, is searched for. An economical way to compute $d_{\min}$ is

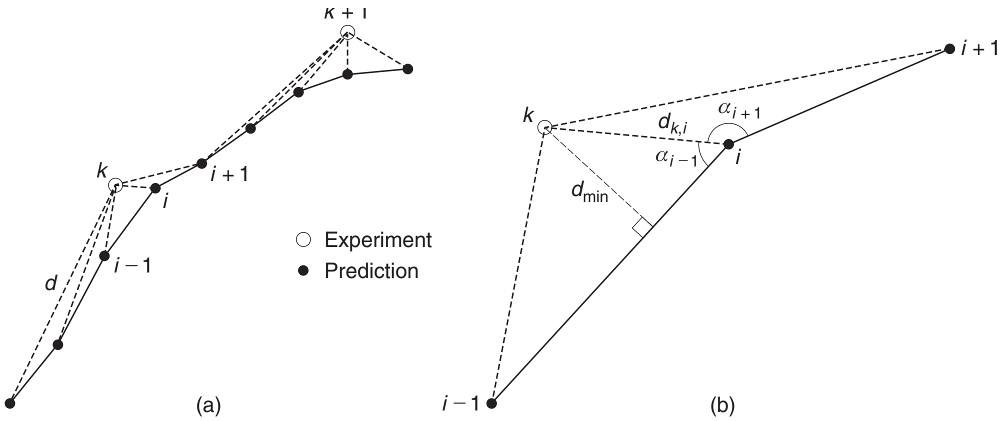

Figure 4.1 The search algorithm for the closest distances

to search for the closest Euclidean distance in Equation (4.8) in one direction, according to **Figure 4.1(a)**. The search proceeds until the closest distance, $d_{k,i} < d_{k,i-1}$ and $d_{k,i} < d_{k,i+1}$, is located. Then the distance d_{min} to an even closer position is searched for on either side of the prediction point i (**Figure 4.1(b)**) by analysing the two triangles.

When the minimum distances for all the experimental points are computed, an absolute individual norm is obtained as

$$E_{abs} = w\frac{1}{(n+1)}\left[\sum_{j=1}^{n} d^{j}_{min} + d_t\right] \tag{4.9}$$

where w is a weight factor, n is the number of experimental points (the first not counted), d^{j}_{min} is the minimum distance for the experimental point j and d_t denotes the distance between the termination points.

The next step is to formulate a final norm, an objective function, based on the individual norms computed for each experimental test included in the optimization. Two different final norms have been used in the past and either can be employed for the objective function. These are the maximum norm and the combined norm, i.e.

$$F_{max} = \max_{1\leq\ell\leq m} E^{\ell} \qquad \text{and} \qquad F_{comb} = m.F_{max} + \sum_{\ell=1}^{m} E^{\ell} \tag{4.10}$$

where m is the number of experimental tests involved in the optimization and E^{ℓ} is the individual norm value for Test No. ℓ.

4.2.4.2 Search strategy and optimization

The solution of the optimization problem is a vector x_o which for any $x_{\ell} \leq x \leq x_u$ satisfies the condition

$$F(x_o) \leq F(x) \tag{4.11}$$

of a global minimum. Two different search strategies have been employed in the past, one based on the method by Rosenbrock (1960) and the other based on the Simplex method by Nelder and Mead (1965), both belonging to the category of direct search methods.

Most optimization routines, however, are only capable of searching for a local minimum. This is also true for the direct search methods discussed here. In the general case, there is no way to check whether the local minimum obtained is also the global one. A possible solution to this problem is to start the search from different initial positions and, if the local minima become the same, then this is most probably also the global minimum.

4.2.4.3 Constitutive driver for simulating soil testing

In a constitutive driver (Mattsson, 1999; Mattsson *et al*., 1999), experimental tests can be simulated with a chosen plasticity model under drained or undrained conditions and with mixed control if needed. The set of constitutive parameters giving the best possible fit against different soils tests is then determined by optimization.

4.2.5 Example: optimization of model parameters for a silty clay

As an example of how to select model parameters based on optimization, results from optimizations against a conventional undrained triaxial compression test on an isotropically normally consolidated soil are briefly commented on.

The laboratory experiment has been performed on a sulphide-rich silty clay, stabilized in the laboratory with air blast-furnace slag and Portland cement (**Table 4.1**). This particular soil sample originates from a field test just outside the city of Lulea, Sweden.

Table 4.1 Soil sample data

Bulk density (Mg/m^3)	Water content (%)	Degree of saturation (%)	Amount of additives (weight % of DS soil)	Mixture (weight %)	Curing time (days)
1.56	70	˜100	14	FS50/PC50[a]	40

[a]FS = air blast-furnace slag (<4 mm grains), PC = Portland cement

Optimizations have been performed by using a 'generalized' Cam clay model and the model described by Nova and Wood (1979). Both these models were considered to have good prospects of predicting the experimental response.

4.2.5.1 Optimization procedure

In the 'generalized' Cam clay model, seven parameters are required, i.e.

1. κ^*, the slope of the unloading–reloading line in the ε_{vol}–ln p' plane, where ε_{vol} is the volumetric strain and p' the effective mean stress;
2. ν', Poisson's ratio;
3. λ^*, the slope of the isotropic compression line in the ε_{vol}–ln p'plane
4. D, deviatoric hardening parameter;
5. M, the slope of the critical state cone;
6. N, parameter for the non-associated flow rule;
7. e_r, parameter for the yield surface dependence on the third deviatoric stress invariant.

The value of the parameter e_r has no influence on the result from a prediction for a conventional triaxial compression test, and is therefore not included in the optimization. The parameters κ^*, ν', λ^*, D and M are also included in the Nova–Wood model, together with two additional parameters: m, that characterizes the yield function, and a dilatancy parameter μ.

The experimental test was carried out with a constant strain rate of 1% per hour in the axial direction and, hence, a linear variation of the axial strain was assumed in the predictions. In the optimizations, an absolute individual norm, Equation (4.9) with $w = 1.0$, was utilized as the objective function, Equation 4.10.

Table 4.2 The optimal set of parameters for the generalized Cam clay model						
	Optimization variables					
F_{max} (Eq. (4.10)) (%)	κ^*	ν'	λ^*	D	M	N
1.21	0.0046	0.3364	0.0311	0.1319	1.9950	1.9950

The optimal set of parameters and the associated value of the objective function are shown in **Table 4.2** for the generalized Cam clay model and in **Table 4.3** for the Nova–Wood model.

In addition to the computation of the optimized values of model parameters, it should also be possible to plot out the simulated test results, computed by the constitutive driver, and compare these with the real test results. In **Figure 4.2**, results from a simulated undrained test, using the generalized Cam clay model with optimized parameters, are compared with the experimental results.

Table 4.3 The optimal set of parameters for the Nova–Wood model							
	Optimization variables						
F_{max} (Eq. (4.10))(%)	κ^*	ν'	λ^*	D	M	m	μ
1.14	0.0053	0.2958	0.0174	0.0721	1.9969	1.9964	1.0000

The parameters that are common for the models in Tables 4.2 and 4.3 received optimal values with a magnitude quite close to each other, which further indicates that the models are able to predict this particular experimental test. On the other hand, it is important to reiterate that good agreement with respect to a single test is not enough to evaluate a model, but it is a promising start. Further, both these models are historically based mostly on data from conventional triaxial tests and it is not certain that an agreement as good as in this example could be obtained for more complex stress/strain paths on the same soil.

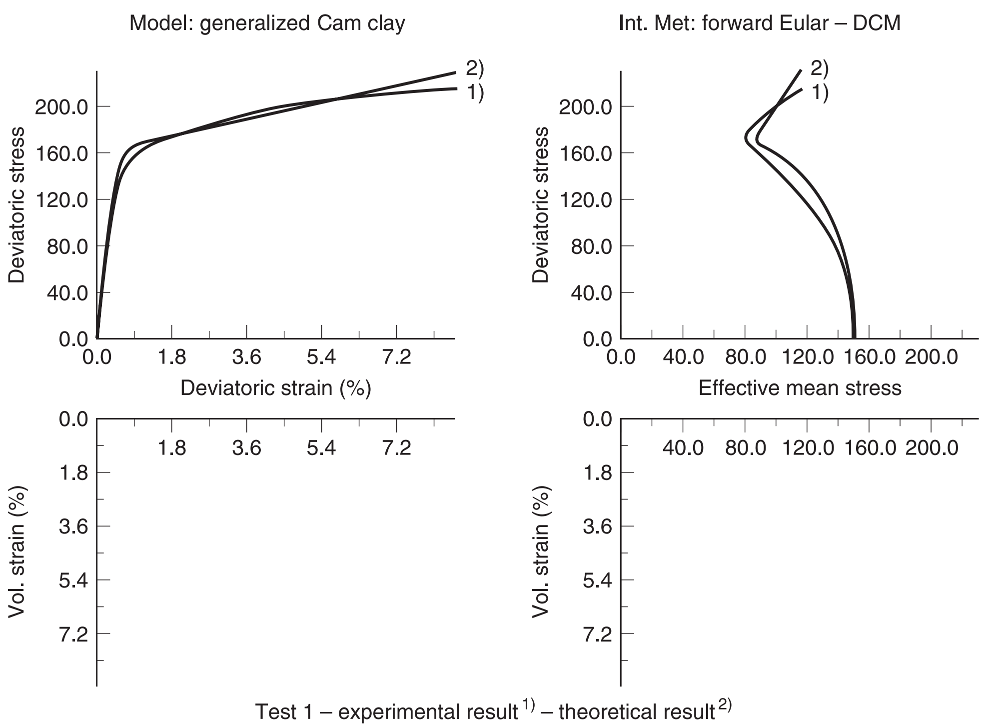

Figure 4.2 Comparison of simulated test with real test results

5

Non-linear analysis

5.1 Introduction

To be able to use non-linear elastic and/or elasto-plastic constitutive models, similar to those described in *Chapter 3*, to represent soil behaviour in a numerical analysis, the basic theory, which is derived for linear material behaviour, must be extended. In the basic theory the soil behaviour is assumed to be elastic and the constitutive matrix [**D**] is therefore constant. If the soil is non-linear elastic and/or elasto-plastic, the equivalent constitutive matrix is no longer constant but varies with stress and/or strain. It therefore changes during a numerical analysis. Consequently, a solution strategy is required that can account for this changing material behaviour. This strategy is a key component of a non-linear analysis, as it can strongly influence the accuracy of the results and the computer resources required to obtain them. Several different solution strategies are described in the literature and three of the most popular schemes used in finite element analysis will be briefly described in this chapter. For a more in-depth description and comparison of the various solution strategies the reader is referred to Potts and Zdravkovic (1999).

Another assumption in the basic theory, especially for finite element analysis, is that the displacements and strains involved are small. This means that the original geometry of the problem under consideration does not change significantly and that all the integrations can be performed over the original, undeformed, geometry. While this assumption has been shown to be adequate for the majority of geotechnical engineering problems, a certain scepticism accompanies the application of this method to problems involving significant amounts of displacement, such as embankments on soft ground or installation of displacement piles. If account is taken of changes in displacement and/or the occurrence of large strains, then the governing equations become non-linear. Such non-linearity is referred to as geometric non-linearity whereas as the non-linearity arising from the constitutive behaviour is called material non-linearity. A brief discussion on the implications of dealing with geometric non-linearity is given subsequently in this chapter.

The basic theory can also be extended to deal with time effects due to dissipation of excess pore water pressures. In such a situation the equations governing the flow of water through the soil skeleton are coupled with those governing the mechanical behaviour of the soil skeleton itself. A brief description of this theory and the main assumptions are presented at the end of this chapter.

5.2 Material non-linearity

As noted in *Chapter 2*, in the analysis of any boundary value problem four basic solution requirements need to be satisfied: equilibrium, compatibility, constitutive behaviour and boundary conditions. Non-linearity introduced by the constitutive behaviour causes the governing finite element equations to be reduced to the following incremental form:

$$[\mathbf{K}_G]^i\{\Delta \boldsymbol{d}\}^i_{nG} = \{\Delta \boldsymbol{R}_G\}^i \tag{5.1}$$

where $[\mathbf{K}_G]^i$ is the incremental global system stiffness matrix, $\{\Delta \boldsymbol{d}\}^i_{nG}$ is the vector of incremental nodal displacements, $\{\Delta \boldsymbol{R}_G\}^i$ is the vector of incremental nodal forces and i is the increment number. To obtain a solution to a boundary value problem, the change in boundary conditions is applied in a series of increments and for each increment Equation (5.1) must be solved. The final solution is obtained by summing the results of each increment. Because of the non-linear constitutive behaviour, the incremental global stiffness matrix $[\mathbf{K}_G]^i$ is dependent on the current stress and strain levels and therefore is not constant but varies over an increment. Unless a very large number of small increments is used, this variation should be accounted for. Hence, the solution of Equation (5.1) is not straightforward and different solution strategies exist. The objective of all such strategies is the solution of Equation (5.1), ensuring satisfaction of the four basic requirements listed above. As some of the strategies are more accurate than others, it is essential that users are familiar with the approach used in the software they are using. To illustrate this, three different categories of solution algorithm are considered next, namely the tangent stiffness, visco-plastic and modified Newton–Raphson (MNR) schemes. While these schemes are mainly applicable to the finite element method, similar alternatives arise with the other numerical methods.

5.2.1 Tangent stiffness method

5.2.1.1 Introduction

The tangent stiffness method, sometimes called the variable stiffness method, is the simplest solution strategy.

In this approach, the incremental stiffness matrix $[\mathbf{K}_G]^i$ in Equation (5.1) is assumed to be constant over each increment and is calculated using the current stress state at the beginning of each increment. This is equivalent to making a piece-wise linear approximation to the non-linear constitutive behaviour. To illustrate the application of this approach, the simple problem of a uniaxially loaded bar of non-linear material is considered (see **Figure 5.1**). If this bar is loaded, the true load–displacement response is as shown in **Figure 5.2**. This might represent the behaviour of a strain-hardening plastic material that has a very small initial elastic domain.

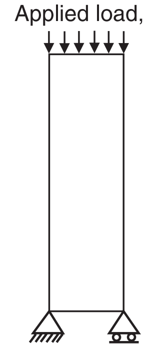

Figure 5.1 Uniaxial loading of a bar of non-linear material

5.2.1.2 Finite element implementation

In the tangent stiffness approach the applied load is split into a sequence of increments. In Figure 5.2 three increments of load are shown, $\Delta \boldsymbol{R}_1$, $\Delta \boldsymbol{R}_2$ and $\Delta \boldsymbol{R}_3$. The analysis starts with the application of $\Delta \boldsymbol{R}_1$. The incremental global stiffness matrix $[\mathbf{K}_G]^1$ for this increment is evaluated on the basis of the unstressed state of the bar corresponding to point ‘a’. For an elasto-plastic material this might be constructed using the elastic constitutive matrix $[\mathbf{D}]$. Equation (5.1) is then solved to determine the nodal displacements $\{\Delta \mathbf{d}\}^1_{nG}$. As the material stiffness is assumed to remain constant, the load–displacement curve follows the straight line ‘ab′’ on Figure 5.2. In reality, the stiffness of the material does not remain constant during this loading increment and the true solution is represented by the curved path ‘ab’. There is therefore an error in the predicted displacement equal to the distance ‘b′b’; however, in the tangent stiffness approach this error is neglected. The second increment of load, $\Delta \boldsymbol{R}_2$, is then applied, with the incremental global stiffness matrix $[\mathbf{K}_G]^2$ evaluated using the stresses and strains appropriate to the end of increment 1, i.e. point ‘b′’ on Figure 5.2. Solution of Equation (5.1) then gives the nodal displacements $\{\Delta \mathbf{d}\}^2_{nG}$. The load–displacement curve follows the straight path ‘b′c′’ on Figure 5.2. This deviates further from the true solution, the error in the displacements now being equal to the distance ‘c′c’. A similar procedure now occurs when $\Delta \boldsymbol{R}_3$ is applied. The stiffness matrix $[\mathbf{K}_G]^3$ is evaluated using the stresses and strains appropriate to the end of

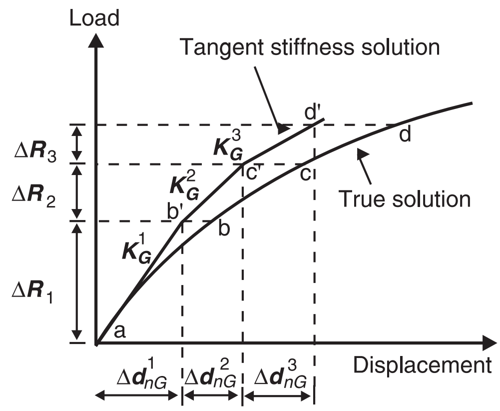

Figure 5.2 Application of the tangent stiffness algorithm to the uniaxial loading of a bar of a non-linear material

increment 2, i.e. point ‘c′’ on Figure 5.2. The load–displacement curve moves to point ‘d′’ and again drifts further from the true solution. Clearly, the accuracy of the solution depends on the size of the load increments. For example, if the increment size was reduced so that more increments were needed to reach the same accumulated load, the tangent stiffness solution would be nearer to the true solution.

From the above simple example it may be concluded that in order to obtain accurate solutions to strongly non-linear problems many small solution increments are required. The results obtained using this method can drift from the true solution and the stresses can fail to satisfy the constitutive relations. Thus the basic solution requirements may not be fulfilled. It can be shown (Potts and Zdravkovic, 1999) that the magnitude of the error is problem dependent and is affected by the degree of material non-linearity, the geometry of the problem and the size of the solution increments used. Unfortunately, in general, it is impossible to predetermine the size of solution increment required to achieve an acceptable error.

The tangent stiffness method can give particularly inaccurate results when soil behaviour changes from elastic to plastic or vice versa. For instance, if an element is in an elastic state at the beginning of an increment, it is assumed to behave elastically over the whole increment. This is incorrect if, during the increment, the behaviour becomes plastic and results in an illegal stress state that violates the constitutive model. Such illegal stress states can also occur for plastic elements if the increment size used is too large; for example, a tensile stress state could be predicted for a constitutive model that cannot sustain tension. This can be a major problem with critical state type models, such as modified Cam clay, which employ a v–lnp' relationship (v = specific volume, p' = mean effective stress, see *Chapter 3*), since a tensile value of p' cannot be accommodated. In that case either the analysis has to be aborted or the stress state has to be modified in some arbitrary way, which would cause the solution to violate the equilibrium condition and the constitutive model.

5.2.2 Visco-plastic method

5.2.2.1 Introduction

This method uses the equations of visco-plastic behaviour and time as an artifice to calculate the behaviour of non-linear, elasto-plastic, time-independent materials (Owen and Hinton, 1980; Zienkiewicz and Cormeau, 1974).

The method was originally developed for linear elastic visco-plastic (i.e. time-dependent) material behaviour. Such a material can be represented by a network of the simple rheological units shown in **Figure 5.3**. Each unit consists of an elastic and a visco-plastic component connected in series. The elastic component is represented by a spring and the visco-plastic component by a slider and dashpot connected in parallel. If a load is applied to the network, then one of two situations occurs in each individual unit. If the load is such that the induced stress in the unit does not cause yielding, the slider remains rigid and all the deformation occurs in the spring. This represents elastic behaviour. Alternatively, if the induced stress causes yielding, the slider becomes free and the dashpot is activated. As the dashpot takes time to react, initially all deformation occurs in the spring. However, with time the dashpot moves. The rate of movement of the dashpot depends on the stress it supports and its fluidity. With time progressing, the dashpot moves at a decreasing rate, because some of the stress the unit is carrying is dissipated to adjacent units in the network, which as a result suffer further movements themselves. This represents visco-plastic behaviour. Eventually, a stationary

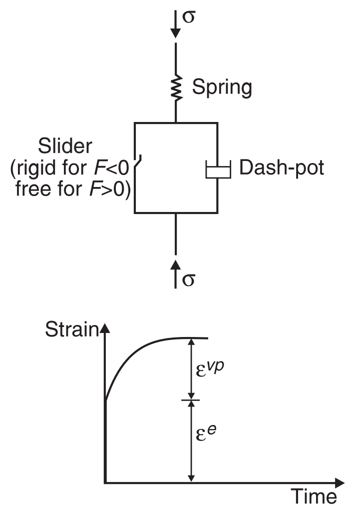

Figure 5.3 Rheological model for visco-plastic material

condition is reached where all the dashpots in the network stop moving and are no longer sustaining stresses. This occurs when the stress in each unit drops below the yield surface and the slider becomes rigid. The external load is now supported purely by the springs within the network but, importantly, straining of the system has occurred, not only due to compression or extension of the springs but also due to movement of the dashpots. If the load was now removed, only the displacements (strains) occurring in the springs would be recoverable, the dashpot displacements (strains) being permanent.

5.2.2.2 Finite element application

Application to finite element analysis of elasto-plastic materials can be summarized as follows. On application of a solution increment the system is assumed to instantaneously behave linear elastically. If the resulting stress state lies within the yield surface, the incremental behaviour is elastic and the calculated displacements are correct. If the resulting stress state violates yield, the stress state can be sustained only momentarily and visco-plastic straining occurs. The magnitude of the visco-plastic strain rate is determined by the value of the yield function, which is a measure of the degree by which the current stress state exceeds the yield condition. The visco-plastic strains increase with time, causing the material to relax with a reduction in the yield function and hence the visco-plastic strain rate. A marching technique is used to step forward in time until the visco-plastic strain rate is insignificant. At this point, the accumulated visco-plastic strain and the associated stress change are equal to the incremental plastic strain and stress change respectively. This process is illustrated for the simple problem of a uniaxially loaded bar of non-linear material in **Figure 5.4**.

For genuine visco-plastic materials the visco-plastic strain rate is given by

$$\frac{\partial\{\varepsilon^{vp}\}}{\partial t} = \gamma\left(\frac{F(\{\sigma\},\{\mathbf{k}\})}{F_o}\right)\frac{P(\{\sigma\},\{\mathbf{m}\})}{\partial\{\sigma\}} \tag{5.2}$$

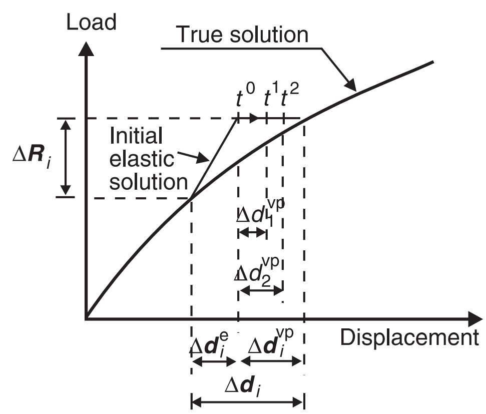

Figure 5.4 Application of the visco-plastic algorithm to the uniaxial loading of a bar of a non-linear material

where γ is the dashpot fluidity parameter and F_o is a stress scalar to non-dimensionalize the yield function $F(\{\sigma\}, \{k\})$ and $P(\{\sigma\}, \{m\})$ is the plastic potential function (Zienkiewicz and Cormeau, 1974). When the method is applied to time-independent elasto-plastic materials, both γ and F_o can be assumed to be unity (Griffiths, 1980) and Equation (5.2) reduces to

$$\frac{\partial\{\varepsilon^{vp}\}}{\partial t} = F(\{\boldsymbol{\sigma}\}, \{\mathbf{k}\})\frac{P(\{\boldsymbol{\sigma}\}, \{\mathbf{m}\})}{\partial\{\boldsymbol{\sigma}\}} \tag{5.3}$$

Over a time step t to $t + \Delta t$ the visco-plastic strain is given by

$$\{\Delta\varepsilon^{vp}\} = \int_{t}^{t+\Delta t} \frac{\partial\{\varepsilon^{vp}\}}{\partial t}\,\mathrm{d}t \tag{5.4}$$

and for small time steps Equation (5.4) can be approximated to

$$\{\Delta\varepsilon^{vp}\} = \Delta t\frac{\partial\{\varepsilon^{vp}\}}{\partial t} \tag{5.5}$$

The visco-plastic algorithm consists of the following steps:

1. At the beginning of a solution increment i, formulate the boundary conditions. In particular, construct the incremental right-hand-side load vector $\{\Delta \boldsymbol{R}_G\}$. Assemble the incremental global stiffness matrix $[\mathbf{K}_G]$ using the linear elastic constitutive matrix $[\mathbf{D}]$ for all elements in the mesh. Zero the visco-plastic strain increment vector, i.e. $\{\Delta\varepsilon^{vp}\} = 0$. Set $t = t_o$.
2. Solve the finite element equations to obtain a first estimate of the nodal displacements

$$\{\Delta \boldsymbol{d}\}^t_{nG} = [\mathbf{K}_G]^{-1}\{\Delta \boldsymbol{R}_G\}^t \tag{5.6}$$

Loop through all integration points in the mesh and for each integration point:

3. Calculate the incremental total strains from the incremental nodal displacements

$$\{\Delta\varepsilon\}^t = [\boldsymbol{B}]\{\Delta \boldsymbol{d}\}^t_{nG} \tag{5.7}$$

where $[\mathbf{B}]$ is the strain matrix containing the derivatives of the element shape functions.

4. The elastic strains are now calculated as the difference between the total strains, from Equation (5.7), and the visco-plastic strains. Note that for the first iteration (i.e. $t = t_o$) the visco-plastic strains are zero. The elastic strains are then used with the elastic constitutive matrix $[\mathbf{D}]$ to evaluate the incremental stress change

$$\{\Delta\boldsymbol{\sigma}\}^t = [\mathbf{D}](\{\Delta\varepsilon\}^t - \{\Delta\varepsilon^{vp}\}) \tag{5.8}$$

5. This incremental stress change is added to the accumulated stress at the beginning of the solution increment, $\{\sigma\}^{i-1}$:

$$\{\boldsymbol{\sigma}\}^t = \{\boldsymbol{\sigma}\}^{i-1} + \{\delta\boldsymbol{\sigma}\}^t \tag{5.9}$$

6. These stresses are then used to evaluate the yield function, $F(\{\boldsymbol{\sigma}\}^t, \{\boldsymbol{k}\})$.
   If the yield function $F(\boldsymbol{\sigma}\}^t, \{\boldsymbol{k}\}) < 0$, the current integration point is elastic. Therefore move to the next integration point (i.e. go to step 3). If the yield function $F(\{\boldsymbol{\sigma}\}^t, \{\boldsymbol{k}\}) \geq 0$ the visco-plastic strains must be calculated:
7. Calculate the visco-plastic strain rate

$$\left(\frac{\partial\{\varepsilon^{vp}\}}{\partial t}\right)^t = F(\{\boldsymbol{\sigma}\}^t, \{\mathbf{k}\})\frac{P(\{\boldsymbol{\sigma}\}^t, \{\mathbf{m}\})}{\partial\{\boldsymbol{\sigma}\}} \tag{5.10}$$

8. Update the visco-plastic strain increment:

$$\{\Delta\varepsilon^{vp}\}^{t+\Delta t} = \{\Delta\varepsilon^{vp}\}^{t} + \Delta t\left(\frac{\partial\{\varepsilon^{vp}\}}{\partial t}\right)^{t} \tag{5.11}$$

Move to next integration point (i.e. go to step 3).

End of integration point loop.

9. Calculate nodal forces equivalent to the change in incremental visco-plastic strains and add them to the incremental global right-hand-side vector. The elastic stress increment associated with the change in visco-plastic strains is given by

$$\{\Delta\sigma^{vp}\} = [\mathbf{D}]\Delta t\left(\frac{\partial\{\varepsilon^{vp}\}}{\partial t}\right)^{t} \tag{5.12}$$

The incremental global right hand side load vector then becomes

$$\{\Delta\boldsymbol{R}_{G}\}^{t+\Delta t} = \{\Delta\boldsymbol{R}_{G}\}^{t} + \sum_{\substack{\text{All}\\\text{elements}}}\int_{Vol}[\mathbf{B}]^{T}[\mathbf{D}]\Delta t\left(\frac{\partial\{\varepsilon^{vp}\}}{\partial t}\right)^{t}\mathrm{d}Vol \tag{5.13}$$

10. Set $t = t + \Delta t$ and return to step 2. This process is repeated until convergence is obtained. When convergence is achieved, the displacements evaluated in step 2, Equation (5.6), hardly change from one time step to the next. The yield function values, step 6, and the visco-plastic strain rates, step 7, become very small and the incremental stresses, step 4, and strain increments, steps 3 and 8, become almost constant with time.
11. Once convergence is achieved the displacements, stresses and strains are updated, ready for the next load increment

$$\{\boldsymbol{d}\}^{i}_{nG} = \{\boldsymbol{d}\}^{i-1}_{nG} + \{\Delta\boldsymbol{d}\}^{t}_{nG} \tag{5.14}$$

$$\{\varepsilon\}^{i} = \varepsilon\}^{i-1} + \{\Delta\varepsilon\}^{t} \tag{5.15}$$

$$\{\varepsilon^{p}\}^{i} = \{\varepsilon^{p}\}^{i-1} + \{\Delta\varepsilon^{vp}\}^{t+\Delta t} \tag{5.16}$$

$$\{\sigma\}^{i} = \{\sigma\}^{i-1} + \{\Delta\sigma\}^{t} \tag{5.17}$$

5.2.2.3 Choice of time step

In order to use the procedure described above, a suitable time step Δt must be selected. If Δt is small, many iterations are required to obtain an accurate solution. However, if Δt is too large numerical instability can occur. The most economical choice for Δt is the largest value that can be tolerated without causing such instability. An estimate for this critical time step is suggested by Stolle and Higgins (1989) and is given by

$$\Delta t_{c} = \frac{1}{\dfrac{\partial F(\{\sigma\},\{\mathbf{k}\})}{\partial\{\sigma\}}^{T}[\mathbf{D}]\dfrac{\partial P(\{\sigma\},\{\mathbf{m}\})}{\partial\{\sigma\}}^{T} + A} \tag{5.18}$$

where A is the hardening modulus (Potts and Zdravkovic, 1999). For simple constitutive models, such as Tresca and Mohr–Coulomb, the yield and plastic potential functions can be written such that Equation (5.18) gives a constant value of the critical time step, which is dependent only on the elastic stiffness and strength parameters. As these parameters are constant, the critical time step has to be evaluated only once during an analysis. However, for more complex constitutive models the critical time step is also dependent on the current state of stress and strain and therefore is not constant. It must therefore be evaluated for each integration point for each iteration. It should be noted that when using the algorithm to solve elasto-plastic problems (i.e. no time-dependent plastic behaviour), the time step does not have to be the same for all integration points during any particular iteration.

5.2.2.4 Potential errors in the algorithm

Owing to its simplicity, the visco-plastic algorithm has been widely used. However, the method has its limitations for geotechnical analysis. Firstly, the algorithm relies on the fact that for each increment the elastic parameters remain constant. The simple algorithm cannot accommodate elastic parameters that vary during the increment because, for such cases, it cannot determine the true elastic stress changes associated with the incremental elastic strains (see Equation (5.8)). The best that can be done is to use the elastic parameters associated with the accumulated stresses and strains at the beginning of the increment to calculate the elastic constitutive matrix [**D**] and assume that this remains constant for the increment. Such a procedure yields accurate results only if the increments are small and/or the elastic non-linearity is not great.

A more severe limitation of the method arises when the algorithm is used as an artifice to solve problems involving non-viscous material (i.e. elasto-plastic materials). As noted above, the visco-plastic strains are calculated using Equations (5.10) and (5.11). In Equation (5.10) the partial differentials of the plastic potential are evaluated at an illegal stress state $\{\sigma\}^t$, which lies outside the yield surface, i.e. $F(\{\boldsymbol{\sigma}'\}, \{\boldsymbol{k}\}) > 0$. As noted for the tangent stiffness method, this is theoretically incorrect and results in failure to satisfy the constitutive equations. The magnitude of the error depends on the constitutive model and in particular on how sensitive the partial derivatives are to the stress state.

Potts and Zdravkovic (1999) show that, while the visco-plastic algorithm works well for simple elasto-plastic constitutive models such as Tresca and Mohr–Coulomb, it has severe limitations when used with critical state type models.

5.2.3 Modified Newton–Raphson method

5.2.3.1 Introduction

The previous discussion of both the tangent stiffness and visco-plastic algorithms has highlighted that errors can arise when the constitutive behaviour is based on illegal stress states. The modified Newton–Raphson (MNR) algorithm described in this section attempts to rectify this problem by only evaluating the constitutive behaviour in, or very near to, legal stress space.

The MNR method uses an iterative technique to solve Equation (5.1). The first iteration is essentially the same as that of the tangent stiffness method. However, it is recognized that the solution is likely to be in error and the predicted incremental displacements are used to calculate the residual load, a measure of the error in the analysis. Equation (5.1) is then solved again with this residual load, $\{\psi\}$, forming the incremental right-hand-side vector. Equation (5.1) can be rewritten as

$$[\mathbf{K}_G]^i \left(\{\Delta \boldsymbol{d}\}^i_{nG} \right)^j = \{\boldsymbol{\psi}\}^{j-1} \tag{5.19}$$

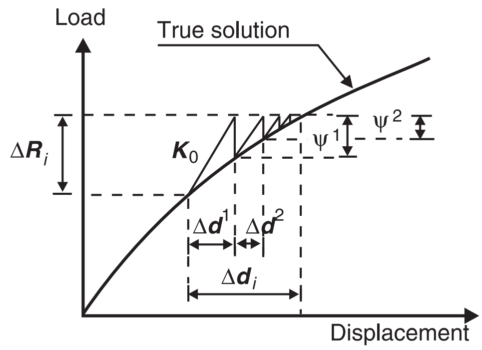

Figure 5.5 Application of the modified Newton–Raphson algorithm to the uniaxial loading of a bar of a non-linear material

The superscript 'j' refers to the iteration number and $\{\psi\}^{\circ} = \{\Delta R_G\}^i$. This process is repeated until the residual load is small. The incremental displacements are equal to the sum of the iterative displacements. This approach is illustrated in **Figure 5.5** for the simple problem of a uniaxially loaded bar of non-linear material. In principle, the iterative scheme ensures that for each solution increment the analysis satisfies all solution requirements.

A key step in this calculation process is to determine the residual load vector. At the end of each iteration the current estimate of the incremental displacements is calculated and used to evaluate the incremental strains at each integration point. The constitutive model is then integrated along the incremental strain paths to obtain an estimate of the stress changes. These stress changes are added to the stresses at the beginning of the increment and used to evaluate consistent equivalent nodal forces. The difference between these forces and the externally applied loads (from the boundary conditions) gives the residual load vector. A difference arises because a constant incremental global stiffness matrix $[\mathbf{K}_G]^i$ is assumed over the increment. Because of the non-linear material behaviour, $[\mathbf{K}_G]^i$ is not constant but varies with the incremental stress and strain changes.

Since the constitutive behaviour changes over the increment, care must be taken when integrating the constitutive equations to obtain the stress change. Methods of performing this integration are termed *stress point algorithms* and both explicit and implicit approaches have been proposed in the literature. There are many of these algorithms in use and, as they control the accuracy of the final solution, users must verify the approach used in their software. Two of the most accurate stress point algorithms are described subsequently.

The process described above is called a Newton–Raphson scheme if the incremental global stiffness matrix $[\mathbf{K}_G]^i$ is recalculated and inverted for each iteration on the basis of the latest estimate of the stresses and strains obtained from the previous iteration. To reduce the amount of computation, the modified Newton–Raphson method calculates and inverts the stiffness matrix only at the beginning of the increment and uses it for all iterations within the increment. Sometimes the incremental global stiffness matrix is calculated using the elastic constitutive matrix, $[\mathbf{D}]$, rather than the elasto-plastic matrix, $[\mathbf{D}^{ep}]$. Clearly, there are several options here and many software packages allow the user to specify how the MNR algorithm should work. In addition, an acceleration technique is often applied during the iteration process (Thomas, 1984).

5.2.3.2 Stress point algorithms

5.2.3.2.1 Introduction

Two classes of stress point algorithm are considered. The *substepping* algorithm is essentially explicit, whereas the *return* algorithm is implicit. In both the substepping and return algorithms, the objective is to integrate the constitutive equations along an incremental strain path. While the magnitudes of the incremental strain components are known, the manner in which they vary during the increment is not. It is therefore not possible to integrate the constitutive equations without making an additional assumption. Each stress point algorithm makes a different assumption and this influences the accuracy of the solution obtained.

5.2.3.2.2 Substepping algorithm

The schemes presented by Wissman and Hauck (1983) and Sloan (1987) are examples of substepping stress point algorithms. In this approach, the incremental strains are divided into a number of substeps. It is assumed that in each substep the strains $\{\Delta\varepsilon_{ss}\}$ are a proportion, ΔT, of the incremental strains $\{\Delta\varepsilon_{inc}\}$. This can be expressed as

$$\{\Delta\varepsilon_{ss}\} = \Delta T\{\Delta\varepsilon_{inc}\} \tag{5.20}$$

It should be noted that, in each substep, the ratio between the strain components is the same as that for the incremental strains and hence the strains are said to vary *proportionally* over the increment. The constitutive equations are then integrated numerically over each substep using either an Euler, a modified Euler or the Runge–Kutta scheme. The size of each substep (i.e. ΔT) can vary and, in the more sophisticated schemes, is determined by setting an error tolerance on the numerical integration. This allows control of errors resulting from the numerical integration procedure and ensures that they are negligible.

The basic assumption in these substepping approaches is therefore that the strains vary in a proportional manner over the increment. In some boundary value problems this assumption is correct and consequently the solutions are extremely accurate. However, in general, this may not be true and an error can be introduced. The magnitude of the error is dependent on the size of the solution increment.

5.2.3.2.3 Return algorithm

The schemes presented by Borja and Lee (1990) and Borja (1991) are examples of one-step implicit-type return algorithms. In this approach, the plastic strains over the increment are calculated from the stress conditions corresponding to the end of the increment. The problem, of course, is that these stress conditions are not known, hence the implicit nature of the scheme. Most formulations involve some form of elastic predictor to give a first estimate of the stress changes, coupled with a sophisticated iterative sub-algorithm to transfer from this stress state back to the yield surface. The objective of the iterative sub-algorithm is to ensure that, on convergence, the constitutive behaviour is satisfied, albeit with the assumption that the plastic strains over the increment are based on the plastic potential at the end of the increment. Many different iterative sub-algorithms have been proposed in the literature. In view of the previous findings, it is important that the final converged solution does not depend on quantities evaluated in illegal stress space. In this respect some of the earlier return algorithms broke this rule and are therefore inaccurate. To simplify this procedure for modified Cam clay, Borja and Lee (1990) assumed that the elastic moduli are constant over an increment. Borja (1991) describes a more rigorous procedure that accounts for the true variation of these moduli. Analyses which make the former assumption are called *constant elasticity* return algorithms, whereas those that correctly account for changes in elastic moduli are called *variable elasticity* return algorithms.

The basic assumption in these approaches is therefore that the plastic strains over the increment can be calculated from the stress state at the end of the increment, as illustrated in **Figure 5.6**. This is theoretically incorrect as the plastic response, and in particular the plastic flow direction, is a function of the current stress state. The plastic flow direction should be consistent with the stress state at the beginning of the solution increment and should evolve as a function of the changing stress state, such that at the end of the increment it is consistent with the final stress state. This type of behaviour is exemplified by the substepping approach, as illustrated in **Figure 5.7**. If the plastic flow direction does not change over an increment, the

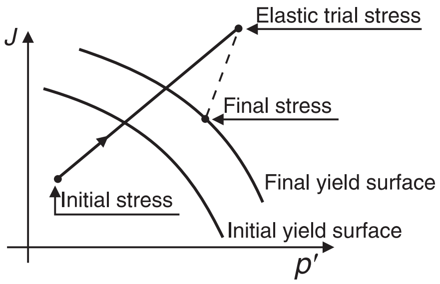

Figure 5.6 Return algorithm approach

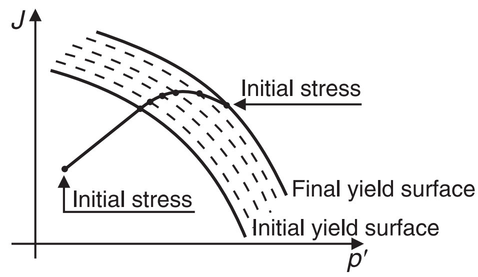

Figure 5.7 Substepping approach

return algorithm solutions are accurate. Invariably, however, this is not the case and an error is introduced. The magnitude of any error is dependent on the size of the solution increment.

5.2.3.2.4 Fundamental comparison

Potts and Ganendra (1994) performed a fundamental comparison of these two types of stress point algorithm and concluded that both algorithms give accurate results but, of the two, the substepping algorithm is slightly more accurate.

Another advantage of the substepping approach is that it is extremely robust and can easily deal with constitutive models in which two or more yield surfaces are active simultaneously and for which the elastic portion of the model is highly non-linear. In fact, most of the software required to program the algorithm is common to any constitutive model. This is not so for the return algorithm which, although in theory can accommodate such complex constitutive models, involves some extremely complicated mathematics. The software to deal with the algorithm is also constitutive model dependent. This means considerable effort is required to include a new or modified model.

5.2.3.2.5 Convergence criteria

As the MNR method involves iterations for each solution increment, convergence criteria must be set. This usually involves setting limits to the size of both the iterative displacements, $(\{\Delta \boldsymbol{d}\}^i_{\mathrm{nG}})^j$, and the residual loads, $\{\psi\}^j$. As both these quantities are vectors, it is normal to express their size in terms of the scalar norms.

$$\left\|\left(\{\Delta \boldsymbol{d}\}^i_{\mathrm{nG}}\right)^j\right\| = \sqrt{\left(\left(\{\Delta \boldsymbol{d}\}^i_{\mathrm{nG}}\right)^j\right)^{\mathrm{T}}\left(\{\Delta \boldsymbol{d}\}^i_{\mathrm{nG}}\right)^j} \tag{5.21}$$

$$\left\|\{\psi\}^j\right\| = \sqrt{\left(\{\psi\}^j\right)^{\mathrm{T}}\{\psi\}^j} \tag{5.22}$$

Often the iterative displacement norm is compared to the norms of the incremental, $\|\{\Delta \boldsymbol{d}\}^i_{\mathrm{nG}}\|$, and accumulated, $\|\{\boldsymbol{d}\}_{\mathrm{nG}}\|$, displacements. It should be remembered that the incremental displacements are the sum of the iterative displacements calculated for that increment so far.

Likewise, the norm of the residual loads is compared to the norms of the incremental, $\|\{\Delta \boldsymbol{R}_{\mathrm{G}}\}^i\|$, and accumulated, $\|\{\boldsymbol{R}_{\mathrm{G}}\}\|$, global right-hand-side load vectors. Typical convergence criteria are usually set such that the iterative displacement norm is less than 1% of both the incremental and accumulated displacement norms, and the residual load norm is less than 1–2% of both the incremental and accumulated global right-hand-side load vector norms. Special attention has to be given to boundary value problems that only involve displacement boundary conditions, as both the incremental and accumulated right-hand-side load vectors are zero.

5.2.4 Comparison of the solution strategies

5.2.4.1 Introduction

A comparison of the three solution strategies presented above suggests the following. The tangent stiffness method is the simplest, but its accuracy is influenced by increment size. The accuracy of the visco-plastic approach is also influenced by increment size, if complex constitutive models are used. The MNR method is potentially the most accurate and is likely to be the least sensitive to increment size. However, considering the computer resources required for each solution increment, the MNR method is likely to be the most expensive, the tangent stiffness method the cheapest and the visco-plastic method probably somewhere in between. It may be possible, though, to use larger and therefore fewer increments with the MNR method to obtain a similar accuracy. Thus, it is not obvious which solution strategy is the most economic for a particular solution accuracy.

Potts and Zdravkovic (1999) provide an extensive comparison of the three methods by considering a range of boundary value problems. Their results for ideal drained and undrained triaxial compression tests are presented here as an example.

5.2.4.2 Idealized triaxial test

Idealized drained and undrained triaxial compression tests were considered. A cylindrical sample was assumed to be isotropically normally consolidated to a mean effective stress, p', of 200 kPa, with zero pore water pressure. The modified Cam clay model was used to represent soil behaviour and the the soil parameters used for the analyses are shown in **Table 5.1**.

Table 5.1 Material properties for the modified Cam clay model

Over-consolidation ratio	1.0
Specific volume at unit pressure on virgin consolidation line, v_1	1.788
Slope of virgin consolidation line in v–$\ln p'$ space, λ	0.066
Slope of swelling line in v–$\ln p'$ space, κ	0.0077
Slope of critical state line in J–p' plane, M_J	0.693
Elastic shear modulus, G/Preconsolidation pressure, p'_o	100

For drained triaxial tests, increments of compressive axial strain were applied to the sample until the axial strain reached 20%, while maintaining a constant radial stress and zero pore water pressure. The results are presented as plots of volumetric strain and deviatoric stress, q, versus axial strain. Deviatoric stress q is defined as

$$\begin{aligned} q = \sqrt{3}J &= \sqrt{\tfrac{1}{2}[(\sigma'_1-\sigma'_2)^2+(\sigma'_2-\sigma'_3)^2+(\sigma'_1-\sigma'_3)^2]} \\ &= \sigma'_1-\sigma'_3 \text{ for triaxial conditions} \end{aligned} \tag{5.23}$$

For the undrained triaxial tests, increments of compressive axial strain were applied to the sample until the axial strain reached 5%, while maintaining the radial total stress constant. A high bulk compressibility of water, K_f, was introduced to ensure undrained behaviour ($= 100\ K'_{\text{skel}}$), where K'_{skel} is the effective bulk modulus of the soil skeleton). The results are presented as plots of pore water pressure, p_f, and q versus axial strain. The label associated with each line in these plots indicates the magnitude of axial strain applied at each increment of that analysis. The tests were deemed ideal as the end effects at the top and bottom of the sample were considered negligible and the stress and strain conditions were uniform throughout. Analytical solutions for both the drained and undrained triaxial tests are given in Potts and Zdravkovic (1999).

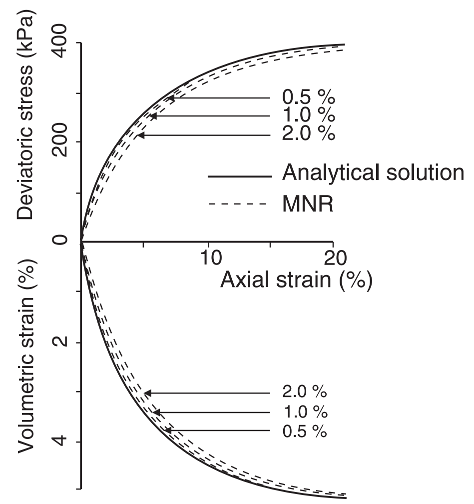

Figure 5.8 Modified Newton–Raphson: drained triaxial test

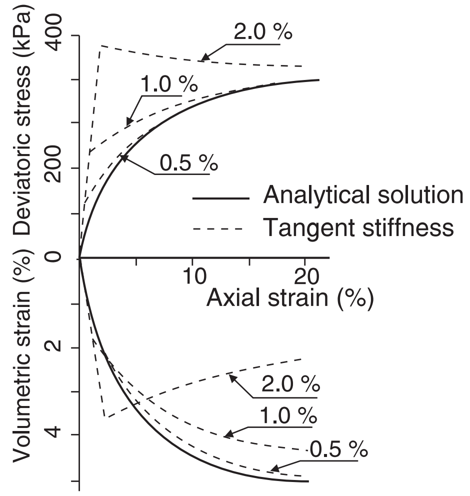

Figure 5.9 Tangent stiffness: drained triaxial test

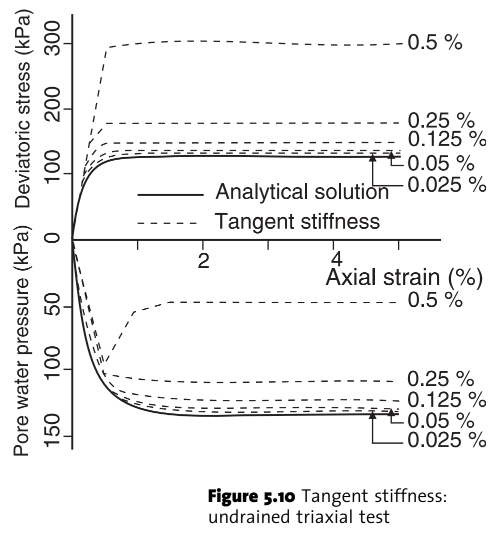

Figure 5.10 Tangent stiffness: undrained triaxial test

Results from the MNR drained triaxial test analyses are compared with the analytical solution in **Figure 5.8**. The results are not sensitive to increment size and agree well with the analytical solution. The MNR undrained triaxial test analyses matched the analytical solution and the errors were negligible, even if the analysis was carried out with just one 5% axial strain increment. Accordingly, the undrained test results are not presented graphically. In an undrained triaxial test the radial and circumferential strains are always equal to minus half of the axial strain. Consequently, all three strains vary proportionally throughout the test. Because such a variation is consistent with the main assumption of a substepping stress point algorithm (see *Section 5.2.3.2.2*), the accuracy of the MNR analysis depends only on the error tolerance controlling the number of substeps. In these analyses the tolerance was set low (i.e. 0.01%), and was the same for all analyses. This explains why the MNR analyses were independent of increment size.

The tangent stiffness results are presented in **Figure 5.9** for the drained test and **Figure 5.10** for the undrained test. The results of both tests are sensitive to increment size, giving very large errors for the larger increment sizes. In both tests, q at failure (20% and 5% axial strain for the drained and undrained tests respectively) is over-predicted. **Figure 5.11** is a plot of p' versus q for the undrained triaxial tests. The analysis with an increment size of 0.5% axial strain gave unrealistic results, predicting an increase in p' and a value of q at failure over twice as large as that of the analytical solution. The analyses with smaller increment sizes gave better results.

The results of the visco-plastic undrained and drained triaxial test analyses are shown in **Figures 5.12** and **5.13** respectively. Inspection of these figures indicates that the solution is also sensitive to increment size. Even the results from the analyses with the smallest increment size of 0.1%, for the drained test, and 0.025%, for the undrained test, are in considerable error.

It is of interest to note that results from the tangent stiffness analyses over-predict the deviatoric stress at any particular value of axial strain for both drained and undrained tests. The opposite is true for the visco-plastic analysis, where q is under predicted in all cases.

For small increment sizes the visco-plastic analyses tend to yield results that are less accurate than the corresponding tangent stiffness analysis, even though the former method requires more computer resources than the latter. Close inspection of the results indicates that the reason for the lack of accuracy of the visco-plastic method is the use of the elasto-plastic equations at illegal stress states outside the yield surface, as explained earlier in this chapter. This results in failure to satisfy the constitutive equations. The MNR approach is more accurate and less dependent on increment size than the other methods.

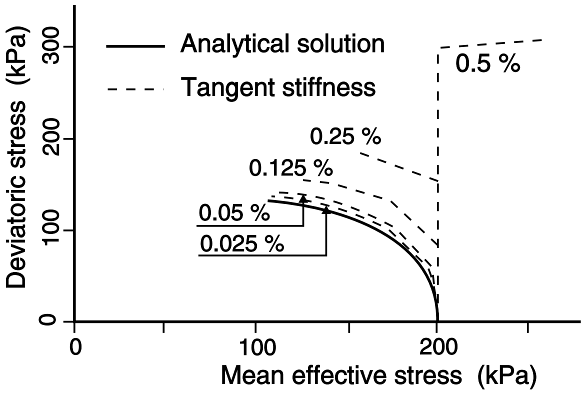

Figure 5.11 Tangent stiffness: undrained stress paths

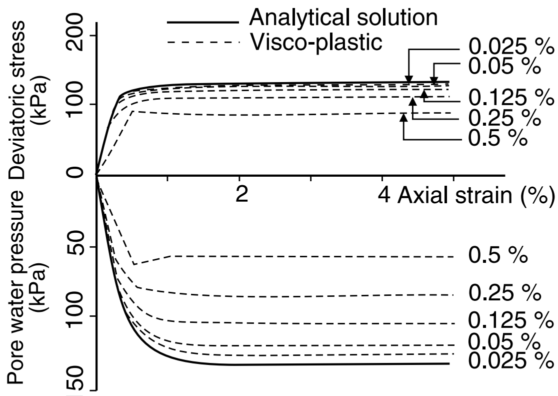

Figure 5.12 Visco-plastic: undrained triaxial test

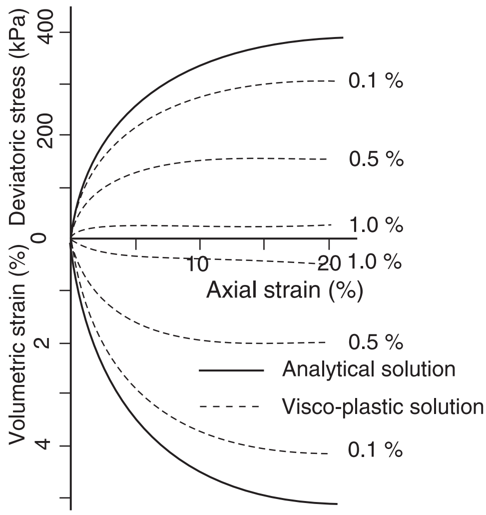

Figure 5.13 Visco-plastic: drained triaxial test

5.3 Geometric non-linearity

The analysis of certain boundary value problems can generate large displacements and strains which, in a finite element implementation, imply a distortion of the original finite element mesh. To deal with these types of problem, the geometry (i.e. finite element mesh) has to be updated during the analysis.

A comprehensive mathematical study of the implications of finite strain on the stress and strain definitions is given by Prager (1961). Attempts to develop complete solution methods have been reported, among others, by Hibbit *et al*. (1970), Hofmeister *et al*. (1971), Osias and Swedlow (1974), Davinson and Chen (1976), Carter *et al*. (1977), Bathe (1982), Van der Heijden and Besseling (1984) and Ziolkowski (1984). Finite strains were coupled with consolidation by, among others, Carter (1977), Carter *et al*. (1977, 1979), Lee and Sills (1981), Booker and Small (1982) and Ziolkowski (1984).

5.3.1 Formulation of the problem

To develop the finite strain formulation, we consider the motion of a general body. As such, the body consists of infinitesimal volumes which have infinitesimal masses. A point within such an infinitesimal volume is called a material point. We assume that during the process of deformation the body under consideration can experience large displacements and large strains. This means that each material point changes its place in space. The aim is to evaluate the equilibrium positions of the complete body at discrete time intervals 0, Δt, $2\Delta t$, . . ., see **Figure 5.14**, where Δt is an increment of time. In this way we follow all the material points of the body in their motion, from the original to the final configuration of the body. This implies the use of

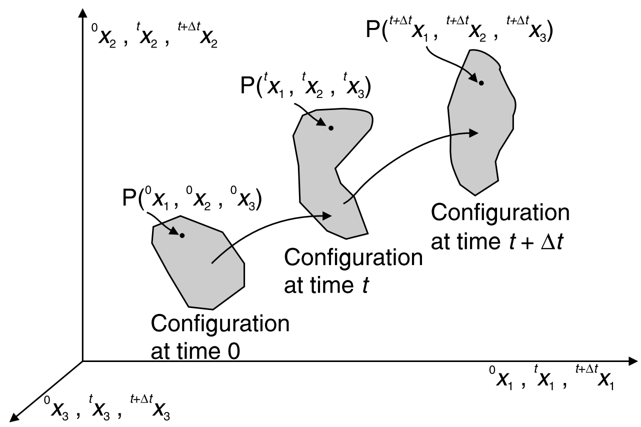

Figure 5.14 Motion of a body in a stationary co-ordinate system

a *Lagrangian* (or material) formulation of the problem, which contrasts with an *Eulerian* formulation (usually used in fluid mechanics problems) in which attention is focused on the motion of the material through a rigid volume. For the analysis of solids, a Lagrangian formulation is more natural than an Eulerian formulation.

A fundamental difficulty in the large strain approach is that the configuration of the body at time $t + \Delta t$ is unknown, which has some important consequences. For example, the Cauchy stress tensor at time $t + \Delta t$ cannot be obtained by simply adding to the Cauchy stress tensor at time t an incremental stress tensor that is due only to the straining of the material. Namely, the calculation of the Cauchy stress tensor at time $t+\Delta t$ must also take into account the rigid body rotation of the material.

The fact that the configuration of the body changes continuously in large deformation analysis is dealt with by using appropriate stress and strain measures and constitutive relations.

5.3.2 Stress and strain tensors

As mentioned in the previous section, in large strain analysis special attention must be given to the fact that the configuration of the body is continuously changing.

One way of dealing with this problem is the use of auxiliary stress and strain measures. Such a stress measure is the *second Piola–Kirchhoff stress tensor*, which defines stresses on the original configuration of a body but uses a deformation gradient to account for the change in mass (Bathe (1982))

$$ {}_{o}^{t}S_{ij} = \frac{{}^{o}\rho}{{}^{t}\rho} \frac{\partial^{o}x_i}{\partial^{t}x_k} {}^{t}\sigma_{kl} \frac{\partial^{o}x_j}{\partial^{t}x_l} \qquad (5.24)$$

where:

${}_{o}^{t}S_{ij}$ is the second Piola–Kirchhoff tensor at time t referred to the configuration at time o (i.e. the original configuration);
$\partial^{o}x_i/\partial^{t}x_j$ is a deformation gradient from time o to time t;
${}^{o}_{\rho}/{}^{t}\rho$ is the ratio of mass densities at time o and time t;
However, the second Piola–Kirchhoff stress tensor has little physical meaning and, in practice, the Cauchy stress tensor must be calculated.

Another stress measure that is effectively used in some formulations is the *Jaumann stress rate tensor*, defined as

$$\hat{\sigma}_{ij} = \dot{\sigma}_{ij} - \sigma_{ik}\Omega_{kj} - \sigma_{jk}\Omega_{ki} \qquad (5.25)$$

where:

$\dot{\sigma}_{ij}$ is the time derivative of the Cauchy stress tensor;
Ω_{ij} is the spin tensor

$$\Omega_{ij} = \tfrac{1}{2}\left(\frac{\partial\,\dot{u}_j}{\partial x_i} - \frac{\partial\,\dot{u}_i}{\partial x_j}\right) \tag{5.26}$$

In Equation (5.26) the velocity $\dot{u}_i$ is the time derivative of the displacement

$$\dot{u}_i = \frac{\partial u_i}{\partial t} \tag{5.27}$$

Physically, the spin tensor represents the angular velocity of the material. Therefore, in Equation (5.25), if $\hat{\boldsymbol{\sigma}}_{ij}$ is zero, then the change in the Cauchy stress tensor is a result of the rigid body rotation of the material.

The important difference between the two stress measures is that the second Piola–Kirchhoff tensor is a total stress tensor that can be calculated from the total current strains (Bathe, 1982), whereas the Jaumann stress rate tensor is related to the rate of straining, which means that an integration process is always required to evaluate the current Cauchy stresses. This difference automatically indicates under what conditions it is more efficient to employ one or the other stress measure. If the constitutive relations are not path dependent and thus do not require an integration process, then the second Piola–Kirchhoff stress tensor is usually more appropriate. However, for the analysis of path-dependent materials the use of the Jaumann stress rate tensor should be considered.

Having discussed briefly the possible stress measures for treating problems that have a continuously changing configuration, it is also necessary to discuss appropriate strain measures. The strain tensor used with the second Piola–Kirchhoff stress tensor is the *Green–Lagrange strain tensor*, defined as

$${}^{t}_{o}\varepsilon_{ij} = \frac{1}{2}\left(\frac{\partial^{t} u_i}{\partial^{o} x_j} + \frac{\partial^{t} u_j}{\partial^{o} x_i} + \frac{\partial^{t} u_k}{\partial^{o} x_i}\frac{\partial^{t} u_k}{\partial^{o} x_j}\right) \tag{5.28}$$

which is a strain tensor in the current configuration (i.e. at time t), referred to the original configuration (i.e. at time 0).

With the Jaumann stress rate tensor it is appropriate to use the *velocity strain tensor*, or rate of deformation tensor

$$l_{ij} = \frac{1}{2}\left(\frac{\partial\,{}^{t}\dot{u}_i}{\partial^{t} x_j} + \frac{\partial\,{}^{t}\dot{u}_j}{\partial^{t} x_i}\right) \tag{5.29}$$

where $\dot{u}_i$ is the velocity, as expressed by Equation (5.27).

Further considerations of the large strain formulation in this handbook will be based on the Jaumann stress rate tensor and the velocity strain tensor.

5.3.3 Numerical implementation

For the solution of the non-linear finite strain problem an incremental formulation is usually employed, similar to the infinitesimal strain formulation. This means that the loading is divided into small increments which are solved sequentially. The configuration of the problem is thus fully defined at the start of each increment. The solution of a typical increment will be described in this section. In the notation that follows, a left superscript will denote the time at which the variables are evaluated. The time at the beginning of an increment is t, and at the end of an increment it is $t+\Delta t$.

The basic problem in a general non-linear analysis is to find the state of equilibrium of a body which corresponds to the applied loads. If the body under consideration is in equilibrium, then

$$ {}^{t}\boldsymbol{R} - {}^{t}\psi = 0 \tag{5.30} $$

where ${}^{t}\boldsymbol{R}$ is the vector of the externally applied nodal forces at time t and ${}^{t}\boldsymbol{\Psi}$ is the vector of nodal forces that correspond to the element stresses in configuration t. The basic approach in an incremental solution is to assume that the solution for the discrete time t is known and that the solution for the discrete time $t+\Delta t$ is required. Hence, from (5.30), the condition is that

$$ {}^{t+\Delta t}\boldsymbol{R} - {}^{t+\Delta t}\boldsymbol{\Psi} = 0 \tag{5.31} $$

Since the solution is known at time t, we can write

$$ {}^{t+\Delta t}\boldsymbol{\Psi} = {}^{t}\boldsymbol{\Psi} + \Delta\boldsymbol{\Psi} \tag{5.32} $$

where $\Delta\boldsymbol{\Psi}$ is the increment of nodal forces, corresponding to the increment of element displacements and stresses from time t to time $t+\Delta t$. This vector can be approximated by using a tangent stiffness matrix ${}^{t}\mathbf{K}_{G}$, which corresponds to the geometric and material conditions at time t

$$ \Delta\boldsymbol{\Psi} \cong {}^{t}\mathbf{K}_{G}\ \Delta\boldsymbol{d} \tag{5.33} $$

where $\Delta\boldsymbol{d}$ is the vector of incremental nodal displacements. Theoretically, ${}^{t}\mathbf{K}_{G}$ should be calculated in the same manner as for small displacement analysis and then augmented by further terms associated with the current stress state (see Bathe, 1982). However, in practice, if a modified Newton–Raphson solution strategy is used, these additional terms can be neglected, as they can be implicitly accounted for by the right-hand-side correction. Substituting Equation (5.33) into (5.32) and (5.31) gives

$$ {}^{t}\mathbf{K}_{G}\Delta\boldsymbol{d} = {}^{t+\Delta t}\mathbf{R} - {}^{t}\boldsymbol{\Psi} \tag{5.34} $$

Solving Equation (5.34) for $\Delta\boldsymbol{d}$ we can calculate an approximation for the displacements at time $t+\Delta t$

$$ {}^{t+\Delta t}\boldsymbol{d} \cong {}^{t}\boldsymbol{d} + \Delta\boldsymbol{d} \tag{5.35} $$

The exact displacements at time $t+\Delta t$ are those corresponding to the applied loads ${}^{t+\Delta t}\mathbf{R}$. In Equation (5.35) we calculate only the approximate displacements because Equation (5.33) was used. From these approximate displacements at time $t+\Delta t$ we can now calculate approximate stresses and strains at time $t+\Delta t$. However, because of the assumption in Equation (5.33), these stresses and strains can be in error, and condition (5.31) will not be satisfied. Therefore, it is necessary to iterate the displacement solution until Equation (5.31) is satisfied with sufficient accuracy. The iteration procedure usually employed is the modified Newton–Raphson method. The problem solution is then based on the following equations

$$ {}^{t}\mathbf{K}\Delta\boldsymbol{d}^{(i)} = {}^{t+\Delta t}\mathbf{R} - {}^{t+\Delta t}\boldsymbol{\Psi}^{(i)} \tag{5.36} $$

$$ {}^{t+\Delta t}\boldsymbol{d}^{(i)} = {}^{t+\Delta t}\boldsymbol{d}^{(i-1)} + \Delta\boldsymbol{d}^{(i)} \tag{5.37} $$

with the initial conditions

$$ {}^{t+\Delta t}\boldsymbol{d}^{(0)} = {}^{t}\boldsymbol{d}; \qquad {}^{t+\Delta t}\boldsymbol{\Psi}^{(0)} = {}^{t}\boldsymbol{\Psi} \tag{5.38} $$

A superscript in brackets on the right-hand side denotes the number of iterations for one solution increment.

In the practical use of the iteration procedure given by Equations (5.36) to (5.38), the convergence properties of the iteration are most important and appropriate convergence criteria must be employed. Consequently, the major differences between small and large deformation finite element analyses are that the Jaumann stress rate tensor must be employed and that account must be taken of the change in geometry when performing various element integrations.

5.3.4 Pitfalls

A potential pitfall when performing large displacement analyses is the use of stress boundary conditions. When such conditions are used, the finite element software must convert the boundary stresses to equivalent nodal forces by integrating the stress over the sides of the elements over which it has been applied. In a small displacement analysis this can be done for the increment that the stress is applied and, as the mesh geometry is assumed not to change, the nodal forces remain constant throughout the analysis. This is not so for a large displacement analysis for, if the stress is constant and the geometry changes, then so will the equivalent nodal forces. The software therefore needs to continually adjust the nodal forces to account for the changing size of the element sides over which the boundary stress is applied. This in turn requires the software to maintain a permanent record of all applied boundary stresses. Such bookkeeping is not trivial in analyses involving excavation and/or construction.

As an example, consider the analysis of an ideal triaxial test. As there are no end effects, behaviour throughout the sample is uniform and therefore a single 4-noded finite element can be used to model the sample (see **Figure 5.15(a)**). If at the start of the analysis a uniform all-round cell pressure of 100 kPa is applied to the sample, the equivalent nodal forces are as shown in **Figure 5.15(b)**. If the sample behaves undrained, there will be no volume change and hence no distortion of the sample. The nodal forces will therefore remain constant. If the sample is now strained vertically so that it shortens by 20%, with the cell pressure kept constant, then vertical nodal displacements must be applied to the nodes along the top of the element. As the sample shortens then so does the vertical height of the element side over which the cell pressure is applied. This means that the equivalent nodal forces due to the cell pressure will change. For example, the values consistent with a 20% shortening are given in **Figure 5.15(c)**. Consequently, it is necessary to constantly adjust the horizontal nodal forces equivalent to the cell pressure as the analysis proceeds. If this is not done and the nodal forces applied in the first stage of the test are left unchanged, the horizontal stress in the sample will increase from 100 kPa to 110 kPa after the 20% shortening.

Another problem frequently encountered in large displacement analyses is ill conditioning, due to severely distorted elements. As the geometry of the finite element mesh is continually updated the shapes of the elements change as the analysis proceeds. In areas of intense straining this can result in elements with large aspect ratios.

As an example, consider the problem of a soil sample squashed between two rough plates (**Figure 5.16(a)**). The soil is modelled as a Tresca material with $S_u = 100$ kPa, $E = 10^5$ kPa, $\mu = 0.3$. The initial finite element mesh is shown in **Figure 5.16(b)**, and the distorted mesh (plotted to natural scale) at various stages of the analysis in **Figure 5.17(a)**, **(b)**, **(c)** and **(d)**. Severe distortion

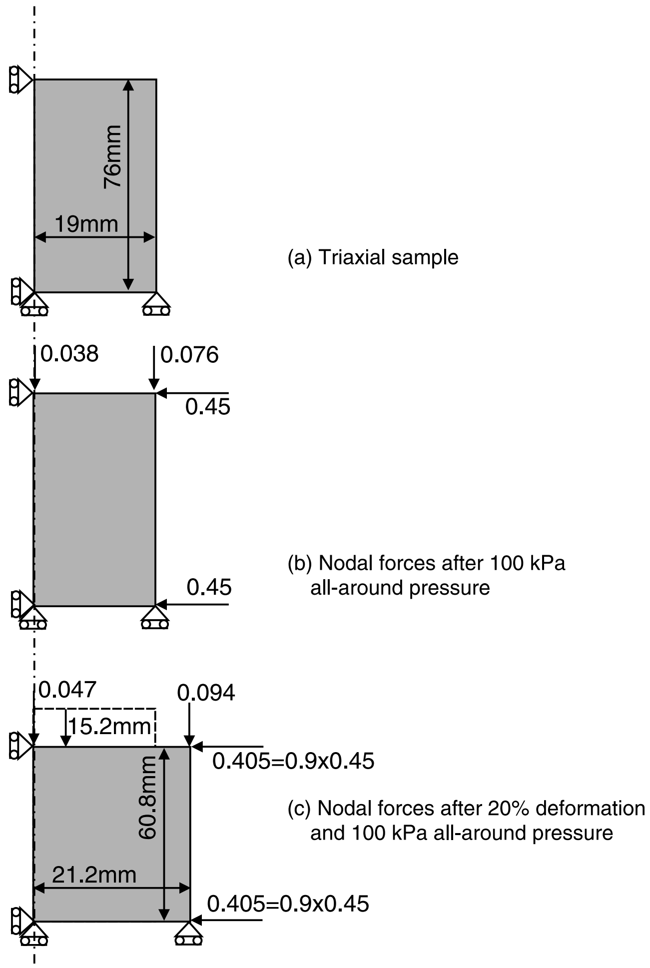

Figure 5.15 Large displacement analysis of a triaxial test

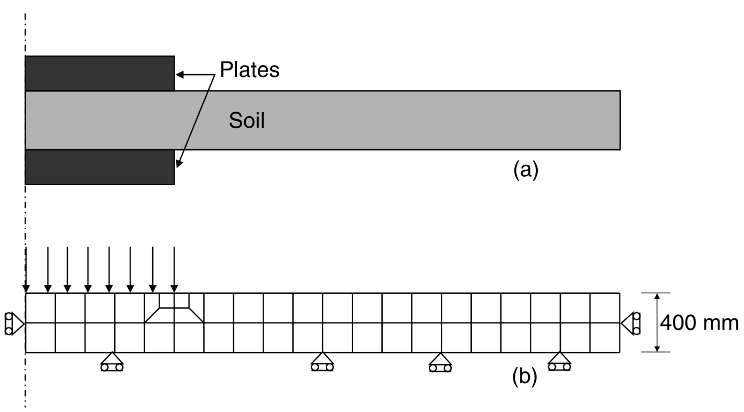

Figure 5.16 Problem of a soil squashed between two rigid plates

of the elements adjacent to the edge of the plate is clearly evident. Such distortion degrades the accuracy of the analysis. In fact the analysis had to be aborted when the vertical displacement of the plate was 200 mm, as a negative Jacobian was calculated for one of the severely distorted elements. This indicates that this element had managed to turn itself inside out.

Potentially there are two options available to overcome this problem. Firstly an Eulerian, as opposed to a Lagrangian, large displacement formulation could be used. Secondly, a new mesh could be constructed once the old mesh had distorted a prescribed amount. This is known as re-meshing. Unfortunately, both of these options have associated problems and drawbacks.

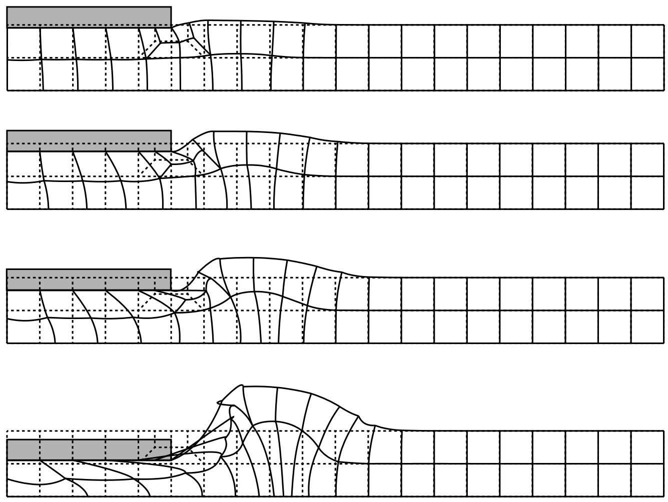

Figure 5.17 Deformation of mesh during displacement analysis of soil squashed between two plates

5.4 Coupled consolidation analysis

5.4.1 Introduction

The basic theory behind most numerical methods considers the mechanical behaviour of the soil; consequently only fully drained or undrained soil behaviour can be considered. While many geotechnical problems can be solved by adopting such extreme soil conditions, real soil behaviour is usually time related, with the pore water pressure response dependent on soil permeability, the rate of loading and the hydraulic boundary conditions. To account for such behaviour it is necessary to combine the equations governing the flow of pore fluid through the soil skeleton with the equations governing the deformation of the soil due to loading. Such theory is called *coupled*, as it essentially couples pore fluid flow and stress strain behaviour together.

As the flow of water within the soil skeleton is now being considered, the hydraulic boundary conditions that control it must be accounted for. These boundary conditions consist of either prescribed flows or changes in pore fluid pressure. Some of the boundary conditions relevant to geotechnical engineering are described in *Chapter 7*.

For the finite element method the governing equations may now be written in the following incremental matrix form

$$\begin{bmatrix} [\mathbf{K}_\mathrm{G}] & [\mathbf{L}_\mathrm{G}] \\ [\mathbf{L}_\mathrm{G}]^\mathrm{T} & -\beta\Delta t[\boldsymbol{\Phi}_\mathrm{G}] \end{bmatrix} \begin{Bmatrix} \{\Delta \boldsymbol{d}\}_{\mathrm{nG}} \\ \{\Delta \boldsymbol{p}_\mathrm{f}\}_{\mathrm{nG}} \end{Bmatrix} = \begin{Bmatrix} \{\Delta \mathbf{R}_\mathrm{G}\} \\ \left([\mathbf{n}_\mathrm{G}] + Q + [\boldsymbol{\Phi}_\mathrm{G}](\{\boldsymbol{p}_\mathrm{f}\}_{\mathrm{nG}})_1\right)\Delta t \end{Bmatrix} \tag{5.39}$$

where

$$[\mathbf{K}_\mathrm{G}] = \sum_{i=1}^{N} [\mathbf{K}_\mathrm{E}]_i = \sum_{i=1}^{N} \left(\int_{Vol} [\mathbf{B}]^\mathrm{T} [\mathbf{D}'] [\mathbf{B}] \mathrm{d}Vol \right)_i \tag{5.40}$$

$$[\mathbf{L}_\mathrm{G}] = \sum_{i=1}^{N} [\mathbf{L}_\mathrm{E}]_i = \sum_{i=1}^{N} \left(\int_{Vol} \{\mathbf{m}\} [\mathbf{B}]^\mathrm{T} [\mathbf{N}_\mathrm{p}] \mathrm{d}Vol \right)_i \tag{5.41}$$

$$\{\Delta \mathbf{R}_\mathrm{G}\} = \sum_{i=1}^{N} \{\Delta \mathbf{R}_\mathrm{E}\}_i = \sum_{i=1}^{N} \left[\left(\int_{Vol} [\mathbf{N}]^\mathrm{T} \{\Delta F\} \mathrm{d}Vol \right)_i + \left(\int_{Srf} [\mathbf{N}]^\mathrm{T} \{\Delta \mathbf{T}\} \mathrm{d}Srf \right)_i \right] \tag{5.42}$$

$$\{m\}^\mathrm{T} = \{1 \quad 1 \quad 1 \quad 0 \quad 0 \quad 0\} \tag{5.43}$$

$$[\mathbf{\Phi_G}] = \sum_{i=1}^{N} [\mathbf{\Phi_E}]_i = \sum_{i=1}^{N} \left[\int_{Vol} \frac{[\mathbf{E}]^T [\mathbf{k}] [\mathbf{E}]}{\gamma_f} \mathrm{d}Vol \right)_i \tag{5.44}$$

$$[\mathbf{n_G}] = \sum_{i=1}^{N} [\mathbf{n_E}]_i = \sum_{i=1}^{N} \left(\int_{Vol} [\mathbf{E}]^T [\mathbf{k}] \{i_G\} \mathrm{d}Vol \right)_i \tag{5.45}$$

[**B**] is the strain matrix containing derivatives of the shape functions [**N**] defining the variation of displacement across the element, [**E**] is a matrix containing the derivatives of the shape functions [$\mathbf{N}_p$] defining the variation of pore water pressures across the element, [**D**] is the constitutive matrix, [**k**] the permeability matrix, $\{\Delta \boldsymbol{F}\}$ the incremental body forces, $\{\Delta \boldsymbol{T}\}$ the incremental surface tractions, $\{\Delta \boldsymbol{d}\}_{nG}$ the incremental nodal displacements, $\{\Delta \boldsymbol{p}_f\}_{nG}$ the incremental nodal pore water pressures, γ_f the bulk unit weight of water, $\{\boldsymbol{i}_G\}$ the unit vector defining the direction of gravity and Δt the increment of time.

To obtain these equations it has been necessary to assume how the pore water pressure varies over the time increment Δt. This is controlled by the parameter β (see Potts and Zdravkovic, 1999). For numerical stability $\beta \geq 0.5$ and for a fully implicit approximation $\beta = 1$. Most software packages allow the user to choose a value for β. It is because of this approximation that the governing equations are expressed in an incremental form.

5.4.2 Implementation

Equation (5.39) provides a set of simultaneous equations in terms of the incremental nodal displacements $\{\Delta \boldsymbol{d}\}_{nG}$ and incremental nodal pore fluid pressures $\{\Delta \boldsymbol{p}_f\}_{nG}$. Once the stiffness matrix and right-hand-side vector have been assembled, the equations can be solved.

As a marching procedure is necessary to solve for the time-dependent behaviour, the analysis must be performed incrementally. This is necessary even if the constitutive behaviour is linear elastic, the permeabilities are constant and geometric non-linearity is not considered. If the constitutive behaviour is non-linear and/or geometric non-linearity is to be accounted for, the time steps can be combined with changes in the loading conditions so that the complete time history of construction can be simulated.

In the above formulation the permeabilities have been expressed by the matrix [**k**]. If these permeabilities are not constant but vary with stress or strain, the matrix [**k**] (and therefore [$\mathbf{\Phi}_G$] and [$\mathbf{n}_G$]) are not constant over an increment of an analysis (and/or a time step). Care must therefore be taken when solving Equation (5.39). This problem is similar to that associated with non-linear stress–strain behaviour where [$\mathbf{K}_G$] is not constant over an increment. As noted above there are several numerical procedures available for dealing with a non-linear [$\mathbf{K}_G$], and, as demonstrated, some of these are more efficient than others. All the procedures described above (e.g. tangent stiffness, visco-plastic and Newton–Raphson) can be modified to accommodate non-linear permeability.

In deriving Equation (5.39), the incremental pore fluid pressure within an element has been related to the values at the nodes using the matrix of pore fluid shape functions [$\mathbf{N}_p$]. If an incremental pore fluid pressure degree of freedom is assumed at each node of every consolidating element, [$\mathbf{N}_p$] is the same as the matrix of displacement shape functions [**N**]. Consequently, pore fluid pressures vary across the element in the same fashion as the displacement components. For example, for an eight-noded quadrilateral element, both the displacements and pore fluid pressures vary quadratically across the element. However, if the displacements vary quadratically, the strains, and therefore the effective stresses (at least for a linear material), vary linearly. There is therefore an inconsistency between the variation of effective stresses and pore water pressures across the element. While this is theoretically acceptable, some users prefer to have the same order of variation of both effective stresses and pore water pressure. For an eight-noded element this can be achieved by having pore fluid pressure degrees of freedom only at the four corner nodes (see **Figure 5.18**). This will result in the [$\mathbf{N}_p$] matrix having contributions from only the corner nodes and therefore differing from [$\mathbf{N}$]. Similar behaviour can be achieved by having pore fluid pressure degrees of freedom only at the three apex nodes of a six-noded triangle, or at the eight corner nodes of a twenty-noded hexahedron. Some software programs allow the user to decide which of these two approaches to use.

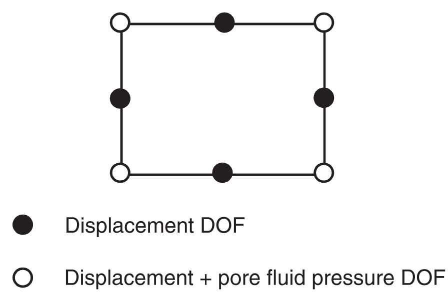

Figure 5.18 Degrees of freedom for an eight-noded element

It is possible to have some elements within a finite element mesh which are consolidating and some which are not. For example, if a situation where sand overlies clay is being modelled, consolidating elements (i.e. elements with pore pressure degrees of freedom at their nodes) might be used for the clay, whereas ordinary elements (i.e. no pore fluid pressure degrees of freedom at the nodes) might be used for the sand (see **Figure 5.19**). The sand is then assumed to behave in a drained manner by specifying a zero value for the bulk compressibility of the pore fluid. Clearly, care has to be taken to ensure the correct hydraulic boundary condition is applied to the nodes at the interface between clay and sand. Some software programs insist that the user decides which elements are to consolidate and which are not at the mesh generation stage. Others are more flexible and allow the decision to be made during the analysis stage.

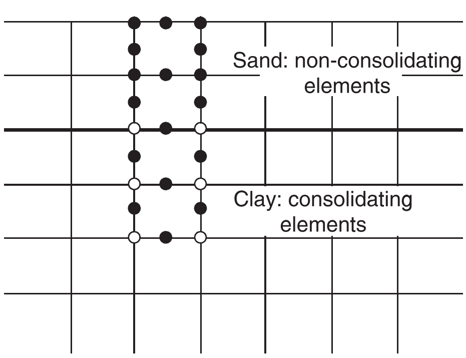

Figure 5.19 Choice of elements for consolidating and non-consolidating layers

In the theory developed above, the finite element equations have been formulated in terms of pore fluid pressure. It is also possible to formulate the equations in terms of hydraulic head, excess pore fluid pressure or excess hydraulic head. In such cases the hydraulic head, excess pore fluid pressure or excess head at the nodes will become degrees of freedom. It is important that the user is familiar with the approach adopted by the software being used, as this will affect the manner in which the hydraulic boundary conditions are specified. It should also be noted that Equation (5.39) assumes that the soil is fully saturated. If partial saturation is to be considered, extra terms must be added to Equation (5.39). One of the consequences of these extra terms is that the final stiffness matrix becomes non-symmetric.

6

Modelling structures and interfaces

6.1 Introduction

Many geotechnical problems involve the interaction between structures and soil. Consequently, in numerical analyses of these problems it is necessary to model both the structure, the ground and the interface between them. For example, when analysing tunnelling problems it is important to realistically model the tunnel lining and its interface with the soil. If the lining is of the segmental type, it will also be necessary to realistically model the interfaces between the segments. In many cases this involves the use of special facilities. For example, in finite element analysis special elements can be used in addition to the conventional continuum elements. This chapter discusses some of the more common assumptions used for modelling structural members and their interface with the soil.

6.2 Modelling structural components

6.2.1 Introduction

Many geotechnical problems involve soil–structure interaction (see **Figure 6.1**). Therefore, when applying numerical analysis to such problems it is necessary to include the structural components, e.g. retaining walls, props, anchors, tunnel linings, foundations, etc., in the finite element mesh (or finite difference grid). In theory, it is possible to use conventional 2D or 3D continuum elements to model these structural components, but in practice this can have drawbacks. For example, in many situations the dimensions of the structural elements are small compared to the overall geometry and therefore to model them with 2D/3D continuum elements would result in either a very large number of elements, or elements with unacceptable aspect ratios. Similar problems arise with finite difference grids.

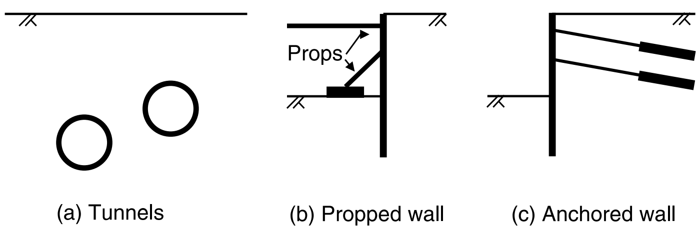

Figure 6.1 Examples of soil–structure interaction

In many instances the interest is not in the detailed distribution of stresses within the structural members but in the distribution of averaged quantities such as bending moments, axial and shear forces. These can be obtained from the stresses within the 2D/3D continuum elements, but additional calculations are required.

To overcome these shortcomings, special finite elements have been developed. These elements are formulated by essentially collapsing one or more dimensions of the structural component to zero. For example, a retaining wall can be modelled using a beam element that has no width. The element is formulated directly in terms of bending moments, axial and shear forces and their associated strains. Consequently, the quantities of engineering interest come directly from the finite element analysis.

There are several different formulations available in the literature for these special structural elements, each of which has advantages and disadvantages. Care must therefore be exercised when using such elements in order to ensure that an appropriate element is used for the problem being investigated. To illustrate the approximations that are made when developing these structural elements, a two-dimensional beam element will be considered (Day and Potts, 1990; Potts and Zdravkovic, 1999).

6.2.2 Strain definitions

The strains for this particular beam element, shown in **Figure 6.2**, are defined as follows (Day, 1990):

Axial strain:

$$\varepsilon_l = -\frac{du_l}{dl} - \frac{w_l}{R} \tag{6.1}$$

Bending strain

$$\chi_l = \frac{d\theta}{dl} \tag{6.2}$$

Shear strain

$$\gamma = \frac{u_l}{R} - \frac{dw_l}{dl} + \theta \tag{6.3}$$

where l is the distance along the beam, u_l and w_l are the displacements tangential and normal to the beam, R is the radius of curvature, and θ is the cross-section rotation. Definitions (6.1) to (6.3) are for a compression-positive sign convention.

It is useful to rewrite Equations (6.1) to (6.3) in terms of the displacements u and v in the global x_G and y_G co-ordinate directions. The transformation of displacements from global to local components is given by

$$\left.\begin{aligned} u_l &= v\sin\alpha + u\cos\alpha \\ w_l &= v\cos\alpha - u\sin\alpha \end{aligned}\right\} \tag{6.4}$$

and noting that (Figure 6.2)

$$\frac{d\alpha}{dl} = -\frac{1}{R} \tag{6.5}$$

gives the following expressions for Equations (6.1) to (6.3) in terms of the global displacements:

Axial strain

$$\varepsilon_l = -\frac{du}{dl}\cos\alpha - \frac{dv}{dl}\sin\alpha \tag{6.6}$$

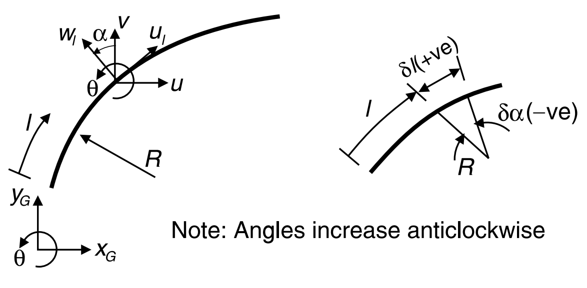

Figure 6.2 Definition of terms and axes

Bending strain

$$\chi_l = \frac{d\theta}{dl} \tag{6.7}$$

Shear strain

$$\gamma = \frac{du}{dl}\sin\alpha - \frac{dv}{dl}\cos\alpha + \theta \tag{6.8}$$

While the above strain terms are sufficient for plane strain analysis, additional terms are required for axisymmetric analysis (Day, 1990):

Circumferential membrane strain

$$\varepsilon_\psi = \frac{w_l \sin\alpha - u_l \cos\alpha}{r_o} = -\frac{u}{r_o} \tag{6.9}$$

Circumferential bending strain

$$\chi_\psi = \frac{\theta\cos\alpha}{r_o} \tag{6.10}$$

where r_o is the circumferential radius (see **Figure 6.3**), and u and v are redefined as the displacements in the directions normal and parallel to the axis of revolution.

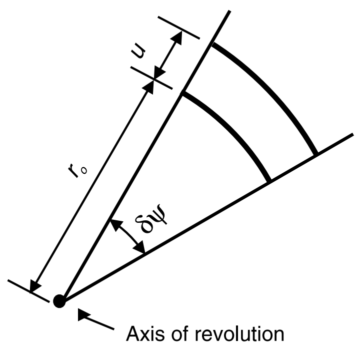

Figure 6.3 Definition of r_o

The major approximation in the above is that the beam geometry can be modelled as having zero thickness and therefore be represented by a line and that the deformation can be expressed in terms of two displacement components u_1 and w_1 (or u and w) and the rotation θ. This in turn implies that cross-sections of the beam remain plane when the beam is deformed. Other, more subtle, implications also arise from the basic assumptions.

For 3D analyses the equivalent structural forms to beams are shells and plates (flat shells). Again these can be modelled by collapsing their thickness to zero and representing them as two-dimensional surfaces. However, the strain formulations become complex and have to be expressed in terms of three displacement components and three rotations.

6.2.3 Constitutive equation

The strain terms presented above are related to the element forces and bending moments by the expression

$$\{\Delta\sigma\} = [\mathbf{D}]\{\Delta\varepsilon\} \tag{6.11}$$

where $\{\Delta\varepsilon\} = [\Delta\varepsilon_l, \Delta\chi_l, \Delta\gamma, \Delta\varepsilon_\psi, \Delta\chi_\psi]^T$, $\{\Delta\sigma\} = [\Delta F, \Delta M, \Delta S, \Delta F_\psi, \Delta M_\psi]^T$, with the incremental components being: ΔF, the meridional force; ΔM, the bending moment; ΔS, the shear force; ΔF_ψ, the circumferential force; and ΔM_ψ, the circumferential bending moment. For plane strain analysis ΔF is the incremental in-plane axial force, ΔF_ψ is the incremental out-of-plane force and $\Delta\varepsilon_\psi = \Delta\chi_\psi = 0$.

For isotropic linear elastic behaviour, the [**D**] matrix takes the form

$$[\mathbf{D}] = \begin{bmatrix} \dfrac{EA}{(1-\mu^2)} & 0 & 0 & \dfrac{EA\mu}{(1-\mu^2)} & 0 \\ 0 & \dfrac{EI}{(1-\mu^2)} & 0 & 0 & \dfrac{EI\mu}{(1-\mu^2)} \\ 0 & 0 & kGA & 0 & 0 \\ \dfrac{EA\mu}{(1-\mu^2)} & 0 & 0 & \dfrac{EA}{(1-\mu^2)} & 0 \\ 0 & \dfrac{EI\mu}{(1-\mu^2)} & 0 & 0 & \dfrac{EI}{(1-\mu^2)} \end{bmatrix} \qquad (6.12)$$

The beam (or shell) properties are the moment of inertia I and cross-sectional area A. In plane strain and axisymmetric analysis these are specified for a unit width of the beam (or shell). E and μ are the Young's modulus and Poisson's ratio and k is a shear correction factor.

The distribution of shear stress across the cross-sectional area of a beam (or shell) in bending is non-linear. The beam element formulation, however, uses a single value to represent the shear strain. The correction factor k is a factor applied to the cross-sectional area so that the strain energy in the finite element model, calculated over the area kA, is equal to the actual strain energy over the area A. The shear correction factor is dependent on the shape of the cross-section. For a rectangular section, $k = 5/6$. Bending deflections of slender beams dominate their behaviour and the solution is very insensitive to the value of k.

For 3D shell and plate elements there are eight strains and eight conjugate forces. The constitutive matrix is therefore represented by an 8×8 matrix.

If plastic behaviour is modelled, then either the constitutive behaviour must be expressed in terms of forces and strains to be consistent with Equation (6.11), or more complex formulations for the beam/shell elements must be used.

Finite elements developed using the above basic formulation can suffer from a phenomenon known as shear and membrane locking. This occurs when full Gauss integration is used to perform the volume integrals and is indicated by widely fluctuating axial and shear forces. It is often claimed that this problem can be avoided by using a selected reduced integration scheme in which some of the strain terms are integrated with a lower-order integration scheme than the others. However, this may not be the case for curved beam or shell elements and in such cases it may be necessary to resort to a reduced integration scheme. Clearly, judgements based on past experience must be made.

6.2.4 Membrane elements

The beam element described above can be degenerated to form another element which cannot transmit bending moments or shear forces. In plane strain and axisymmetric analyses it is a pin-ended membrane element, capable of transmitting forces tangential to the surface only (membrane forces). It is essentially a spring, but differs from a spring in that it can be curved, and it is treated in the same way as all other elements in the analysis.

This element has two degrees of freedom per node: the displacements u and v in the global x_G and y_G directions respectively. In plane strain analysis the element has only one strain term, the longitudinal strain ε_l, given by

$$\varepsilon_l = -\frac{\mathrm{d}u_l}{\mathrm{d}l} - \frac{w_l}{R} \tag{6.13}$$

In axisymmetric analysis the additional circumferential strain is given by

$$\varepsilon_\psi = -\frac{u}{r_o} \tag{6.14}$$

These definitions are the same as for beam elements (Equations (6.1) and (6.9)).

The terms in the constitutive matrix [**D**], are equal to the corresponding terms in the beam element constitutive matrix and are as follows

$$[\mathbf{D}] = \begin{bmatrix} \dfrac{EA}{(1-\mu^2)} & \dfrac{EA\mu}{(1-\mu^2)} \\ \dfrac{EA\mu}{(1-\mu^2)} & \dfrac{EA}{(1-\mu^2)} \end{bmatrix} \tag{6.15}$$

The advantages of using an element of this type as opposed to the use of spring boundary conditions (which are discussed in *Chapter 7*) are:

- Different behaviour can easily be specified through a constitutive law and an elasto-plastic formulation. For example, a maximum axial force may be specified by a yield function, F, of the form F = axial force $\pm$ constant.
- In axisymmetric analysis, hoop forces can provide significant restraint. These are included in an analysis by using membrane elements. Spring boundary conditions do not account for the effect of hoop forces.

Membrane elements are useful for the analysis of soil–structure interaction problems. A constitutive law that does not allow tension can be used to model pin-ended retaining wall props that fall out if the wall moves away from the prop after installation. An element which can only resist tensile forces (i.e. not compression) can be used to model flexible reinforcing strips, such as geofabrics, embedded in the soil.

It is a relatively easy matter to extend the above formulation to three dimensions, in which case there are two in-plane direct strains, a shear strain and corresponding direct and shear membrane forces. It is also possible to formulate both the 2D and 3D elements in terms of membrane stresses as opposed to membrane forces. In such a situation the terms in the [**D**] matrix given by Equation (6.15) are divided by A which represents the thickness of the membrane.

6.3 Modelling interfaces

6.3.1 Introduction

In any soil–structure interaction situation, relative movement of the structure with respect to the soil can occur. The use of continuum elements, with compatibility of displacements, in a finite element analysis of these situations prohibits relative movement at the soil–structure interface (**Figure 6.4**). Nodal compatibility of the finite element method constrains the adjacent structural and soil elements to move together. Interface elements, or joint elements as they are sometimes called, can be used to model the soil–structure boundary such as the sides of a wall or pile, or the underside of a footing. Particular advantages are the ability to vary the constitutive behaviour of the soil–structure interface (i.e. the maximum wall friction angle) and to allow differential movement of the soil and the structure, i.e. slip and separation. Many methods have been proposed to model discontinuous behaviour at the soil–structure interface, as listed below.

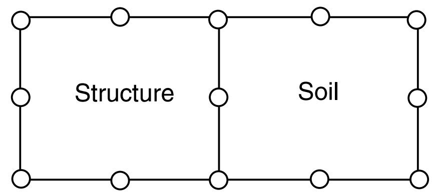

Figure 6.4 Soil–structure interface using continuum elements

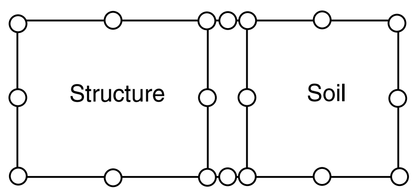

Figure 6.5 Use of continuum elements to model interface

- Use of thin continuum elements with standard constitutive laws (Pande and Sharma, 1979; Griffiths, 1985) (**Figure 6.5**).
- Linkage elements in which only the connections between opposite nodes are considered (Hermann, 1978; Frank *et al*., 1982). Usually opposite nodes are connected by discrete springs (**Figure 6.6**).
- Special interface or joint elements of either zero or finite thickness (Goodman *et al*., 1968; Ghaboussi *et al*., 1973; Carol and Alonso, 1983; Wilson, 1977; Desai *et al*., 1984; Beer, 1985) (**Figure 6.7**).
- Hybrid methods where the soil and structure are modelled separately and linked through constraint equations to maintain compatibility of force and displacement at the interface (Francavilla and Zienkiewicz, 1975; Sachdeva and Ramakrishnan, 1981; Katona, 1983; Lai and Booker, 1989).

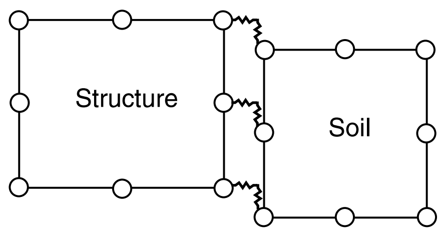

Figure 6.6 Use of springs to model interface

Among these alternatives, the use of zero thickness interface elements is probably the most popular. Consequently a brief description of the basic theory for this type of element will be given and some of its shortcomings described.

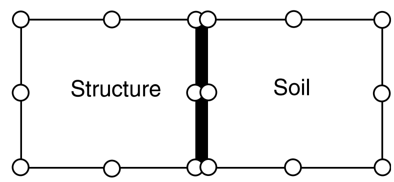

Figure 6.7 Use of special interface elements

6.3.2 Zero thickness interface elements

The isoparametric two-dimensional zero thickness interface element is described by Beer (1985) and Carol and Alonso (1983). The element (see **Figure 6.8**) with four or six nodes is fully compatible with four- and eight-noded quadrilateral, and three- and six-noded triangular, isoparametric 2D elements.

The interface stress consists of the normal and shear components. The normal stress σ and the shear stress τ are related by the constitutive equation to the normal and tangential element strains, ε and γ

$$\begin{Bmatrix} \Delta\tau \\ \Delta\sigma \end{Bmatrix} = [\mathbf{D}] \begin{Bmatrix} \Delta\gamma \\ \Delta\varepsilon \end{Bmatrix} \tag{6.16}$$

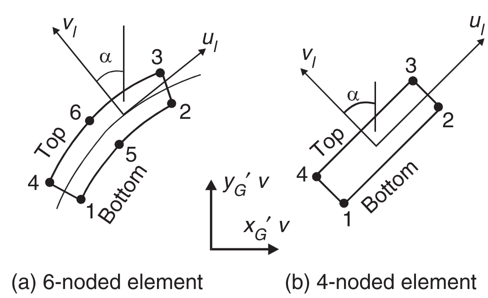

Figure 6.8 Isoparametric interface elements

For isotropic linear elastic behaviour the [**D**] matrix takes the form

$$[\mathbf{D}] = \begin{bmatrix} K_s & 0 \\ 0 & K_n \end{bmatrix} \tag{6.17}$$

where K_s and K_n are the elastic shear stiffness and normal stiffness respectively.

The interface element strain is defined as the relative displacement of the top and bottom of the interface element

$$\gamma = \Delta u_l = u_l^{bot} - u_l^{top} \tag{6.18}$$

$$\varepsilon = \Delta v_l = v_l^{bot} - v_l^{top} \tag{6.19}$$

where

$$\left.\begin{aligned} u_l &= v \sin\alpha + u \cos\alpha \\ v_l &= v \cos\alpha - u \sin\alpha \end{aligned}\right\} \tag{6.20}$$

and u and v are the global displacements in the x_G and y_G directions respectively. Hence

$$\left.\begin{aligned} \gamma &= (v^{bot} - v^{top}) \sin\alpha + (u^{bot} - u^{top}) \cos\alpha \\ \varepsilon &= (v^{bot} - v^{top}) \cos\alpha - (u^{bot} - u^{top}) \sin\alpha \end{aligned}\right\}$$

The formulation for 3D interface elements is similar to that described above, except that there are three interface stresses (a normal stress, σ, and two mutually perpendicular shear stresses, τ_a and τ_b) and strains (ε, γ_a and γ_b), and three displacements (u_l, v_l and w_l).

From Equations (6.18) and (6.19) it is evident that the *strains* are defined as the relative displacements of the top and bottom of the interface element. Consequently the strains are not dimensionless, but have the same dimensions as the displacements (i.e. length). The constitutive matrix, given by Equation (6.17), is in terms of the shear stiffness K_s and normal stiffness K_n. These stiffnesses relate stresses (in units of force/(length)^2) to strains (in units of length) via Equation (6.16), which implies that they must have units of force/(length)^3. They therefore have different units to the Young's modulus E of the soil and/or structure adjacent to them (i.e. E has the same units as stress: force/(length)^2). As it is difficult to undertake laboratory tests to determine K_n and K_s, selecting appropriate values for an analysis is therefore difficult. For this reason some software packages automatically select interface stiffness values for the user. Usually these stiffnesses are based on the stiffness of the solid elements either side of the interface element and the dimensions of the interface element. Clearly the user should make sure that such default values are suitable for the problem under investigation.

If a pore fluid exists in the interface, undrained behaviour can be modelled by including the effective bulk stiffness of the pore fluid (again in force/(length)^3) in the stiffness matrix. It is also possible to allow the interface elements to consolidate by implementing one-dimensional consolidation along their length.

The interface stresses can also be limited by imposing a failure criterion. This is conveniently achieved by using an elasto-plastic constitutive model. For example, the Mohr–Coulomb failure criterion can be used to define the yield surface

$$F = |\tau| + \sigma' \tan\varphi' - c' \tag{6.22}$$

along with the gradient of the plastic potential function, P:

$$\frac{\partial P}{\partial \sigma'} = \tan v; \qquad \frac{\partial P}{\partial \gamma} = \pm 1 \tag{6.23}$$

where φ' is the maximum angle of shearing resistance, c' is the cohesion (see **Figure 6.9**) and v is the dilation angle. If the interface moves such that the maximum normal tensile strength is exceeded ($c'/tan\,\varphi'$), the interface is allowed to subsequently open and close and in a finite element analysis the residual tensile stress is redistributed via the non-linear solution algorithm. When the interface is open, the normal stress remains equal to $c'/tan\,\varphi'$ and the shear stress remains zero. The amount of opening of the interface is recorded. When the interface re-closes and reforms contact, the constitutive model again defines the interface behaviour.

The facility for opening and closing of the interface element is particularly useful in the analysis of problems where tensile cracks may form, for example behind a laterally loaded pile or behind a retaining wall.

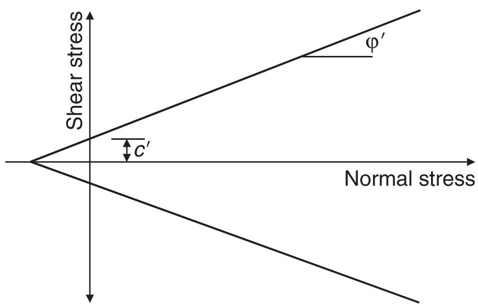

Figure 6.9 Mohr–Coulomb yield function

A common problem when using zero thickness interface elements is ill conditioning of the global stiffness matrix, which results in large oscillations in the stresses in the interface elements. This arises from large differences between the element stiffness matrices of the interface elements and the adjacent elements and/or to high stress and strain gradients (Potts and Zdravkovic, 1999). The former problem arises as a result of both the stiffness values input for the interface element and the size and stiffness of the adjacent elements.

7 Boundary and initial conditions

7.1 Introduction

The term *boundary conditions* is used to cover all possible additional conditions that may be necessary to fully describe a particular problem. The types of boundary conditions can be classified according to their influence on the global system of equations given by

$$[\mathbf{K}_G]\{\Delta \boldsymbol{d}\}_{nG} = \{\Delta \boldsymbol{R}_G\} \tag{7.1}$$

The first group of boundary conditions affects only the right-hand side (i.e. $\{\Delta \boldsymbol{R}_G\}$) of the system equations. These boundary conditions are loading conditions such as *point loads*, *boundary stresses*, *body forces*, *seepage flows (consolidation analysis), construction* and *excavation*.

The second group of boundary conditions affects only the left-hand side (i.e. $\{\Delta \boldsymbol{d}\}_{nG}$) of the system equations. These are kinematic conditions such as *prescribed displacements* and *pore water pressures (consolidation analyses)*.

The final group of boundary conditions is more complex, since the conditions affect the whole structure of the system equations. These conditions include: *local axes*, which require a transformation of the stiffness matrix and the right-hand-side load vector; tied freedoms, which affect the numbering of the degrees of freedom and the stiffness matrix assembly procedure; and *springs*, which again affect the stiffness matrix assembly procedure.

The following sections of this chapter describe in detail the boundary condition options necessary for performing geotechnical finite element analysis. For plane strain (and axi-symmetric) problems it is necessary to specify an x (r) and y (z) boundary condition at each node on the boundary of the finite element mesh. For three-dimensional analyses it is also necessary to specify a boundary condition in the third co-ordinate direction (z) at each boundary node. The boundary condition can either be a prescribed nodal displacement or a nodal force. In addition, for coupled consolidation analyses it is also necessary to specify either a prescribed pore water pressure or seepage flow at all boundary nodes that have a pore water pressure degree of freedom. It should be noted that many finite element programs do not insist that the user specifies all these conditions. In such a situation the program makes an implicit assumption for the unspecified nodal conditions. Usually, if a boundary condition is not prescribed, the program assumes that the appropriate nodal force is zero and, for a coupled consolidation, analyses that the nodal seepage flow is zero. The chapter finishes by considering the specification of initial conditions (i.e. stresses and state parameters).

7.2 Local axes

In most applications, the degrees of freedom at each node (e.g. the two nodal displacements for plane strain or axisymmetric problems) are referred to the global system of axes. Thus, for compatibility, the stiffness matrices and load conditions are also determined with respect to the global axes. However, in order to apply boundary conditions at an angle to the global directions, it is sometimes necessary to define a set of *local axes* at certain nodes. In such cases the stiffness matrices and load conditions, for the elements containing the nodes with local axes, need to be transformed.

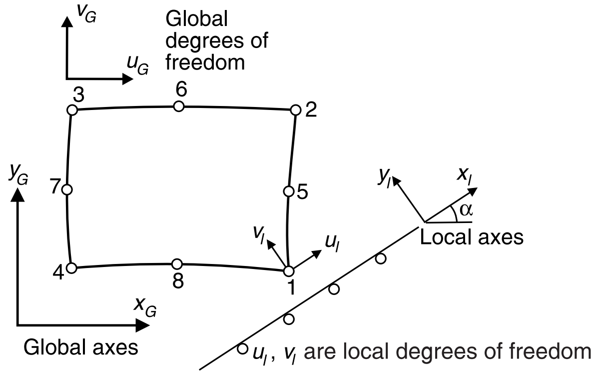

Figure 7.1 Sliding boundary condition

As an example, **Figure 7.1** shows a problem with a sliding boundary condition. In this case, node 1 is required to move only parallel to the x_l direction, where x_l makes an angle α with the global x_G axis. This is most easily achieved by defining local axes x_l, y_l for node 1 and setting the second degree of freedom at node 1 to zero (v_l = 0).

If local axes are defined, it is necessary to transform the element stiffness matrices and the load boundary conditions prior to assembling the global system of equations. For 2D plane strain and axisymmetric analyses the element stiffness matrix $[\mathbf{K_E}]$ is transformed from global axes to local axes by

$$[\mathbf{K_E}]_{\text{local}} = [\mathbf{Q}]^{\mathrm{T}}[\mathbf{K_E}]_{\text{global}}[\mathbf{Q}] \tag{7.2}$$

where $[\mathbf{Q}]$ is a rotation matrix of direction cosines defined by the expression

$$\{\Delta \boldsymbol{d}\}_{\text{global}} = [\mathbf{Q}]\{\Delta \boldsymbol{d}\}_{\text{local}} \tag{7.3}$$

which relates the local displacements to the global displacements. For example, for a 4-noded isoparametric element, the rotation matrix $[\mathbf{Q}]$ takes the form:

$$[\mathbf{Q}] = \begin{bmatrix} \cos\alpha_1 & -\sin\alpha_1 & 0 & 0 & 0 & 0 & 0 & 0 \\ \sin\alpha_1 & \cos\alpha_1 & 0 & 0 & 0 & 0 & 0 & 0 \\ 0 & 0 & \cos\alpha_2 & -\sin\alpha_2 & 0 & 0 & 0 & 0 \\ 0 & 0 & \sin\alpha_2 & \cos\alpha_2 & 0 & 0 & 0 & 0 \\ 0 & 0 & 0 & 0 & \cos\alpha_3 & -\sin\alpha_3 & 0 & 0 \\ 0 & 0 & 0 & 0 & \sin\alpha_3 & \cos\alpha_3 & 0 & 0 \\ 0 & 0 & 0 & 0 & 0 & 0 & \cos\alpha_4 & -\sin\alpha_4 \\ 0 & 0 & 0 & 0 & 0 & 0 & \sin\alpha_4 & \cos\alpha_4 \end{bmatrix} \tag{7.4}$$

where angles α_1, α_2, α_3, α_4 define the orientation of the local axes with respect to the global axes at each of the four nodes. In practice, the number of multiplications performed in evaluating Equation (7.2) is greatly reduced by processing only the non-zero sub-matrices of the matrix (7.4).

The transformation of the right-hand-side load vector can be performed in a similar manner

$$\{\Delta \boldsymbol{R}_{\mathrm{E}}\}_{\text{local}} = [\mathbf{Q}]^{\mathrm{T}}\{\Delta \boldsymbol{R}_{\mathrm{E}}\}_{\text{global}} \tag{7.5}$$

where $[\mathbf{Q}]$ is again of the form of Equation (7.4) (note: $[\mathbf{Q}]^{-1} = [\mathbf{Q}]^{\mathrm{T}}$). The transformation equation (7.5) is indicated at the element level; however, in practice it is more convenient to take account of the local axes in the assembled right-hand-side vector, $\{\Delta \boldsymbol{R}_{\mathrm{G}}\}$.

7.3 Prescribed displacements

In addition to the application of prescribed displacement conditions to represent structural boundaries, a sufficient number of displacement components must be specified to restrict any rigid body translations or rotations. If these conditions are not prescribed, the global stiffness matrix becomes singular and the system equations cannot be solved.

To remove the rigid body modes, which for two dimensions consist of two translations and one rotation, the user should effectively prescribe the values of at least three degrees of freedom. Care should be taken, particularly with the rotational mode, that the prescribed displacements

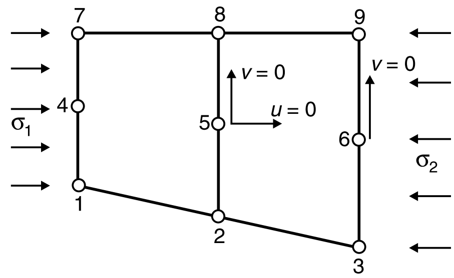

Figure 7.2 Removal of rigid body modes

do restrain *all* the rigid body modes. **Figure 7.2** shows an example of a plane strain body deformed by stress boundary conditions. The choice of prescribed displacements, which restrain the rigid body modes, is not unique and depends on the displacement solution required. Figure 7.2 shows the case where the rigid body modes are removed by specifying three degrees of freedom: these are u = 0, v = 0 at node 5 and v = 0 at node 6.

Problems involving symmetrical bodies and symmetrical boundary conditions can be solved by analysing only half of the total body. For such cases displacement boundary conditions can be applied to ensure that the line of symmetry remains undeformed. These displacement conditions may also be useful in removing certain rigid body modes.

Defining a prescribed displacement component is equivalent to specifying the value of a degree of freedom. Thus, if local axes are also specified at certain nodes, the prescribed displacements refer to the displacement components with respect to the new local system of axes. The application of the prescribed displacements is performed simultaneously with the solution of the global system of equations.

The global equilibrium equations (7.1) can be partitioned in the form

$$\begin{bmatrix} \mathbf{K}_u & \mathbf{K}_{up} \\ \mathbf{K}_{up}^{\mathrm{T}} & \mathbf{K}_p \end{bmatrix} \begin{Bmatrix} \Delta \boldsymbol{d}_u \\ \Delta \boldsymbol{d}_p \end{Bmatrix} = \begin{Bmatrix} \Delta \boldsymbol{R}_u \\ \Delta \boldsymbol{R}_p \end{Bmatrix} \tag{7.6}$$

where $\Delta \boldsymbol{d}_{\mathrm{u}}$ are the unknown degrees of freedom and $\Delta \boldsymbol{d}_p$ corresponds to the prescribed displacements. The first matrix equation from Equation (7.6) gives

$$[\mathbf{K}_u]\{\Delta \boldsymbol{d}_u\} = \{\overline{\Delta \boldsymbol{R}_{\mathrm{u}}}\} \tag{7.7}$$

where

$$\{\overline{\Delta \boldsymbol{R}_u}\} = \{\Delta \boldsymbol{R}_u\} - [\mathbf{K}_{up}]\{\boldsymbol{d}_p\} \tag{7.8}$$

Thus the unknown displacements $\{\Delta \boldsymbol{d}_u\}$ can be calculated from a modified system of global equilibrium equations (7.7).

Having determined $\{\Delta \boldsymbol{d}_u\}$ from Equation (7.7), the second matrix equation (7.6) gives

$$\{\Delta \boldsymbol{R}_p\} = [\mathbf{K}_{up}]^{\mathrm{T}}\{\Delta \boldsymbol{d}_u\} + [\mathbf{K}_p]\{\boldsymbol{d}_p\} \tag{7.9}$$

Hence, the *reaction forces* corresponding to each prescribed displacement can also be calculated.

In many solution schemes the application of prescribed displacements is performed without rearranging the global system of equations as implied by Equation (7.6). The equations corresponding to $\{\Delta \boldsymbol{R}_p\}$ are skipped over whilst the Equations (7.7) are solved, and the coefficients of $[\mathbf{K}_{up}]^{\mathrm{T}}$ and $[\mathbf{K}_p]$ are then used to determine the reaction forces.

If beam (shell) elements are being used to model structural components, these elements have a rotational degree of freedom, θ, in addition to the two displacements. To realistically model the behaviour of the structural components it may be necessary to prescribe values of some of the nodal rotations.

If a dynamic analysis is being undertaken, then velocities and/or accelerations may be specified at the nodes. Before they are applied to the analysis, the software will convert these to equivalent nodal displacements based on the dynamic algorithm being used.

7.4 Tied degrees of freedom

This boundary condition option allows a condition of equal displacement components to be imposed at one or more nodes, whilst the magnitudes of the components remain unknown.

To explain where this concept might be useful, the problem of a smooth rigid strip footing is considered. Such a situation is shown in **Figure 7.3**, where symmetry has been assumed and half the footing is between nodes A and B. The footing is subject to a vertical load *P*, and it is required to calculate the magnitude of the resulting footing settlement. Because the behaviour of the footing under a given load is required, this load has to form part of the boundary conditions. As the footing is rigid, it is also required that it displaces vertically by the same amount across its width. Unfortunately, the magnitude of this vertical displacement is not known, in fact the reason for doing the analysis is to determine just this quantity.

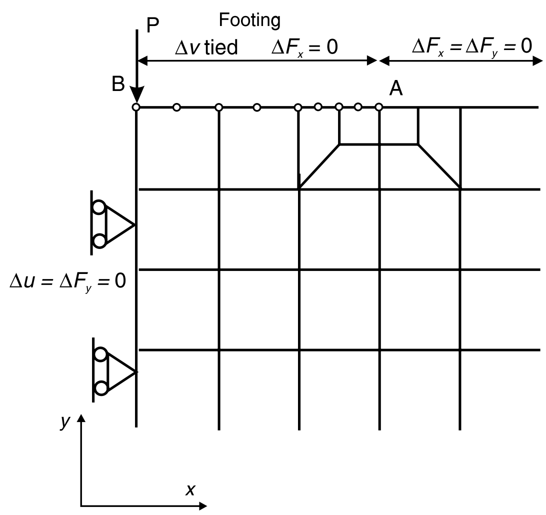

Figure 7.3 Boundary conditions for a smooth strip footing subject to a vertical load *P*

One solution to this problem is to use the tied freedoms concept. The boundary conditions to be applied to the mesh boundary immediately below the position of the strip footing are shown in Figure 7.3. A vertical nodal force, $\Delta F_y = P$, is applied to node B, on the line of symmetry, and zero horizontal nodal forces, $\Delta F_x = 0$, are applied to nodes on the boundary between A and B. In addition, the nodes between A and B are constrained to move vertically by the same amount by using tied freedoms. This is achieved in the finite element analysis by assigning a single degree of freedom number to the vertical degree of freedom at each of the nodes along the boundary between A and B.

In general, the set of tied displacement components is given a single degree of freedom number, which appears only once in the assembled global equilibrium equations. Thus, tying degrees of freedom alters the structure of the global stiffness matrix and in some cases may increase the total profile (i.e. the number of terms of $[\mathbf{K}_G]$ which need to be stored).

As an example, **Figure 7.4** shows a problem of frictionless contact between two bodies. The nodes 25, 26, 27, 28 in the upper body are defined to be coincident with the nodes 19, 20, 21, 22

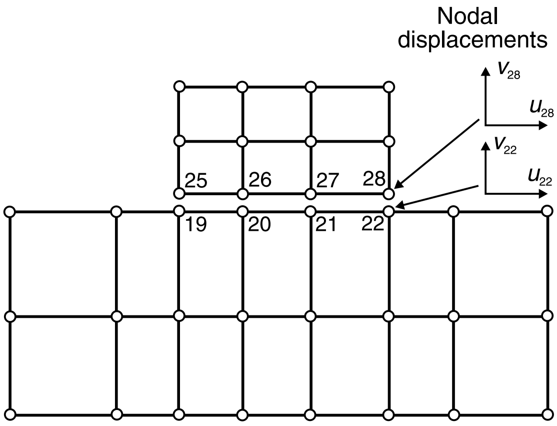

Figure 7.4 Frictionless contact problem

respectively, of the lower body. The problem is to find the indentation stresses induced from the weight of the upper body. Since the two bodies are in contact, a condition of 'no penetration' must be specified for the contact zone. This condition is most easily imposed by tying the degrees of freedom with a set of constraint equations

$$v_{19} = v_{25}; \qquad v_{20} = v_{26}; \qquad v_{21} = v_{27}; \qquad v_{22} = v_{28} \tag{7.10}$$

The incorporation of Equations (7.10) in the solution procedure is achieved by simply numbering the displacement components at the tied nodes with the same degree of freedom numbers. Thus, for example, v_{19} and v_{25} will be given the same degree of freedom number.

Since the degrees of freedom (or displacements) are measured positive with respect to the local system of axes at each node, the flexibility of this feature is greatly increased if it is combined with the *local axes* feature described in *Section 7.2*. **Figure 7.5** shows the effective global constraints that can be achieved by tying the two degrees of freedom at a single node and by adjusting the orientation of the local axes x_l, y_l which make an angle α with the global axes x_G, y_G. The global displacements (measured positive in the x_G, y_G directions) are indicated by u and v.

If the degrees of freedom are tied between two nodes, the effective global constraints depend on the orientation of the local axes at both of the nodes. As an example, **Figure 7.6** shows the case where the degrees of freedom are tied between two nodes labelled A and B. The local axes at node A are, for simplicity, chosen to be coincident with the global axes, and the local axes at node B are varied. The orientation of the local axes, and hence the degrees of freedom, are again indicated by notation x_l, y_l; the global displacements are given by u and v.

A further option for defining tying constraints is to tie the degrees of freedom over a range of boundary nodes, as indicated in the strip footing problem shown in Figure 7.3.

The tied freedom concept can also be applied to pore pressure degrees of freedom in a coupled

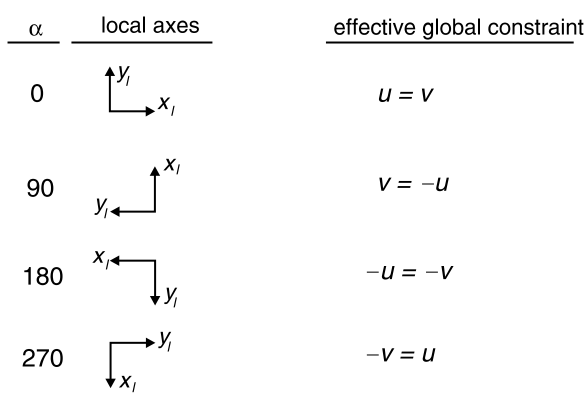

Figure 7.5 Effective global constraints for tying at a single node

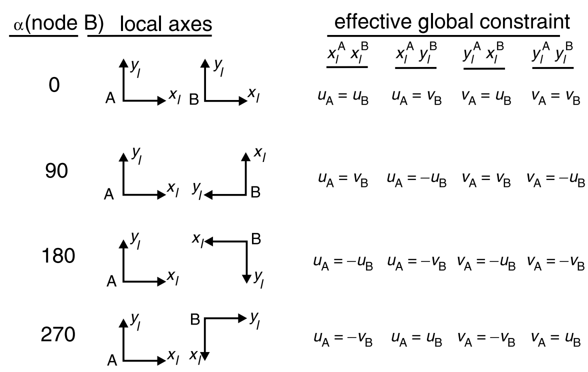

Figure 7.6 Effective global constraints for tying between two nodes

consolidation analysis. However, because pore fluid pressure is a scalar quantity, there is only one tying option, compared to the several that are available for displacement which is a vector (see above). As an example of the use of tied pore fluid pressure, consider the example of two consolidating layers of soil, separated by interface elements, shown in **Figure 7.7**. Because interface elements have zero thickness, they are not usually formulated to account for consolidation. In the situation shown in Figure 7.7, there is a set of nodes along the underside of soil layer 1 and another set on the upper surface of soil layer 2, corresponding to the upper and lower sides of the row of interface elements respectively. Because the interface elements do not account for consolidation, there is no seepage link between these two rows of nodes and, unless a boundary condition is specified for these nodes, most software programs will treat each row as an impermeable boundary (i.e. zero incremental nodal flow). If the interface is to be treated as a permeable boundary, the solution is to tie the incremental pore fluid pressures of adjacent nodes across the interface elements. For example, tie the incremental pore fluid pressures for nodes AB, CD, . . ., etc.

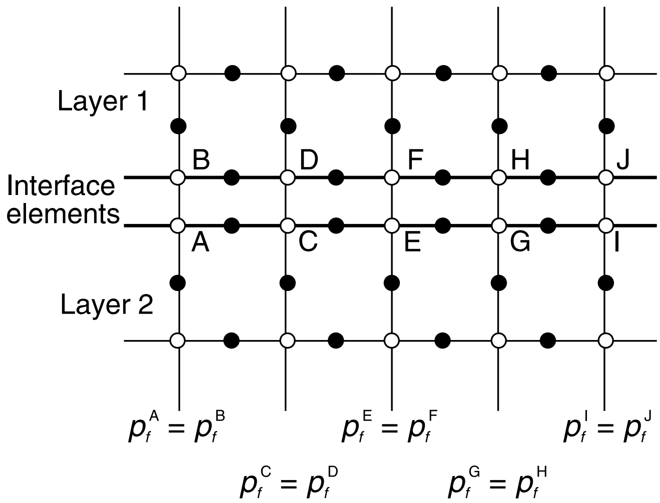

Figure 7.7 Tied pore fluid pressures

7.5 Springs

As an alternative to using membrane elements to model structural components which can sustain only membrane (i.e. axial) forces, spring boundary conditions can be used. Springs are usually assumed to be linear, with a constant stiffness k_s, and can be applied in finite element analysis in three different ways.

Firstly, they can be placed between two nodes in the mesh. **Figure 7.8** shows a very crude excavation problem in which two such springs are used. The first spring spans between nodes *i* and *j* and represents a prop. The second spring spans between nodes *m* and *n* and represents an end bearing pile. These springs essentially act as linear two-noded membrane elements. They therefore contribute to the global stiffness matrix. The equilibrium equation for the spring between nodes *i* and *j* is

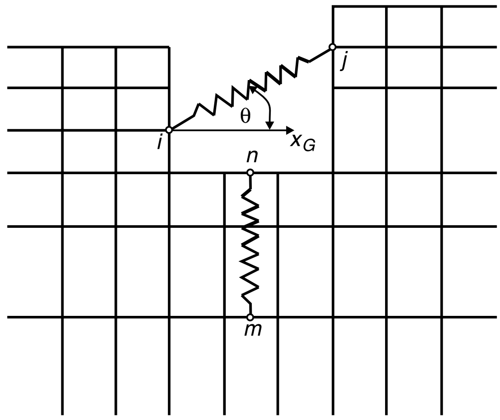

Figure 7.8 Spring between two nodes

$$k_s \begin{bmatrix} \cos^2\theta & \sin\theta\cos\theta & -\cos^2\theta & -\sin\theta\cos\theta \\ \sin\theta\cos\theta & \sin^2\theta & -\sin\theta\cos\theta & -\sin^2\theta \\ -\cos^2\theta & -\sin\theta\cos\theta & \cos^2\theta & \sin\theta\cos\theta \\ -\sin\theta\cos\theta & -\sin^2\theta & \sin\theta\cos\theta & \sin^2\theta \end{bmatrix} \begin{Bmatrix} \Delta u_i \\ \Delta v_i \\ \Delta u_j \\ \Delta v_j \end{Bmatrix} = \begin{Bmatrix} \Delta R_{xi} \\ \Delta R_{yi} \\ \Delta R_{xj} \\ \Delta R_{yj} \end{Bmatrix} \tag{7.11}$$

where θ is the inclination of the spring to the global x_G axis (see Figure 7.8). The equation above must be added to the global stiffness matrix during the assembly process. It affects the terms relating to the displacement degrees of freedom of nodes *i* and *j*.

Secondly, springs can be applied at a single node. Such an example is shown in **Figure 7.9** which shows a symmetric excavation with a spring applied at node *i* to represent a prop. In this situation it is implicitly assumed that the end of the spring not attached to the node is 'grounded' and restrained from moving in any direction. Such springs also contribute to the global stiffness matrix. The equilibrium equation for this spring is

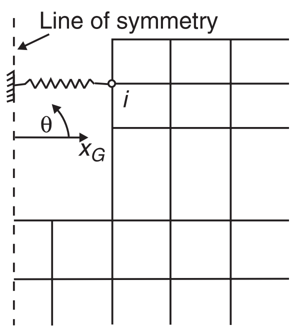

Figure 7.9 Spring at a single node

$$k_s \begin{bmatrix} \cos^2\theta & \sin\theta\cos\theta \\ \sin\theta\cos\theta & \sin^2\theta \end{bmatrix} \begin{Bmatrix} \Delta u_i \\ \Delta v_i \end{Bmatrix} = \begin{Bmatrix} \Delta R_{xi} \\ \Delta R_{yi} \end{Bmatrix} \tag{7.12}$$

where, in general, θ is the inclination of the spring to the global x_G direction. In the above example $\theta = 0°$. Again, above equation must be added to the global stiffness matrix during the assembly process.

The third option is to apply a continuous spring along a part of the boundary of the mesh. An example is shown in **Figure 7.10** where such a spring is placed along the bottom boundary of the mesh. It is important to note that these are not discrete springs positioned at nodes, but are continuous along the mesh boundary. They must therefore be converted into equivalent nodal springs before they can be assembled into the global stiffness matrix.

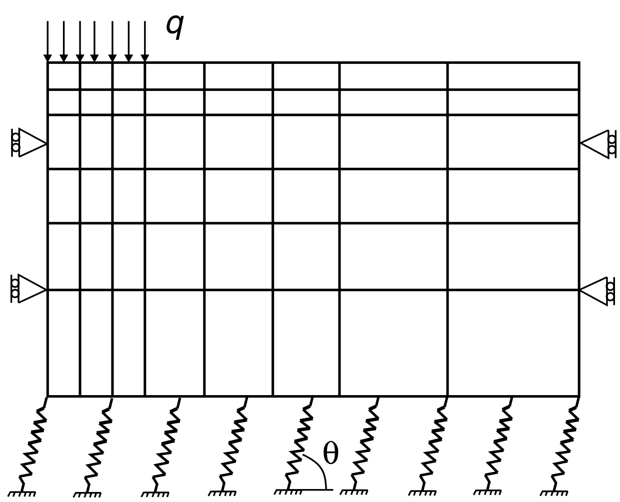

Figure 7.10 Continuous spring along mesh boundary

It can be shown that, for a single element side, the contribution to the global stiffness matrix takes the form

$$\int_{Srf} [\mathbf{N}]^T [\mathbf{K_s}][\mathbf{N}] d\mathbf{Srf} \tag{7.13}$$

where

$$[\mathbf{K_s}] = \mathbf{k_s} \begin{bmatrix} \cos^2\theta & \sin\theta\cos\theta \\ \sin\theta\cos\theta & \sin^2\theta \end{bmatrix}$$

and *Srf* is the element side over which the spring acts. Clearly, the above equation only contributes to the global stiffness terms of the nodes along the element side. If the spring spans across more than one element, then the contribution from each element must be added into the global stiffness matrix. The integral in Equation (7.13) can be evaluated numerically for each element side, in a similar fashion to that described for boundary stress in *Section 7.6*.

7.6 Boundary stresses

Stress boundary conditions have to be converted into equivalent nodal forces. In many finite element programs the calculation of the equivalent nodal forces is performed automatically for generally distributed boundary stresses and for arbitrarily shaped boundaries.

To illustrate this, **Figure 7.11** shows an example of the type of boundary stresses which may be defined. Between the points 1 and 2 a linearly decreasing shear stress is applied; between points 2 and 3 a generally varying normal stress is applied; the side 3 to 4 is stress free; and between points 4 and 1 a linearly increasing normal stress is applied. To determine the nodal forces, which are equivalent to the stress boundary conditions, the expression for the surface traction contribution to the element right-hand-side load vector is utilized

$$\{\Delta \boldsymbol{R}_E\} = \int_{Srf} [\mathbf{N}]^T \{\Delta \boldsymbol{T}\} dSrf \tag{7.14}$$

where [**N**] is the shape function matrix, $\{\Delta \boldsymbol{T}\}$ is the incremental global surface traction vector (i.e. boundary stresses) and *Srf* (i.e. Surface) is the element side over which tractions are prescribed. The integral (7.14) can be evaluated numerically for each element side over which the tractions act.

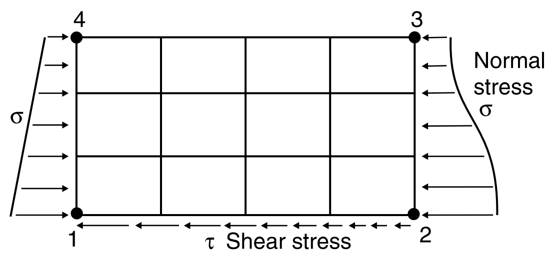

Figure 7.11 Example of stress boundary conditions

To determine the integration point value of the surface traction vector $\{\Delta \boldsymbol{T}\}$, the applied stress must be transformed according to the orientation of the surface element at the integration point and the defined sign convention for stresses. One such sign convention is that normal stresses (σ) are positive if oriented outwards from the boundary of the body, while shear stresses (τ) are positive if oriented in a tangentially anticlockwise sense with respect to the boundary of the body. Using this convention gives

$$\{\Delta \boldsymbol{T}_I\} = \boldsymbol{\sigma}_I \begin{Bmatrix} \cos\theta_I \\ \sin\theta_I \end{Bmatrix} \tag{7.15}$$

if normal stresses are prescribed, or

$$\{\Delta \boldsymbol{T}_I\} = \tau_I \begin{Bmatrix} -\sin\theta_I \\ \cos\theta_I \end{Bmatrix} \tag{7.16}$$

if shear stresses are prescribed, where θ_I is the angle between the boundary normal and the global x_G axis, and the subscript I denotes the integration point value.

In all cases the equivalent nodal forces, calculated from Equation (7.14), are initially referred to the global system of axes. If local axes are defined, the nodal forces are transformed accordingly, as described in *Section 7.2*.

7.7 Point loads

A further option for applying traction boundary conditions is to apply discrete nodal point loads. For plane strain and axisymmetric analyses they are line loads, with their length perpendicular to the plane of the mesh. This allows the user to manually define stress boundary conditions over a range of the boundary, or to define a point load at a single node. Point loads can be defined with respect to a set of *point loading axes*.

As an example, **Figure 7.12** shows the case where a single point load is applied at an angle to the boundary of the body. If point loads are defined over a part of the mesh boundary and are required to represent a continuous stress distribution, the values of the point loads must be calculated in a manner consistent with minimizing the potential energy of the body. This requires that the work done by the point loads in displacing the nodal points is equal to the work done by the continuous stress distribution in deforming the boundary. The point loads must therefore be calculated from an integral of the form given in Equation (7.14).

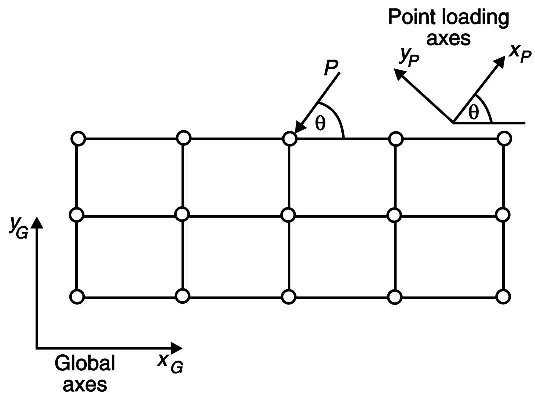

Figure 7.12 Orientation of point loading axes

For simple element shapes and simple stress distributions the equivalent nodal forces can be evaluated exactly. Some examples are illustrated in **Figure 7.13** for element sides with two and three nodes.

In all cases the point loads, which are initially defined with respect to the x_p, y_p point loading axes, or with respect to the boundary normal, are transformed to the global system of axes. If local axes are defined, the nodal forces are transformed again as described in *Section 7.2*.

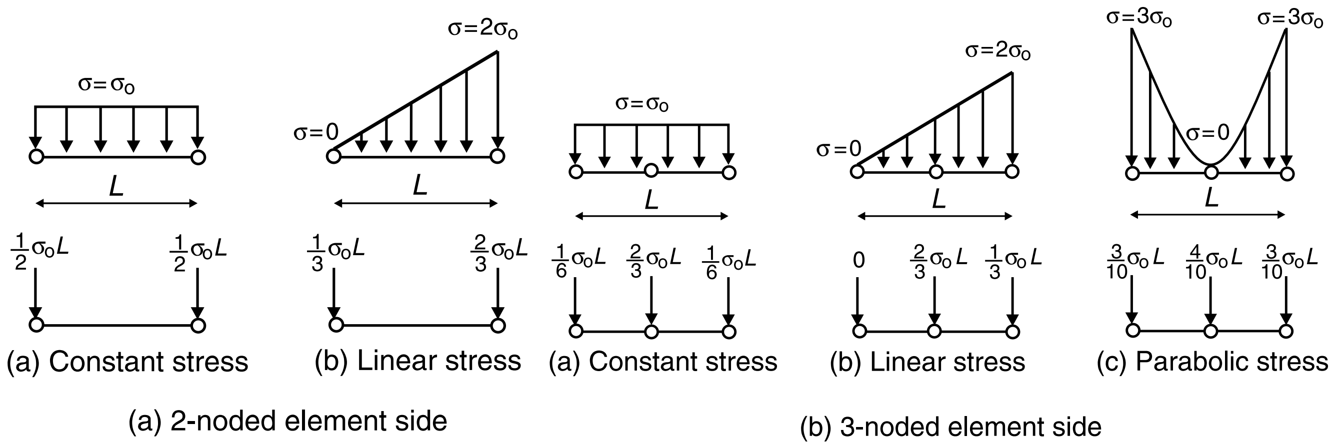

Figure 7.13 Equivalent nodal forces for element side with (A) two nodes and (B) three nodes

7.8 Body forces

Gravity loading, or body forces, plays an important role in most geotechnical problems. In a similar fashion to the other loading conditions discussed above, the application of body forces as a boundary condition requires the calculation of equivalent nodal forces. In most finite element programs the calculation of nodal forces corresponding to body forces is performed automatically. The body force can act in any direction and its magnitude over the mesh can be varied.

To illustrate the application of body forces and the definition of the body force axes, consider the example shown in **Figure 7.14**. This example shows a cross-section of an embankment which lies on a slope and is deforming under its own weight. For convenience, the global axes are chosen to be parallel to the slope. Thus, in order to apply the gravitational field, a set of body force loading axes x_B, y_B must be defined, where x_B makes an angle θ with the global x_G axis. The gravitational field is then defined with respect to the y_B axis.

The nodal forces equivalent to the body force are calculated element-wise, using the body force contribution to the right-hand-side vector:

$$\{\Delta \boldsymbol{R}_{\mathbf{E}}\} = \int_{Vol} [\mathbf{N}]^{\mathrm{T}} \{\Delta \boldsymbol{F}_{\mathbf{G}}\} \mathrm{d}Vol \tag{7.17}$$

where [**N**] is the shape function matrix, $\{\Delta \boldsymbol{F}_{\mathbf{G}}\}$ is the global body force vector and *Vol* is the volume of the element. The body force vector $\{\Delta \boldsymbol{F}_{\mathbf{G}}\}$ is determined with respect to the global axes by using

$$\left\{ \begin{array}{c} \Delta F_{xG} \\ \Delta F_{yG} \end{array} \right\} = \Delta\gamma \left\{ \begin{array}{c} \cos\beta \\ \sin\beta \end{array} \right\} \tag{7.18}$$

where Δy is the increment of bulk unit weight; $\beta = \theta$ or $\theta + 90^\circ$ depending on whether Δy refers to the x_B or y_B component of body force, respectively; and θ is the angle between the x_B and x_G axes.

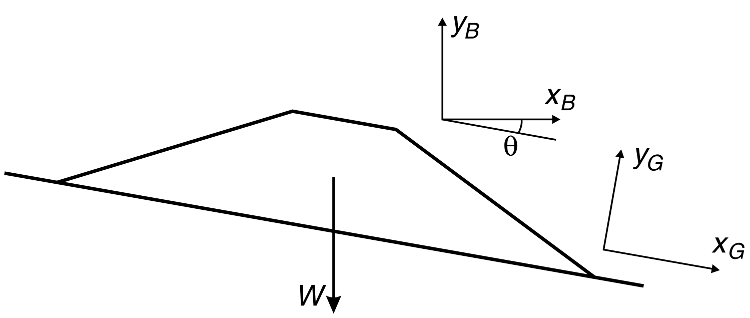

Figure 7.14 Body force loading axes for an embankment on a slope

7.9 Construction

Many geotechnical problems, such as embankment construction and backfilling behind a retaining wall, involve the placing of new material. Simulation of such activities in a finite element analysis is not straightforward. The software must be able to accommodate the following:

- Elements representing the material to be constructed must be present in the original finite element mesh, but must be *deactivated*, either by prior excavation or at the outset of the analysis. On construction the elements are reactivated.
- Construction of material must be performed incrementally since, even for a linear elastic material, superposition does not hold. When constructing an embankment the layered construction procedure must be followed, with each increment of the analysis simulating the construction of a layer of fill.
- During construction, the elements representing the new material must have a constitutive model which is consistent with its behaviour during construction. Once constructed, the constitutive model should change to represent the behaviour of the material once placed.
- When an element is constructed, the addition of its weight to the finite element mesh must be simulated by applying self-weight body forces to the constructed element.

When constructing material, the following procedure is recommended:

- Divide the analysis into a set of increments and make sure that all elements to be constructed are deactivated prior to the increment at which construction starts.
- For a particular increment the elements to be constructed are reactivated and given a constitutive model appropriate to the material behaviour during placing. This often means that the material has a low stiffness.
- Nodal forces due to the self-weight body forces of the constructed material are calculated in a similar fashion to that explained for body forces in *Section 7.8*, and added to the right-hand-side load vector.
- The global stiffness matrix and all other boundary conditions are assembled for the increment. The equations are solved to obtain the incremental changes in displacements, strains and stresses.
- Before application of the next increment, the constitutive model for the elements just constructed is changed to represent the behaviour of the fill material once placed. Displacements of any nodes which are connected only to the constructed elements (i.e. not connected to elements that were active at the previous increment) are zeroed. Depending on the constitutive models used to represent the constructed material, it may be necessary to establish state parameters (e.g. hardening parameters for elasto-plastic models) and/or adjust the stresses in the constructed elements. If the stresses are adjusted, then care must be taken that equivalent changes are made to the accumulated right-hand-side vector to ensure equilibrium is maintained.
- Apply the next increment of analysis.

As an example, consider the problem of constructing the embankment shown in **Figure 7.15**. The embankment has been split into four horizontal layers of material and therefore is constructed in four increments. At the outset of the analysis all elements in the embankment are deactivated. In

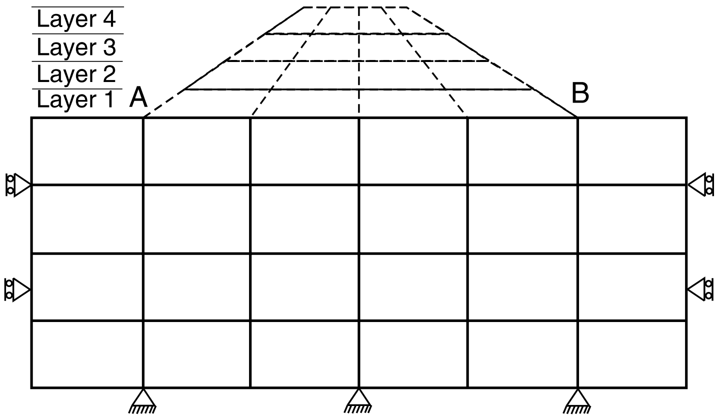

Figure 7.15 Embankment construction

increment 1, layer 1 is to be constructed and therefore, at the beginning of the increment, all the elements in this layer are reactivated (i.e. added to the active mesh) and assigned a constitutive model appropriate to the material behaviour during placing. Self-weight body forces are then assumed for these elements and the equivalent nodal forces calculated and added to the incremental right-hand-side vector. The global stiffness matrix and other boundary conditions are assembled and a solution found. The incremental displacements calculated for the nodes connected to the constructed elements, but not connected to those elements forming the original ground (i.e. all active nodes above line AB), are zeroed. A new constitutive model appropriate to the behaviour of the fill once placed is then assigned to the elements just constructed. Any material state parameters are then calculated and any stress adjustments made.

The procedure for construction of layers 2, 3 and 4 follows similar steps. The final result is obtained by accumulating the results from each increment of the analysis. Clearly, the results of the analysis will depend on the number and therefore thickness of the construction layers.

Deactivation of elements can be accounted for in one of two ways. The best way is not to include the deactivated elements in the formulation of the finite element equations. This means that no account is taken of their element stiffness matrices or of the nodal degrees of freedom, which are connected only to deactivated elements, during assembly of the global stiffness matrix and right-hand-side vector. As far as the finite element formulation is concerned, it is as if the deactivated elements do not exist. Although this is the recommended way of dealing with deactivated elements, it implies that the finite element software must have sophisticated book-keeping arrangements for keeping track of data, as the active mesh will change throughout an analysis. An alternative procedure, which simplifies the book-keeping, is to leave the deactivated elements in the active mesh but assume that they have a very low stiffness. The deactivated elements are often called ‘ghost elements’. In this procedure the elements do contribute to the element equations and all degrees of freedom remain active. Their effect on the solution depends on the stiffnesses that they assume. Most software that use this approach automatically set low stiffness values for the ghost elements, or encourage the user to set low values. However, care must be taken that the resulting Poisson’s ratio does not approach 0.5. If it does, the ghost elements become incompressible, which can have a serious effect on the predictions.

Because of the complexities involved in simulating construction, many finite element programs oriented towards structural engineering are unsuitable for performing such analyses.

7.10 Excavation

Excavation of soil is involved in many geotechnical problems. Its simulation in a finite element analysis can be summarized as follows. **Figure 7.16(a)** shows a body of soil from which the shaded portion A is to be excavated, leaving the unshaded portion B. No displacements or changes in stress occur if material is removed but replaced by tractions (T) which are equal to

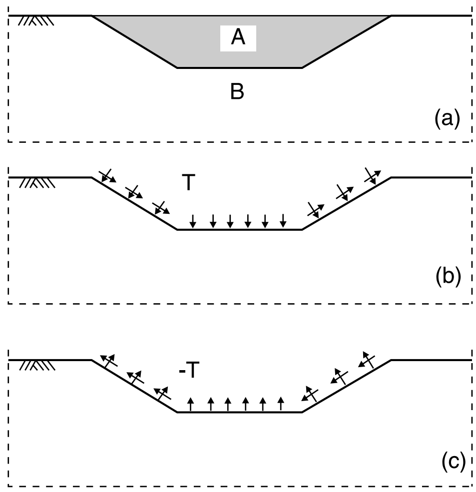

Figure 7.16 Simulation of excavation

the internal stresses in the soil mass that act on the excavated surface before A is removed (see **Figure 7.16(b)**). The behaviour of B due to the excavation of A will be identical to the behaviour of B when the tractions (*T*) are removed, for example by applying equal and opposite tractions as indicated in **Figure 7.16(c)**.

Simulation of a stage of excavation therefore involves determination of the tractions T at the new soil boundary, determination of the stiffness of the soil mass B, and application of tractions $-T$ to that new soil boundary. Finite element implementation of this process involves determination of the nodal forces that are equivalent to the tractions shown in Figure 7.16(c). These forces can be calculated from the excavated elements adjacent to the excavation boundary, using

$$\{\boldsymbol{R}_{\mathrm{E}}\} = \int_{Vol} [\mathbf{B}]^{\mathrm{T}}\{\sigma\}\mathrm{d}Vol - \int_{Vol} [\mathbf{N}]^{\mathrm{T}}\gamma\,\mathrm{d}Vol \tag{7.19}$$

where $\{\sigma\}$ is the stress vector in the element, γ is the bulk unit weight and *Vol* is the volume of the excavated element. Only the forces appropriate to the nodes on the excavated surface are placed in $\{\boldsymbol{R}_E\}$. This calculation is repeated for all excavated elements adjacent to the excavation boundary. This procedure is based on that in Brown and Booker (1985).

When simulating excavation in a geotechnical problem it is usual that structural elements or supports are added as excavation proceeds. It is therefore necessary to split the analysis into a sequence of increments. This is also necessary if non-linear constitutive models are used. The procedure followed in the analysis is therefore as follows:

- Specify the elements to be excavated for a particular increment.
- Using Equation (7.19), determine the equivalent nodal forces to be applied to the excavation boundary to simulate removal of the elements. Tag the elements to be excavated as *deactivated* and remove them from the active mesh.
- Assemble the remaining boundary conditions and the global stiffness matrix, using the active mesh. Solve the finite element equations to give the incremental changes in displacements, stresses and strains.
- Add the incremental changes of displacements, stresses and strains to the accumulated values existing before the increment to give the updated accumulated values.
- Perform the next increment of the analysis.

7.11 Pore pressures

When performing non-consolidating (i.e. uncoupled) analyses in which the total stresses are expressed in terms of effective stresses and pore water pressures it may be appropriate to specify changes in pore water pressure.

In the finite element analysis it is necessary to specify changes in pore fluid pressure in terms of equivalent nodal forces. It can be shown that for an element with a specified change in pore fluid pressure, Δp_f, the equivalent nodal forces are given by

$$\{\boldsymbol{R}_E\} = -\int_{Vol} [\mathbf{B}]^T \{\Delta\sigma_f\} dVol \tag{7.20}$$

where $\{\Delta\sigma_f\} = \{\Delta p_f, \Delta p_f, \Delta p_f, 0, 0, 0\}^T$ is a stress vector containing the change in pore water pressure.

Two scenarios often occur:

Firstly, a set change in the pore water pressure in part of a finite element mesh may be required. For example, during excavation in layered soils it may be necessary to dewater granular layers to prevent bottom heave (see **Figure 7.17**).

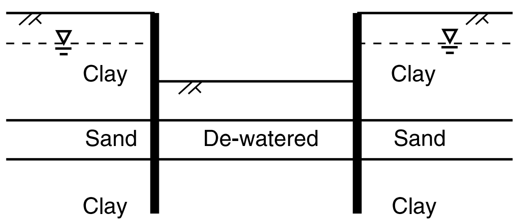

Figure 7.17 Excavation dewatering

Secondly, dissipation of excess pore water pressures may be needed. For example, consider a strip footing which has initially been loaded under undrained conditions. The original part of the analysis could be performed with the equivalent bulk modulus of the pore water, K_e, set to a high value. Excess pore water pressures would then be calculated (see **Figure 7.18**). Once the footing is loaded, K_e could be set to zero and the excess pore water pressures dissipated by specifying changes equal and opposite to those calculated during loading. An estimate of the effects of full consolidation could therefore be calculated. However, no information would be available about intermediate states during the consolidation process. Such an approach is appropriate if the soil behaviour is linear elastic. An approximation is involved if the constitutive behaviour is non-linear. This arises because there is an implicit assumption that stress changes are proportional throughout the consolidation period. In practice, stress changes may be far from proportional. Under the loaded footing pore water pressures will dissipate first at the edge, causing a relatively rapid effective stress change in this region. The effective stresses at the centre will change more slowly. The extent of the error involved depends on the constitutive model. To model the consolidation process accurately, coupled analyses should be performed.

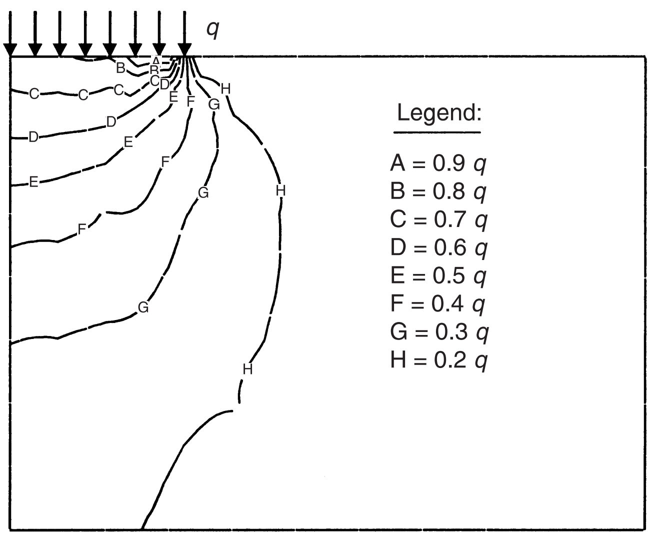

Figure 7.18 Excess pore water pressures under smooth flexible strip footing

If a coupled consolidation analysis is being performed, it will probably be necessary to specify prescribed incremental changes in nodal pore fluid pressures, $\{\Delta \boldsymbol{p}_f\}_{nG}$. As pore fluid pressure is a scalar quantity, local axes are irrelevant. Prescribed changes in pore fluid pressures are dealt with in a similar way to prescribed displacements, as described in *Section 7.3*.

Although it is the incremental change in pore fluid pressure that is usually the required quantity when solving the governing non-linear equations, it is often more convenient for the user to specify the accumulated value at the end of a particular increment. It is then left to the software to work out the incremental change from the prescribed value, given by the user for the end of the increment, and the value stored internally in the computer, for the beginning of the increment. It is noted that not all software packages have this facility. It should also be noted that some software packages may use change in head or excess pore fluid pressure, instead of pore fluid pressure, as the nodal degree of freedom. Consequently, the boundary conditions will have to be consistent.

As an example of the use of prescribed pore fluid pressures, consider the excavation problem shown in **Figure 7.19**. Throughout the analysis it is assumed that on the right-hand side of the mesh the pore fluid pressures remain unchanged from their initial values. Consequently, for all the nodes along the boundary AB, a zero incremental pore fluid pressure (i.e. $\Delta p_f = 0$) is specified for every increment of the analysis. The first increments of the analysis simulate excavation in front of the wall and it is assumed that the excavated surface is impermeable. Consequently, no pore fluid pressure boundary condition is prescribed along this surface and a default condition of zero nodal flow is imposed. However, once excavation is completed, as shown in Figure 7.19, the excavated soil surface is assumed to be permeable, with a zero pore fluid pressure. Therefore, for the increment after excavation has been completed, the final accumulated value (i.e. $p_f = 0$) is specified along CD. As the program knows the accumulated pore fluid pressure at the nodes along this boundary at the end of excavation, it can evaluate Δp_f. For subsequent increments the pore fluid pressure remains at zero along CD and consequently $\Delta p_f = 0$ is applied.

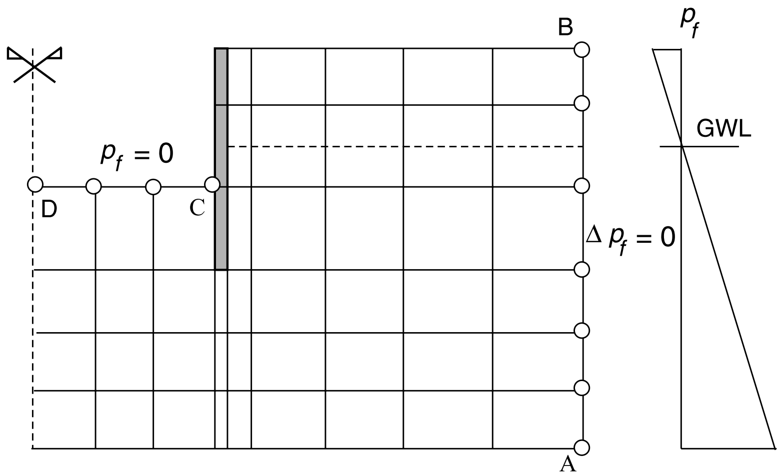

Figure 7.19 Prescribed pore fluid boundary conditions

7.12 Infiltration

When it is necessary to prescribe pore fluid flows across a boundary of the finite element mesh (i.e. in coupled consolidation analysis) for a particular increment of the analysis, infiltration boundary conditions are used. These flows are treated in a similar fashion to boundary stresses as described in *Section 7.6*.

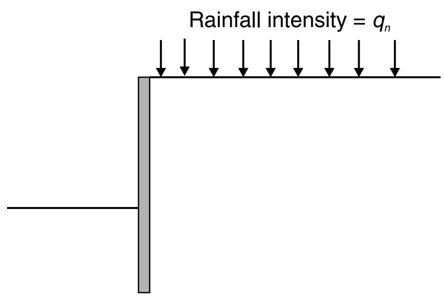

Figure 7.20 Example of infiltration boundary conditions

An example of an infiltration boundary condition is shown in **Figure 7.20**, where it is assumed that rainfall provides a flow rate q_n on the soil surface adjacent to the excavation. In general, the flow rate may vary along the boundary over which it is active. To apply such a boundary condition in finite element analysis, the flow over the boundary must be converted into equivalent nodal flows. Many finite element programs will do this automatically for generally distributed boundary flows and for arbitrarily shaped boundaries.

The nodal flows equivalent to the infiltration boundary condition are determined from the equation

$$\{\boldsymbol{Q}_{\text{infil}}\} = \int_{Srf} [\mathbf{N}_p]^{\mathrm{T}} q_n \mathrm{d}Srf \tag{7.21}$$

where *Srf* is the element side over which the infiltration flow is prescribed. As with boundary stresses, this integral can be evaluated numerically for each element side on the specified boundary range.

7.13 Sources and sinks

A further option for applying flow boundary conditions is to apply sources (inflow) or sinks (outflow) at discrete nodes, in the form of prescribed nodal flows. For plane strain and axisymmetric analyses these are essentially line flows acting perpendicularly to the plane of the finite element mesh.

An example of a source and sink boundary condition is shown in **Figure 7.21** in the form of a simple dewatering scheme involving a row of extraction wells (sinks) within an excavation and, to limit excessive settlements behind the retaining wall, a row of injection wells (sources). The effect of the extraction wells could be modelled by applying a flow rate equivalent to the pumping rate at node A, and the effect of the injection wells could be modelled by applying a flow rate equivalent to the injection rate at node B.

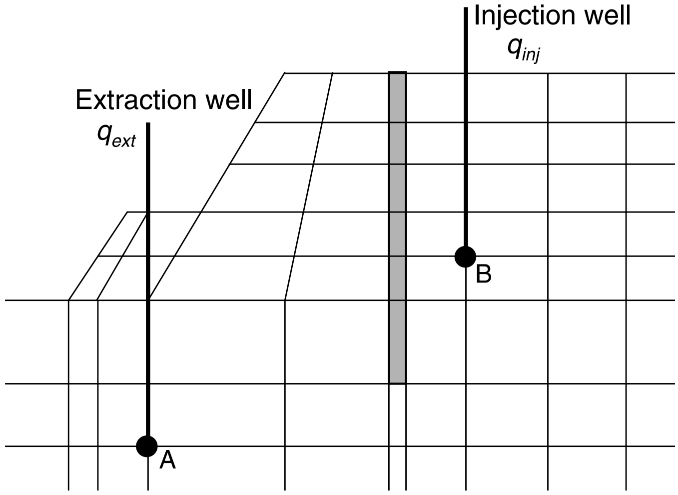

Figure 7.21 Example of sources and sinks boundary conditions

7.14 Precipitation

This boundary condition option allows the user essentially to prescribe a dual boundary condition to part of the mesh boundary. Both an infiltration flow rate q_n and a pore fluid pressure p_{fb} are specified. At the start of an increment, each node on the boundary is checked to see whether the pore fluid pressure is more compressive than p_{fb}. If it is, the boundary condition for that node is taken as a prescribed incremental pore fluid pressure Δp_f, the magnitude of which gives an accumulated pore fluid pressure equal to p_{fb} at the end of the increment. Alternatively, if the pore fluid pressure is more tensile than p_{fb}, or if the current flow rate at the node exceeds the value equivalent to q_n, the boundary condition is taken as a prescribed infiltration with the nodal flow rate determined from q_n. The following two examples show how this boundary condition may be used.

7.14.1 Tunnel problem

After excavation for a tunnel, assuming the tunnel boundary to be impermeable, the pore fluid pressure in the soil adjacent to the tunnel could be tensile. If for subsequent increments of the analysis (tunnel boundary now permeable) a prescribed zero accumulated pore fluid pressure boundary condition is applied to the nodes on the tunnel boundary, flow of water from the tunnel into the soil would result (see **Figure 7.22(a)**). This is unrealistic, because there is unlikely to be a sufficient supply of water in the tunnel. This problem can be dealt with by using the precipitation boundary option with $q_n = 0$ and $p_{fb} = 0$. Initially (after excavation), the pore fluid pressures at the nodes on the tunnel boundary are more tensile than p_{fb}; consequently a flow boundary condition with $q_n = 0$ (i.e. no flow) is adopted (see **Figure 7.22(b)**). With time the tensile pore fluid pressures reduce owing to swelling and eventually become more compressive

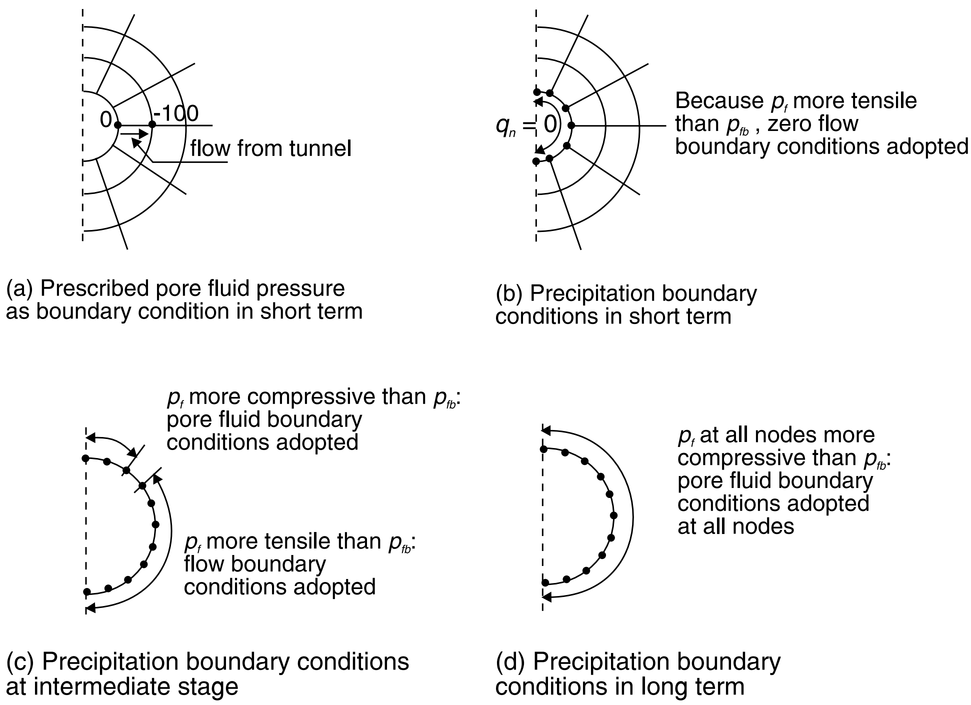

Figure 7.22 Precipitation boundary conditions in tunnel problem

than p_{fb}. When this occurs, the pore fluid stress boundary condition is applied, with a magnitude set to give an accumulated pore fluid pressure at the end of the increment equal to p_{fb} (see **Figure 7.22(d)**). The pore fluid pressure checks are made on a nodal basis for all nodes on the tunnel boundary for each increment. This implies that the boundary condition can change at individual nodes at different increments of the analysis. At any one increment some nodes can have a prescribed pore fluid stress boundary condition, while others can have a flow condition (see **Figure 7.22(c)**).

7.14.2 Rainfall infiltration

In this case the problem relates to a boundary that is subject to rainfall of a set intensity. If the soil is of sufficient permeability and/or the rainfall intensity is small, the soil can absorb the water and a flow boundary condition is appropriate (see **Figure 7.23(a)**). However, if the soil is less permeable and/or the rainfall intensity is high, the soil will not be able to absorb the water, which will pond on the surface (see **Figure 7.23(b)**). There is a finite depth to such ponding, which is problem specific, and consequently a pore fluid pressure boundary condition would be applicable. However, it is not always possible to decide which boundary condition is relevant before an analysis is undertaken, because the behaviour will depend on soil stratification, permeability and geometry. The dilemma can be overcome by using the precipitation boundary condition, with q_n set equal to the rainfall intensity and p_{fb} set to have a value more compressive (i.e. equivalent to the ponding level) than p_{fi}, the initial value of the pore fluid stress at the soil boundary. Because p_{fi} is more tensile than p_{fb}, a flow boundary condition will be assumed initially. If during the analysis the pore fluid pressure becomes more compressive than p_{fb}, the boundary condition will switch to that of a prescribed pore fluid pressure.

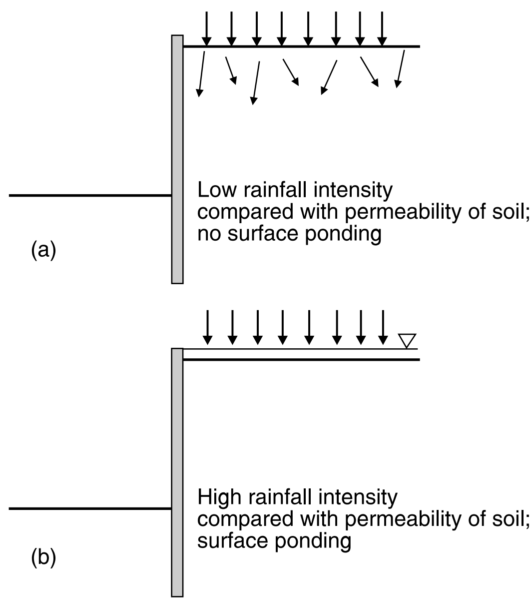

Figure 7.23 Rainfall infiltration boundary conditions

7.15 Initial stresses

The initial stress state in the ground, prior to any stress redistribution taking place as a result of construction activities or applied loading, plays an important role in a numerical analysis. In particular when advanced constitutive models are employed, the initial stress state may have a significant influence on the predicted mechanical behaviour.

There are several methods available to arrive at the initial stress state in a numerical analysis:

- The most common method in geotechnical programmes is to initialize the domain with a certain stress state corresponding to the unit weight and a K_o value. In this case of course no displacements are associated with these stresses. Depending on whether the soil is normally consolidated or over-consolidated, care must be taken in choosing the appropriate initial size of yield surface(s) when using the more advanced constitutive models. It has to be noted that this procedure is applicable only for horizontal ground surfaces. It should be checked whether the software used checks the initial stress state for violation of the failure criterion used.

- The second method is to apply gravity to the soil body. In this case the resulting displacements have to be set to zero before analysis of the boundary value problem is undertaken. Again care has to be taken in the choice of the constitutive model because this can have a significant influence on the resulting K_o value. It is worth mentioning that a gravity load case with an elastic material restricts the horizontal stress to be calculated from this procedure to a K_o value of $v/(1-v)$, where v is the Poisson's ratio. The same holds true for a Mohr–Coulomb model when the domain has a horizontal surface and standard boundary conditions apply. For these reasons this method may be an acceptable approximation for normally consolidated ground conditions but is certainly not suitable for over-consolidated soils.
- If the geological history is known it is possible (and sometimes advisable) to model the history, especially when preconsolidation and unloading of the area has been significant (e.g. ice cover). Again the choice of the constitutive model (e.g. the behaviour in primary loading–unloading) has a significant influence on the calculated stresses and therefore on the results of a subsequent analysis.

Guidelines for input and output

8.1 Introduction

There is a basic need to provide a consistent form of the minimum input and output documentation for a finite element (FE) or finite difference (FD) analysis. This is beneficial for the user as it establishes an easy control and checking procedure, as well as facilitating any quality control system. The client profits from a traceable and easily understandable procedure. Standardization of input and output parameters also facilitates the verification of data consistency. The guidelines in this chapter suggest minimum basic and standardized information required for an FE analysis. An interpretation of the questions to be solved and an explanation of the meaning of the results should be provided too.

Equivalent information as standardized here for FE analysis should be given for FD analysis as well as for boundary element (BE) calculations or for mixed forms such as the coupled FE–BE methods.

8.2 Basic information

Before describing the most likely input and output data, a set of basic information is needed. This should include:

- full identification of the code, including the version and any additional (installed) features used;
- the element types used (if not indicated in the plots themselves);
- the material models used for the different soil strata and structural components;
- implied simplifications in the calculation as, for example: plane strain, axisymmetry, etc.

8.3 Input

It is most important that the data input is replotted by the program so that its consistency can be visualized and confirmed. The different soil layers should be clearly identified so that possible confusion and inconsistency in the input data may be easily detected.

8.3.1 Plot of the finite element mesh

Figure 8.1 shows an example of a finite element mesh used to analyse a natural slope. This plot provides the basic information about the mesh. It allows for a straight forward preliminary check of the undeformed mesh in order to judge whether it is appropriate. The importance of this check is obvious, since many numerical difficulties that are encountered in using full numerical analysis stem from an incorrect or confused mesh geometry.

When interface elements are used, their types and their locations should be given either in the main plot or in a separate figure.

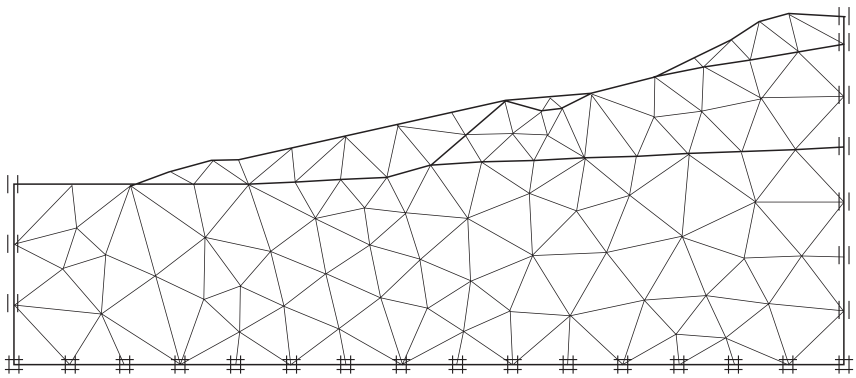

Figure 8.1 Plot of the finite element mesh

8.3.2 Plot of boundary conditions

A plot showing the type and position of the boundary conditions is also essential for judging the quality of the numerical model. It also demonstrates the simplifying assumptions that have been made. **Figure 8.2** gives an example showing the boundary fixities (bottom line) and the horizontally restrained and vertically free deformation boundaries (side boundaries).

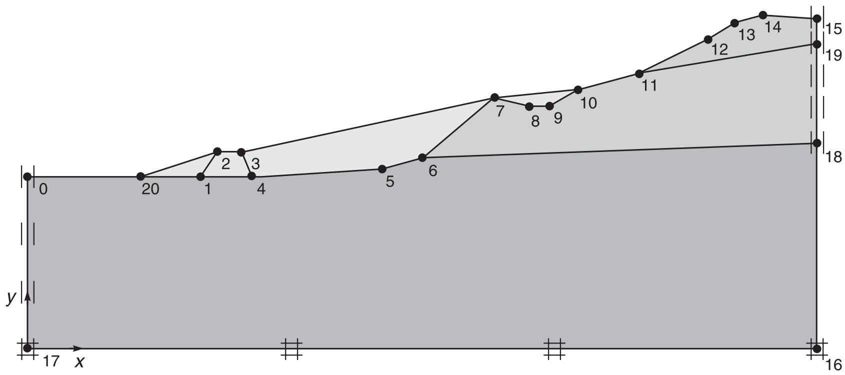

Figure 8.2 Plot of the soil strata for a natural clay slope

8.3.3 Plot of soil strata

A plot of the soil strata, see Figure 8.2, is the third of the necessary standard plots. It is again useful for judging and comparing the numerical model with the real situation. The plot of the soil strata should be followed by a description of the material models used and a table of the associated input parameters.

8.3.4 Table of used material parameters and material models

In this table the constitutive models used and their associated input parameters should be given. It is essential to provide information on how these parameters have been derived. This information should be provided as complete as possible in order to demonstrate the inherent assumptions and simplifications. An example is given in Table 8.1. As far as possible the physical meaning of the parameters and the flow rule used should also be indicated.

8.3.5 Plots illustrating the behaviour of the chosen material models

It is a good idea to simulate relevant laboratory tests (triaxial tests, oedometer tests) with the parameters chosen, and to compare these numerical simulations with the possible test data at hand for the problem that is under investigation.

Table 8.1 Example table for displaying constitutive models used and their associated parameters
Used material model: differentiate between different soils and their constitutive models.
Special applications of the model: e.g. including cap, hardening, softening, etc. If possible refer to the constitutive model in the manual or include a short description.
List the input parameters and **indicate** how these were derived. Probably the software will have click boxes here to indicate the different possibilities: ■ Laboratory tests ■ Derived from *in situ* tests (which way) ■ Empirical data ■ Estimated data ■ Curve-fitting data (e.g. recalculation of a triaxial test to derive the complex input parameters) ■ Parameter extracted from the manual.

8.3.6 Plots showing the initial stress conditions, pore water pressures and state variables

These plots should provide both the client and the user with information concerning the initial starting conditions for the numerical model. They should include the stress conditions, the pore water pressures and the distribution of state variables such as the stiffness distribution or the state of an element in terms of its hardening/softening parameters before the modelling starts. This information also helps the user to judge the consistency of the input data and to show any inherent idealizations.

Figure 8.3 shows the initial stress state in a normally consolidated sediment. The length and direction of the lines represent the magnitude and orientation of the principal stresses at integration points. The buried 'structure' shown by the thick horizontal and short vertical lines is not yet loaded. The soil layer above the structure is merely added to simulate the preconsolidation effect of the previous overlying soil.

In **Figure 8.4** the upper soil layer has been removed. Note that with the soil model used in this example (not a perfectly elastic one) the horizontal stress profile tends to reflect the previous soil surface, switching the principal stress axis close to the current terrain surface.

Assumptions concerning the initial stress situation may be very crucial for the later calculation stages.

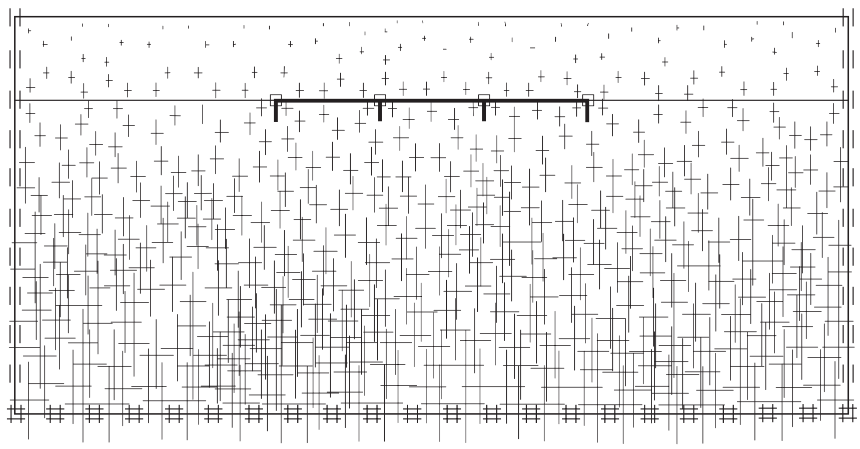

Figure 8.3 Initial stress state for a normally consolidated sediment

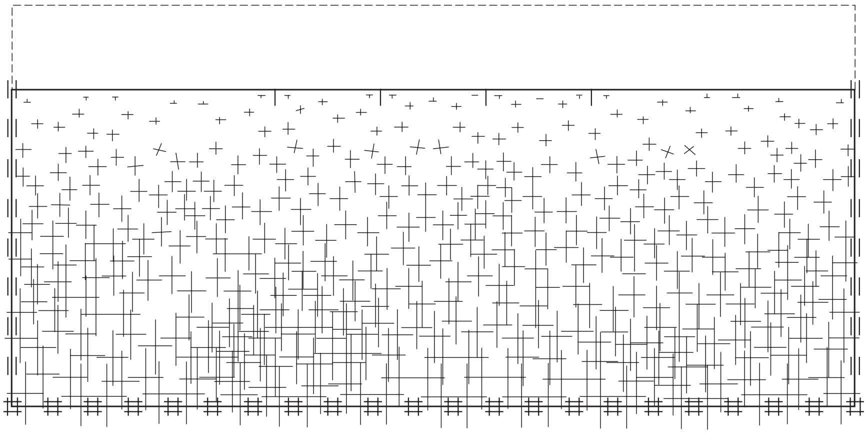

Figure 8.4 Over-consolidated stress situation after removal of upper soil layer

8.3.7 Table of solution stages and convergence criteria

This table should indicate the sequence of loading/construction/excavation stages for the entire numerical modelling process. It should be accompanied by geometrical plots in cases involving excavation and/or construction (i.e. removal or adding of elements) etc. The table allows the client to follow the entire modelling procedure from the mesh generation stage through to the different boundary conditions applied during the analysis. For undrained–drained analysis it is necessary to state the time sequence in which something is modelled. In addition, the required or assumed convergence criteria should be indicated.

8.4 Ouput

The output documentation should again consist of a set of standard plots. These may vary in appearance because of the options offered in the different computer codes and the nature of the specific problem that is to be analysed. However, it should be clearly shown which calculations have been conducted and how they affect the model itself. Thus a set of minimum necessary plots is described here. They consist of the following.

8.4.1 Plot of the deformed element mesh

A plot of the deformed FE mesh may give an overview of where and how the deformations of the soil body and adjacent structures have taken place. **Figure 8.5(a)** and **(b)** show an example of a natural slope where the upper part of the slope clearly has undergone the most severe deformations.

8.4.2 Plot of displacement vectors

Figure 8.6(a) and **(b)** show examples of plots of displacement vectors. These plots could present accumulated displacements during the whole calculation or sub-accumulated displacements occurring during each different calculation step.

An incremental plot is useful for certain sequences. This may apply in particular to sequences that model the removing/adding of elements or the removing/adding of a load.

For long-term calculations involving consolidation or creep, one should also include plots of intermediate steps.

8.4.3 Contours of stress and strain

Figure 8.7(a) and **(b)** show contour plots of shear strain. Contour plots of the stress and strain states for intermediate and final stages of the analysis should be given. The number of plots

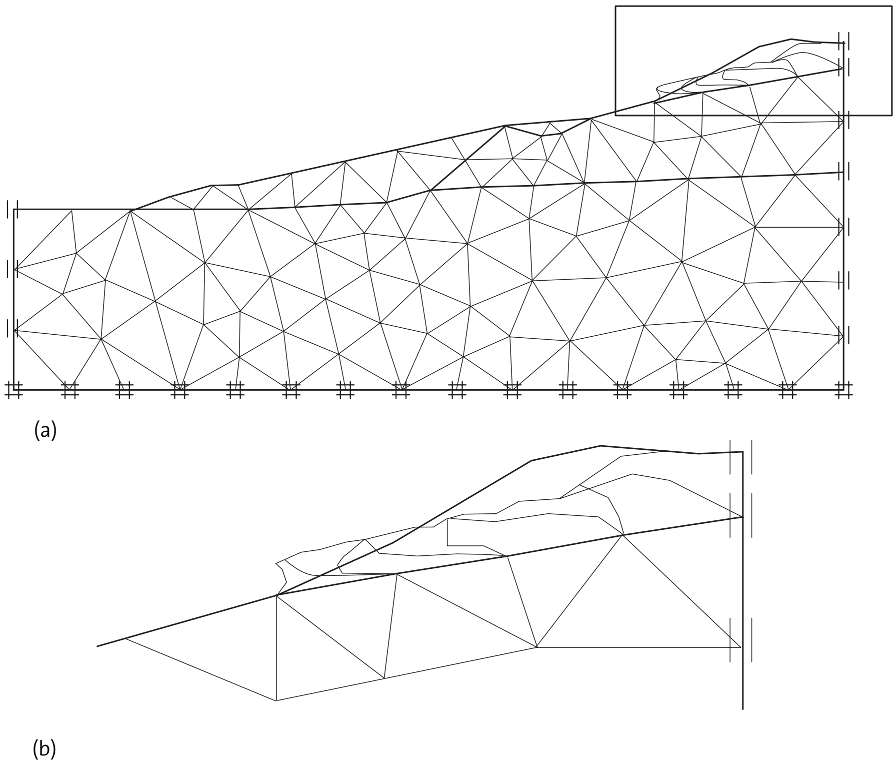

Figure 8.5 (a) Example of a deformed element mesh. (b) Close-up of the upper part of the slope

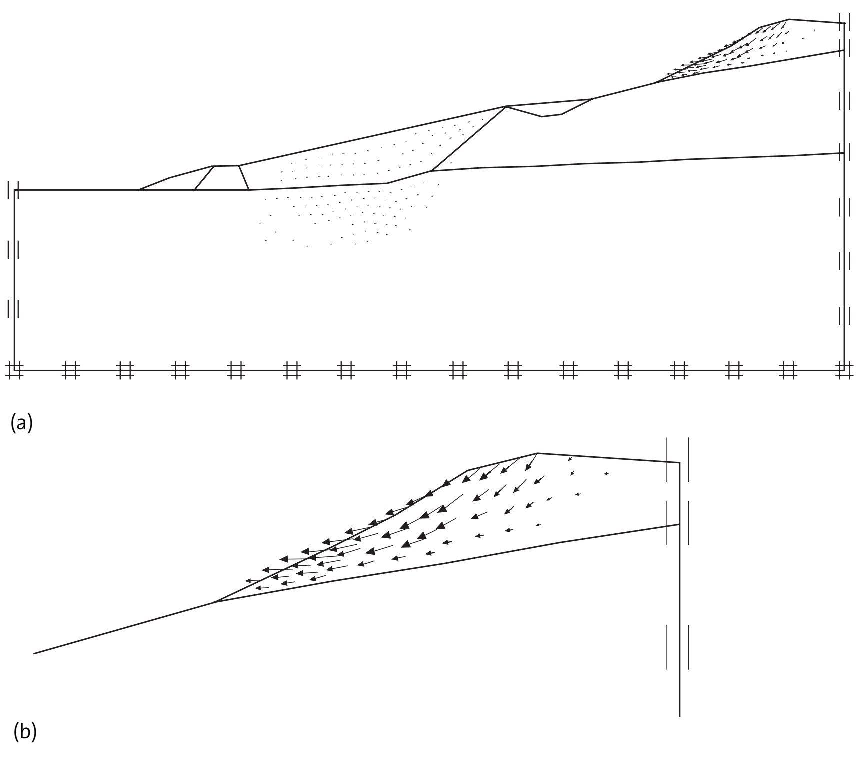

Figure 8.6 (a) Displacement vectors for a natural slope (note the upper part of the slope is critical). (b) Total displacement vectors – enlarged plot of upper slope

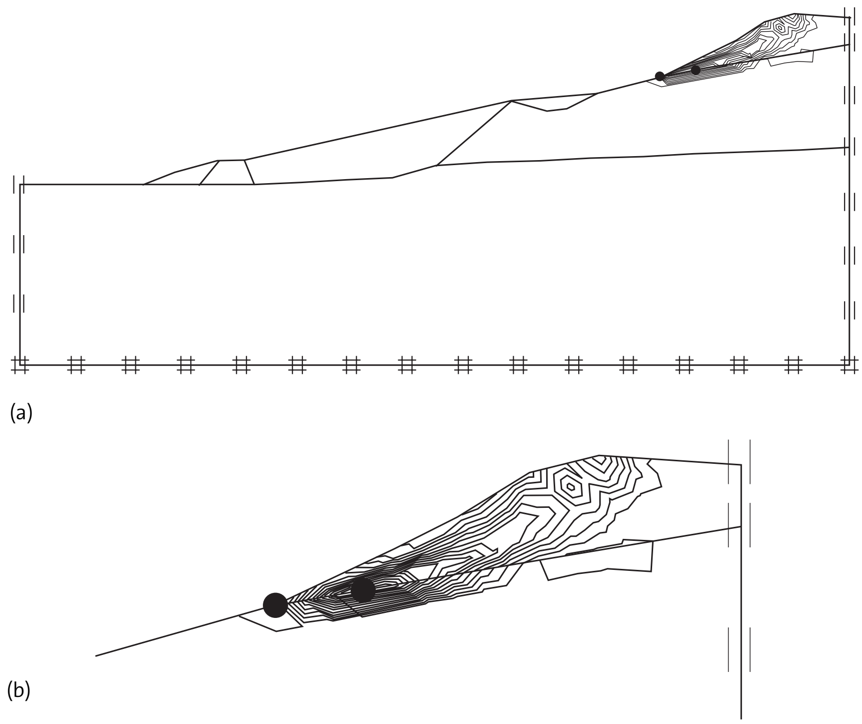

Figure 8.7 (a) Shear strain contours for a natural slope. (b) Close-up view of the strain contours in the upper slope

depends on the difficulty and the complexity of the modelling procedure. The client should be able to get a visual idea of the changes taking place in the soil as the analysis proceeds. The range and the resolution in the contour plots should be related to the problem.

8.4.4 Contours of stress levels and state variables

An indication of stress levels and state variables by means of contour plots helps (in addition to the suggestions given under *Section 8.4.2*) to establish the quality of the FE mesh. Of major importance (depending on the constitutive models adopted) are the identification of zones reaching plasticity (see **Figure 8.8**) and changes in stiffness and strength of the soil or the boundary forces.

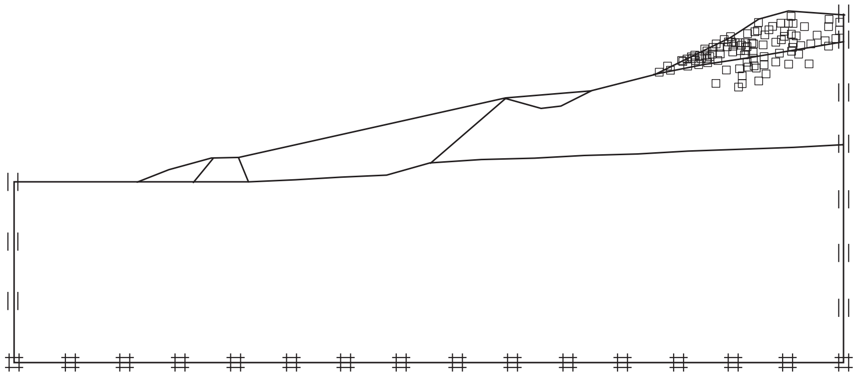

Figure 8.8 Plastic integration points

In order to properly interpret the changes in the stresses and strains predicted during an analysis, one must bear in mind the two-(or three-) dimensional nature of the problem. Plots of volumetric and shear components of stresses and strains are therefore often more meaningful than concentrating on horizontal and vertical components. Often the shear strength of the soil materials will vary with the average effective stress level; thus plots of the degree of shear mobilization (often denoted as relative shear) will be more instructive than plots of the shear stress itself (in kPa).

8.5 Conclusion

Full numerical analysis requires the handling of a vast amount of data. It is vital to utilize graphical plots to secure and demonstrate the consistency of the input and output data. The series of plots that should be presented may grow prohibitive. It is important that at least the basic plots showing the geometry and boundary conditions, the initial stress assumptions and the intermediate and final stress, strain and displacements are given.

In addition, the material parameters and their implications should be summarized.

9 Modelling specific types of geotechnical problems

9.1 General aspects

9.1.1 Size of problem domain

Numerical methods such as the finite element method (FEM) yield approximate solutions to boundary value problems of continuum mechanics. In this approach the problem domain, which is a part of the continua, is subdivided into finite elements. The size of the problem domain should be selected in such a way that the influence of the omitted part of the continua has a negligible effect on the results of the numerical solution.

With regard to a linear elastic boundary value problem, the optimal size of the domain should be large enough to ensure that no significant displacements along the boundaries are induced by the numerical solution. Enlargement of the domain may also be required to account for other factors such as unbalanced external loads, which could induce unacceptable reactive loads along the boundaries (Meissner, 1991). On the other hand, the size of the domain influences the number of degrees of freedom (DOF) and hence the cost of the solution, therefore it should be kept as small as possible. In order to reduce the size of the domain, it is important to utilize all of the possible symmetry conditions of the structure and its surroundings. Another option is to use infinite elements, or a combination of the FEM and the BEM (boundary element method).

The soil–structure interaction problems under consideration in this report involve modelling the behaviour of soils that can rarely be treated as elastic. Therefore a number of additional geomechanical aspects should be taken into account when the size of the problem domain is selected:

- Depending on the specific *geological conditions* of any site, the size of the domain could be either reduced or enlarged. For example, if a layer of compressible subsoil is underlain by incompressible rock then the thickness of the compressible subsoil determines the depth of the domain. On the other hand, a rectangular domain with inclined strata or an inclined system of joints requires an enlargement of the domain size.
- The size of the domain depends also on the *constitutive model* used to represent the various soil layers and structural components. The response of an elastic material to loading and unloading can be infinite. This can produce an unrealistic heave of a tunnel, or an unrealistic settlement of an embankment, which increases as the depth of the model is increased if elastic or elastic–perfectly-plastic (e.g. Mohr–Coulomb) constitutive models are used. To avoid this effect, the depth of the model should be restricted to (2–3)D tunnel diameters below a tunnel invert (Meissner, 1996), and to the so called 'active depth' (depth at which the subsoil structural strength exceeds the vertical stress increment due to surface load (Swoboda *et al*., 2001)) below shallow foundations and embankments. Alternatively the elastic stiffness can be allowed to increase with depth. Such restrictions are unnecessary if more advanced constitutive models, which take proper account of non-linearity and deviatoric and volumetric loading/unloading in the pre-peak regime, are employed.

9.1.2 Appropriate use of numerical analysis

Numerical analysis should be undertaken in cases where the problem cannot be solved using conventional analysis, or where such a conventional solution is incomplete or oversimplified. As a rule, complex geotechnical problems of large civil engineering structures belong to this category, especially when:

- the geological and geotechnical conditions of the site are complicated (e.g. heterogeneous and/or inclined strata, over-consolidated, anisotropic and swelling soils, etc.) and no prior experience with these conditions exists;
- soil–structure interaction problems with complex geometry and geological conditions are addressed;
- deformation of interacting structures should be predicted, or the effect on existing nearby underground or above-ground structures concerning stability and cracking resistance should be determined;
- the effect of complex material behaviour, including non-linearity, plasticity and creep, should be considered;
- the solution is considerably influenced by the *in situ* stress state, including over-consolidation;
- the effect of construction techniques and construction sequence should be estimated;
- irregular results of laboratory or full-scale *in situ* tests or other field tests have been obtained;
- the influence of the stiffness of above-ground structures should be taken into account;
- the effect of different construction techniques should be compared and evaluated;
- evaluation of a field trial is necessary;
- monitoring is planned and limiting values of the expected displacements, pore pressures and other quantities are required;
- possible failure mechanisms and the corresponding deformation criteria should be determined;
- specification of an optimum construction speed, for example control of pore pressure development in the subsoil beneath embankments, is required to secure the safety of the structure during construction;
- back analysis of measurement results is performed and the material properties (constitutive models and parameters) are to be identified.

9.1.3 Parametric studies of the effects of chosen input parameters

Since numerical analyses are undertaken to solve complex problems in difficult geological and geotechnical conditions, there will always be limitations regarding the quality and quantity of input parameters. Therefore a parametric study is a basic tool for appropriate use of numerical analysis for solving geotechnical problems. The main objective is to obtain a range of responses for a given range of input data and to understand the behaviour of the structure. In order to minimize the process, only the key parameters of a given problem should be analysed and their realistic range and reasonable combination specified.

Concerning soil–structure interaction problems, the following list of input data is provided as a basis for specification of items to be studied:

- initial state: K_o, size (width) of domain, groundwater level;
- type of constitutive model: elastic–perfectly-plastic with non-linearity (small strain stiffness) in pre-peak regime, Mohr–Coulomb, double hardening;

- material properties: stiffness, cohesion, undrained shear strength, permeability (note there is interdependence of deformational, strength and hydraulic parameters), degree of anisotropy of mechanical and hydraulic parameters;
- construction techniques and sequence.

9.2 Piles and piled rafts

9.2.1 General aspects

The behaviour of piles, together with the use of numerical analysis to analyse pile behaviour, is of course a subject which receives much attention in the literature. In this chapter some general points will be raised. For a more detailed treatment of the subject, the reader is referred to Potts and Zdravkovic (2001a).

9.2.2 Soil behaviour aspects

Soil dilation can have a dominant effect on pile behaviour and consequently care must be exercised when selecting an appropriate constitutive model and its parameters.

When analysing axially loaded piles using an effective stress constitutive model, it is unwise to use a model that predicts finite plastic dilation indefinitely without reaching a critical state condition (e.g. the Mohr–Coulomb model with $v > 0^o$). Such analyses will not predict an ultimate pile capacity.

9.2.3 Interface elements

When analysing a single pile subject to axial loading, either thin solid elements or special interface elements should be placed adjacent to the pile shaft. If solid elements are used and they are not sufficiently thin, the analysis will overestimate the pile shaft capacity.

If interface elements are positioned adjacent to the pile shaft, care should be taken in selecting their normal and shear stiffness. These values, if not sufficiently large, can dominate pile behaviour. However, if the values are too large, numerical ill conditioning can occur.

9.2.4 2D or 3D analysis

In several cases 2D plane strain modelling provides accuracy good enough to enable proper simulation of a problem. A railway or road embankment can be mentioned as such. However, a simulation of a laterally loaded pile group requires 3D modelling because of the discontinuous effects in orthogonal directions.

Although several finite element codes provide capabilities for 3D and 2D modelling of soil structure problems, 3D modelling is highly complex. Little experience exists in its application and caution should be taken when using such techniques.

An efficient way to reduce the number of degrees of freedom in finite element modelling is to utilize planes of symmetry. This is possible in many problems. In certain cases it is even possible to have two symmetry planes, thus leading to a significant reduction of the number of degrees of freedom and savings in computer resources.

An example of such an analysis, for a piled raft foundation, is shown in **Figure 9.1**. The geometric model of the continuum and the piles consists of 3D isoparametric finite elements while the raft is modelled with shell elements. At the borders infinite elements are used, which respond like an elastic half-space. Because of the symmetry of the geometry, the finite element mesh is reduced to cover only one-eighth of the original area to be considered.

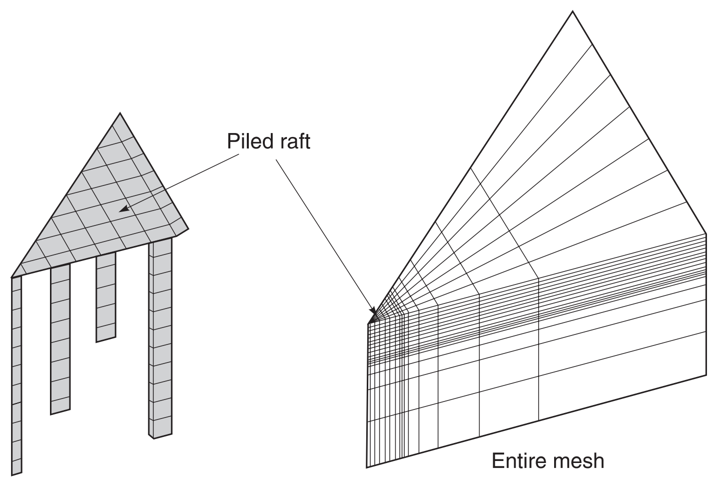

Figure 9.1 3D finite element mesh for a piled raft foundation (after Katzenbach *et al.*, 1998)

9.2.5 Lateral loading

Field evidence shows that during cyclic lateral loading of single piles (particularly in offshore situations) a crack forms down the back of the pile (i.e. gapping) (e.g. Long *et al.*, 1992). If this is to be taken into account in analysis, interface elements should be installed along the pile–soil interface, which cannot sustain tensile normal stresses. Whether or not gapping is likely to occur depends on the soil strength and in particular its distribution with depth (Potts and Zdravkovic, 2001a).

9.2.6 Back analysis of pile tests

Back analysis of pile tests is used for modelling pile behaviour under known loading conditions. The objectives are usually to determine the development of the base and shaft resistance in the soil layers, to determine the stress and strain distribution in the soil layers adjacent to the pile, or to develop a well behaved soil–structure interaction model for the tested pile type.

The pile tests used as a reference for the analysis should be performed under controlled conditions, either in a laboratory test pit or as a field test. Soil conditions of the test site must be known as accurately as possible. The soil layers and layer boundaries should be determined by soundings and at least one soil sample from each stratum should be tested in the laboratory to determine the necessary elastic and plastic soil parameters needed for the soil model used.

The test pile should be instrumented in a manner such that at least the load–displacement behaviour of the pile is well recorded. If possible, also the stress distribution along the pile shaft and the stress level under the pile base should be known.

The back analysis can be performed for individual piles or pile groups under static, cyclic or dynamic loading. The reference data of the tests as well as the determined soil parameters of the test site should be consistent with the type of modelling to be performed.

The back analysis of the pile test can be performed by using either a 2D axisymmetric or a 3D model, or by using the combination of 3D beam elements and non-linear springs to model the soil response. The dimensioning of the model depends on the load type and its direction, the physical complexity of the pile and the test environment or the symmetry of the pile group in respect of the load and soil conditions. The main objective is to create a model that corresponds as accurately as possible to the test conditions and that uses material models for the soil and structural elements that are suitable for the purpose.

9.3 Tunnelling

9.3.1 Scope of the problem

This section focuses on numerical analysis of shallow tunnels, which frequently cause soil–structure interaction problems in urban areas. Their construction, as a rule, affects existing underground and above-ground structures and there is a need to keep the settlement induced by tunnelling as small as possible. Such complex soil–structure interaction problems can only be solved by numerical analysis, which provides complete information on the stress–strain conditions of the tunnel, the surrounding soil mass and nearby structures.

The stress state induced by construction of a shallow tunnel (secondary stress state) is three-dimensional (3D) in general and depends on the following factors:

- tunnel geometry, determined by cross-section and depth;
- geological and hydro-geological conditions of the site;
- *in situ* (primary) stress state determined by the depth of overburden and the lateral pressure coefficient at rest K_0;
- deformational, strength and rheological properties of the ground and the lining; and
- construction sequence, i.e. excavation stages in transverse and longitudinal directions and temporary support placement and permanent lining installation techniques.

The correct simulation of the 3D load transfer, occurring ahead of and behind the tunnel face and resulting in transverse and longitudinal arching around the unsupported section at the tunnel face, is of particular importance (see **Figure 9.2**).

9.3.2 Type of numerical analysis

9.3.2.1 3D analysis

In principle all the above factors can be taken into account by using an advanced numerical code, appropriate constitutive models for the materials and a 3D computational model. The

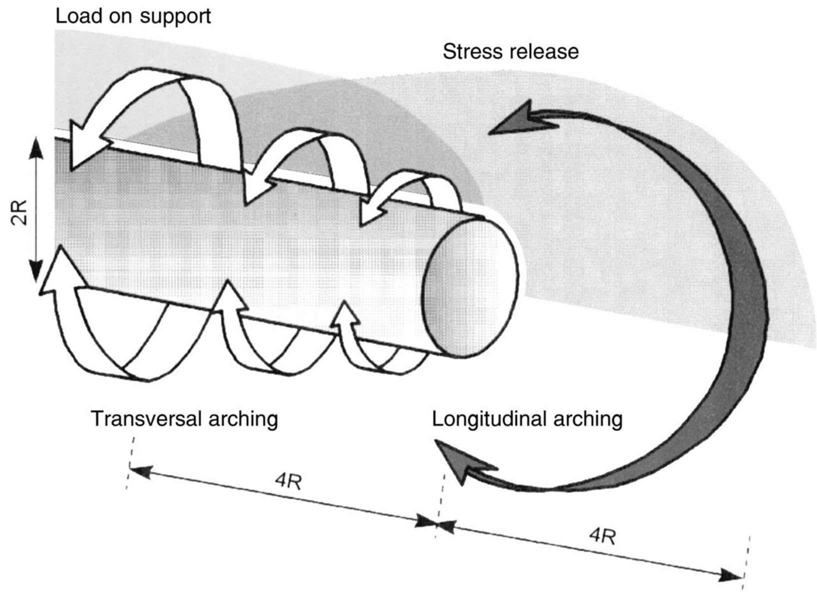

Figure 9.2 Sketch showing three-dimensional stress transfer at tunnel face

software should provide efficient 3D-mesh generation and 3D graphical presentation of the results as well.

However, as stated above, there is little international experience of 3D analyses and they should be undertaken only by an experienced operator and the results treated with caution. Also, such 3D analyses are costly and time consuming and should be applied only to complex problems.

9.3.2.2 Axisymmetric analysis

Axisymmetric analysis of a tunnel and its surroundings provides a full 3D solution of the transverse and longitudinal load transfer for the cost and run-time of a 2D analysis. The tunnel face advance and support installation procedure (stability of the face, influence of the support distance from the face on the tunnel convergence and lining load, etc.) can be investigated in this way. Furthermore, the effect of the ground properties on these matters can be studied and the initial convergence, which occurs ahead of the tunnel face, determined (Panet and Guenot, 1982; Renati and Roessler, 1998).

However, this type of analysis is limited to tunnels of circular cross-section built in homogeneous subsoil at depth, where axisymmetric boundary conditions and an *in-situ* stress state with $K_o = 1$ can be assumed. These assumptions are hardly valid for a shallow tunnel.

9.3.2.3 Plane strain analysis

For a completed tunnel, plane strain conditions with zero axial strain are often valid, which sometimes justifies the wide use of this type of analysis for tunnels. Problems arise, however, with the adequate modelling of the following aspects:

- geological conditions where bedding planes and/or discontinuities are not parallel to the tunnel axis;
- *in situ* stress states;
- simulation of the construction sequence in the longitudinal direction, especially when modelling the support installation distance from the tunnel face;
- support measures such as anchors and micro-piles.

By performing a standard plane strain analysis with staged excavation and support installation only the transverse load transfer can be simulated. Each excavation stage is performed in one step and either an unsupported tunnel or a wished-in-place tunnel support can be modelled.

Neither can the tunnel face stability problem be solved, nor can the effect of the longitudinal load transfer on tunnel convergence and support pressure be simulated.

9.3.3 Methods of 2D approximation of the 3D tunnel face effect

To overcome the above limitations, methods approximating the 3D conditions at the tunnel face by a sequence of 2D analyses have been developed (Sakurai, 1978; Panet and Guenot, 1982; Dolezalova *et al.*, 1991). The process of stress release due to excavation and the process of support installation are carried out in *n* loading steps with variable support forces. To control the steps, different approaches have been developed:

- reduction of the support forces according to a stress release factor (λ method);
- reduction of the support forces until a given volume loss is achieved (V_l method);
- reduction of both the support forces and stiffness of the excavated elements.

Concerning the first method, the factor λ expressing the degree of stress release is determined by the ratio $\lambda = u_n/u_{\max}$. Here u_n denotes the actual radial displacement close to the tunnel face and $u_{\max}$ is the maximum radial displacement far away from the face. At distances $>4R$ ahead of the face $\lambda = 0$, whereas $\lambda = 1.0$ at distances $>4R$ behind it (**Figure 9.3**). Assuming that the support forces are indirectly proportional to λ, a reduction factor $\beta = 1 - \lambda$ was introduced for calculation of the actual support force vector $\boldsymbol{P}_n = \beta\, \boldsymbol{P}_{\max}$. Here $\boldsymbol{P}_{max}$ is the maximum

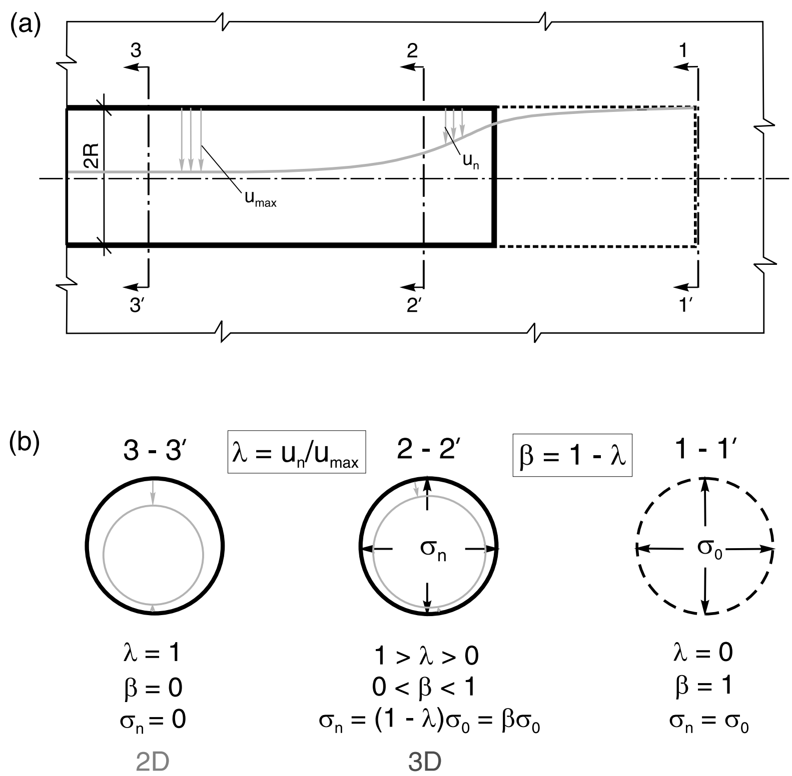

Figure 9.3 (a) Tunnel convergence due to working face advance. (b) Concept of the λ method for 2D analysis

support force vector corresponding to the *in situ* stress state σ_o (Pan and Hudson, 1988; Panet and Guenot, 1982; Dolezalova *et al*., 1991).

For a known degree of stress release λ_{rel} and load reduction factor β_{rel} before the placement of the lining, the 2D loading steps can be carried out in two stages: for the unsupported part of the tunnel with reduction factors $1 > \beta_n > \beta_{rel}$, and for the supported part of the tunnel with factors $\beta_{rel} > \beta_n \geq 0$. In this way the effect of the support distance from the tunnel face can be considered and more realistic tunnel convergence, surface settlement and lining loads can be calculated from a 2D numerical model.

There are, however, at least three problems with the 2D approximation of the 3D tunnel face effect. The first one is the realistic estimation of λ_{rel}, which is in fact a 3D problem depending on all the factors listed in *Section 9.3.1*. The second problem is the tunnel face stability, which cannot be assessed by this approach. The third one is the validity of the basic assumption of the method that a tunnel section far away from the face satisfies plane strain conditions.

To solve the first problem, estimation of the distribution of u_n in the longitudinal direction according to some 3D analytical solution (elastic, viscoelastic, elastoplastic) of an unsupported circular tunnel has been recommended and used in the past (Sakurai, 1978). Nowadays, information on tunnel convergence or volume loss according to *in situ* measurements obtained for a given type of tunnel are preferred for selecting λ_{rel} or β_{rel}. Another approach is to perform parametric studies of the face effect on the tunnel convergence, surface settlement and lining load, introducing different percentages of β_{rel}. In this way, input for the application of the convergence-confinement method can also be obtained (Renati and Roessler, 1998).

While performing all these 2D approximations of a 3D tunnel face problem, the modeller should be aware that plane strain conditions far away from the tunnel face are satisfied only for a particular case. This is the case of an unsupported tunnel in a linear elastic medium with *in situ* stress field, where $K_o = v/1 - v$. Otherwise, there is a considerable influence of the axial normal stress component σ_z and hence of the average normal stress σ_{oct}, which do not correspond to plane strain conditions, on the computed stress–strain field (Pan *et al*., 1989). This is especially important for modelling tunnels excavated in over-consolidated soil with $K_o > 1$. Because of this difference, the use of physically more correct non-linear constitutive models produces a bigger discrepancy between the results of a 3D FEM solution and the λ method (Vogt *et al*., 1998; Dolezalova and Danko, 1999). Even the elastic–perfectly-plastic Mohr–Coulomb model, which is independent of σ_2, gives considerable differences if yielding occurs. The reason is that for a 3D solution $\sigma_z = \sigma_3$ can occur at the face, which differs from the 2D assumptions. It has also been found that the surface settlement and tunnel convergence calculated by a 3D FEM analysis are often difficult to simulate with the λ method using the same value of λ_{rel} (Vogt *et al*., 1998; Dolezalova and Danko, 1999).

With respect to the above problems, 2D approaches for simulating 3D behaviour of shallow tunnels can be recommended primarily for parametric studies and for tunnels where either the site conditions are known or *in situ* measurement results (especially on volume loss V_l) are available. Otherwise, for modelling 3D construction sequences and for predicting realistic tunnel convergence, surface settlement and lining loads, 3D numerical analysis with advanced constitutive models may have to be considered.

9.3.4 Tunnelling—size of problem domain

When the size of the domain for a shallow tunnel is selected, the expected width of the *settlement trough* should be taken into account. According to field measurements (**Figures 9.4** and **9.5** and **Table 9.1**), the settlement trough width is about 1*H* to 1.5*H* for tunnels in sand (*H* is the depth to the tunnel axis), while for tunnels in clay it is about 1.5*H* to 2.5*H* (see also Mair and Taylor, 1997).

S/Smax vs x/D

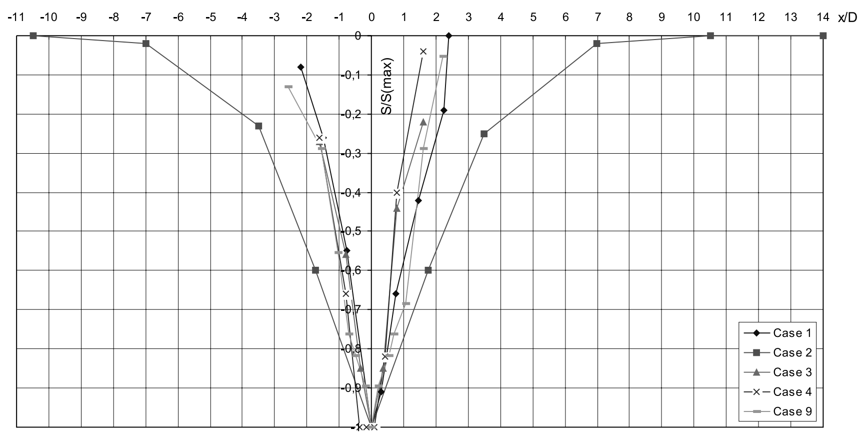

x - distance
H - depth at the tunnel axis

S - settlement
S(max) - maximum settlement

S/Smax vs x/H

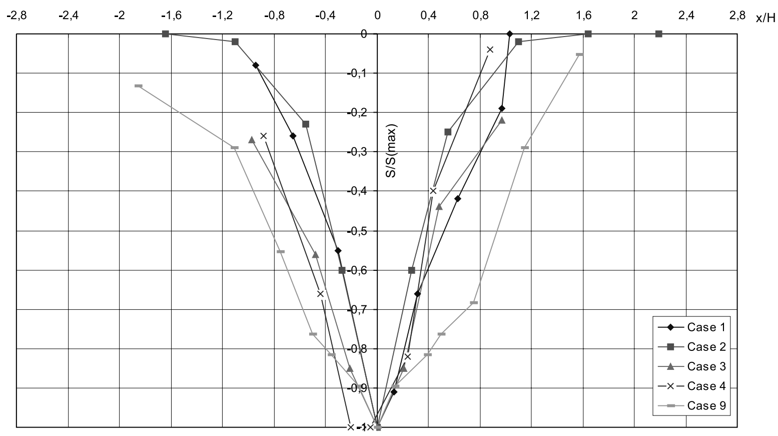

Figure 9.4 Normalized settlement troughs due to shallow tunnelling in sand

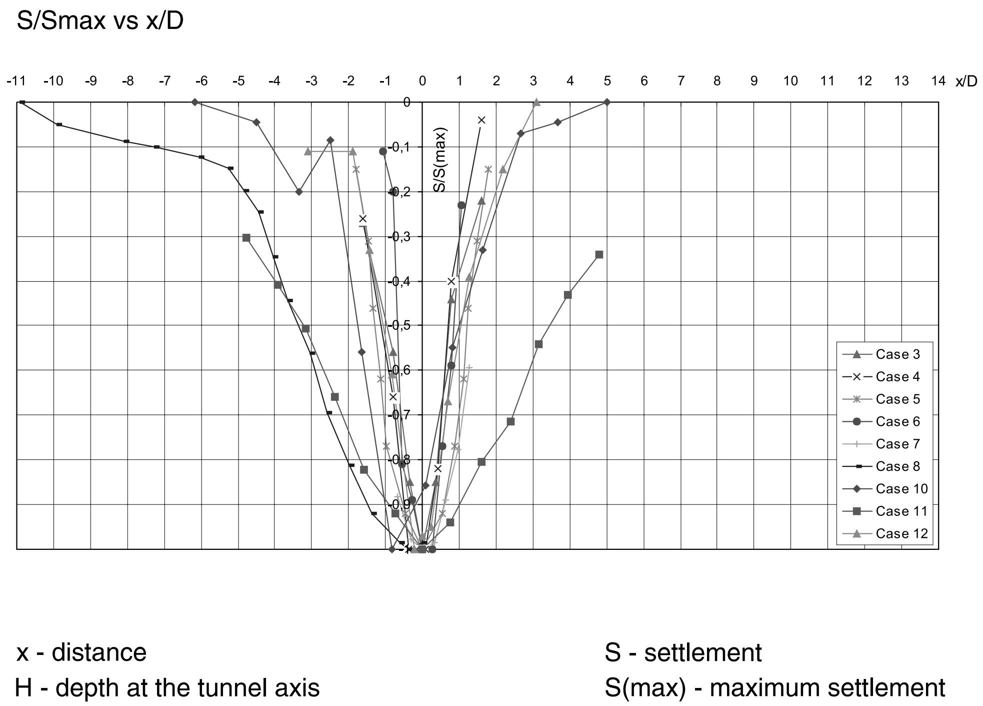

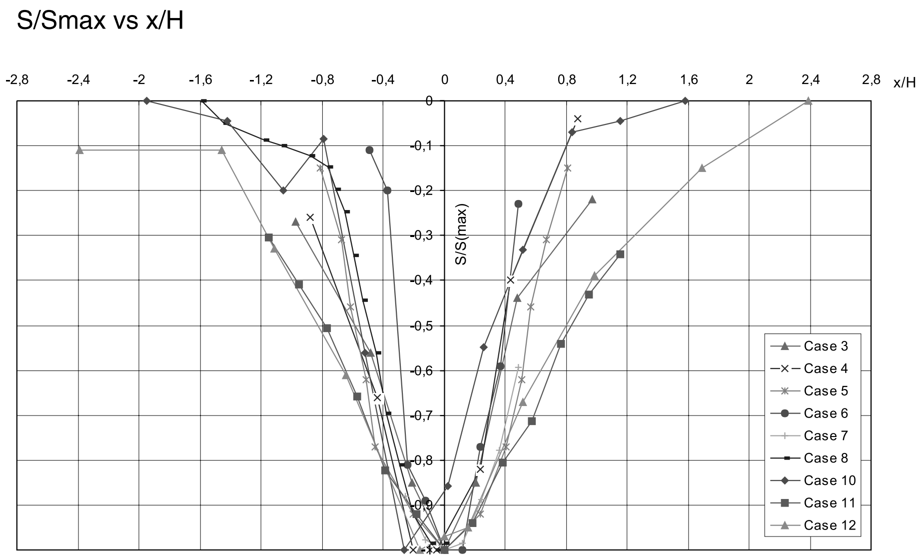

Figure 9.5 Normalized settlement troughs due to shallow tunnelling in clay

The size of the domain is also affected by the magnitude and orientation of the principal stresses corresponding to the *in situ stress state*. For a common case of a shallow tunnel in a rectangular domain, where the *in situ* stresses are parallel with the domain sides, zero horizontal displacement along the sides can be assumed at a distance of about 6*D* to 11*D*, depending on the above factors. However, a larger domain or a specific solution (calculation of *in situ* stresses by a 'macromodel' and their transfer to the boundaries of the 'micromodel' of the tunnel (Swoboda *et al*., 2001) should be applied if the *in situ* stresses are inclined. Also, to avoid underestimation of displacements, larger domains should be applied for underground openings at larger depths.

Table 9.1 Summary of case history data for measurements of tunnel behaviour.

Case	Tunnel	Diameter (m)	Depth to axis (m)	S_{max} (mm)	Excavation method and soil type	Reference
1	Val-de-Marne	3.35	7.75	5.3	Slurry shield; silt, sand, gravels	Atahan *et al.* (1996)
2	Sudden Valley Sewer	1.43	9.12	43.0	Pipe-jacking with EPB; water-borne glacial sands	Dyer *et al.* (1996)
3	Madrid Underground (Section 1)	9.38	15.50	18.0	TBM with EPB; clayey sand and sandy clay	Hernández and Romera (2001)
4	Madrid Underground (Section 2)	9.38	17.00	21.2	TBM with EPB; clayey sand and sandy clay	Hernández and Romera (2001)
5	Shanghai (Tunnel I)	11.20	24.54	650.0	Shield with mechanical excavating; silty clay	Hou *et al.* (1996)
6	Shanghai (Tunnel II)	11.20	24.50	17.9	Slurry shield; silty clay	Hou *et al.* (1996)
7	Lyon Metro, D line	6.27	16.40	13.5	Slurry shield; fine silty sands and clays	Kastner *et al.* (1996)
8	Jubilee Line, St James's Park	4.95	34.00	21.00	NATM; Lower London clay	Potts and Zdravkovic (2001b)
9	Tunnel in Japan	10.00	14.00	38.00	Highly jointed rock	Sakurai (1992)
10	Singapore, Southbound Tunnel	6.00	19.00	17.5	NATM; very stiff clay	Mair and Taylor (1997)
11	Mrazovka Adit, St. 4.859	3.76	15.58	18.5	NATM; highly jointed shale	Kamenicek *et al.* (1997)
12	Mrazovka Tunnel, St. 4.930	16.60	21.45	22.7	NATM; jointed shale	Rozsypal (2000)

9.3.5 Construction sequence

The basic steps of tunnel construction involve excavation stages in both the transverse and longitudinal directions, placement of temporary support and installation of the permanent lining. Obviously each stage needs to be modelled separately.

The following construction steps can be modelled:

- Assigning $\beta = 0$ and γ_n (stiffness reduction factor) = 0, full excavation of a selected area can be realized either in a 3D or in a 2D solution.
- If a small value $\gamma_n = 0.001$ is assigned and β_n is a variable load reduction factor which depends on the degree of stress release λ, then the tunnel face effect according to the λ method (*Section 9.3.3*) can be modelled by a sequence of 2D solutions.
- In order to follow a step-by-step stress release by the λ method, increasing values of stress release $\lambda_n > \lambda_{n-1}$ with $\sum_{n=1}^{nn}(\lambda_n - \lambda_{n-1}) = 1$ (*nn* is the number of stress release steps) are introduced. The corresponding values of loading factor β_n are given by

$$\beta_n = \frac{1 - \lambda_n}{1 - \lambda_{n-1}}$$

- Increasing the percentage of the stress release λ_n and changing the loading factor in the range $1 \geq \beta_n \geq \beta_{rel}$, the ground reaction curve for the convergence-confinement method can be computed (Renati and Roessler, 1998). Here β_{rel} corresponds to λ_{rel}, the value associated with lining installation.
- It should be noted that, to get a proper elasto-plastic solution, each loading step with a given β_n should be further divided into a number of sub-increments.
- Often only the maximum tunnel convergence occurring before placement of the lining is of interest. In this case the calculation is carried out in two stages. In the first stage $\lambda_n = \lambda_{rel}$ and $\beta_n = \beta_{rel}$ are introduced and convergence produced by the unlined part of the tunnel is calculated. In the second stage $\lambda = 1$ and $\beta = 0$ are used and the lining is installed. In this way the lining load is reduced to $\beta_{rel}\ \sigma_0$, where σ_0 is the initial stress state before excavation.
- The lining is represented by added elements with zero initial stresses. Use of three-noded beam elements, which are compatible with eight-noded isoparametric quadrilateral elements and six-noded isoparametric triangular elements, is recommended in 2D.
- The λ method can be applied not only for full-face excavation, but also for modelling multistage excavation (**Figure 9.6**). In this case the lining load for the first excavated section (crown section in Figure 9.6) will correspond to the prescribed value $\beta = \beta_{rel}$. The remaining

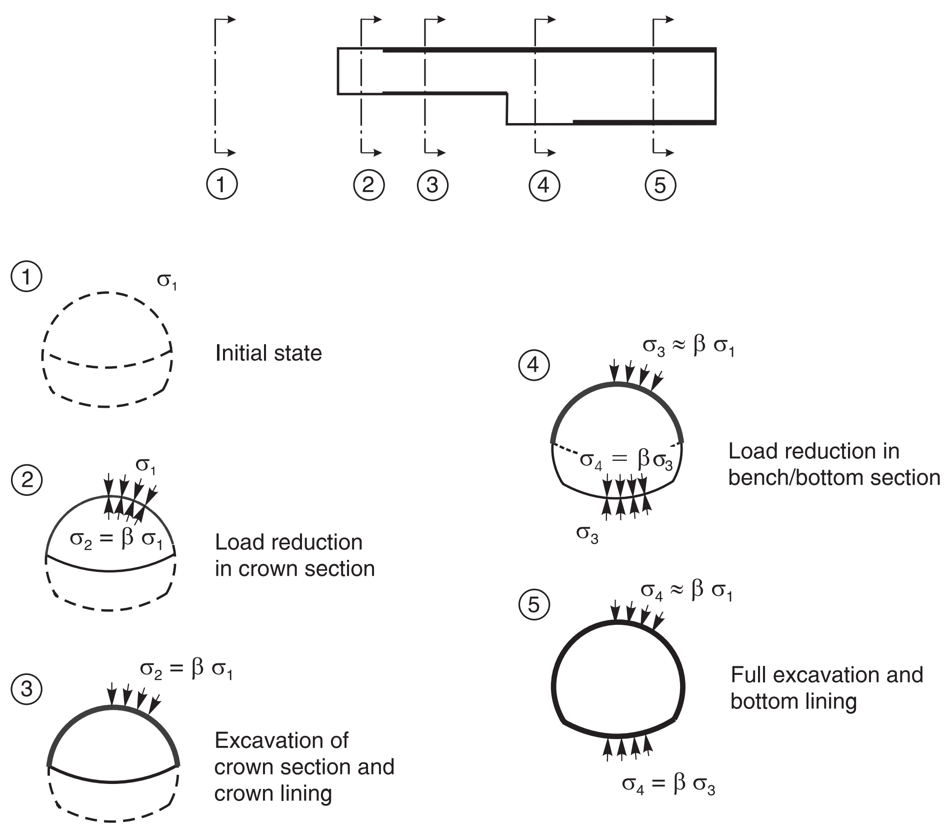

Figure 9.6 Construction sequence of staged excavation approximated by λ method

sections are influenced by the stress release of the preceding sections, which results in an additional lining load reduction (bottom lining in Figure 9.6).

If a suitable value of β_{rel} is specified, even the effect of the excavation round length in the longitudinal direction, i.e. the effect of the support distance from the tunnel face, can be simulated. However, to determine this value, either appropriate field measurements or results from a relevant 3D FEM solution should be available.

- The value of β_{rel} can be determined according to a given volume loss V_l^{meas}, which is derived from field measurements for similar tunnels in comparable ground conditions (Mair and Taylor, 1997). The volume loss is given by $V_l = V_s/A$, where V_s is the volume of the surface settlement trough per metre length of tunnel and A is the cross-sectional area of the tunnel.

β_{rel} can be found by a trial-and-error procedure in which the λ method with gradually increasing λ_{rel} and decreasing β_{rel} is applied. For each solution with a given β_{rel} the settlement trough area V_s and the volume loss V_l are calculated and checked against the measured value of volume loss V_l^{meas}.

The measured volume loss expresses the suitability of the applied excavation and support installation techniques for the given ground conditions and also the advances in tunnel construction techniques. From this point of view, it is interesting to compare the data on V_l^{meas} given in O'Reilly and New (1982) with data published in Mair and Taylor (1997). While the range of V_1^{meas} is from 0.5 to 20% (maximum 40%) in 1982, it is reduced to a narrow range from 0.5 to 2% (maximum 4%) in 1997. With such information, the λ method can be used with confidence in tunnel design.

However, there are only a few areas, such as London, where reliable information on V_l^{meas} is available. In the remaining cases, where no relevant field measurements are available, 3D FEM modelling may have to be considered in order to simulate the construction sequence.

If a sprayed concrete tunnel construction sequence such as that shown in Figure 9.6 is modelled in 3D, multistage partial face excavation with corresponding excavation round lengths can be simulated. First, full excavation of a face section with a given round length is performed, assigning $\beta = 0$ and $\gamma = 0$ in removing the excavated elements. Then the lining is installed by introducing added elements. Elements that are added have zero initial stresses and this should be considered when the constitutive model for the lining is selected. Thin layers of 20-noded brick elements can be used for modelling a sprayed concrete lining.

Apart from 2D approximation by the λ method, closer simulation of the real construction sequence by a 3D model, where this is achievable, allows:

- a correct stress state for a given K_o and the possibility of applying advanced constitutive models;
- an assessment of the face stability and its influence on surface settlement;
- an estimate of the effect of the support distance from the face on tunnel convergence and lining load; and also
- a determination of the reduction factor β_n corresponding to a given face distance, provided the λ method is applied simultaneously.

Another important feature of 3D modelling of the tunnel construction sequence is that the unbalanced forces due to excavation act always on the excavated soil surface and the lining loads are solely produced by stress transfer. In this case unrealistic heave of a tunnel lining is not computed, which is a frequent drawback of 2D modelling of tunnel construction. 3D modelling of a shield driven tunnel is more difficult as the support provided by the tunnelling shield must be simulated. In addition it is necessary to simulate accurately the articulated nature of the tunnel segments when they are erected. Neither of these phenomena are easy to model and consequently it is often difficult to justify the expense of 3D analysis.

9.3.6 Hydraulic problems: groundwater in tunnelling

During tunnel excavation in water-bearing ground, seepage flow towards the opening takes place because the pressure at the excavation boundary is, in general, atmospheric and therefore the tunnel acts as a groundwater drain. The seepage flow may lead to a drawdown of the water level, to a decrease in the discharge (or even a drying-up) of wells, or to severe subsidence due to consolidation. Besides these—in the broader sense—environmental consequences, large water inflows may impede excavation work. Water can affect both the stability and the deformation of a tunnel by reducing the effective stress and thus the resistance to shearing; by generating seepage forces towards the excavation boundary; and by washing out fine particles from the ground. The movement of water in low-permeability soils is one major cause of time-dependent effects in tunnelling. Furthermore, when tunnelling in soft ground, the seepage forces acting towards the tunnel face may impair its stability. **Figure 9.7** gives an overview of the typical questions arising when tunnelling through water-bearing ground.

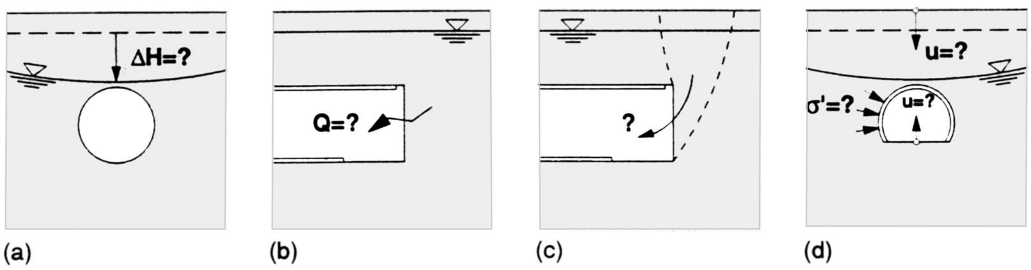

Figure 9.7 Problems when tunnelling through water-bearing ground: (a) drawdown of the water table; (b) water ingress; (c) stability of the tunnel face; (d) deformations of the ground surrounding the tunnel and changes in the ground pressure acting on the tunnel lining

Numerical analyses represent an important design aid because they provide useful indications regarding the ground response to the tunnelling operation. Depending on the nature of the design objective, a numerical seepage-flow analysis, a stress analysis or a coupled stress–seepage-flow analysis has to be carried out.

9.3.7 Boundary and initial conditions

For a complete problem formulation the initial stress field as well as the initial hydraulic head field have to be specified (usually a homogeneous field according to the elevation H of the undisturbed groundwater table). Concerning the *mechanical* boundary conditions (fixed boundaries or prescribed tractions), a careful distinction between *effective* and *total* boundary tractions is important when studying problems of ground–tunnel–lining interaction (**Figure 9.8**). The deformations of a tunnel lining depend on the total stresses acting upon it, whereas the ground response is studied in terms of effective stresses. Although trivial, this is a common source of error.

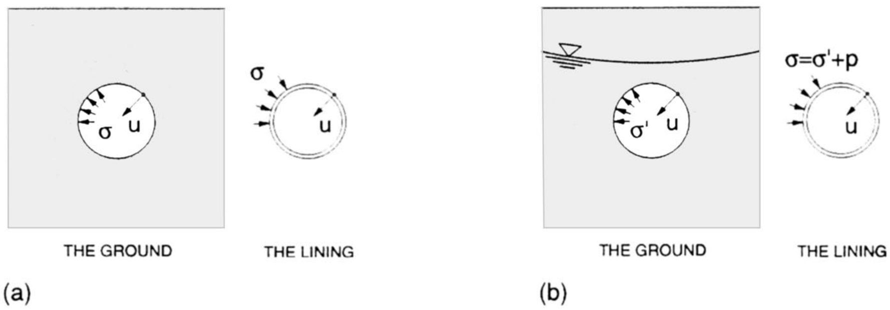

Figure 9.8 Ground–support interaction: (a) without water; (b) in water-bearing ground

Figures 9.9 and **9.10** show examples of typical *hydraulic* boundary conditions. At the far-field boundary of the seepage flow domain (BCDA, Figure 9.9(a)), the hydraulic head Φ is fixed to its initial value. In problems involving a symmetry plane, a no-flow boundary condition applies ($Q = 0$, Figure 9.9(b)). It should be noted that the far-field boundary conditions (and, consequently, the size of the numerical model) are more important in a seepage-flow analysis than in a stress analysis, particularly in problems with a drawdown of the water table (Arn, 1987). In general, the greater the distance between the far-field boundary and the tunnel, the more the water table will be depressed. According to the results of numerical studies by Arn (1987) and Anagnostou (1995b), the far-field boundaries should be located at a distance of at least 15–20 diameters from the tunnel.

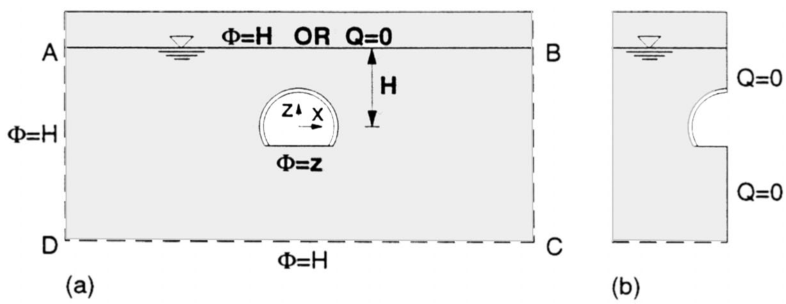

Figure 9.9 Examples of hydraulic boundary conditions

The boundary conditions along AB depend on the hydrogeological conditions and are, in general, time dependent. Subsequently, two important borderline cases will be discussed. In the first case, the position of the water table remains constant due to natural replenishment by, e.g., rainfall or an adjacent river, lake or well. The respective boundary condition is a fixed head along AB ($\Phi = H$). In this case tunnel excavation causes a decrease in the pore water pressures in the surrounding ground. In the other borderline case, accretion does not occur. Tunnel excavation causes a drawdown of the water table. The evolution of the drawdown can be computed by considering the free surface as a boundary of the flow (Bear, 1972). This approach is not appropriate for a coupled numerical analysis because it presupposes a successive modification of the finite element mesh. A better alternative is to consider the free surface as part of a continuum comprising the saturated ground and the overlying unsaturated zone up to the soil surface (Marsily, 1986). The free surface is defined as the surface on which the pressure p is atmospheric ($p = 0$, $\Phi = z$). Since accretion is assumed to be zero, a no-flow boundary condition is applied to AB ($Q = 0$).

An open tunnel heading represents a seepage face under atmospheric pressure, while a no-flow boundary condition applies when tunnelling with a slurry or earth pressure balance shield, provided that a filter cake or a practically impervious plug is formed in the working chamber (Anagnostou and Kovári, 1996, 1999). At the tunnel walls, the no-flow boundary condition ($Q = 0$) applies in the presence of a waterproofing membrane (Figure 9.10(c)). Open surfaces (e.g. the tunnel floor in Figure 9.9(a)), surfaces with a high-conductivity drainage layer (Figure 9.10(d)) or unsealed lined surfaces (Figure 9.10(e)) are modelled as seepage faces ($p = 0$ or, equivalently, $\Phi = z$). This condition, in combination with the pressure-dependence of the permeability ensures that water can seep into (but not out of) the opening. Besides these

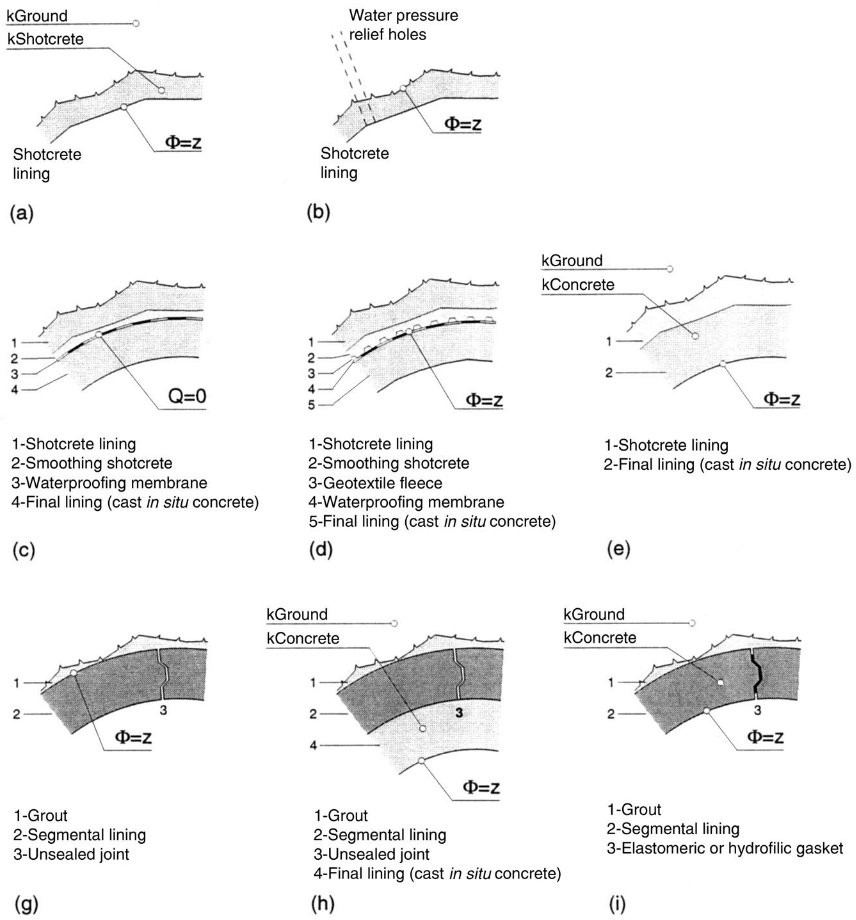

Figure 9.10 Hydraulic boundary conditions at the tunnel walls

simple boundary conditions, mixed-type conditions have also been proposed in order to model specific types of problems with ground surfaces exposed to the air (Anagnostou, 1995a).

9.3.8 Water table drawdown and seepage during tunnel construction

9.3.8.1 Water table drawdown during tunnel construction

A drawdown of the water table will take place when the groundwater recharge rate is lower than the quantity of water seeping into the tunnel. With the exceptions of closed-shield tunnelling (slurry or earth pressure balanced shields) or tunnelling under compressed air, the tunnel heading represents a seepage face (atmospheric pressure). Consequently, seepage flow takes place not only in the tunnel's cross-section plane but also towards the tunnel face. The problem of estimating the drawdown during tunnel excavation is therefore a three-dimensional one.

The loss of hydraulic head in the vicinity of the tunnel face does not take place immediately after excavation. The lower the permeability and the higher the storativity of the ground, the more time is required to achieve a steady state (Marsily, 1986). The time-dependence of the seepage flow phenomenon can be neglected in the cases of a high-permeability ground, or of a low advance rate, or of a longer excavation standstill. In these cases, the drawdown of the water table can be estimated by *steady state* 3D seepage flow analyses.

In general, however, a *transient* (or coupled) analysis is required, because the alteration of the hydraulic head field takes place simultaneously with the process of excavation (Goodman *et al.*, 1965). One can readily verify by dimensional analysis that the time development of the hydraulic head field is governed by the ratio of excavation advance rate *v* to ground permeability *k*. The higher the *v:k* ratio, the smaller will be the excavation-induced disturbance of the hydraulic head field. In the case, for example, of rapid excavation in a low-permeability ground, the water table will not be affected at all by the construction if an impervious lining is installed close to the heading.

A discussion of alternative methods of dealing with the problem of an advancing tunnel face can be found in Anagnostou (1995b). Following the simplest approach, a spatially fixed flow domain is considered, whereby excavation is simulated through the successive removal of finite elements. After a certain number of time-steps, the hydraulic head field will achieve a quasi-steady state, that is a steady state with respect to a frame of reference, which is fixed to the advancing tunnel face. This method makes it possible to simulate excavation without any modification of a standard finite element code, but it has obvious disadvantages. The computation of the quasi-steady state requires many time iterations whereby a non-linear iterative computation must be carried out for every time-step. Since the hydraulic head gradients are high close to the tunnel face, and since the position of the tunnel face changes over the course of time, the finite-element mesh has to be fine everywhere, leading to an extremely large system of equations. Furthermore, due to the successive deactivation of finite elements, the hydraulic conductivity matrix must be updated and refactorized at every time-step, even when the step size is kept constant.

Pursuing the approach proposed by Anagnostou (1995b), the diffusion equation is re-formulated within a frame of reference that is fixed to the advancing tunnel face. The governing equations contain the advance rate as an additional parameter, and can easily be implemented into existing finite element codes. This method has considerable advantages in terms both of computer time and of numerical stability and accuracy, because forecasts of the quasi-steady hydraulic head field can be made by means of a single computational step.

Note that in both methods mentioned above the deformability of the ground is taken into account indirectly through the specific storage coefficient (Marsily, 1986). Conceptually, a hydraulic–mechanical coupled model would be more satisfactory. An uncoupled analysis presupposes that the first invariant of the total stress tensor will remain constant, which is strictly true only in very special cases.

Figure 9.11 shows the results of a parametric study concerning the effect of advance rate on the drawdown of the water table. These results are useful as a guide for the selection of the appropriate analysis type (transient or steady state). Accordingly, when the dimensionless parameter *Dsv/k* is lower than 0.10, the effect of advance rate can be neglected and consequently the drawdown can be estimated by means of a relatively simple steady state analysis.

9.3.8.2 Water inflows during construction

Water inflows in the vicinity of the tunnel heading may seriously impede the construction works. The quantities of water can be estimated by a simple 3D *steady state* seepage flow analysis, i.e., it is not necessary to take into account the tunnel excavation process. According to the results of a parametric study (Anagnostou, 1995b) the advance rate has an effect on the water inflows only in low-permeability soils; in such soils, however, the question of inflows lacks practical relevance.

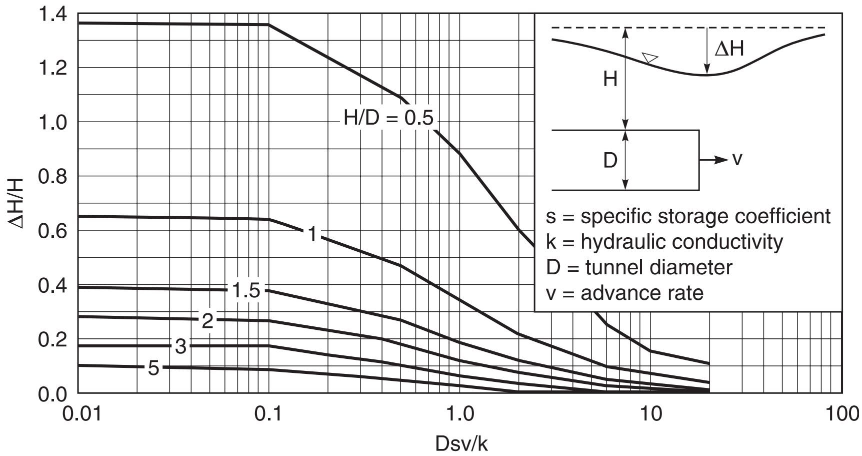

Figure 9.11 Drawdown of the water table for a cylindrical tunnel with impervious lining (after Anagnostou, 1995b)

9.3.8.3 Seepage flow during the operation phase

Since long-term conditions are considered, the drawdown of the water table can be studied by means of steady state, two-dimensional seepage-flow analyses with the boundary conditions according to Figures 9.9 and 9.10. Such calculations can also be used to estimate water inflows in order to design the tunnel drainage system in the case of high-permeability ground. A three-dimensional analysis is necessary only if the hydrogeological conditions vary considerably within short distances along the tunnel alignment. It should be noted, however, that permanent groundwater drainage and a permanent drawdown of the water table are usually not admissible in urban areas.

9.4 Deep basements

An important number of analyses of braced excavations have been reported in the literature, many of them listed by Duncan (1994). Two other very useful publications on this subject are by:

- Gens (1995) on prediction, performance and design; and
- Hight and Higgins (1995) on an approach to the prediction of ground movements in engineering practice.

9.4.1 Modelling building load, stiffness of buildings and surcharge loading

The surcharge loading to be used should be compatible with the particular situation being modelled. However, in most cases a surcharge loading to model construction traffic, storage of material adjacent to a retaining wall, etc. should be included. BS 8002 (British Standards Institution, 1994), for example, recommends that a surcharge of 10 kN/m^2 should be included to model such effects.

The pressure of compacted fill on retaining walls may be a significant factor in the imposed loading. Clayton and Symons (1992) outline an approach for calculating these pressures.

There is no doubt that the building stiffness alters the pattern of retaining wall and ground movement over the 'greenfield' situation. This problem has been addressed for tunnelling problems by:

- Potts and Addenbrooke (1997), who established design curves by introducing relative stiffness parameters which combine the bending and axial stiffness of the structure with its width and the stiffness of the soil.
- Simpson (1994), who used finite elements to model both the structure and soil together.

9.4.2 Soil/retaining wall interface problems

The possible alternative approaches to modelling soil–structure interfaces are discussed in *Chapter 6*. Among these alternatives, the use of zero thickness interface elements is perhaps the most popular.

Powrie et al. (1999) discuss some problems associated with not using any special interface elements between the soil and the wall. An analysis of a retaining wall in a stiff boulder clay, using the elastic/Mohr–Coulomb plastic analysis, calculated negative bending moments over the top portion of the wall. Powrie et al. (1999) suggest this could be overcome by reducing the soil stiffness near the retained surface. Long and Brangan (2001) have also successfully used this approach in the back analysis of a retaining wall in hard glacial till.

9.4.3 Props and anchor modelling

A variety of techniques is used to model props and anchors. When the prop is external to the structure, it may be convenient to model the prop as a linear elastic spring with spring stiffness being specified in the relevant directions. Full moment connection, such as that due to a reinforced concrete slab acting as a prop, can be modelled using solid 2D elements. The load distribution can be obtained from the compressive stresses at the integration points. Anchors can be modelled by bar elements and it is relatively easy for the program to calculate the excess force over the initial (pre-stress) value.

Beam elements have rotational as well as displacement degrees of freedom and therefore are capable of transmitting moments as well as axial forces.

If a joint between a permanent slab and a retaining wall is being modelled, it is possible to model full connection using a quadrilateral type element or a pinned connection using a triangular element (see **Figure 9.12**).

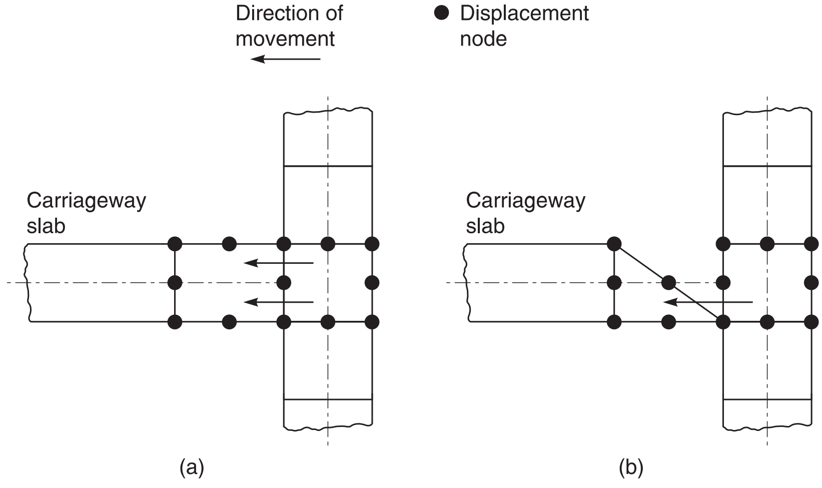

Figure 9.12 Detail of joint between wall and permanent slab: (a) rigid connections; (b) pinned joint

Temperature effects can have a significant influence on the actual forces generated in props. Powrie and Batten (2000) and Boone and Crawford (2000) give detailed discussions on how these effects should be modelled.

In all cases hand calculation checks of nodal forces should be made to ensure equilibrium is satisfied.

9.4.4 Prediction of ground movements in deep basement analyses

It is now well recognized that, in order to satisfactorily predict wall and ground movements resulting from deep basement excavations, a constitutive model which assumes linear elasticity should not be used.

Gens (1995) states that a review of published analyses strongly suggests that the lateral wall movements are not very sensitive to the type of constitutive law adopted, at least as far as excavations in stiff soil are concerned. The situation is different regarding vertical ground movements. Burland and Hancock (1977) illustrate this finding, for example, in their classic paper on the deep excavation at New Palace Yard, London. They assumed a linear elastic constitutive model and were able to predict the maximum measured movement relatively accurately. However, the pattern of movements predicted was inaccurate. This included a prediction that the Big Ben clock tower would tilt in a direction exactly opposite to that which occurred. Also, the linear elastic model tended to over-predict the movement of the toe of the retaining wall.

Thus a constitutive model which incorporates non-linear elasticity, particularly at small strain, should be used in these circumstances. When choosing a constitutive model the following aspects need to be considered:

- soil non-linearity;
- actual resulting strains in the ground due to excavation;
- technique for determination of ground stiffness.

9.4.4.1 Soil non-linearity

It is well accepted that soil stiffness is non-linear and that the stiffness degrades rapidly with strain. The concept of the S-shaped curve (similar to that shown in **Figure 9.13**) to describe this phenomenon has been well documented in the literature.

9.4.4.2 Actual resulting strains in the ground due to excavation

It must be recognized that the strains in the ground resulting from deep excavation are very small. **Figure 9.14** shows that the (predicted) shear strains resulting from a wall displacement of 0.2% its height (*H*) vary between 0.01% and 0.1%. The figure of 0.2% *H* is relatively high, thus real strains are likely to be even smaller than this. The stiffness values used in any analysis must be the appropriate values for the likely strains.

9.4.4.3 Technique for determination of ground stiffness

Figure 9.13 shows that, for strains in the typical range encountered in retaining walls, conventional triaxial test results are not applicable. This is because of bedding-type errors associated with measuring displacement in conventional triaxial cells. Special triaxial equipment, with local transducers mounted on the specimens, is necessary. If stiffness values at

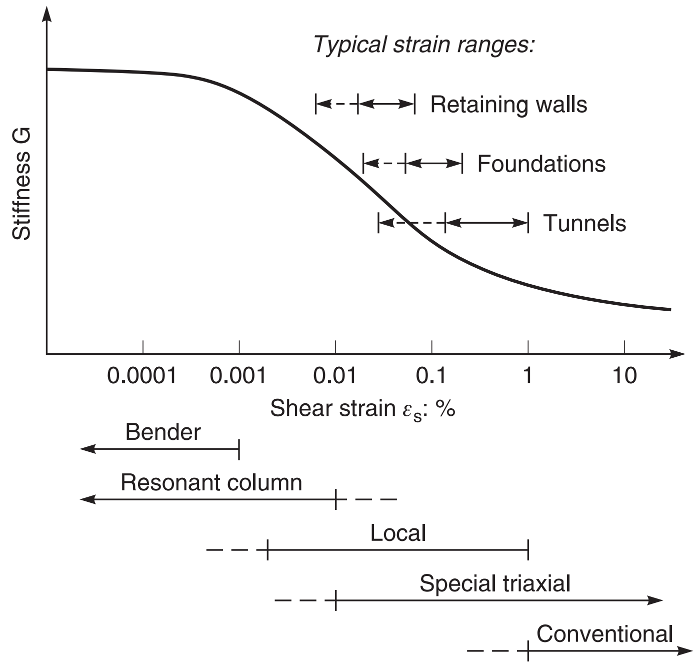

Figure 9.13 Approximate strain limits for reliable measurement of soil stiffness

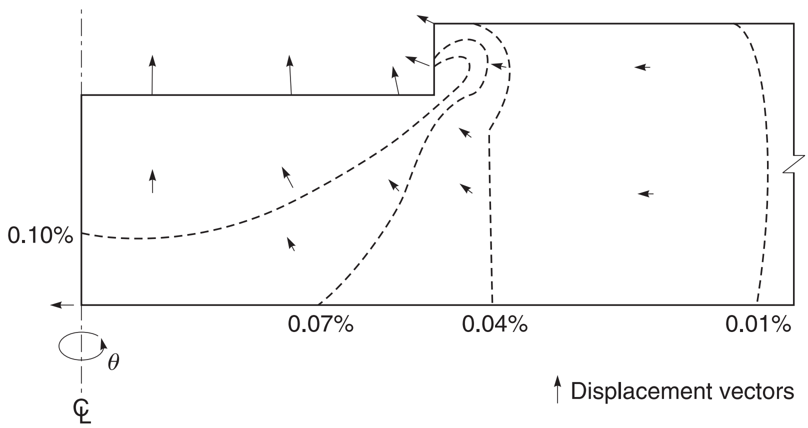

Figure 9.14 Strain contours around an excavation (after Simpson *et al.*, 1979)

strains lower than about 0.001% strain are required, then data from equipment such as the resonant column or bender elements are needed.

As the mechanical behaviour of soils depends on the current effective stress state and stress history, it may be important to obtain soil stiffness estimates from tests which follow a stress path compatible with that experienced by the soil at the particular site. Ng (1999) discusses this problem, and his approach is shown in **Figure 9.15**.

Hight and Higgins (1995) discuss the influence of the following factors on the derived soil parameters. They feel that a better understanding of these parameters is required in order to improve predictions of ground movements:

- the influence of fabric;
- sample disturbance effects;
- initial anisotropy;
- induced and evolving anisotropy; and
- rate and time effects.

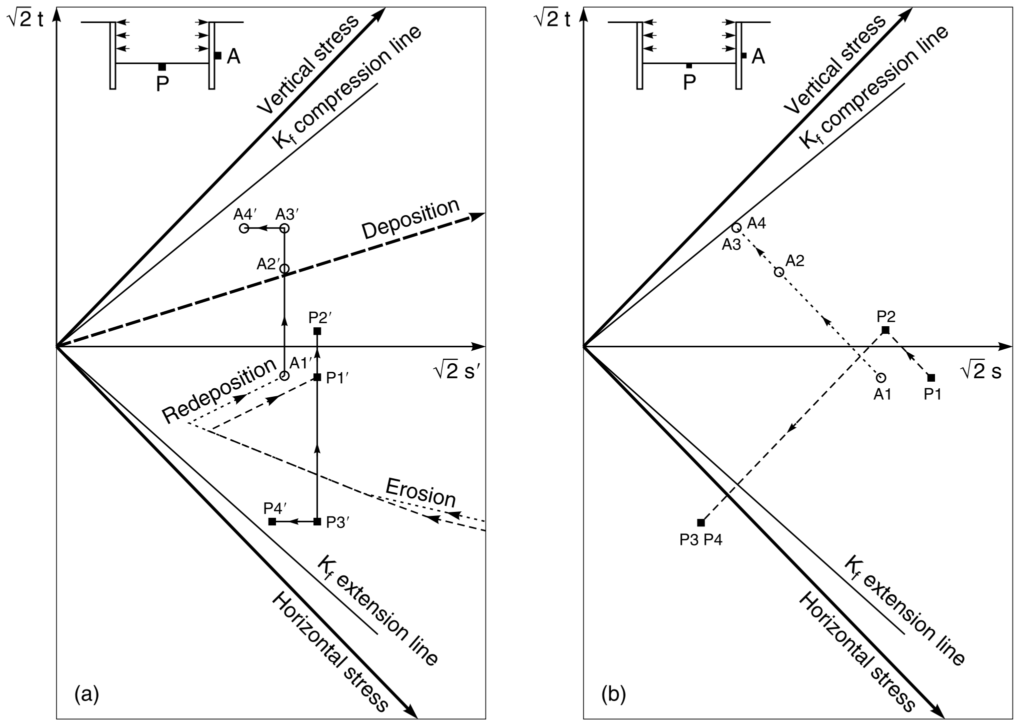

Figure 9.15 Idealized stress paths associated with stress relief due to excavation (after Ng, 1999). (a) Effective stress paths; (b) total stress paths

9.4.4.4 Constitutive models

There are many constitutive models available in commercial finite element packages for carrying out analyses involving non-linear or small strain stiffness. Some examples are given in Simpson *et al*. (1979), Simpson (1992), Gunn (1992), Stallebrass and Taylor (1997), Jardine *et al*. (1986) and Jardine et al. (1991).

9.4.4.5 Yield surface

The consideration of an anisotropic yield surface has significant consequences in the case of excavation in soft to medium soils. As **Figure 9.16** shows, on the passive side the main yielding of the soil occurs much earlier if a more realistic anisotropic bounding surface is adopted.

9.4.5 Water drawdown and underwater construction

Loading due to groundwater is clearly a very important component of the forces acting on a retaining wall. Often there will be a lack of relevant information in ground investigation reports. In order to overcome this BS 8002: 1994, for example, suggests 'a conservative ground water regime' should be assumed for design purposes.

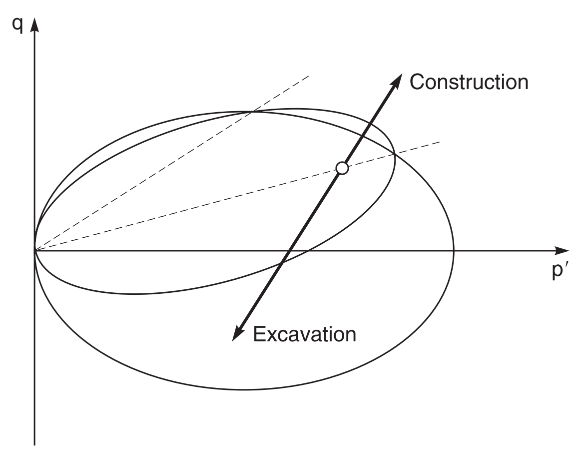

Figure 9.16 Excavation (passive side) and construction stress paths in relation to the type of yield surface (after Gens, 1995)

9.4.6 Modelling wall installation, excavation and pore pressure equalization

When analysing the installation of a diaphragm wall or bored pile retaining wall there are three different strategies that one might adopt:

(a) Begin the analysis with the wall already in place (the so called 'wished in place' wall).
(b) Begin with original undisturbed ground and then swap the relevant soil and concrete elements in the same time increment.
(c) Begin with original undisturbed ground and then simulate the excavation of the soil, the placing of wet concrete and the subsequent hardening of the concrete.

Higgins et al. (1989) compare strategies (a) and (c) in the analysis of the Bell Common tunnel retaining walls using undrained analysis in the short term and imposed pore pressure changes to model the long term. Gunn *et al*. (1993) give further details of the numerical aspects of strategy (c), using a coupled consolidation approach. In these analyses there is sometimes a spatial and temporal oscillation of pore pressure and effective stress in the lateral direction and care needs to be taken in the choice of time step.

Gens (1995) points out that strut loads are related to the existing horizontal stresses before excavation, which are highly dependent on the process of wall installation and/or construction.

Ng and Yan (1999) report on a successful 3D analysis of a diaphragm wall construction sequence for the Lion Yard, Cambridge, retaining wall.

Watson and Carder (1994) suggest that, as a compromise, an axisymmetric analysis to provide an assessment of the movement and stress relief caused by the installation of a single bored pile could be carried out.

9.4.7 Constitutive models for walls

The retaining wall material is usually modelled using a linear elastic constitutive model. This should be adequate in most normal situations. Young's modulus, for concrete walls, can be obtained from test results on concrete cores. Care should be taken in the calculation of bending moments in the wall. The calculation may be based on the:

(a) transverse stress distributions in the wall elements;
(b) horizontal soil pressures acting externally on the wall elements;
(c) nodal forces acting between the wall elements;
(d) nodal forces from the soil acting externally on the wall elements.

The first two methods seem intuitively reasonable as they make use of stresses calculated at integration points. However, stress distributions can be far from reliable. Comparisons of these two methods have shown significant discrepancies (Powrie and Li, 1991). Methods (c) and (d) on the other hand make use of nodal forces, which can be expected to be more reliable.

Ng *et al*. (1992) suggest techniques for modelling partially cracked concrete walls.

9.4.8 Modelling accidental over-dig

On many sites, accidental over-dig below the intended formation level frequently occurs. This is often associated with installation of service pipes or may be due to imprecise site control. BS 8002: 1994 suggests that an over-dig of 0.5 m should be included to account for these effects.

10

Limitations and pitfalls in full numerical analyses

10.1 Introduction

Full numerical analyses are powerful and versatile tools for investigating the influence of various factors and parameters on a given boundary value problem. With modern graphical output facilities these numerical tools are also very fascinating. However, one has always to keep in mind that the numerical analyses are done on the basis of the given input, not from an inherent understanding of the physics of the problem.

Thus, numerical analyses may be most beneficially used for enhancing the understanding of a physical problem that has already been identified. Preferably, the problem should even be largely understood aside of the numerical analysis itself. Much insight may then be achieved by elaborating on constitutive equations and their parameters and by manipulating the boundary conditions and other idealizations that one cannot avoid in the theoretical modelling of reality. By parametric studies the relative influence of the most important factors may be studied, and this will bring confidence to the predicted behaviour in a given design situation.

Full numerical analysis may also be used for testing out a hypothesis made on physical phenomena; in that case it should always be done in combination with model and/or full-scale testing. It is vitally important that such investigations are done with the purpose of learning about the physics of the phenomena, not necessarily for 'benchmarking' the software towards sometimes poorly understood tests.

It is also very important to be aware of the limitations that lie in a full numerical analysis. The analysis can never encompass physical phenomena that are not more or less deliberately taken account of. It is clear to everybody that a structural beam analysis that does not incorporate second-order effects from deformations can never predict buckling problems. Parallels to this limitation are abundant; often a good insight is required for identifying the presence of a limitation in a given case.

One of the more serious problems arises when a strain-softening material is modelled. In this case the numerical analysis will evidently try to concentrate large shear strains in very narrow bands, and the result is extremely dependent on boundary conditions, the finite element mesh and geometry. Extreme care should be taken when entering into full numerical analysis with strain softening materials.

Another phenomenon that often causes great difficulty is the modelling of undrained (constant volume) behaviour of a dilatant soil material. Specifying dilatant behaviour of the soil skeleton together with undrained behaviour may lead to extreme effective stresses and thus incredible values of strength and stiffness. Again, great care should be taken when approaching undrained problems in highly dilatant soils. It is vitally important to verify by testing that both the total volumetric constraint and the dilatant behaviour of the soil skeleton actually apply to the real situation in question.

A third phenomenon that may be encountered is a mismatch between kinematical deformation possibilities and prescribed flow rules. One may lock the deformation pattern by using too 'advanced' an element with too many degrees of freedom, thus ending up with capacity overshoots. This stems from the fact that the material has to deform elastically in order to remedy the discrepancy between the flow rule deformation pattern and the deformation pattern allowed through the displacement functions. Sometimes a simpler element would give a better performance in the plastic state.

To summarize, one is strongly advised to carry out full numerical analyses, but the results from these analyses should never be fully believed to represent reality, and they must always be compared thoroughly with practical experience and adopted engineering practice, provided these have been properly calibrated for the problem at hand. Moreover, much emphasis should be laid on trying to understand the 'physics' and mathematics behind the problem behaviour predicted by the analysis. Is the behaviour of a fundamental or a problem-specific type? Are the stress and deformation fields trustworthy or do they reflect 'arbitrary' boundary or geometrical conditions?

Modern computers allow for powerful checks and visualizations of input parameters and output results. Since the complexity is very large, much emphasis should be laid in testing out the material behaviour, preferably by modelling standard laboratory tests with the constitutive laws and parameters chosen. As a minimum, oedometer, shear box or simple shear and triaxial tests (drained and undrained) should be simulated for all parameter combinations chosen for the 'real' simulation of the design situation.

To check the performance of a computer code it is useful to test a given software package by running specified benchmarking tests. Such tests are purely aimed at checking the logic and mathematical performance versus some ideal calibration data obtained by thoroughly checked 'official calibration software'. The need for verification, both for software packages and even for 'best practice' is clearly demonstrated by the benchmarking tests run by this workgroup (see *Chapter 11*).

The following part of this chapter focuses on more specific pitfalls related to the different parts of a full numerical analysis. Recommendations of how one may present and structure the input and output data related to a given analysis are given in *Chapter 8*.

10.2 Discretization errors

This section sets out the errors that most frequently occur in relation to discretization on constructing a mesh of finite elements. Other types of errors have therefore not been included; these are involved in the choice of a 2D or 3D model, plane strain or plane stress, etc. Also omitted are errors connected with the analysis of appropriate constitutive laws, and errors arising from a particular kind of construction process. These and other aspects are dealt with in other sections of this chapter.

The following types of errors should be noted.

10.2.1 Errors originating from incorrect data

These errors are made when defining nodes, lines, areas, key points, assigning properties, entering actions, etc. In general, these errors are easily detected, since most codes have a facility for displaying the data entered as well as the corresponding records. Graphical interpretation of geometry, soil layering, mesh and boundary conditions is highly recommended.

It is important to take care with the units. In this sense, it is advisable always to use the International System (SI) of units.

10.2.2 Errors originating from the dimensions of the mesh

In the analysis of geotechnical problems, in terms of both soil mechanics and rock mechanics, it is usual to work with meshes that have lateral and vertical sides where the prescribed horizontal movement is zero. At the bottom boundary of the mesh, all movements are usually prevented.

The dimensions of the mesh should be appropriate to the problem in question so that the boundaries do not exercise undue influence. In general, these conditions are met if, during the various stages of the analysis process, movement in the proximity of the lateral boundaries is very small in comparison with movement in other parts of the mesh, or if there are no plastic points in the proximity of the said boundaries when a plastification criterion is applied. With regard to the lower boundary, it should also be far enough away from the situation under analysis, although this does not generally occur. For example, in the analysis of underground excavations, the location of the lower boundary can have a great influence on the results. The geomechanical properties of the soil can also influence the suitable location of the mesh boundaries.

10.2.3 Errors originating from inadequate identification of features

Errors can occur due to the inadequate identification of certain features such as small layers which could be significant in the analysis of a problem. Thus, for example, failure to take into account a small layer of sand or silty sand located between two clayey levels gives rise to results that are different from those that would have been expected in a consolidation analysis. Other types of error can occur when using interface elements and their links etc. These elements are dealt with in the next section of this chapter.

10.2.4 Boundary conditions

Once the stiffness matrix has been formed, the boundary conditions are put in place. A part of these conditions is made up of imposed movements and a part consists of the applied loads. All of these actions, the movements as well as the loads, should be subject to the global axes.

As previously stated, in most geotechnical problems the lateral boundaries are vertical with horizontal displacement prevented and, on the horizontal lower boundary, horizontal and vertical displacement prevented. The possibility of other movements at certain points or in particular areas of the mesh should also be considered. We should also be aware of movements that occur as a result of the symmetrical forms under analysis. For example, at a point where a structural element is subjected to bending, located at an axis of symmetry, a zero rotation condition should be prescribed.

When the conditions prescribed do not match the global axes in question, a rotation of axes should be carried out beforehand. Alternatively, the conditions should be applied in accordance with the axes that are active at the time. In any case, the prescribed movements should be in such a way as to avoid rigid body movement of the mesh as a whole.

Other types of action consisting of line loads, surcharge pressures, body forces, etc. also form part of the boundary conditions. In addition, these include the actions that arise from the analysis of construction stages in which the birth (i.e. construction) and death (i.e. excavation) of elements leads to nodal forces around the affected geometry.

10.2.5 The selection of elements

When making a stress–strain analysis, the user of a finite element program must take a number of decisions. One of the main decisions concerns the selection of the appropriate element group (some codes have more than a hundred available). In this sense, the simplifications made during a model's conception must be compatible with its correct functioning.

Next, the user should select the element(s) most appropriate to the problem. The analyst should take into account relevant factors in deciding which is the most appropriate theory. He/she should also choose between multi-node elements and simple ones with nodes only at the element vertices. The user must also decide whether to include degenerated elements (triangles, prisms, tetrahedra). They are sometimes necessary for geometric reasons.

Multi-node elements provide greater precision than the simpler elements which have nodes only at their vertices. As far as their function in a mesh is concerned, it should be remembered that the corner nodes and the side nodes have different characteristics. They are neither interchangeable nor connectable. The corner node of one element should not be placed alongside the side node of another.

The shape functions of simple elements (3-noded triangles in plane strain or 4-noded tetrahedra in 3D) are linear. Therefore, they provide constant stresses, strains and fields which in general give a bad representation of the stress and strain state.

The shape of the elements and in particular the way in which they differ from the regular form (i.e. a right triangle with equal sides, a square or a cube) affects the quality of the results. As a general rule, the mesh elements should have as regular a shape as possible.

Thus, for example, if quadrilaterals are used, the ratio of the lengths of the sides should be no more than 20. Likewise, the acute angle defined by the straight lines linking midpoints on opposite sides should be more than 45°–50° in quadrilaterals with nodes on the vertices, and more than 30° if the quadrilaterals have nodes on the middle of the sides. The loss of parallelism of opposite sides is another factor that adversely affects the results.

For three-dimensional prismatic elements, the overall appearance is determined by the geometrical shape of their sides in accordance with the criteria applied to quadrilaterals. It is also conditioned by the torsion factor such as the angle formed by the edges that connect opposite sides with the straight line that links the baricentres of these sides. This value is zero for a cube.

10.2.6 Density and refinement of the mesh

It should be borne in mind that solving a problem using the finite element method is no more than an approximate representation of reality. The exact solution can be approached when the size of the largest element in the mesh tends to zero.

The analyst should choose the size and the density of the mesh. Most times, this decision will be based on his/her experience and there will be a compromise between precision and calculation time. In cases where there is doubt, it is necessary to make the analysis with several meshes with the aim of guaranteeing a solution that matches reality.

An estimate of the effectiveness of the solution can be made by using the energy error norm defined by Zienkiewicz and Zhu (1992). These and other considerations regarding errors can lead to the need to refine the mesh in areas in which concentrations of stresses and strains occur.

If different materials exist in the model, as is usually the case in soil mechanics, identical movements of the contact nodes give rise to the need for a discontinuity in the stresses. This means that it is appropriate to calculate the nodal stresses in subdivisions made up of elements of the same material. Likewise, the calculation of the energy error should also be made in subdivisions of the same material.

When the mesh does not provide the required accuracy, it is necessary to increase the density of the meshing. Initially, this can be done in two ways:

- maintaining the number of simple elements (only having nodes at their vertices), and using multi-node elements
- increasing the number of elements.

However, there are situations in which it is not necessary to increase the density of the meshing in the whole model in the same way because of the concentration of stresses and strains that exist in a particular area. In these situations, selective meshing can be used, thus increasing the density in especially interesting areas.

In very large meshes, in dynamic analysis and in non-linear situations, where the performance of two parts of the model can be separated, it may be useful to carry out substructuring. This involves replacing one part of the model with a 'macroelement'. A simpler but less accurate solution is submodelling. In this approach, the initial model is analysed. Next, the area to be made more dense is selected and a finer mesh is produced. The appropriate loads are applied to this part. The movements obtained in the first calculation are applied as the boundary conditions for nodes that should be in contact with the rest of the model. For the submodel nodes that would not have been present in the first analysis, it is necessary to carry out an interpolation in order to determine the boundary conditions.

10.3 Modelling of structural members in plane strain analysis

Various commercial finite element codes began to be developed in the 1970s and the 1980s. Most of these codes offer a wide scope for analysis (elements, constitutive laws, the simulation of processes, etc.). The analysis may even be three-dimensional. However, these are general codes which are often designed for structural analysis. Consequently, they are not specifically developed for geotechnical applications. This sometimes leads to great difficulty when, for example, effective stresses are to be used, the at-rest pressure coefficient is to be used to define initial stresses, or the safety factor for a particular stage of construction is required.

A more recent innovation, from the last fifteen or twenty years, has been the advent of commercial codes specifically developed for geotechnical applications. These facilitate the analysis of problems concerning stability, stress–strain and consolidation or water flow. They can also simulate construction processes and ground improvement. The main problem with these codes is that they only allow one to work in two dimensions, assuming either plane strain or axisymmetrical conditions. There undoubtedly exist finite element codes for analysing 3D models, but they are normally restricted to the field of research in universities and other institutions.

Although plane strain and axisymmetrical models provide a fairly accurate representation of reality for many geotechnical problems (slopes, embankments, deep excavations, underground excavations, etc.), it is necessary to take a number of factors into account or to make some simplifications when these models are used in the analysis of a specific problem.

This section provides a description of certain aspects concerning the modelling of structural elements (retaining wall, tunnel lining, strip footing, props, etc.) which form a part of the model in a typical analysis of 2D soil–structure interaction.

Most structural elements can be modelled by means of 2D elements (triangles and quadrilaterals) like the ones used to model the soil. However, this entails some disadvantages. These structural elements normally have a small thickness and, as a result, their meshing with continuous 2D elements would lead to a high number of elements. If coarse meshing is used for the structural elements, there could be an unsuitable balance among the dimensions of the elements.

Bearing in mind these disadvantages, the codes for geotechnical applications provide for the use of beam elements in order to discretize structural elements which are compatible with the 2D continuous elements used to model the soil. The beam elements available in the codes are usually based on Mindlin beam theory, which takes into account the shear strain.

Various beam elements have been developed. They have three degrees of freedom per node (two displacements and a rotation). The simplest is the two-node one with linear shape functions. However, the most popular beam elements have three nodes and quadratic shape functions.

Both the two- and three-node beam elements can lock the solution when full integration is used. Various techniques have been developed in order to prevent the locking of the solution. Perhaps the most usual and the best known of these is reduced integration. In this technique, fewer Gauss points are used to integrate the stiffness matrix than in the case of complete integration. Another alternative consists of decomposing the stiffness matrix and considering the effects of bending and shear separately. Selective integration is used here. It is complete in the case of the bending stiffness matrix and reduced for the shear stiffness matrix. Some techniques involve different shape functions (polynomials of different degrees) for displacements and rotations. This procedure should be used with caution as in some instances it is incapable of reproducing simple shear force laws. Other procedures can be found in the technical literature.

Unfortunately, user manuals provide little more than the minimum information necessary for operating the program. They do not usually give certain technical details about the functioning of the elements. The user must either request this information or carry out his/her own checks with the aim of getting to know the limitations of a certain element.

It is feasible to model retaining walls, strip footings and continuous tunnel linings by means of two- or three-node beam elements or other more complex ones (some codes have five-node beam elements with fourth-order shape functions). The user needs to provide the program with the values of EI (bending stiffness, where I is the moment of inertia and E is Young's modulus), EA (axial stiffness, where A is the cross-sectional area) and Poisson's ratio. In plane strain and axisymmetrical analysis, A and I are specified for a unit width of the beam. The analysis gives the bending moments as well as the axial and shear forces for a unit width.

On occasions, the codes determine the shear stiffness (kGA), assuming that the section is rectangular. In this instance, $k = 5/6$. This would be correct, for example, in the case of a solid wall. However, in the case of steel profile elements such as sheet pile walls, secant piles or contiguous bored piles, the computed shear strain would be erroneous.

Some codes allow for the possible plastification of structural elements, specifying a maximum bending moment and limiting the axial force.

At the point where two beams join, there exists only one degree of rotational freedom. Therefore, the rotation is continuous, i.e. the connection is rigid. Various techniques are used in order to define a hinge connection. This depends on the scope of the program. The hinge connection is sometimes defined by means of two different nodes with the same co-ordinates and by the application of the condition that the displacement (both horizontal and vertical) must be the same at each node. On other occasions, the code allows the user to define the hinge connection directly.

The beam element allows another element to be obtained, a bar (pin-jointed) element, which transmits neither bending moments nor shear forces. This element is defined by two degrees of freedom for each node and is capable of transmitting only axial forces. It is similar to a spring but it has the advantage that it can transmit axial forces in curved elements. It is possible to model props in a deep excavation by means of either these elements or springs. In fact, this is a three-dimensional problem, as props are several metres apart, but it is modelled in two dimensions. To model the equivalent stiffness per metre, the out-of-plane spacing between props must be accounted for. Likewise, springs can be used to simulate anchors. These springs only work from traction and can be defined by introducing axial stiffness and anchor separation. If the material type selected is elastoplastic, a maximum anchor force can be entered.

Interface elements can be used to model the interaction between the soil and structures. In any soil–structure interaction, relative movements between the soil and the structure can occur. These movements cannot be simulated when compatibility of movement between elements that simulate the structure (beam elements) and those that represent the soil (2D elements) is established.

Various methods have been put forward for considering relative movements between retaining walls, foundations, tunnel linings, etc. and the ground. Some methods use continuous elements with their own constitutive laws. Alternative methods establish connections between opposite nodes (springs), while others involve joint elements with a certain thickness. As in other aspects, the codes on the market are not very explicit even when they have these interface elements available. At most, they provide a factor for reducing the shear strength parameters around the structure.

The modelling of interface elements is a subject of great importance. The user should study it and take his/her own decisions in each case, but must also be aware of the repercussions for bending moments, shear and axial forces and movements in structural elements.

Interface elements with zero thickness occasionally pose numerical problems, depending on the stiffness of the adjoining elements (ground and/or structure).

10.4 Construction problems

The analysis of new geotechnical problems involves making important changes to the geometry of the mesh of elements in accordance with the various stages of construction. This occurs, for example, when carrying out a stress–strain analysis of an embankment, taking into account the different stages of construction, even the improvement in the ground on which the embankment is built. Another typical example can be seen in the analysis of movements, shear forces and bending moments in a retaining wall during the excavation process.

The modelling of these and other geotechnical problems is covered in *Chapter 7*. Here only some aspects regarding the activation and deactivation of solid elements, such as the ones used to model the soil, are covered.

For the last few years, some general codes have included an option involving the birth and death of elements or, to be more exact, the activation and deactivation of elements. However, the codes that are geared towards geotechnical problems are the ones that have most fully developed this potential for simulating construction problems.

Among other recommendations and considerations, the user who analyses a construction problem should take into account the following points.

The elements which are going to be activated at some time during the construction process should be present in the initial mesh. Their properties should be identified. When the analysis begins, these elements will be deactivated.

The analysis of a construction involves simulating the construction process as accurately as possible. This does not mean that the geometry created by the activated elements has to exactly match progress made in the actual construction. For example, in order to simulate the construction of an embankment 8–9 m high, it may be enough to analyse 3 to 4 stages. New elements are activated in each of these phases.

Deactivated elements have zero stress. When they are activated, the self-weight body forces are calculated and added to the active model. The elements that become active do so in the position occupied by the deformed mesh in the previous construction phase.

In line with the objective of reflecting reality, each stage should allow for possible changes to the properties of previously activated elements (an improvement in stiffness and in the strength properties) and for changes to the nature of the soil before construction begins.

Many codes maintain the deactivated elements in the mesh, allocating a very low stiffness for them. This way of working is acceptable as long as Poisson's ratio is not near 0.5. In this case, the deactivated elements would be practically incompressible.

10.5 Underwater excavation

Water is present in the soil on many occasions. When this happens, many geotechnical problems should be analysed, taking into account the permeability of the soil, the hydraulic boundary conditions and the loads applied. There are two types of boundary conditions:

- a prescribed groundwater head or prescribed pore fluid pressure, the latter being equal to water weight × (groundwater head − vertical position); the pore fluid pressure can be prescribed for internal points of the mesh or for the edges of the mesh;
- a prescribed discharge; if the discharge is zero, the boundary is a closed (or no-flow) boundary.

Various hypotheses can be adopted for permeability:

- linear isotropic permeability;
- linear anisotropic permeability;
- non-linear permeability, according to the void ratio or the mean effective stress.

An excavation below groundwater level in front of a retaining wall is a typical case for analysis. On the vertical side of the mesh behind the wall, the pore fluid pressure remains constant (or the head remains constant). The bottom of the mesh is a no-flow boundary. While the excavation in front of the wall is simulated, thereby deactivating elements, it is necessary to apply a zero pore fluid pressure on the excavated surface. A groundwater flow calculation must be made by the code for each of the excavation stages, taking into account the boundary conditions applied and obtaining the discharge. The way in which the boundary conditions are introduced may vary from one code to another.

Interface elements play a very important role in these analyses. They are usually associated with a much lower permeability than that of the surrounding soil. If placed behind either a retaining wall or a tunnel lining, they can be used to restrict the flow of water.

A limitation of most of the available codes is that they do not allow for the analysis of flow in partially saturated soil. The relation between soil permeability, the degree of saturation and tensile pore pressure is more complex than for fully saturated soil.

10.6 Lack of consistency in input parameters

The material model(s) used in a specific analysis should be checked with respect to the material parameters by simulating 'standard' laboratory tests at relevant stress levels and stress ratios. As a minimum, an oedometer and a triaxial test should be simulated for each material.

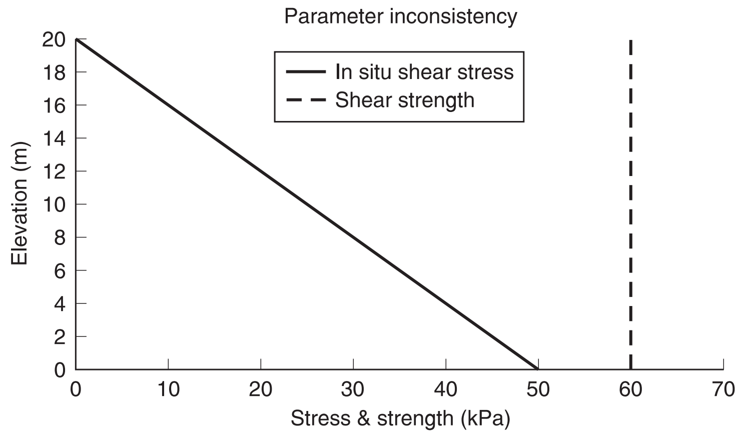

Figure 10.1 Inconsistent stress and strength distributions

When simulating undrained strength, attention must be paid to the description of the initial stress condition. Some codes offer the possibility of prescribing both a constant shear strength (with depth) and a constant stress ratio $K_o = \sigma_h/\sigma_v = \text{const}$. Even for a horizontal terrain the initial stress state then implies that the deepest layers are closest to or even at failure, a situation that seldom is relevant for a practical problem. **Figure 10.1** illustrates this problem.

In the example the initial *in situ* shear stress is given as

$$\tau_{max} = \frac{1}{2}(\sigma'_v - \sigma'_h) = \frac{1}{2}(1 - K'_o)\gamma' z$$

For the example chosen:

$$K_o = 0.5 \text{ and } \gamma' = 10\,\text{kN/m}^3$$

The undrained shear strength is set to 60 kPa. If it was less than 50 kPa, the initial stress condition so specified would have led to an inconsistency in the bottom soil layers.

An over-consolidated soil layer may possess higher horizontal stresses than a normally consolidated layer. One may think that this could be described by a higher stress ratio $K'_o = \sigma'_h/\sigma'_v$. However, this may be very erratic, as illustrated in **Figure 10.2**. In this figure, the following stress states are shown:

1. NC-equivalent (normally consolidated) denotes the horizontal stresses in a virtual 'fresh' sediment, i.e. a sediment that has carried no overburden, $K'_o = 0.5$.
2. OC sediment (over-consolidated), represented by $K'_o = 2.0$ (OCR=2).
3. NC sediment with 22 m overlying soil (Prehistoric state).
4. OC sediment as analysed with a non-elastic soil model after removing the overlying 22 m of soil (current state).

It may be noted that there is no way to match alternatives 2 and 4.

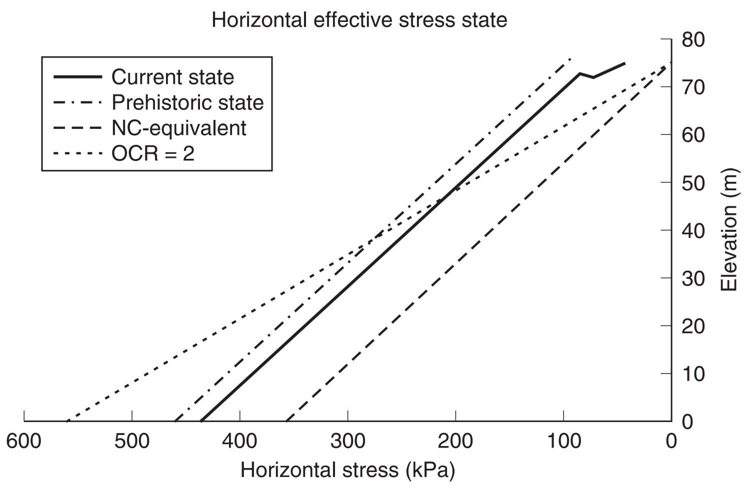

Figure 10.2 Descriptions of the horizontal stress distribution in an over-consolidated sediment

11

Benchmarking

11.1 Introduction

Benchmarking is of significant importance in geotechnical engineering, probably more so than in other engineering disciplines such as structural engineering. The reason for this follows from the previous chapters, where specific problems of numerical analyses in geotechnical engineering with special emphasis on soil–structure interaction have been discussed. These may be summarized as follows:

- the domain to be analysed is generally not clearly defined by the structure;
- a wide variety of constitutive models exists in the literature, but there is no 'approved' model for each type of soil;
- in most cases construction details cannot be modelled very accurately in time and space (excavation sequence, prestressing of anchors, etc.), at least not from a practical point of view;
- soil–structure interaction is important and may lead to numerical problems (e.g. certain types of interface elements);
- implementation details and solution procedures for commercial codes differ and are often not fully described (implicit versus explicit strategies, stress point algorithms, etc.).

These problems have been addressed by, amongst others, the Working Group 1.6 'Numerical Methods in Geotechnics' of the German Society for Geotechnics (DGGT) and it is the aim of this group to provide recommendations for numerical analyses in geotechnical engineering. So far the group has published general recommendations (Meissner, 1991), recommendations for numerical simulations in tunnelling (Meissner, 1996) and recommendations for deep excavations (Meissner, 2002). In addition, benchmark examples are specified and the results obtained by various users employing different software are compared. The work presented in the following summarizes the efforts of the working group and may be seen as a first step towards more objectivity in numerical analyses of geotechnical problems in practice. The results from three examples given by Working Group 1.6 of the DGGT are briefly presented and an additional example, an undrained analysis of a shield tunnel excavation, has been specified by Working Group A of this COST Action and solved by a number of its members. The results from this exercise are also included.

11.2 Specifications for benchmark examples

Keeping in mind the purpose of benchmarking from a practical point of view, the following requirements for benchmark examples can be postulated:

- no analytical solution available;
- a practical problem should be addressed, simplified in such a way that the solution can be obtained with reasonable computational effort;
- no calibration of constitutive models by analysing laboratory tests (this is done extensively in research and is of minor interest for engineers in practice);
- examples should be preferably set in such a way that, in addition to global results, specific aspects can be checked (e.g. handling of initial stresses, dilation behaviour, excavation procedures, etc.);

- influence of constitutive models on results should become apparent;
- the problem of identifying parameters for various constitutive models should be addressed.

11.3 Example No. 1—Tunnel excavation

11.3.1 Specification of problem

Figure 11.1 depicts the geometry of the example and **Table 11.1** lists the material parameters given. Additional specifications were as follows:

- plane strain conditions;
- linear elastic–perfectly plastic analysis with Mohr–Coulomb failure criterion;
- perfect bonding: shotcrete/ground;
- shotcrete lining: beam or continuum elements, two rows of elements over cross-section if continuum elements with quadratic shape function are used;
- to account for deformations occurring ahead of the face (pre-relaxation) the load reduction method or a similar approach should be used.

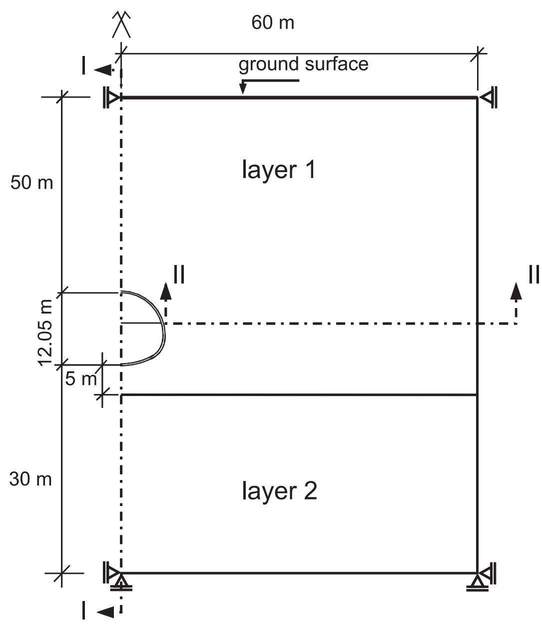

Figure 11.1 Geometry for example No. 1

Shotcrete ($d = 25$ cm): linear elastic. Young's modulus $E = 15 \times 10^6$ kN/m^2; Poisson's ratio $\mu = 0.15$.

The following computational steps were specified:

Initial stress state is given by $\sigma_v = \gamma H$, $\sigma_h = K_o \gamma H$ (deformations = 0). Note that it was assumed that there is no water present in the soil. The following pre-relaxation factors are valid for the load reduction method:

Construction stage 1: pre-relaxation across full cross-section of 40%;
Construction stage 2: excavation of full cross-section (i.e. remaining 60%) with shotcrete in place.

In addition to a full face excavation, excavation of top heading and bench was also considered, but these results will not be discussed here (see Schweiger, 1997, 1998).

Table 11.1 Material parameters for example tunnel excavation

Layer	Young's modulus E (kN/m²)	Poisson's ratio μ	Angle of shearing resistance φ'	Cohesion c' (kN/m²)	Coef. of earth pressure at rest K_o	Bulk unit weight γ (kN/m³)
Layer 1	50 000	0.3	28°	20	0.5	21
Layer 2	200 000	0.25	40°	50	0.6	23

11.3.2 Selected results

In **Figure 11.2** surface settlements obtained from ten different analyses are compared. Fifty percent of the calculations give 5.2 to 5.3 cm as the maximum settlement and most of the others are within approximately 20% of this value and each other. However, calculations TL1A and TL10 show significantly lower settlements, the reason being that in both cases it was not possible to apply the load reduction method correctly and therefore alternative excavation procedures have been used. For example, TL10 used the stiffness reduction method and it is well known that it is difficult to match results from this procedure with those from the load reduction method.

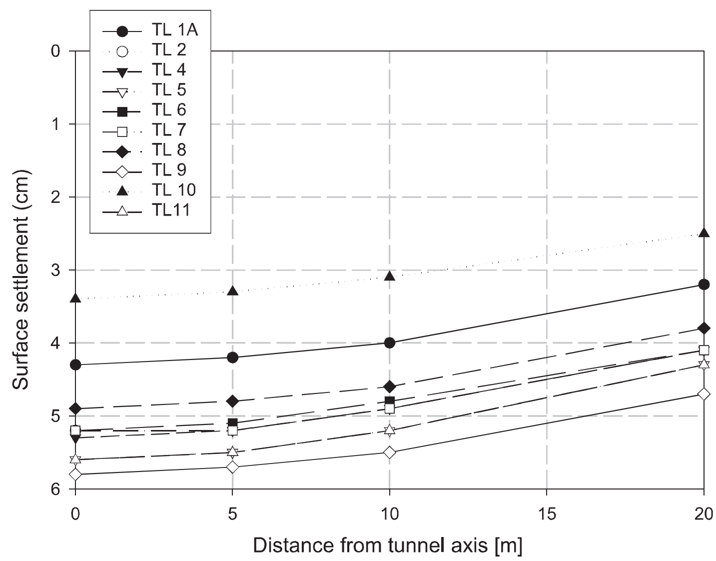

Figure 11.2 Surface settlements for example No. 1

Figure 11.3 shows the calculated normal forces in the shotcrete lining. Reasonable agreement is observed, with the exception of TL1 and TL10. **Figure 11.4** indicates the magnitudes and locations of the maximum bending moments and the significant differences in magnitude (approximately 300%) and location are obvious. Even if TL1, TL9 and TL10 are excluded because they did not refer exactly to the specification, the variation is still 70%. Unfortunately it was not possible, from the information available, to clearly identify the reasons for these discrepancies, but most probably these are due to different element formulations for modelling the lining and different procedures for calculating the internal forces within continuum elements.

11.4 Example No. 2—Deep Excavation

11.4.1 Specification of problem

Figure 11.5 illustrates the geometry and excavation stages and **Table 11.2** lists the relevant material parameters. Additional specifications were as follows:

- plane strain conditions;
- linear elastic–perfectly plastic analysis with Mohr–Coulomb failure criterion;

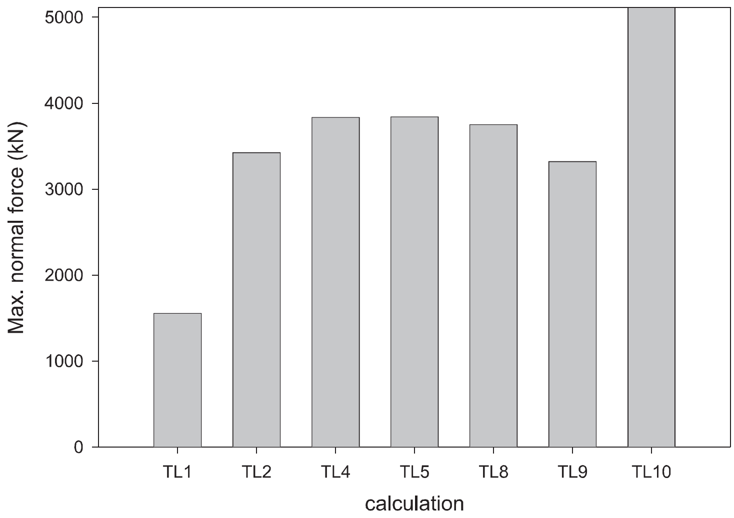

Figure 11.3 Comparison of maximum normal forces in lining for example No. 1

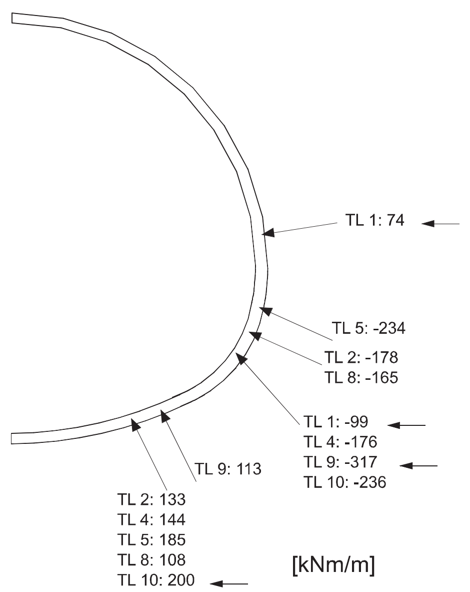

Figure 11.4 Comparison of maximum bending moments in lining for example No. 1

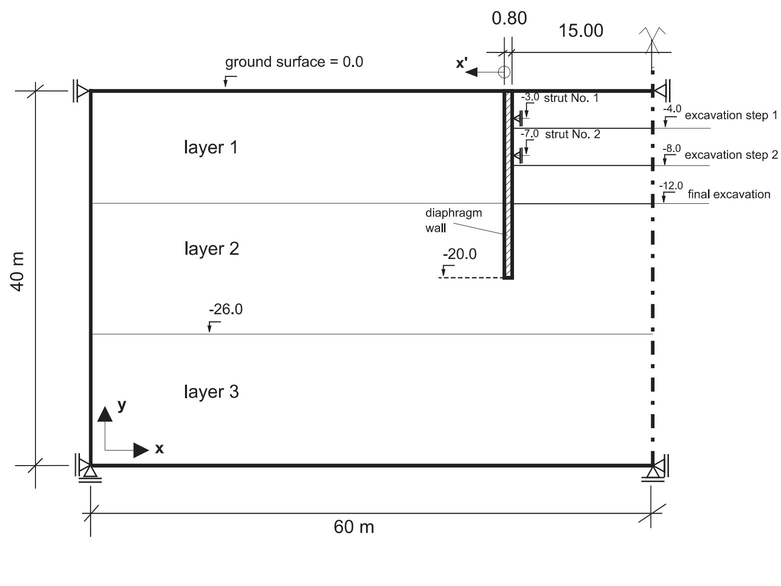

Figure 11.5 Geometry for example No. 2

Table 11.2 Material parameters for deep excavation example						
Layer	Young's modulus E (kN/m²)	Poisson's ratio μ	Angle of shearing resistance (φ')	Cohesion c' (kN/m²)	Coef. of earth pressure at rest K_o	Bulk unit weight γ (kN/m³)
1	20 000	0.3	35	2.0	0.5	21
2	12 000	0.4	26	10.0	0.65	19
3	80 000	0.4	26	10.0	0.65	19

- perfect bonding: diaphragm wall/ground;
- struts to be modelled as rigid (i.e. horizontal degree of freedom fixed);
- influence of diaphragm wall construction may be neglected, i.e. initial stresses without wall, then wall 'wished-in-place';
- diaphragm wall modelling: beam or continuum elements, two rows of elements over cross-section if continuum elements with quadratic shape function are used.

Diaphragm wall ($d = 80$ cm): linear elastic. $E = 21 \times 10^6$ kN/m²; $\mu = 0.15$; $\gamma = 22$ kN/m³.

The following computational steps were specified:

Initial stress state is given by: $\sigma_v = \gamma_n H$, $\sigma_h = K_o \gamma H$ (deformations = 0, then wall 'wished-in-place'). Note again that no water is present in the soil.

Construction stage 1: excavation step 1 (to level −4.0 m);
Construction stage 2: excavation step 2 (to level −8.0 m), with strut No. 1 (at −3.0 m) active;
Construction stage 3: final excavation (to level −12.0 m), with struts Nos. 1 and 2 (at −7.0 m) active.

11.4.2 Selected results

It is worth mentioning that five out of the twelve calculations that were submitted for comparison were made by different users, but with the same computer programme. **Figure 11.6** compares heave/settlement of the retained ground surface after construction stage 1 and shows two groups of results. The lower values for the heave, from calculations BG1 and BG2, may be explained by their use of interface elements which were incorporated in their analyses despite not being part of the problem specification. The results of BG3 and BG12 could not be explained

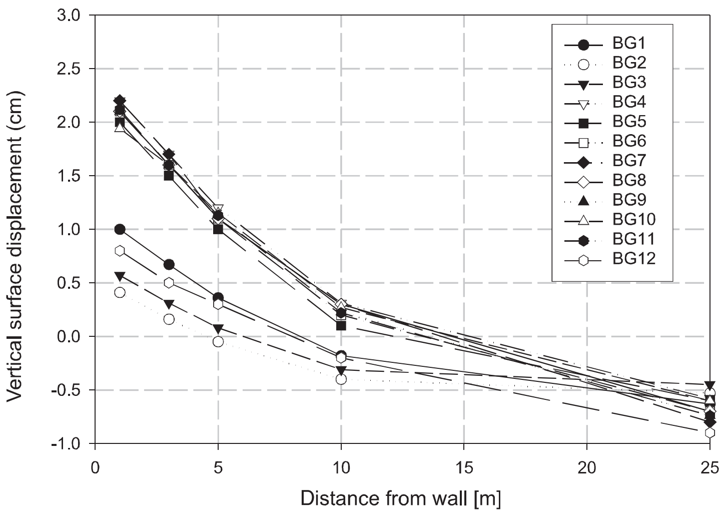

Figure 11.6 Vertical displacements of surface behind wall: construction stage 1

in detail. There were indications, though, that for the particular computer program used to obtain these predictions a significant difference in vertical displacements was observed when either beam or continuum elements were used for modelling the diaphragm wall. This emphasizes the significant influence of different modelling assumptions and the need to evaluate the validity of these models under certain conditions. It may be worth mentioning that this effect was not observed to such an extent in the other computer programs used.

Figure 11.7 shows the retained ground surface displacements for the final excavation stage; the results are now almost evenly distributed between the limiting values. It is apparent from Figures 11.6 and 11.7 that the simple linear elastic–perfectly plastic constitutive model specified is not well suited for analysing the displacement pattern around deep excavations, especially for the ground surface behind the wall, because the heave predicted is certainly not realistic. However, it was not the aim at this stage to compare results with actual field observation but merely to see what differences are obtained when using slightly different modelling assumptions with a rather tight problem specification. It is interesting to compare the horizontal displacement of the head of the wall after the first excavation step (**Figure 11.8**). Fifty percent of the analyses predicted horizontal displacements towards the retained soil, which is not very realistic for a cantilever situation. The horizontal displacements of the bottom of the wall, the heave inside the excavation and earth pressure distributions on the wall did not show significant differences. Calculated bending moments varied within 30% and strut forces for excavation step 2 varied from 155 to 232 kN/m. A more detailed examination of this example can be found in Schweiger (1997, 1998).

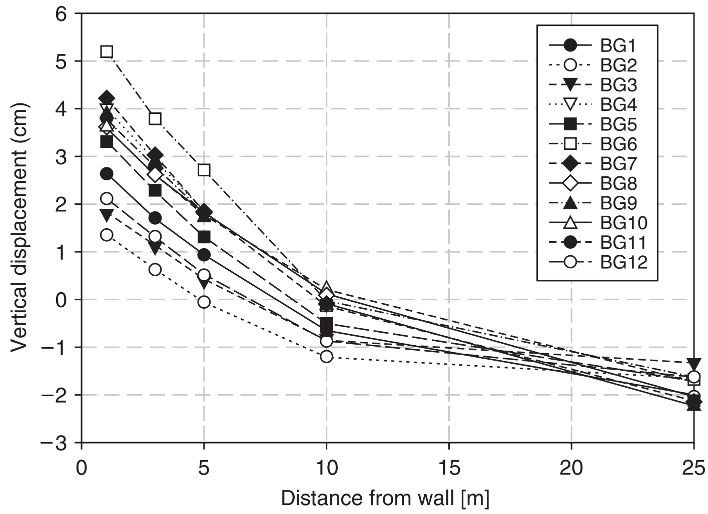

Figure 11.7 Vertical displacements of surface behind wall: construction stage 3

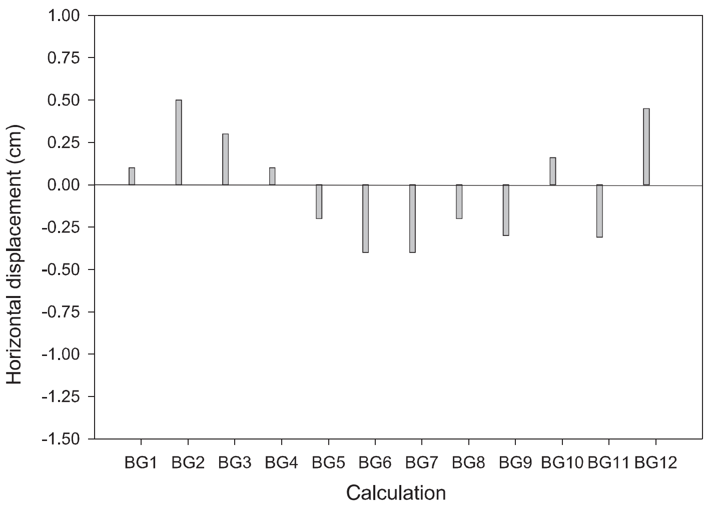

Figure 11.8 Horizontal displacement of wall head: excavation step 1

11.5 Example No. 3—Tied-back deep excavation

11.5.1 Background

This example again considers an excavation supported by a retaining wall, but this time it is closely related to an actual project in Berlin. Slight modifications have been introduced in modelling the construction sequence, such as the groundwater lowering which has been performed in various steps *in situ* but is modelled here in one step prior to excavation. In this example the constitutive model to be used for the soil has not been prescribed, but was left to the analyst. Some basic material parameters were taken from the literature and these, along with additional results from one-dimensional compression tests on loose and dense samples, were given together with results from triaxial tests on dense samples. Thus the exercise represents closely the situation one faces in practice.

Inclinometer measurements made during construction provided information on the actual behaviour in the field. However, owing to the simplifications mentioned above, a one-to-one comparison is not possible. Of course the measurements have not been disclosed to the authors of the analyses. As the objective of this chapter is to demonstrate the necessity of performing benchmarking exercises, and because of space restrictions, only the most relevant part of the specification will be given here; see also **Figure 11.9**. A detailed description can be found in Schweiger (2000). Only a limited number of results will be presented; they indicate, however, the wide scatter of predictions one may get due to different interpretations of the available data.

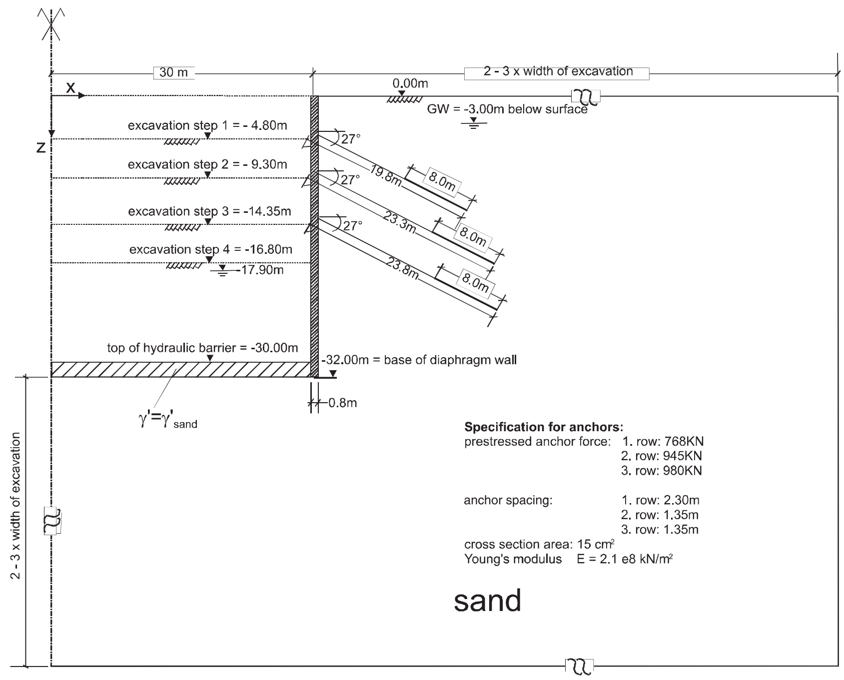

Figure 11.9 Geometry and excavation stages for example No. 3

11.5.2 Specification of problem

Values for stiffness and strength parameters from the literature frequently used in the design for excavations in Berlin sand are given below.

$E_s \approx 20\,000\sqrt{z}$ kN/m² for $0 < z \leq 20$ m ($z =$ depth below ground surface)
$E_s \approx 60\,000\sqrt{z}$ kN/m² for $z > 20$ m
$\varphi = 35°$ (medium dense)
$\gamma = 19$ kN/m³
$\gamma' = 10$ kN/m³ (effective bulk unit weight)
$K_0 = 1 - \sin\varphi'$

Diaphragm wall:
$E \;= 30\,000 \times 10^3\ \mathrm{kN/m^2}$
$\mu \;= 0.15$
$\gamma \;= 24\ \mathrm{kN/m^3}$
$\delta \;= \varphi'/2$ (wall friction)

The given moduli E_s from oedometer tests may be used to arrive at approximate values for Young's modulus for calculations with linear elastic–perfectly plastic material models (Mohr–Coulomb) assuming an appropriate Poisson's ratio.

In addition to these values, results from oedometer tests (on loose and dense samples) and triaxial tests ($\sigma_3 = 100$, 200 and 300 kN/m²) were provided. It was not possible to include a significantly large number of test results and consequently the question arose whether the stiffness values obtained were representative; e.g., if the constitutive model requires as an input parameter the oedometric stiffness at a reference pressure of 100 kN/m², a value of only 12 000 kN/m² was obtained from the data provided. This value was considered too low by many authors and indeed did not compare well with data from the literature. However, this again represents the situation frequently met in practice where a limited amount of test data is available and the question arises whether the stiffness values obtained from laboratory tests are representative of field conditions. This inevitably leaves a lot of room for engineering judgement in defining parameters as input for numerical analysis.

General assumptions

- plane strain conditions;
- influence of diaphragm wall construction may be neglected, i.e. initial stresses without wall, then wall 'wished-in-place';
- diaphragm wall modelling: beam or continuum elements;
- interface elements between wall and soil;
- domain to be analysed (suggested: see Figure 11.9);
- horizontal hydraulic cut-off at depth -30.00 m not to be considered as structural support;
- given anchor forces are design loads.

Computational steps to be performed:

Initial stress state is given by $\sigma'_v = \gamma' z$, pore water pressure hydrostatic below groundwater level, i.e. $u = (z - 3.0)\gamma_w$, $\sigma'_h = K_0\ \sigma'_v$ (wall 'wished-in-place', deformations = 0).

Construction stage 1: GW-lowering to -17.90 m;
Construction stage 2: excavation step 1 (to level -4.80 m);
Construction stage 3: activation of anchor 1 at level -4.30 m and prestressing;
Construction stage 4: excavation step 2 (to level -9.30 m);
Construction stage 5: activation of anchor 2 at level -8.80 m and prestressing;
Construction stage 6: excavation step 3 (to level -14.35 m);
Construction stage 7: activation of anchor 3 at level -13.85 m and prestressing;
Construction stage 8: excavation step 4 (to level -16.80 m).

Table 11.3 Summary of all analyses submitted

Analysis	Constitutive model	Stiffness	Reference stiffness (loading/unloading) (kPa)	φ (°)	ν (°)	Domain analysed, width x depth [m]	Element type, soil	Element type, wall	Interface	Note
B1	elastic–perfectly plastic	stress dependent	$z < 20$ m: 14 900 $z > 20$ m: 44 700	35	5	100 × 64	quadratic	9-noded continuum	yes	—
B2 B2a	elastic–plastic ($z < 40$ m) elastic–perfectly plastic ($z > 40$ m)	stress dependent	$z < 40$ m: 15 000/39 000 (B2) $z < 40$ m: 60 000/180 000 (B2a) $z > 40$ m: 253 000 (B2), 227 000 (B2a)	36	6	100 × 100	quadratic	beam	yes	—
B3 B3a	hypoplastic without (B3) with intergranular strains (B3a)					161 × 162	linear	4-noded continuum	yes	error in prestress force
B4	elastic–perfectly plastic	constant, per layer 43 layers (1)	$z < 2$ m: 10 500 $102 < z < 107$ m: 457 000	35	0	105 × 107	linear	4-noded continuum	—	—
B5	elastic–perfectly plastic	constant, per layer 6 layers (1)	$z < 5$ m: 32 600 $32 < z < 60$ m: 303 000	35	15	80 × 60	—	beam	no	—
B6	elastic–perfectly plastic	constant, per layer 20 layers (1)	$z < 20$ m: 20 000 $\sqrt{z}$ $z > 20$ m: 44 700 $\sqrt{z}$	35	15	122 × 90	—	—	—	error in prestress force
B7	elastic–perfectly plastic	constant	60 000	40.5	13.5	90 × 60	quadratic	continuum	yes	c = 2.5 kPa capillary cohesion

B8	elastic–plastic	stress dependent	$z < 20$ m: 20 000/ 74 400 $z > 20$ m: 60 000/120 000	35	10	90 × 70	quadratic	beam	yes	—
		constant	$z < 20$ m: 39 400	35	5	150 × 100	quadratic	beam	yes	—
B9 B9a	elastic–perfectly plastic elastic–plastic	per layer 3 layers (1)	$z > 40$ m: 310 000 25 000/100 000							
B10	elastic–plastic	stress dependent	60 000/180 000	36	6	100 × 72	quadratic	beam	yes	—
B11	elastic–plastic	stress dependent	$z < 20$ m: 20 000/ 100 000 $z > 20$ m: 60 000/ 300 000	35	0	150 × 120	quadratic	beam	yes	error in prestress force
B12	elastic–perfectly plastic	constant, per layer 9 layers (1)	$z < 5$ m: 23 000 $42 < z < 92$ m: 365 000	35	4	90 × 92	quadratic	beam	yes	error in prestress force
B13	hypoplastic with intergran. strains					100 × 100	linear	beam	yes	anchor fixed at boundary
B14	elastic–plastic with small strain stiffness	stress/strain dependent	G_{min} = 30 000 $G_{\text{small strain}}$ = 240 000	35	5	120 × 100	quadratic	8-noded continuum	yes	—
B15	elastic–plastic (0–20 m) elastic–plastic (> 20 m)	stress dependent	$z < 20$ m: 32 000/ 96 000 $z > 20$ m: 192 000/ 384 000	35 41	7 14	95 × 50	quadratic	beam	yes	—

(1) Stepwise increase in stiffness with depth

11.5.3 Brief summary of assumptions of submitted analyses

In **Table 11.3** the main features of all the analyses submitted have been summarized in order to highlight the different assumptions made. Only a limited number utilized the provided laboratory test results to calibrate their model. Most of the analysts used data from the literature for Berlin sand or their own experience to arrive at input parameters for their analysis. Looking more closely at Table 11.3, it is found that only marginal differences exist in the assumptions for the strength parameters (many of the analysts trusted the experiments in this respect), the angle of shearing resistance φ' was taken as 36° or 37° and a small cohesion was assumed by many authors to increase numerical stability. A significant variation is observed, however, in the assumption of the dilatancy angle *v*, ranging from 0° to 15°. In addition, a significant scatter is observed in the assumptions for the stiffness parameters. Most analysts assume an increase with depth, either by introducing some sort of power law similar to the formulation presented by Ohde (1951) which in turn corresponds to the formulation of Janbu (1963), or by defining different layers with different Young's moduli. An additional variation is introduced by different formulations for the interface elements, element types, domains analysed and modelling of prestressed anchors. Some computer codes obviously have problems in modelling the prestressing of the ground anchors and lose part of the force because of deformation in the ground. Where this is the case, a remark has been included in Table 11.3.

11.5.4 Selected results

A total number of 15 organizations (university institutes and consulting companies from Germany, Austria, Switzerland and Italy) submitted solutions, termed B1 to B15 in the following. A detailed inspection of the results from the analyses indicated that a number of them obviously used extremely low values for the stiffness of the sand (see Table 11.3). These are those analyses that derived their input parameters from the oedometer tests provided, which gave very low stiffnesses as compared to values found in the literature. These calculations result in excessive deformations which are clearly unrealistic and therefore they have not been included in the comparison presented below.

As mentioned earlier, field measurements are available for this project and, although the example here has been slightly modified in order to facilitate the calculations, the order of magnitude of displacements is known. **Figure 11.10** shows measured wall deflections for the final construction stage, together with the calculated results. The scatter is significant. It should be mentioned that measurements have been taken by inclinometer but unfortunately no geodetic survey of the wall head is available. It is very likely that the base of the wall does not remain fixed, as assumed by the inclinometer measurement, and that a parallel shift of the measurement of about 5–10 mm would reflect the *in situ* behaviour more correctly. This is confirmed by other measurements made under similar conditions in Berlin. The calculated maximum horizontal wall displacement varies between 7 and 57 mm and the shape of the deflection curve is also quite different. **Figure 11.11** depicts the calculated surface settlements. Settlements of approximately 50 mm have to be compared with a heave of about 15 mm. Considering the fact that the calculation of surface settlements is one of the main objectives of such an analysis, the need for recommendations and guidelines in order to minimize unrealistic modelling assumptions is obvious. **Figure 11.12** shows the development of anchor forces for the upper anchor layer. Maximum anchor forces for the final excavation stage range from 106 to 634 kN/m. Some of the analyses did not model the prestressing of the anchors correctly because

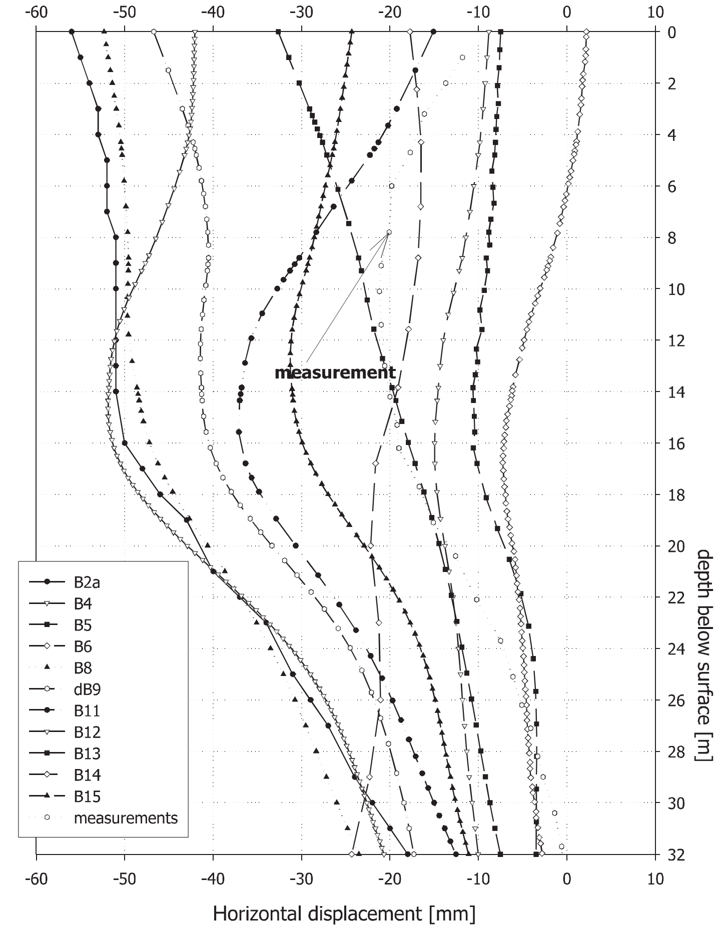

Figure 11.10 Wall deflection and inclinometer measurements

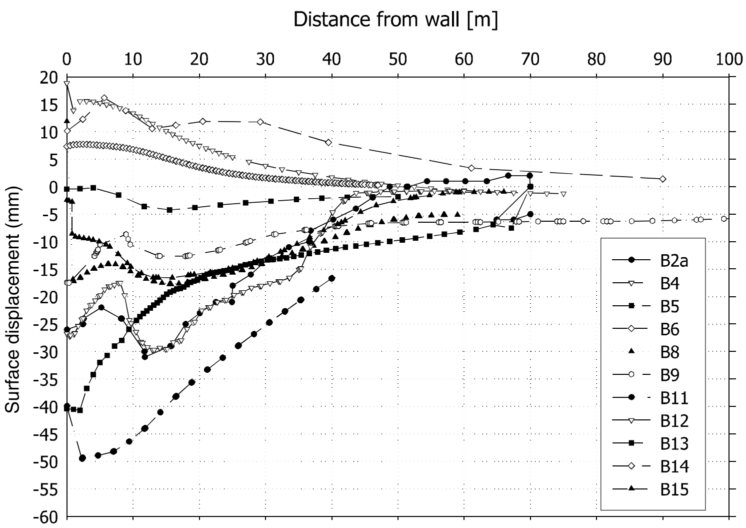

Figure 11.11 Surface displacements

they do not show the specified prestressing force in the respective construction step. Bending moments, which are important from a design aspect, also differ significantly, ranging from 500 to 1350 kN/m.

Combining Figures 11.10 to 11.12 and Table 11.3, it is interesting to see that no conclusions are possible with respect to the constitutive model or assumptions concerning element types etc. It is worth mentioning that even with the same computer code and the same constitutive model significant differences in the results are observed, depending entirely on the interpretation of

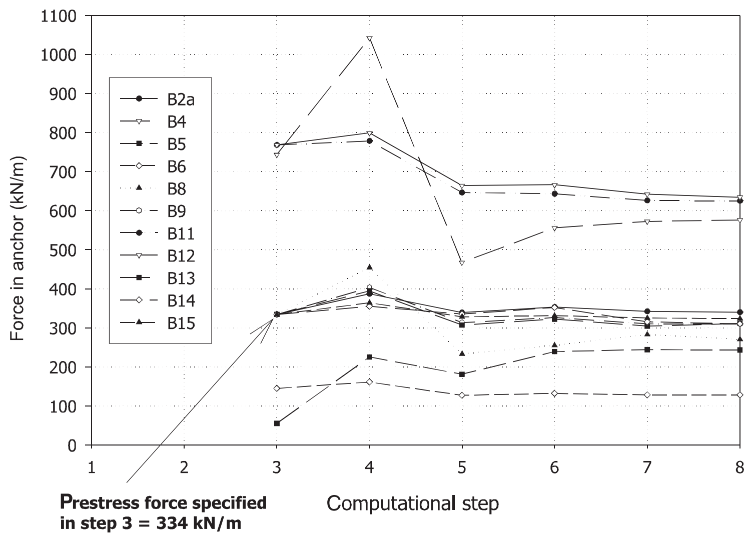

Figure 11.12 Forces in first layer of anchors

the stiffness parameters from the information available. Again, a more comprehensive coverage of this exercise is beyond the scope of this handbook and may be found in Schweiger (2000).

For this example a 'reference solution' is now being prepared and, based on this, a parametric study will be performed, varying the most significant modelling parameters in order to provide some guidelines for modelling these types of problem. It is anticipated that this work will be published soon and will be continued within Technical Committee ETC7 of the International Society for Soil Mechanics and Geotechnical Engineering (ISSMGE).

11.6 Example No. 4—Undrained analysis of a shield tunnel

11.6.1 Specification of problem

This example has been specified by Working Group A of this COST Action and has been deliberately chosen to be very simple in order to avoid the large discrepancies in results experienced especially in Example No. 3 described in the last section. The problem consists of excavating a circular hole, under plane strain conditions, in either an elastic or an elasto-plastic soil. For the latter, the soil is assumed to have an undrained strength constant with depth.

Undrained conditions were assumed and a set of three analyses was required, all performed in terms of total stresses under plane strain conditions:

- Analysis A: elastic, no lining, uniform initial stress state;
- Analysis B: elastic–perfectly plastic, no lining, $K_o = 1.0$;
- Analysis C: elastic–perfectly plastic, segmental lining, $K_o = 1.0$ with a given ground loss.

The tunnel diameter is given as 10 m and the overburden (measured from crown to surface) is assumed to be 15 m. At a depth of 45 m below ground surface bedrock can be assumed (see **Figure 11.13**).

11.6.1.1 Specification for analysis A

Soil parameters (elastic):

- elastic shear modulus, $G = 12\,000$ kPa; Poisson's ratio, $\mu = 0.495$;
- uniform initial stress state: $\sigma_v = \sigma_h = 400$ kPa;
- no lining to be considered.

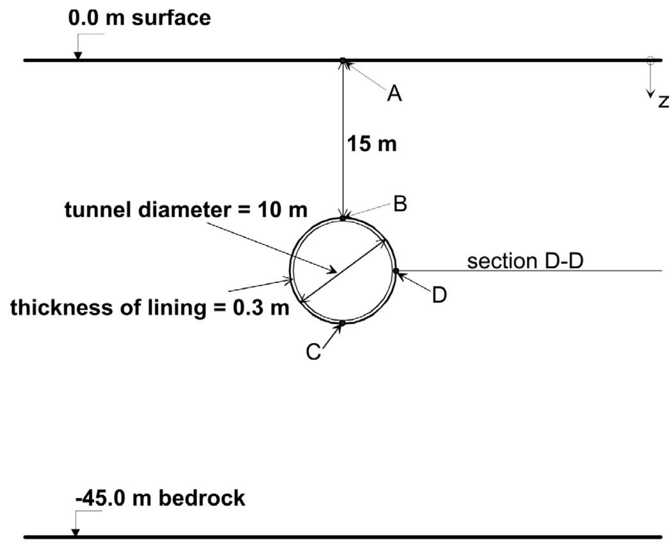

Figure 11.13 Geometric data for example No. 4

Computational step to be performed:

- full excavation.

11.6.1.2 Specification for analysis B

Soil parameters (elastic–perfectly plastic):

- $G = 12\,000$ kPa, $\mu = 0.495$, undrained shear strength, $S_u = 130$ kPa;
- initial stress state: $\sigma_v = \gamma z$, $\sigma_h = K_o \gamma z$, where $\gamma = 20\,\text{kN/m}^3$ and $K_o = 1.0$;
- no lining to be considered.

Computational step to be performed:

- full excavation.

11.6.1.3 Specification for analysis C

Soil parameters (elastic–perfectly plastic):

- $G = 12\,000$ kPa, $\mu = 0.495$, $S_u = 60$ kPa;
- initial stress state: $\sigma_v = \gamma\, z$, $\sigma_h = K_o\, \gamma\, z$, where $\gamma = 20\,\text{kN/m}^3$ and $K_o = 1.0$.

Parameters for segmental lining:

- $E = 2.1 \times 10^7$ kPa (value assumed to cover possible reduction due to hinges);
- lining thickness, $d = 0.3$ m;
- $\mu = 0.18$;
- $\gamma = 24\,\text{kN/m}^3$.

Computational step to be performed:

- full excavation with assumed ground loss of 2% (i.e. lining inserted at the appropriate stage of the analysis to give this final volume loss).

Note: for simplicity it is assumed here that no ground loss occurs at the tunnel face (approximately justified for an earth pressure balance (EPB) shield).

11.6.2 Selected results

11.6.2.1 Analysis A

Figure 11.14 shows calculated settlements of the ground surface. Even in this simple elastic case some scatter in the results is observed. Some of the discrepancies are due to different boundary conditions. For example, analysis ST5 restrained both the vertical and horizontal displacements of the far field vertical boundary, while most of the other analyses restrained only the horizontal displacements of this boundary. Also, the distance of this far field vertical boundary from the tunnel centre-line has some influence. The effect of this lateral boundary becomes more pronounced when **Figure 11.15**, which shows the horizontal displacement at the ground surface, is examined. It should be noted that some of the analysts did not assume that this lateral boundary was fixed in the horizontal direction, but introduced an elastic spring or a stress boundary condition.

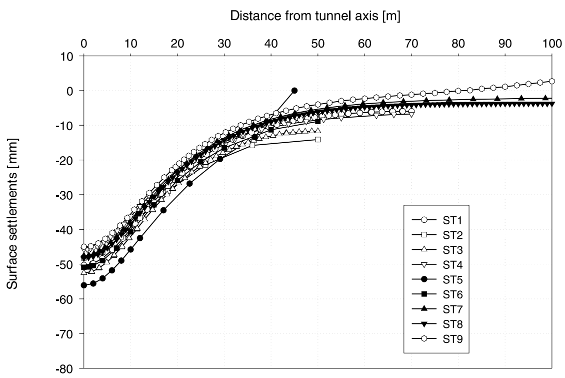

Figure 11.14 Surface settlements: Analysis A

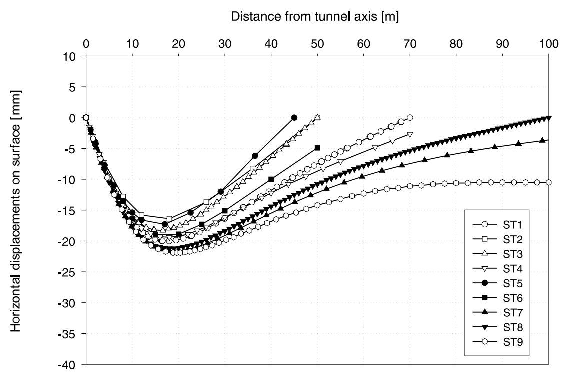

Figure 11.15 Horizontal displacements at surface: Analysis A

Table 11.4 summarizes calculated displacement values at specific points, the locations of which are indicated in Figure 11.13. It can be seen that a maximum of 10 mm difference (this is roughly 20%) exists in the vertical displacement of point A; this can be considered as too high for a linear elastic analysis.

Table 11.4 Analysis A—Calculated displacements of points A, B, C, D (mm)

	A	B	C	D_{vert}	D_{horiz}
ST1	−50	−115	62	−24	−80
ST2	−48	−110	64	−21	−79
ST3	−53	−116	62	−25	−79
ST4	−46	−111	67	−20	−82
ST5	−56	−118	60	−27	−79
ST6	−51	−115	62	−26	−81
ST7	−48	−114	63	−24	−83
ST8	−48	−114	63	−24	−83
ST9	−45	−111	62	−22	−82

11.6.2.2 Analysis B

Figures 11.16 and **11.17** show settlements and horizontal displacements at the ground surface for this elasto-plastic solution with constant undrained shear strength. In Figure 11.16 a similar scatter to that in Figure 11.14 is observed, with the exception of ST4 and ST9 which show an even larger deviation from the 'mean' of all analyses submitted. Again, ST5

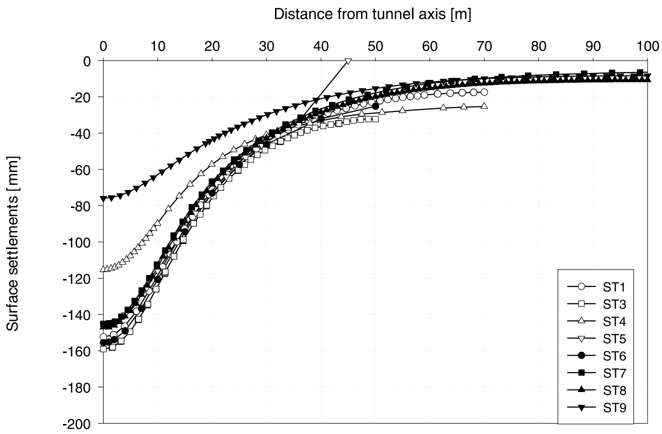

Figure 11.16 Surface settlements: Analysis B

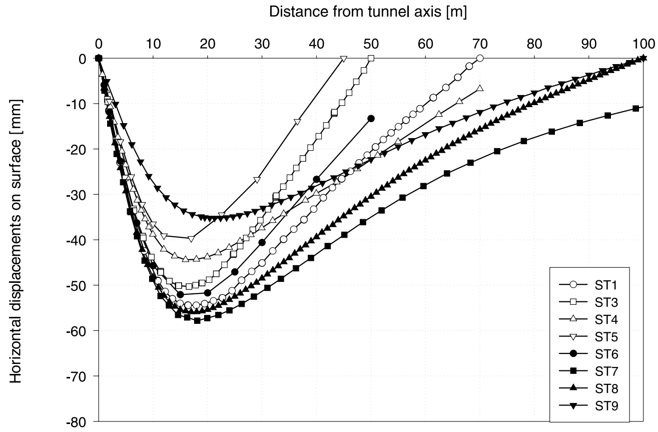

Figure 11.17 Horizontal displacements at surface: Analysis B

restrained vertical displacements on the far field vertical boundary and thus the settlement is zero here. Large differences, mainly depending on the distance of the far field vertical boundary from the symmetry axes of the tunnel, are observed. **Figures 11.18** and **11.19** depict vertical and horizontal displacements at the springline (section D–D, see Figure 11.13) respectively. ST9 gives a horizontal displacement of only 165 mm, whereas most of the other analyses yield values around 260 mm. Significant differences are also observed in the vertical displacements at the springline (Figure 11.18). **Table 11.5** summarizes the displacement values for points A to D.

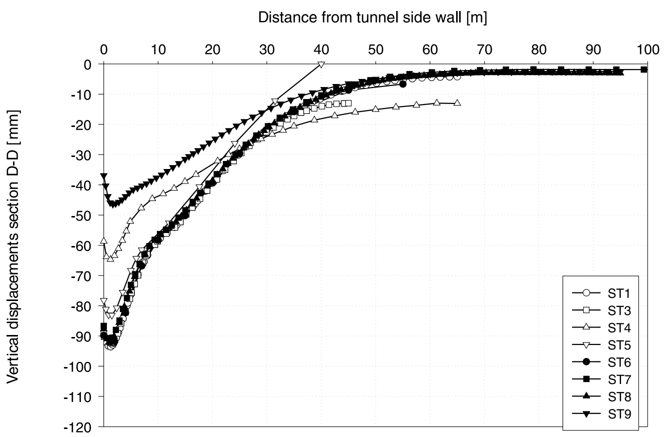

Figure 11.18 Vertical settlements at section D–D: Analysis B

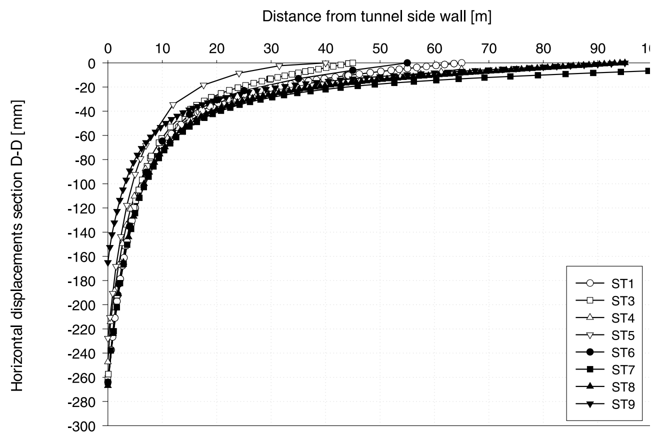

Figure 11.19 Horizontal displacements at section D–D: Analysis B

11.6.2.3 Analysis C

Figure 11.20 plots the ground surface settlements for this elastic–perfectly plastic analysis with a specified volume loss of 2%. A wide scatter in the results is evident. The large settlements of ST7 can be explained because there was a misinterpretation of volume loss and actually 4% has been applied. ST5 used a vertical restraint on the far field vertical boundary, which influences the result. However, in the other solutions no obvious cause for the differences could be found, except that the far field lateral boundary has been placed at different distances from the symmetry axes. Only ST8 and ST5 explicitly stated that they checked the achieved volume loss, and therefore it can be concluded that most of the other authors did not. **Figure 11.21** shows the horizontal displacements at the ground surface, and a similar picture to that of the previous

Table 11.5 Analysis B—Calculated displacements of points A, B, C, D (mm)

	A	B	C	D_{vert}	D_{horiz}
ST1	−152	−252	233	−90	−266
ST3	−159	−244	221	−92	−260
ST4	−115	−219	267	−59	−247
ST5	−146	−220	183	−78	−228
ST6	−156	−249	227	−90	−264
ST7	−145	−259	247	−87	−264
ST8	−147	−256	242	−88	−267
ST9	−76	−166	173	−37	−165

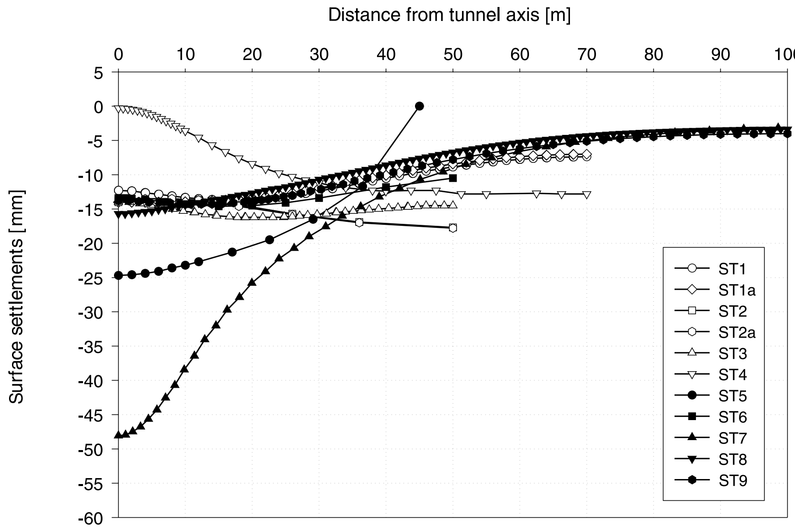

Figure 11.20 Surface settlements: Analysis C

analyses can be found. In these plots ST1, ST1a and ST2 and ST2a indicate different modelling of the volume loss by the same author. Similar arguments hold for comparison of vertical and horizontal displacements at the springline (**Figures 11.22** and **11.23**).

11.6.3 Corrected results

Because of the obvious influence of the position of the far field vertical boundary of the finite element mesh (or finite difference grid), which has been chosen at various distances from the line of symmetry of the tunnel, and the different boundary conditions applied to this boundary, a second round of analysis was performed in which all authors were asked to redo their analysis with this boundary at 100 m distance from the centre-line of the tunnel, with only the horizontal displacements fixed. As follows from **Figures 11.24–11.27**, which present the new results for case A, all calculations give the same results; thus the discrepancies described above are entirely caused by the location of, and boundary conditions applied to, the far field vertical boundary. In Figures 11.24 and 11.25 the analytical solution is also plotted and the influence of the boundary becomes apparent again.

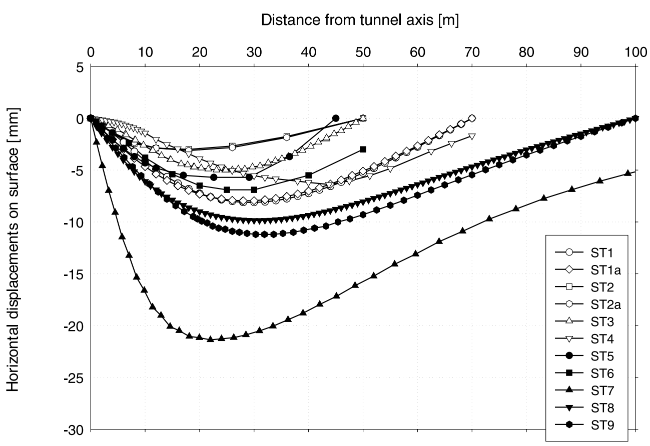

Figure 11.21 Horizontal settlement at surface: Analysis C

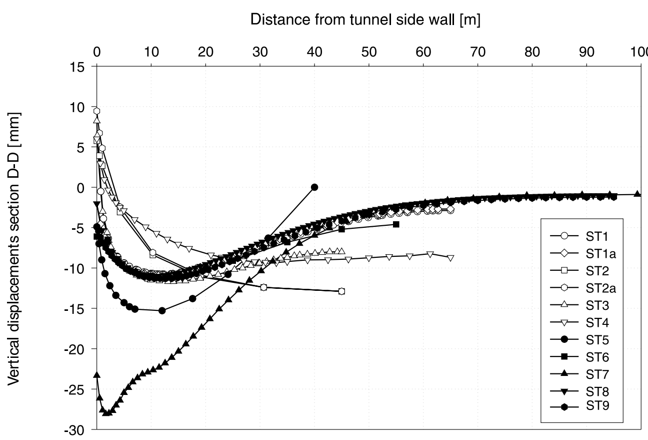

Figure 11.22 Vertical displacements at section D–D: Analysis C

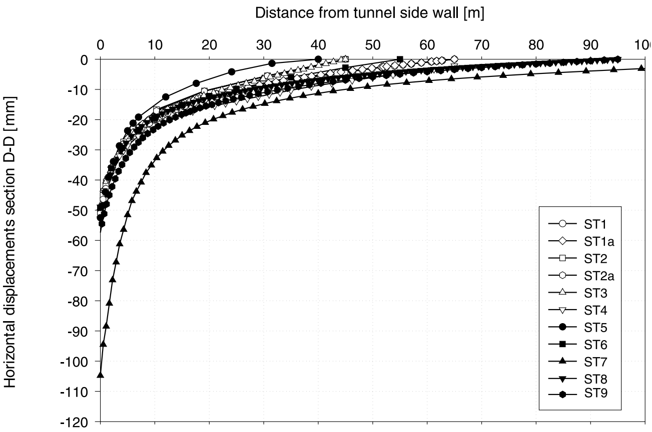

Figure 11.23 Horizontal displacements at section D–D: Analysis C

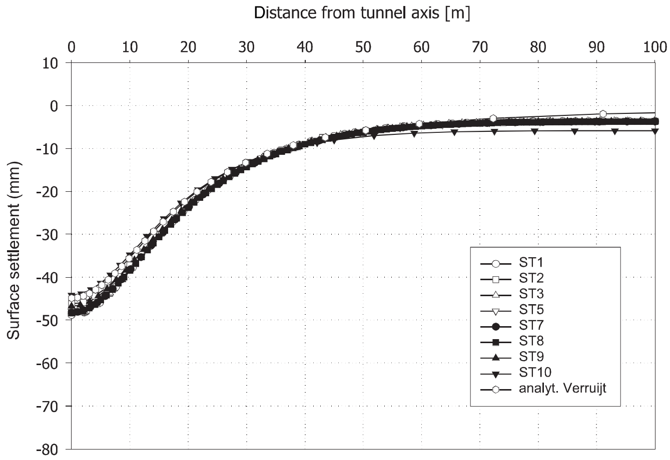

Figure 11.24 Surface settlements: Analysis A/100

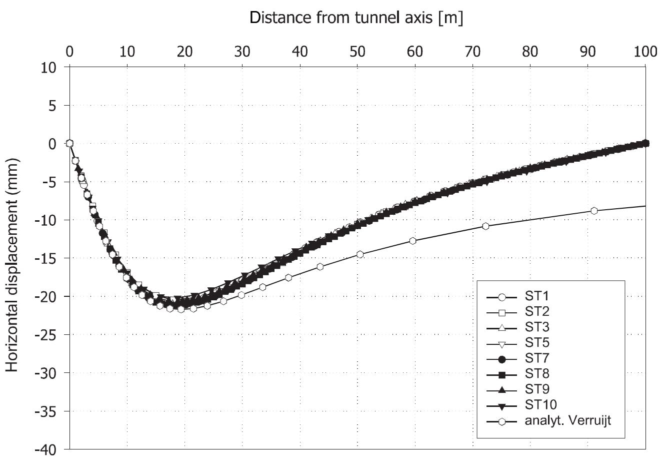

Figure 11.25 Horizontal displacements at surface: Analysis A/100

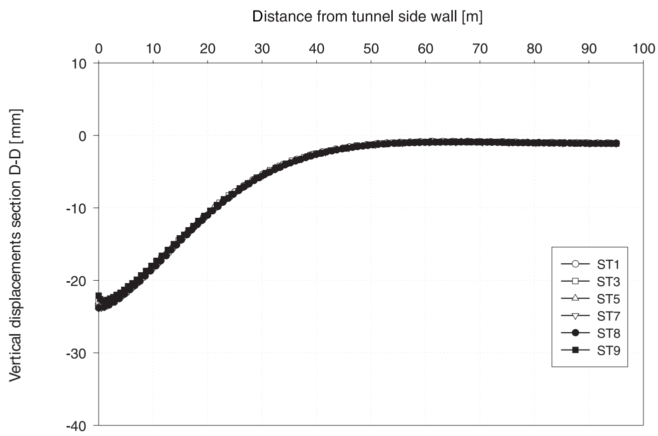

Figure 11.26 Vertical displacements at section D–D: Analysis A/100

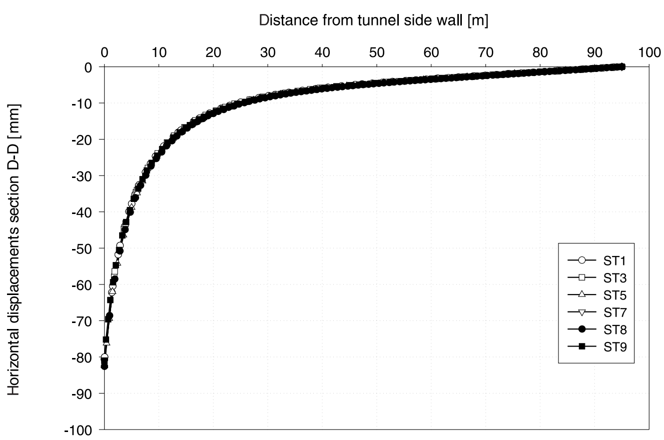

Figure 11.27 Horizontal displacements at section D–D: Analysis A/100

For case B similar results were also obtained, although some small differences were observed for analysis ST9 which used a Von Mises failure criterion instead of a Tresca criterion. Although analyses ST9 and ST9a both used the Von Mises criterion, they differed in the strength value assigned to the soil. For analysis ST9 a reduced failure strength was adopted in order to match the Tresca criterion for a stress path with a Lode angle of 0°, whereas for analysis ST9a the strength was not reduced (**Figures 11.28–11.31**).

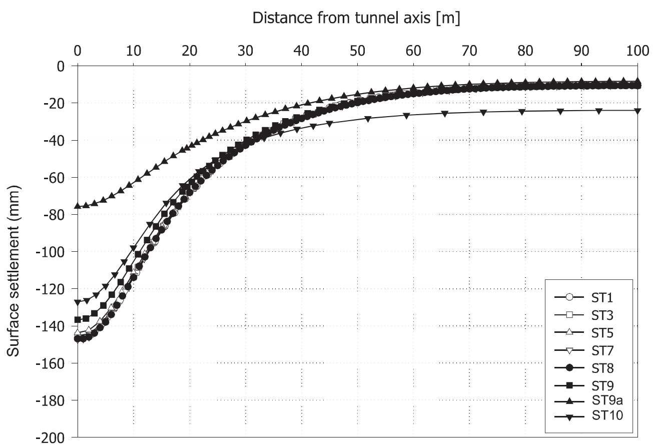

Figure 11.28 Surface settlements: Analysis B/100

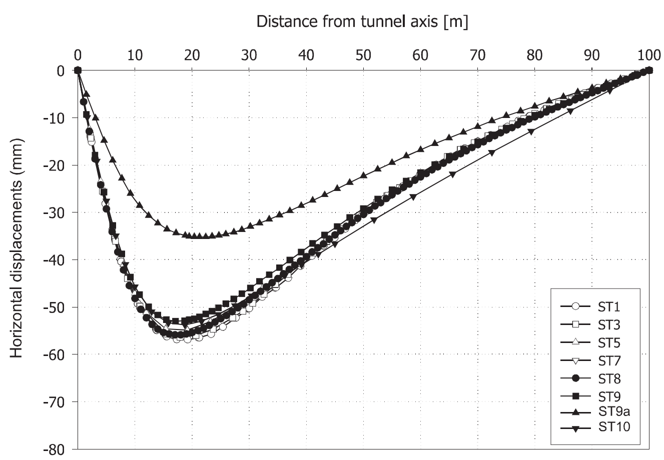

Figure 11.29 Horizontal displacements at surface: Analysis B/100

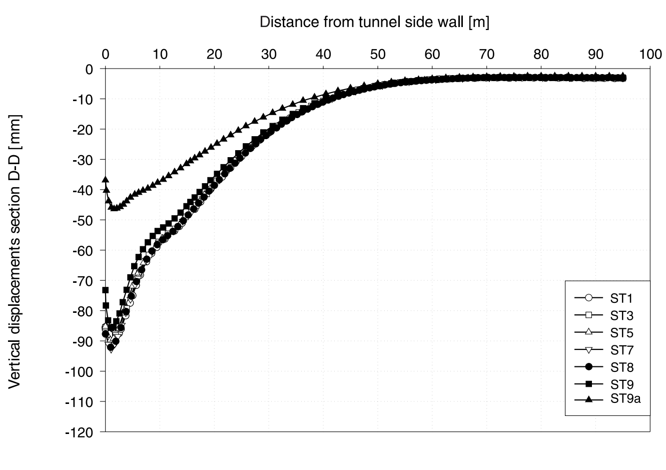

Figure 11.30 Vertical displacements at section D–D: Analysis B/100

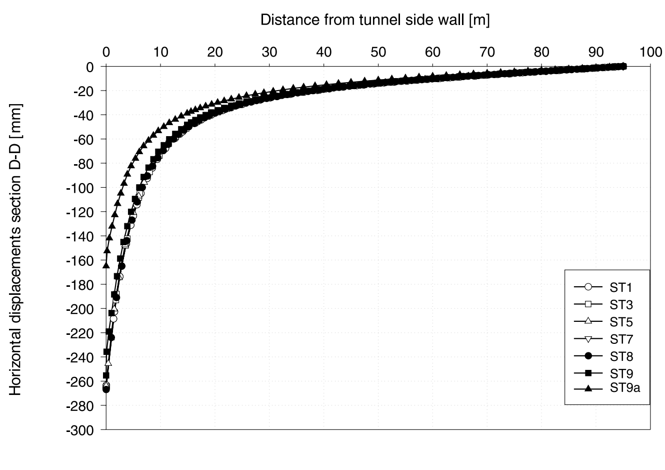

Figure 11.31 Horizontal displacements at section D–D: Analysis B/100

For case C (**Figures 11.32–11.35**) the comparison also improves, but some major differences remain and these are almost certainly due to the fact that the computer programs handle the specified volume loss in different ways. At section D–D the vertical displacements shown at the tunnel perimeter differ but this value probably depends on whether or not the lining is included over its entire thickness as given in the diagram.

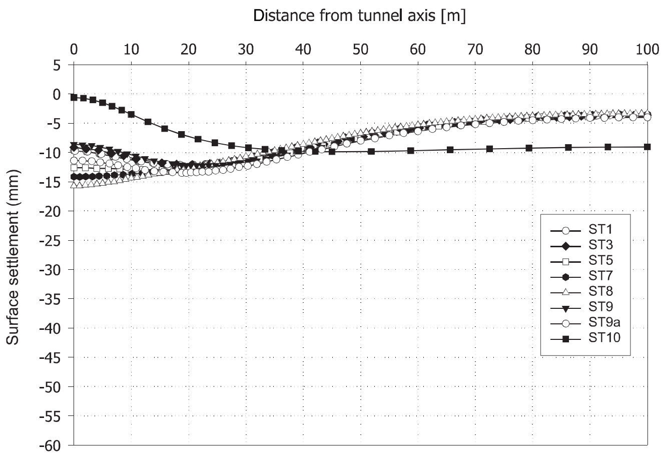

Figure 11.32 Surface settlements: Analysis C/100

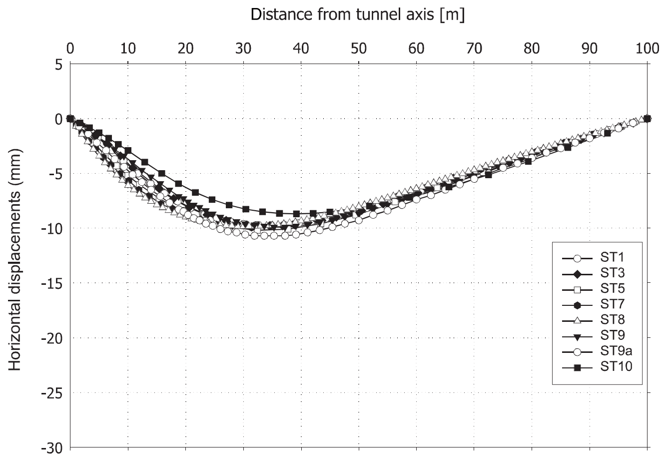

Figure 11.33 Horizontal displacements at surface: Analysis C/100

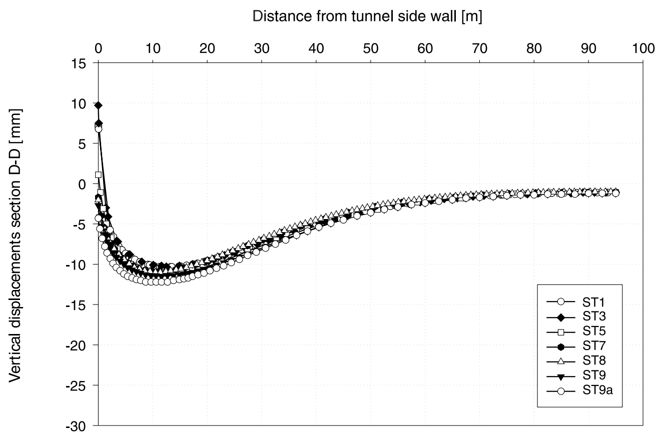

Figure 11.34 Vertical displacements at section D–D: Analysis C/100

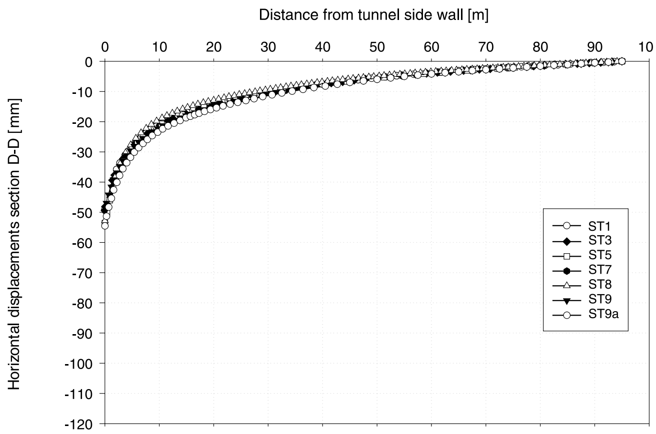

Figure 11.35 Horizontal displacements at section D–D: Analysis C/100

In order to show that the influence of the far field vertical boundary is especially important under undrained conditions (i.e. constant volume soil behaviour), an analysis has been performed for case A with exactly the same parameters except that Poisson's ratio corresponds to that for drained soil behaviour. The influence of assuming a rough or a smooth base to the finite element mesh (or finite difference grid) has also been studied. It follows from **Figure 11.36** that the surface settlements are virtually independent of either the distance to the far field vertical boundary or the displacement restraints applied to the bottom boundary. The corresponding horizontal surface displacements shown in **Figure 11.37** differ, but these differences are not significant.

11.7 Conclusions

The comparison of results obtained from several benchmarking exercises clearly shows the need for such exercises. In the first two examples differences in results have been obtained although very strict specifications have been prescribed. Even analyses using the same software but different users showed significant differences. In these cases a re-analysis has not been possible and thus not all of the discrepancies could be explained. In the third example the choice of the constitutive model was not specified and therefore the wide scatter in results is largely dependent on the personal interpretation of the available data, which formed the basis for determination of material parameters, and is perhaps not surprising. However, this is the

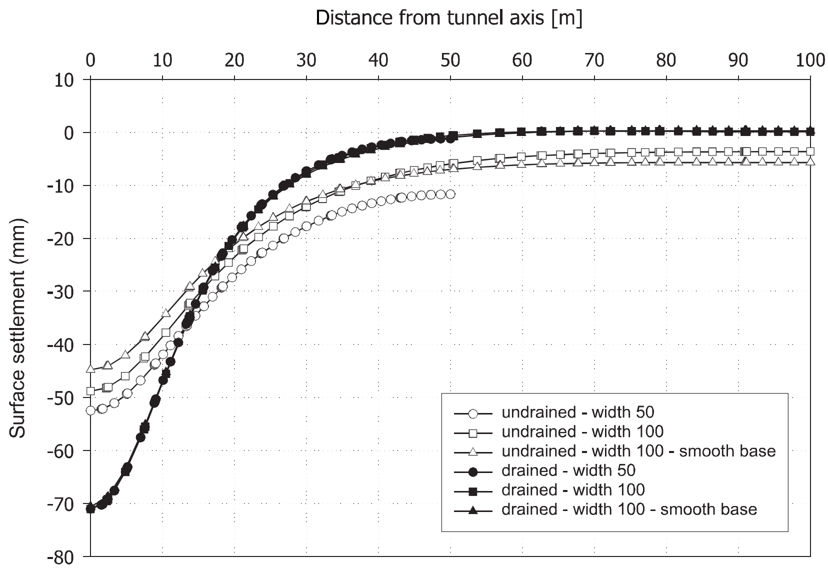

Figure 11.36 Surface settlements: Analysis A/100—drained/undrained

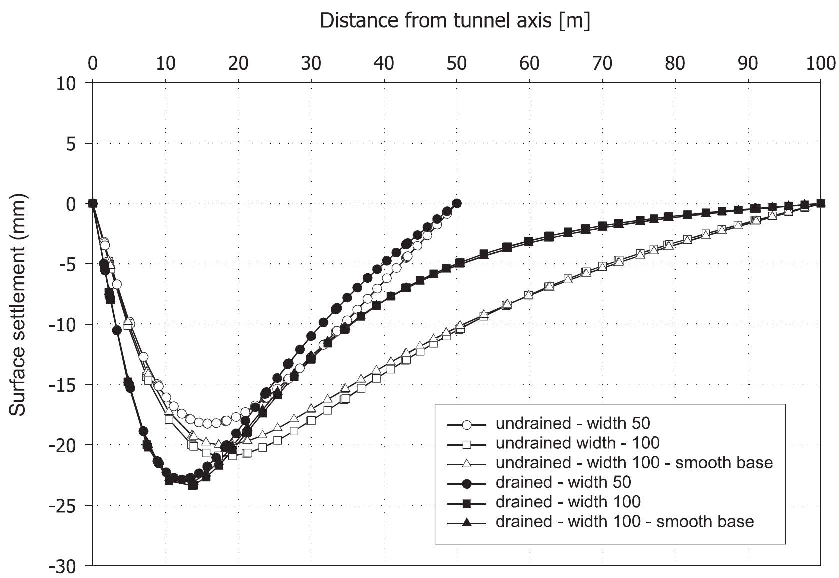

Figure 11.37 Horizontal displacements at surface: Analysis A/100—drained/undrained

situation one faces in practice, and much future work needs to be done in order to arrive at standard procedures for the determination of input parameters for numerical analysis.

The final, very simple example also revealed that the differences observed in the analysis were mainly due to the modelling assumptions made by the user. When a second round of analyses was initiated for the same problem, specifying the boundary conditions in detail, smaller differences in results were obtained, although software-specific differences come into the analysis when modelling the volume loss, as was necessary for this exercise.

These examples clearly show that a sufficient amount of experience and theoretical background from the user is required in order to obtain sensible results in numerical analyses. Neither the software (at least in most cases) and certainly not the numerical method are to be blamed exclusively for unrealistic results.

References

Alawaji, H., Runesson, K., Sture, S. and Axelsson, K. (1992). Implicit integration in soil plasticity under mixed control for drained and undrained response. *Int. J. Numer. Anal. Methods Geomech.*, **16**, 737–756.

Al-Tabbaa, A. (1987) Permeability and stress–strain response of speswhite kaolin, PhD thesis, Cambridge University.

Al-Tabbaa, A. and Wood, D.M. (1989) An experimentally based 'bubble' model for clay. *International Conference of Numerical Models in Geomechanics, NUMOG III*, Pietruszczak and Pande (eds), Balkema, pp. 91–99.

Anagnostou, G. (1995a) Seepage flow around tunnels in swelling rock. *Int. J. Numer. Anal. Methods Geomech.,* **19**, 705–724.

Anagnostou, G. (1995b) The influence of tunnel excavation on the hydraulic head. *Int. J. Numer Anal. Methods Geomech.*, **19**, 725–746.

Anagnostou, G. and Kovári, K. (1996) Face stability conditions with earth pressure balanced shields. *Tunnell. Undergrd Space Technol.*, **11**(2), 165–173.

Anagnostou, G. and Kovári, K. (1999) Tunnelbau in Störzonen. *Symposium Geologie AlpTransit, Zürich.*

Arn, Th. (1987) *Numerische Erfassung der Stroemungsvorgaenge im geklueftteten Fels*. Swiss Federal Institute of Technology, Zurich, IBETH, Mitteilung 1/89.

Atahan, C., Leca, E. and Guilloux, A. (1996) Performance of a shield driven sewer tunnel in the Val de Marne, France. In: Mair and Taylor (eds), *Geotechnical Aspects of Underground Construction in Soft Ground*, London, Balkema, Rotterdam, pp. 641–646.

Atkinson, J.H. and Potts, D.M. (1975) A note on associated field solutions for boundary value problems in a variable φ–variable ν soil. *Géotechnique*, **25**(2) 379–384.

Bathe, K.J. (1982) *Finite element procedures in engineering analysis*. New Jersey: Prentice Hall.

Bazant, Z.P. (1978) Endochronic inelasticity and incremental plasticity. *Int. J. Solids Struct.*, **14**, 691–714.

Bear, J. (1972) *Dynamics of Fluids in Porous Media*, New York: American Elsevier, p. 764.

Beer, G. (1985) An isoparametric joint/interface element for finite element analysis. *Int. J. Numer. Methods Eng.*, **21**, 585–600.

Booker, J.R. and Small, J.C. (1982) Finite element analysis of consolidation, Papers I and II. *Int. J. Numer. Methods Geomech.*, **6**, 151–194.

Boone, S.J. and Crawford, A.M. (2000) Braced excavations: Temperature elastic modulus and strut loads. *ASCE J. Geotech. Geoenviron. Engn.,* **126**(10), 870–881.

Borin, D.L. (1989) Wallap—Computer program for the stability analysis of retaining walls. Geosolve.

Borja, R.I. (1991) Cam clay plasticity, part II: Implicit integration of constitutive equations based on nonlinear elastic stress prediction. *Comput. Methods Appl. Mech. Eng.*, **88**, 225–240.

Borja, R.I. and Lee, S.R. (1990) Cam clay plasticity, part I: Implicit integration of constitutive relations. *Comput. Methods Appl. Mech. Eng.*, **78**, 49–72.

British Standards Institution (1994) BS 8002: *Code of Practice for Earth Retaining Structures*.

Brown, P.T. and Booker, J.R. (1985) Finite element analysis of excavation. *Comput. Geotech.*, **1**, 207–220.

Burland, J.B. and Hancock, R.J.R. (1977) Underground car park at the House of Commons, London: geotechnical aspects. *Struct. Eng.*, **55**(2), 87–105.

Calladine, V.R. (1963) Correspondence. *Géotechnique*, **13**, 250–255.

Carol, I. and Alonson, E.E. (1983) A new joint element for the analysis of fractured rock. *5th International Congress on Rock Mechanics*, Melbourne, Australia, Vol. F, pp. 147–151.

Carter, J.P. (1977) Finite deformation theory and its application to elastoplastic soils. PhD thesis, University of Sydney, Australia.

Carter, J.P., Booker, J.R. and Davies, E.H. (1977) Finite deformation of an elastoplastic soil. *Int. J. Numer. Methods Geomech.*, **1**.

Carter, J.P., Booker, J.R. and Small, J.C. (1979) The analysis of finite elastoplastic consolidation. *Int. J. Numer. Anal. Methods Geomech.*, **3**, 107–129.

Castro, G. (1969) Liquefaction of sands. PhD thesis, Harvard University, USA. Soil Mechanics Series No. 81.

Chambon, R., Desrues, J., Hammad, W. and Charlier, R. (1994) CLoE, a new rate-type constitutive model for geomaterials—Theoretical basis and implementation. *Int. J. Numer. Anal. Methods Geomech.*, **18**(4), 253–278.

Chen, W.F. (1975) Limit analysis and plasticity. In: *Developments in Geotechnical Engineering*, Vol. 7, Elsevier, Amsterdam.

Clarke, B.G. (1995) *Pressuremeters in Geotechnical Design*, London: Blackie.

Clayton, C.R.I. and Symons, I.F. (1992) The pressure of compacted fill on retaining walls. *Géotechnique*, **42**(1), 127–130.

Coulomb, C.A. (1776) Essai sur une application des règles de maximis et minimis à quelques problèmes de statique, relatifs à l'architecture. *Mém. Math. Phys. Acad. R. Sci.*, **7**, 343–382.

Dafalias, Y.F. (1975) On cyclic and anisotropic plasticity. PhD thesis, University of California, Berkeley, CA.

Dafalias, Y.F. and Popov, E.P. (1975) A model of nonlinearly hardening materials for complex loadings. *Acta Mech.*, **21**, 173–192.

Davinson, H.L. and Chen, W.F. (1976) Nonlinear analyses in soil and solid mechanics. *Proceedings of 2nd Conference on Numerical Methods in Geomechanics*, Desai (ed.), Blacksburg, VA, pp. 205–216.

Day, R.A. (1990) Finite element analysis of sheet pile retaining walls. PhD thesis, Imperial College, University of London.

Day, R.A. and Potts, D.M. (1990) Curved Mindlim beam and axi-symmetric shell elements—A new approach. *Int. J. Numer. Methods Eng.*, **30**, 1263–1274.

Desai, C.S. (1999) *Mechanics of Materials and Interfaces: The Disturbed State Concept*, Boca Raton, FL: CRC Press.

Desai, C.S., Zaman, M.M., Lightner, J.G. and Siriwardane, H.J. (1984) Thin-layer element for interfaces and joints. *Int. J. Numer. Anal. Method. Geomech.*, **8**, 19–43.

Di Maggio, F.L. and Sandler, I.S. (1971) Material model for granular soils. *ASCE EM Div.*, **97**, 935–950.

Dolezalová, M. and Danko, J. (1999) Effect of dimension of the analysis and other factors on the accuracy of numerical prediction of surface settlements due to tunnelling. *Scientific Seminar on Soil–Structure Interaction*, Bratislava, pp. 13–20 (in Czech).

Dolezalová, M., Havlena, V., Karhanek, J., Hamza, P. and Stavicek, J. (1991) Numerical analysis of staged excavation of a sewer tunnel. *Proceedings, Underground Structures '91*, Prague, pp. 16–25 (in Czech).

Dolezalová, M., Zemanová, V. and Danko, J. (1998) An approach for selecting rock mass constitutive model for surface settlement predictions. *Proceedings of 1st International Conference on Soil–Structure Interaction in Urban Civil Engineering*, Darmstadt, **1**(4), 44–66.

Drucker, D.C. and Prager, W. (1952) Soil mechanics and plasticity analysis or limit design. *Q. Appl. Math.*, **10**(2), 157–165.

Drucker, D.C., Gibson, R.E. and Henkel, D.J. (1957) Soil mechanics and work hardening theories of plasticity. *Trans. ASCE*, **122**, 338–349.

Duncan, J.M. (1994) The role of advanced constitutive relations in practical applications. *Proceedings of 13th ICSMFE*, New Delhi, vol. 5, pp. 31–48.

Duncan, J.M. and Chang, C.-Y. (1970) Nonlinear analysis of stress and strain in soils. *J. Soil Mech. Found. Div. ASCE* (SM5) **96**, 1629–1653.

Dyer, M.R., Hutchinson, M.T. and Evans, N. (1996) Sudden Valley Sewer: A case history. In: Mair and Taylor (eds), *Geotechnical Aspects of Underground Construction in Soft Ground*, pp. 671–676, London, Balkema, Rotterdam.

Francavilla, A. and Zienkievicz, O.C. (1975) A note on numerical computation of elastic contact problems. *Int. J. Numer. Methods Eng.*, **9**, 913–924.

Frank, R., Guenot, A. and Humbert, P. (1982) Numerical analysis of contacts in geomechanics. *Proceedings of 4th International Conference on Numerical Methods in Geomechanics*, Balkema, Rotterdam, pp. 37–42.

Ganendra, D. (1993) Finite element analysis of laterally loaded piles, PhD thesis, Imperial College, University of London.

Ganendra, D. and Potts, D.M. (1995) Discussion on 'Evaluation of constitutive model for overconsolidated clays, by A.J. Whittle. *Géotechnique*, **45**(19), 169–173.

Gens, A. (1995) General report: Prediction, performance and design. In: Shibuya, Mitachi and Miura (eds), *Pre-failure Deformation of Geomaterials*, Rotterdam: Balkema.

Ghaboussi, J., Wilson, E.L. and Isenberg, J. (1973) Finite element for rock joint interfaces. *ASCE (SM10)* **99**, 833–848.

Goodman, R.E., Moye, D.G., van Schalkwyk, A. and Javendel, I. (1965) Ground water inflows during tunnel driving. *Eng. Geol.*, **2**, 39–56.

Goodman, R.E., Taylor, R.L. and Brekke, T.L. (1968) A model for the mechanics of jointed rock. *ASCE (SM3)*, **94**, 637–659.

Griffiths, D.V. (1980) Finite element analyses of walls, footings and slopes, PhD thesis, University of Manchester.

Griffiths, D.V. (1985) Numerical modelling of interfaces using conventional finite elements. *Proceedings of the 5th International Conference on Numerical Methods in Geomechanics*, Nagoya, Balkema, Rotterdam. pp. 837–844.

Gudehus, G. (1996) A comprehensive constitutive equation for granular materials. *Soils Found.*, **36**(1), 1–12.

Gunn, M. (1992) Small strain stiffness model for CRISP. *Proceedings of Wroth Memorial Symposium, Predictive Soil Mechanics*, Oxford, July, Houlsby and Schofield (eds), London: Thomas Telford.

Gunn, M.J., Satkunananthan, A. and Clayton, C.R.I. (1993) Finite element modelling of installation effects. In: *Retaining Structures*, Clayton, C.R.I. (ed) London: Thomas Telford, pp. 46–55.

Hashash, Y.M.A. (1992) Analysis of deep excavations in clay, PhD thesis, Massachusetts Institute of Technology.

Hermann, L.R. (1978) Finite element analysis of contact problems. *ASCE (EM5)*, **104**, 1043–1057.

Hernández, S. and Romera, L.E. (2001) A non-linear finite element procedure for evaluation of settlement induced by tunnel excavation. *Computer Methods and Advances in Geomechanics*, Tucson, Arizona, Desai *et al.* (ed), Balkema, Rotterdam. pp. 641–646.

Hibbit, H.D., Marchal, P.V. and Rice, J.R. (1970) Formulation for problems of large strain and large displacements. *Int. J. Solids Struct.*, **6**, 1069–1086.

Higgins, K., Potts, D.M. and Symons, I.F. (1989) Comparison of predicted and measured performance of the retaining walls of the Bell Common tunnel, *TRL Report CR 124*, Crowthorne: Transport Research Laboratory.

Hight, D.W. and Higgins, K.G. (1995) An approach to the prediction of ground movements in engineering practice: Background and application. In: Shibuya, Mitachi and Miura (eds), *Pre-failure Deformation of Geomaterials*, Rotterdam: Balkema, pp 909–945.

Hoeg, K., Christian, J.T. and Whitman, R.V. (1968) Settlement of strip load on elastic–plastic soil. *J. Soil Mech. Found. Div. ASCE (SM2)* **94**, 431–445.

Hofmeister, L.D., Greenbaum, G.A. and Evensen, D.A. (1971) Large strain, elastoplastic finite element analysis. *AIAA J.*, **9**, 1248–1254.

Hou, X.Y., Liao, S. and Zhao, Y. (1996) Field measurements from two tunnels in Shanghai. In: Mair and Taylor (eds), *Geotechnical Aspects of Underground Construction in Soft Ground*, London, Balkema, Rotterdam, pp. 689–694.

Hvorslev, M.J. (1937) *Über die Festigkeitseigenschaften gestörter bindiger Böden*, Danmarks Naturvidenskaplige samfund, Ingeniorvidenskaplige Skrifter A45, Copenhagen.

Janbu, N. (1963) Soil compressibility as determined by oedometer and triaxial tests. *Proceedings of European Conference for Soil Mechanics and Foundation Engineering*, Wiesbaden, pp. 19–25.

Jardine, R.J., Potts, D.M., Fourie, A.B. and Burland, J.B. (1986) Studies of the influence of non-linear stress–strain characteristics in soil–structure interaction. *Géotechnique*, **36**(3), 377–396.

Jardine, R.J., Potts, D.M., St John, H.D. and Hight, D.W. (1991) Some practical applications of a non-linear ground model. *Proceedings of Xth European Conference for Soil Mechanics and Foundation Engineering*, Firenze, vol. 1, pp. 223–228.

Kamenicek, I. *et al*. (1997) Mrazovka Exploratory Adit, 1st stage, Technical Report. Monitoring NATM, IKE Ltd, Prague: PUDIS (in Czech).

Kastner, R., Ollier, C. and Guibert, G. (1996) In situ monitoring of the Lyons Metro D line extension. In: Mair and Taylor (eds), *Geotechnical Aspects of Underground Construction in Soft Ground*, London, Balkema, Rotterdam, pp. 701–706.

Katona, M.G. (1983) A simple contact-friction interface element with application to buried culverts. *Int. J. Numer. Anal. Methods Geomech.*, **7**, 371–384.

Katzenbach, R., Arslan, U., Moormann, C. and Reul, O. (1998) Piled raft foundations—interaction between piles and raft. *Proceedings of the 1st International Conference on Soil–Structure Interaction in Urban Civil Engineering*, Darmstadt, October, vol. 2, pp. 279–296.

Kavvadas, M. and Amorosi, A. (2000) A constitutive model for structured soils. *Géotechnique*, **50**(3), 263–273.

Klisinski, M. (1998) On constitutive equations for arbitrary stress–strain control in multi-surface plasticity. *Int. J. Solids Struct.*, **35**, 2655–2678.

Klisinski, M., Mroz, Z. and Runesson, K. (1992) Structure of constitutive equations in plasticity for different choices of state and control variables. *Int. J. Plast.*, **8**, 221–243.

Kolymbas, D., Herle, I. and von Wolffersdorff, P.A. (1995) Hypoplastic constitutive equation with back stress. *Int. J. Numer. Anal. Methods Geomech.*, **19**(6), 415–446.

Kondner, R. (1963) Hyperbolic stress–strain response: cohesive soils. *J. Soil Mech. Found. Div. ASCE (SM1)* **89**, 115–143.

Krieg, R.D. (1975) A practical two-surface plasticity theory. *J. Appl. Mech.*, **42**, 641–646.

Lade, P.V. (1977) Elasto-plastic stress–strain theory for cohesionless soil with curved yield surfaces. *Int. J. Solids Struct.*, **13**, 1019–1035.

Lade, P.V. and Duncan, J.M. (1973) Cubical triaxial tests on cohesionless soil. *J. Soil Mech. Found. Div. ASCE, (SM10)*, **99**, 793–812.

Lade, P.V. and Duncan, J.M. (1975) Elasto-plastic stress–strain theory for cohesionless soil. *ASCE, GT Div.*, **101**, 1037–1053.

Lai, J.Y. and Booker, J.R. (1989) A residual force finite element approach to soil–structure interaction analysis. *Research Report No. 604*, University of Sydney.

Lee, K. and Sills, G.C. (1981) The consolidation of a soil stratum including self weight effects and large strains. *Int. J. Numer. Methods Geomech.*, **5**, 405–428.

Long, M. and Brangan, C. (2001) Behaviour of a deep basement in Dublin glacial till. *Geotech. Eng. J.* (submitted).

Long, M.M., Hamilton, J., Clarke, J.C. and Lambson, M.D. (1992) Cyclic lateral loading of an instrumented pile in over consolidated clay at Tilbrook Grange. *Proceedings of a Conference on Recent Large Scale Fully Instrumented Pile Tests in Clay*, London: ICE, June.

Lunne, T., Robertson, P.K. and Powell, J.J.M. (1997) *Cone penetration testing in geotechnical practice*, Blackie, London.

Magnan, J.P., Belkeziz, A., Humbert, P. and Mouratidis, A. (1982) Finite element analysis of soil consolidation with special reference to the case of strain hardening elasto-plastic stress–strain models. *1st International Conference on Numerical Methods in Geomechanics*, Zürich, pp. 601–609.

Mair, R.J. and Taylor, R.N. (1997) Bored tunnelling in the urban environment. *Proceedings of 14th International Conference for Soil Mechanics and Foundation Engineering*, Hamburg, Balkema, Rotterdam, pp. 2353–2385.

Marchetti, S. (1997) Flat dilatometer design applications. *Geotechnical Engineering Conference*, Cairo University, January, vol. 3.

Marsily, G. de (1986) *Quantitative Hydrogeology. Groundwater Hydrology for Engineers*, London: Academic Press, p. 434.

Matsuoka, H. and Nakai, T. (1977) Stress–strain relationship of soil based on the 'SMP'. Constitutive equations of soils. Proceedings of specialty session 9, *IX ICSMFE*, Tokyo, pp. 153–162.

Mattsson, H. (1999) On a mathematical basis for constitutive drivers in soil plasticity. PhD thesis, Lulea University of Technology, Lulea, Sweden.

Mattsson, H., Axelsson, K. and Klisinski, M. (1997) A method to correct yield surface drift in soil plasticity under mixed control and explicit integration. *Int. J. Numer. Anal. Methods Geomech.*, **21**, 175–197.

Mattsson, H., Axelsson, K. and Klisinski, M. (1999) On a constitutive driver as a tool in soil plasticity. *Adv. Eng. Software*, **30**, 511–528.

Mattsson, H., Klisinski, M. and Axelsson, K. (2000) Optimisation routine for identification of model parameters in soil plasticity. *Int. J. Numer. Anal. Methods Geomech.* (submitted).

Meissner, H. (1991) Empfehlungen des Arbeitskreises 1.6 'Numerik in der Geotechnik', Abschnitt 1, 'Allgemeine Empfehlungen'. *Geotechnik*, **14**, 1–10.

Meissner, H. (1996) Tunnelbau unter Tage-Empfehlungen des Arbeitskreises 1.6 'Numerik in der Geotechnik', Abschnitt 2. *Geotechnik*, **19**, 99–108.

Meissner, H. (2002). Baugruben-Empfehlungen des Arbeitskreises 1.6 'Numerik in der Geotechnik', Abschnitt 3. *Geotechnik*, **25**, 44–56.

Mohr, O. (1882). Über die Darstellung des Spannungszustandes und des Deformationszustandes eines Körperelements und über die Anwendung derselben in der Fesigkeitslehre. *Civilingenieur*, **28**, 113–156.

Mouratides, A. and Magnan, J.P. (1983) Un modèle élastoplastque anisotrope avec écrouissage pour les argilles molles naturelles. MELANIE. *Rev. Fr. Geotech.*, **25**, 55–62.

Mroz, Z. (1967) On the description of anisotropic work hardening. *J. Mech. Phys. Solids*, **15**, 163–175.

Mroz, Z. and Norris, V.A. (1982) Elastoplastic and viscoplastic constitutive models for soils with application to cyclic loading. In: Pande, G.N. and Zienkiewicz, O.C. (eds), *Soil Mechanics. Transient and Cylic Loads*, pp. 173–217.

Naylor, D.J., Pande, G.N., Simpson, B. and Tabb, R. (1981) *Finite Elements in Geotechnical Engineering*, Swansea: Pineridge Press.

Nelder, J.A. and Mead, R. (1965) A simplex method for function minimization. *Comput. J.*, **7**, 308–313.

Ng, C.W.W. (1999) Stress paths in relation to deep excavation, *ASCE J. Geotech. Geoenviron. Eng.*, **125**(5), 357–363.

Ng, C.W.W. and Yan, R.W.M. (1999) Three-dimensional modelling of a diaphragm wall construction sequence. *Géotechnique*, **46**(6), 825–834.

Ng, C.W.W., Lings, M.L. and Nash, D.F.T. (1992) Back-analysing the bending moment in a concrete diaphragm wall. *Struct. Eng.*, **70** (23 & 24), 421–426.

Nieminis, A. and Herle, I. (1997) Hypoplastic model for cohesionless soils with elastic strain range. *Mech. Cohes. Frict. Mater.*, **2**(4), 279–299.

Nova, R. (1989) Liquefaction, stability, bifurcations of soil via strain hardening plasticity. In: Dembicki, E., Gudehus, G. and Sikora, Z. (eds), *Numerical Methods for Localization and Bifurcation of Granular Bodies*, TU Gdansk, pp. 117–131.

Nova, R. and Wood, D.M. (1979) A constitutive model for sand in triaxial compression. *Int. J. Num. Anal. Methods Geomech.*, **3**(3), 255–278.

Nuebel, K., Karcher, C. and Herle, I. (1999) Ein einfaches Konzept zur Abschaetzung von Setzugnen. *Geotechnik*, **22**(4), 251–258.

Ohde, J. (1939) Zur Theorie der Druckverteilung im Baugrund. *Bauingenieur*, **20**, 451–459.

Ohde, J. (1951) *Grundbaumechanik*, Huette, BD, III, 27. Auflage.

Ohta, H. and Wroth, C.P. (1976) Anisotropy and stress reorientation in clay under load. *Second International Conference on Numerical Methods in Geomechanics*, Blacksburg, vol. 1, pp. 319–328.

O'Reilly, M.P. and New, B.M. (1982) Settlements above the tunnels in the United Kingdom—their magnitude and prediction. *Tunnelling '82*, London, pp. 173–182.

Osias, J.R. and Swedlow, J.L. (1974) Finite elastoplastic deformation—theory and numerical examples. *Int. J. Solids Struct.*, **10**, 321–339.

Owen, D.R.J. and Hinton, E. (1980) *Finite Elements in Plasticity: Theory and Practice*, Swansea: Peneridge Press.

Pan, X.D. and Hudson, J.A. (1988) Plane strain analysis in modelling three-dimensional tunnel excavations. *Int. J. Rock Mech. Min. Sci. Geomech. Abstr.*, **25**(5), 331–337.

Pan, X.D., Hudson, J.A. and Cassie, J. (1989) Large deformation of weak rocks at depth—A numerical case study. *Rock at Great Depth*, **2**, 613–620.

Pande, G.N. and Pietruszczak, S. (1986) A critical look at constitutive models for soils. In: Dugnar, R. and Studer, J.A. (eds), *Geomechanical Modelling in Engineering Practice*, Balkema, Rotterdam, pp. 369–395.

Pande, G.N. and Sharma, K.G. (1983) Multilaminate model for clays—a numerical evaluation of the infleunce of rotation of the principal stress axes. *Int. J. Numer. Anal. Methods Geomech.*, **7**, 397–418.

Pande, G.N., Beer, G. and Williams, J.R. (1990) *Numerical Methods in Rock Mechanics*, Chichester: John Wiley & Sons.

Panet, M. and Guenot, A. (1982) Analysis of convergence behind a face of a tunnel. *Proceedings of International Symposium on Tunnelling '82*, pp. 197–204.

Pani, M., Battelino, D. and Zanette, N. (2001) The new computer aided design using cell method. *International Workshop on Computational Mechanics of Materials, IWCM11*, Freiberg.

Papin, J.W., Simpson, B., Felton, P.J. and Raison, C. (1985) Numerical analysis of flexible retaining walls. *Conference on Numerical Methods in Engineering, Theory and Application*, Swansea, pp. 789–802.

Pietruszczak, S. and Pande, G.N. (1987) Multi-laminate framework of soil models—plasticity formulation. *Int. J. Numer. Anal. Methods Geomech*, **11**, 651–658.

Potts, D.M. and Addenbrooke, T.I. (1997) A structure's influence on tunnelling-induced ground movements. *Proc. ICE, Geotech. Eng.*, **125**, 109–125.

Potts, D.M. and Ganendra, D. (1994) An evaluation of substepping and implicit stress point algorithms. *Comput. Methods Appl. Mech. Eng.*, **119**, 341–354.

Potts, D.M. and Zdravkovic, L. (1999) *Finite Element Analysis in Geotechnical Engineering: Theory*, London: Thomas Telford.

Potts, D.M. and Zdravkovic, L. (2001a) *Finite Element Analysis in Geotechnical Engineering—Application*, London: Thomas Telford.

Potts, D.M. and Zdravkovic, L. (2001b) Prediction and reality in geotechnical practice. In: Desai *et al*., (eds) *Computer Methods and Advances in Geomechanics*, Tucson, AZ, pp. 57–65.

Powrie, W. and Batten, M. (2000) Comparison of measured and calculated temporary-prop loads at Canada Water Station. *Géotechnique*, **50**(2), 127–140.

Powrie, W. and Li, E.S.F. (1991) Finite element analysis of an in situ wall propped at formation level. *Géotechnique*, **41**(4), 499–514.

Powrie, W., Chandler, R.J., Carder, D. and Watson, G.V.R. (1999) Back analysis of an embedded retaining wall with a stabilising base. *Proc. ICE, Geotech. Eng*., **127**, 75–86.

Prager, W. (1961) An elementary discussion of definitions of stress rate. *Q. Appl. Math*., **17**, 403–407.

Prevost, J.H. and Hoeg, K. (1975) Effective stress–strain–strength model for soils. *ASCE, GT Div*., **10**, 257–278.

Puzrin, A.M. and Burland, J.B. (1998) Nonlinear model of small strain behaviour of soils. *Géotechnique*, **48**(2), 217–233.

Randolph, M.F. and Houlsby, G.T. (1984) The limiting pressure on a circular pile loaded laterally in cohesive soil. *Géotechnique*, **34**(4), 613–623.

Renati, E.B. and Roessler, K. (1998) Tunnel design and construction in extremely difficult ground conditions. *Tunnel*, **8**, 23–31.

Riggs, C.O. (1982) Proposed standard test method for a free fall penetration test. *ASTM Geotech. Test. J.*, **5** (3/4), 89–92.

Roscoe, K.H. and Burland, J.B. (1968) On the generalised stress–strain behaviour of 'wet' clay. In: *Engineering Plasticity,* Cambridge University Press, pp. 535–609.

Roscoe, K.H. and Schofield, A.N. (1963) Mechanical behaviour of an idealised 'wet' clay. *European Conference for Soil Mechanics and Foundation Engineering*, Wiesbaden, vol. 1, pp. 47–54.

Roscoe, K.H., Schofield, A.N. and Wroth, C.P. (1958) On the yielding of soils. *Géotechnique*, **8**, 22–52.

Rosenbrock, H.H. (1960) An automatic method for finding the greatest or least value of a function. *Comput. J.*, **3**, 175–184.

Rouainia, M. and Muir Wood, D. (2000) A kinematic hardening constitutive model for natural clays with loss of structure. *Géotechnique,* **50**(2), 153–164.

Rozsypal, A. (2000) Influence of tunnelling on surface subsidence. *Proceedings of International Conference on Underground Construction*, Prague, pp. 156–163 (in Czech).

Runesson, K., Axelsson, K. and Klisinski, M. (1992) Characteristics of constitutive relations in soil plasticity for undrained behaviour. *Int. J. Solids Struct*., **29**, 363–380.

Sachdeva, T.D. and Ramakrishnan, C.V. (1981) A finite element solution for the two dimensional elastic contact problem. *Int. J. Numer. Methods Eng*., **17**, 1257–1271.

Sakurai, S. (1978) Approximate time dependent analysis of tunnel support structure considering progress of tunnel face. *Int. J. Numer. Anal. Methods Geomech*., **2**, 159–175.

Sakurai, S. (1992) The deformation behaviour of underground openings excavated in soils and jointed rocks. *Proceedings of International Conference, NUMEG '92*, Prague, Balkema, Rotterdam.

Sandler, I.S., Di Maggio, F.L. and Baladi, G.Y. (1976) Generalised cap model for geological materials. *ASCE, GT Div*., **102**, 683–697.

Schofield, A.N. and Wroth, C.P. (1968) *Critical State Soil Mechanics*, London: McGraw-Hill.

Schweiger, H.F. (1997) Berechnungsbeispiele des AK 1.6 der DGGT—Vergleich der Ergebnisse für Beispiel 1 (Tunnel) und 2 (Baugrube). *Tagungsband Workshop 'Numerik in der Geotechnik'*, DGGT/AK 1.6, 1–29.

Schweiger, H.F. (1998) Results from two geotechnical benchmark problems. *Proceedings of 4th European Conference on Numerical Methods in Geotechnical Engineering*, Cividini, A. (ed.), pp. 645–654.

Schweiger, H.F. (2000) Ergebnisse des Berechnungsbeispieles Nr. 3 '3-fach verankerte Baugrube'. *Tagungsband Workshop 'Verformungsprognose für tiefe Baugruben'*, DGGT/AK 1.6, 7–67.

Sekiguchi, H. and Ohta H. (1977) Induced anisotropy and time dependency in clays. *Ninth International Conference for Soil Mechanics and Foundation Engineering*, Tokyo, Special Session 9, pp. 163–175.

Simpson, B. (1992) Retaining structures, displacement and design, 32nd Rankine Lecture. *Géotechnique*, **42**(4), 541–576.

Simpson, B. (1994) A model of interaction between tunnelling and a masonry structure. In: Smith (ed.), *Numerical Methods in Geotechnical Engineering*, Rotterdam: Balkema.

Simpson, B., O'Riordan, N.J. and Croft, D. (1979) A computer model for the analysis of ground movements in London clay. *Géotechnique*, **29**, 149–175.

Sloan, S.W. (1987) Substepping schemes for numerical integration of elasto-plastic stress–strain relations. *Int. J. Numer. Methods Eng.*, **24**, 893–911.

Small, J.C. and Chung, M.O. (1991) Finite element analysis of excavation in jointed rock. In *Computer Methods and Advances in Geomechanics*; Beer *et al.* (eds), Balkema, Rotterdam, Cairns, 1227–1232.

Sokolovski, V.V. (1960) *Statics of Soil Media*, London: Butterworth.

Sokolovski, V.V. (1965) *Statics of Granular Media*, Oxford: Pergamon Press.

Stallebrass, S.E. and Taylor, R.N. (1997a) The development and evaluation of a constitutive model for the prediction of ground movements in overconsolidated clay. *Géotechnique*, **47**(2), 235–254.

Stolle, D.F. and Higgins, J.E. (1989), Viscoplasticity and plasticity—numerical stability revisited. *International Conference on Numerical Methods in Geomechanics, NUMOG III*, pp. 431–438.

Stroud, M.A. (1971) Sand at low stress levels in the S.S.A., PhD thesis, Cambridge University.

Swoboda, G., Mahmoud, M. and Hladik, I. (2001) Simulation of initial stresses for tunnel models. *10th IACMAG*, Tucson, AZ, vol. 2, Balkema, Rotterdam.

Tatsuoka, F. and Ishihara, K. (1974) Yielding of sand in triaxial compression. *Soils Found.*, **14**(2), 63–76.

Tavenas, F. (1981) Some aspects of clay behaviour and their consequences on modelling techniques. *ASTM STP*, **740**, 667–677.

Thomas, J.N. (1984) An improved accelerated initial stress procedure for elasto-plastic finite element analysis. *Int. J. Numer. Methods Geomech.*, **8**, 359–379.

Timoshenko, S. and Goodier, J.N. (1951) *Theory of Elasticity*, New York: McGraw-Hill.

Tonti, E. (2001) A direct discrete formulation of field laws: the cell method. *Comput. Model. Eng. Sci.*, **2**.

Truesdell, C. and Noll, W. (1965) The non-linear field theories of mechanics. In: *Handbuch der Physik III/c*, Berlin: Springer-Verlag.

Valanis, K.C. (1971) A theory of viscoplasticity without a yield surface, Part I, General theory. *Arch. Mech.*, **23**, 517–534.

Valanis, K.C. (1982) An endochronic geomechanical model for soils. *IUTAM Conference on Deformation and Failure of Granular Materials*, Delft. Vermeer and Luger Delft (eds), Balkema, pp. 159–165.

Van der Heijden and Besseling (1984) A large strain plasticity theory and the symmetry properties of its constitutive equations. *Int. J. Comput. Struct.*, **19**, 271–276.

Vermeer, P. (1982) A five-constant model unifying well-established concepts. *International Workshop on Constitutive Relations for Soils*, Grenoble, Balkema, pp. 477–483.

Vogt, C., Bonnier, P. and Vermeer, P.A. (1998) Analysis of NATM tunnels with 2D and 3D FEM. *NUMGE98*, Udine, pp. 211–220.

Watson, G.V.R. and Carder, D.R. (1994) Comparison of the measured and computed performance of a propped bored pile retaining wall at Walthamstow. *Proc. ICE, Geotech. Eng.*, **107**, 127–133.

Whittle, A.J. (1987) A constitutive model for overconsolidated clays with application to the cyclic loading of friction piles, PhD thesis, Massachusetts Institute of Technology.

Whittle, A.J. (1991) MIT-E3: A constitutive model for overconsolidated clays. In: *Computer Methods and Advances in Geomechanics*, Beer *et al*. (eds) Rotterdam: Balkema.

Whittle, A.J. (1993) Evaluation of a constitutive model for overconsolidated clays. *Géotechnique*, **43**, 289–313.

Wilson, E.L. (1977) Finite elements for foundations, joints and fluids. Chapter 10 In: Gudehus (ed), *Finite Elements in Geomechanics*, John Wiley & Sons, New York.

Wissman, J.W. and Hauck, C. (1983) Efficient elasto-plastic finite element analysis with higher order stress point algorithms. *Comput. Struct*., **17**, 89–95.

Wu, W. and Bauer, E. (1994) A simple hypoplastic constitutive model for sand. *Int. J. Numer. Anal. Methods Geomech*., **18**, 833–862.

Zienkiewicz, O.C. and Cormeau, I.C. (1974) Visco-plasticity, platicity and creep in elastic solids—a unified numerical solution approach. *Int. J. Numer. Methods Eng.*, **8**, 821–845.

Zienkiewicz, O.C. and Naylor, D.J. (1973) Finite element studies of soils and porous media. Lecture, finite elements, Oden and de Arantes (eds), UAH Press, pp. 459–493.

Zienkiewicz, O.C. and Zhu, J.Z. (1992) The super convergent patch recovery and a posteriori error estimates, Part 2: error, estimates and adaptivity. *Int. J. Numer. Methods Eng.*, **33**, 1365–1382.

Ziolkowski, J.C. (1984) Numerical study of strain rate effects on stress–strain response of soils, PhD thesis, Imperial College, University of London.